Dissertation

Thermodynamics of the Fractional Quantum Hall System: The High–Temperature Expansion Method

Sivinee Sawatdiaree

Thermodynamics of the Fractional Quantum Hall System: The High–Temperature Expansion Method

Vom Fachbereich Physik der Universität Hannover

zur Erlangung des Grades
Doktor der Naturwissenschaften
Dr. rer. nat.

genehmigte Dissertation

von

Sivinee Sawatdiaree, M. Sc.
geboren am 19.08.1972 in Chiang Mai, Thailand

2001

Referent:	Priv.–Doz. Dr. Walter Apel
Korreferent:	Prof. Dr. Mario Liu
Tag der Promotion:	26.06.2001

Meinen Eltern

"... not just connected but proper ..."

Kurzzusammenfassung

Die thermodynamischen Eigenschaften des gebrochenzahligen Quanten Hall Systems – wechselwirkende Elektronen, die sich in zwei Dimensionen im starken Magnetfeld bewegen – wurden untersucht. Das großkanonische thermodynamische Potential wurde mit Hilfe einer Hochtemperaturentwicklung bis zur achten Ordnung in der Entwicklung nach der Wechselwirkung berechnet. Daraus wurden Energie und freie Energie abgeleitet und als Funktionen der Teilchendichte und der Temperatur ausgedrückt. Auf Grund einer besonderen Symmetrie des Landauniveaus konnte ein gemeinsamer Faktor, "Muster", für zusammenhängende Diagramme definiert werden, die dieselbe Frequenzsumme ergeben. Die Einführung dieser "Muster" reduziert die Anzahl der Summanden, die berechnet werden müssen, um einen Faktor von der Größe der Ordnung der Entwicklung. Mit der vorliegenden Methode wurden das Resultat der herkömmlichen störungstheoretischen Behandlung bis zur dritten Ordnung der Entwicklung und das Resultat der Virialentwicklung in der tiefsten Ordnung für beliebige Wechselwirkung reproduziert.

Zwei kurzreichweitige Modellwechselwirkungen, für die Laughlins Wellenfunktionen die exakten Grundzustände zu zwei verschiedenen Teilchendichten sind, wurden benutzt um die Zuverlässigkeit der Ergebnisse zu überprüfen. Wenn die Temperatur erniedrigt wird, entwickelt die Energie pro Teilchen, wie erwartet, einen Knick nahe der Teilchendichte, die der Wechselwirkung entspricht. Für eine Summe zweier kurzreichweitiger Wechselwirkungen ist nur ein Knick in der Energie pro Teilchen sichtbar. Die Teilchendichte, an der sich dieser Knick entwickelt, verändert sich mit dem Verhältnis der Wechselwirkungen in der Summe.

Die Kurven der inversen Kompressibilität zu verschiedenen Temperaturen überkreuzen sich bei bestimmten Teilchendichten, die der untersuchten kurzreichweitigen Wechselwirkung entsprechen. Diese Überkreuzungspunkte wurden als Indikator für die Existenz des Grundzustandes des gebrochenzahligen Quanten Hall Effektes erkannt. Die Existenz der Überkreuzungspunkte wird analytisch durch die Temperaturunabhängigkeit eines Integrals der inversen Kompressibilität über die Teilchendichte garantiert. Diese Summenregel zeigt, daß die Überkreuzungspunkte durch die Wechselwirkung zustande kommen. Die numerischen Resultate demonstrieren auf der anderen Seite, daß die Position der Überkreuzungspunkte auf der Achse der Teilchenzahl in der Nähe des Punktes ist, wo man eine verschwindende Kompressibilität bei Temperatur Null für die gegebene kurzreichweitige Wechselwirkung erwartet. Mit der Hilfe der Überkreuzungspunkte wurde die gleichzeitige Existenz zweier Quanten Hall Zustände beobachtet, die für eine kombinierte Wechselwirkung erwartet wird. So erweisen sich die Überkreuzungspunkte in der inversen Kompressibilität als sehr nützliche Hilfsmittel, um das gebrochenzahlige Quanten Hall System bei endlichen Temperaturen zu studieren.

Schlagworte: Quanten Hall Effekt; Nicht–Fermiflüssigkeits Grundzustände; Fermionen in reduzierten Dimensionen.
PACS: 73.43.–f; 71.10.Hf; 71.10.Pm

Abstract

The thermodynamics of the fractional quantum Hall system – interacting electrons moving in two dimensions in a strong magnetic field – has been studied. A high–temperature expansion method has been used to calculate the grand canonical thermodynamic potential. The calculation has been carried out up to the eighth order of the expansion in the interaction. From the grand canonical thermodynamic potential, the energy and the canonical free energy have been derived and expressed as functions of the particle density and the temperature. Due to a special symmetry of the Landau level, a common factor, *pattern*, can be defined for connected diagrams which yield the same frequency sum. The introduction of the patterns reduces the number of terms needed to be calculated by a factor of the order of the expansion. With the present method, the result of the traditional perturbative treatment up to the third order of the expansion, and the result of the Virial expansion in the lowest order have been reproduced for an arbitrary interaction.

Two zero–range model interactions, for which Laughlin's wave functions are the exact ground states at two different particle densities, have been used to check the reliability of the results. As the temperature is lowered, the energy per particle develops a cusp, as expected, near the particle density corresponding to the interaction. For a sum of two zero–range interactions, only one cusp is visible in the energy per particle. The particle density, where the cusp develops, changes with the ratio of the interactions in the sum.

The curves of the inverse compressibility of different temperatures cross at certain particle densities corresponding to the zero–range interaction studied. These *crossing points* are found to be an indication of the existence of the fractional quantum Hall ground states. Analytically, the existence of the crossing point is ensured by the temperature independence of an integral of the inverse compressibility on the particle density. This sum rule shows that the crossing points are due to the interaction. Numerical results, on the other hand, demonstrate that the position of the crossing points on the particle density axis is close to where a vanishing compressibility at zero temperature is expected for a given zero–range interaction. With the aid of the crossing points, the existence of the two quantum Hall states which is expected for a combined interaction has been simultaneously observed. Thus, the crossing points in the inverse compressibility prove to be a very useful tool in studying the fractional quantum Hall system at finite temperatures.

Keywords: Quantum Hall effect; Non–Fermi–liquid ground states; Fermions in reduced dimension
PACS: 73.43.–f; 71.10.Hf; 71.10.Pm

Contents

List of Figures

List of Tables

Part I

Introduction & Motivation

Chapter 1

Introduction

It was in the beginning of the 80's when the "quantum Hall effect" came under spotlight. Since then, the field keeps fascinating scientists by a number of phenomena hidden under the already observed phenomena or between two of them. In the past two decades, the field has been enlarged and expanded as new physics has been found. The phenomenon discovered first, the "integer quantum Hall effect", gave a new way to determine the fine structure constant and also a new way to maintain the standard resistance. The phenomenon is explained within the single–particle description. Two years later, an even more fascinating phenomenon was found, the "fractional quantum Hall effect". Experimentally, both effects look much alike, but they contain different physics. The single–particle picture fails dramatically and a theoretical description of the fractional quantum Hall effect starts from an interacting many–body system. Thus, only in the first two years, the field is enlarged from one particle in a random potential field to a many–body system. The enlargement is still going on. This already lead us to new physics and many new questions but, perhaps, there are more phenomena awaiting to be discovered. Thus, the field of the quantum Hall effect continues to be a fascinating field in condensed matter physics.

1.1 Historical Aspects

The integer quantum Hall effect (IQHE) was discovered in 1980 by K. von Klitzing, G. Dorda and M. Pepper [1] as a surprise. Although some properties of the system of electrons moving in two dimensions in a strong magnetic field were discussed earlier by Ando, Matsumoto and Uemura [2] and Kawaji, et. al. [3] in 1975, the precision of the quantised Hall plateaus was completely unexpected. A first general explanation was suggested a year later, known as the Laughlin argument [4]. The Laughlin argument was generalised by Halperin in Ref. [5]. Generally, an explanation of the effect is searched within the single particle description under the condition that the Fermi level lies between two Landau levels. The role of disorder is crucial here.

After the discovery of the integer quantum Hall effect, the fractional quantum Hall effect (FQHE) was the next unexpected discovery in 1982 by D. C. Tsui, H. L. Störmer and A. C. Gossard [6], a surprise to both experimental and theoretical physicists. The experimental discovery was followed by the theoretical proposal of a new ground state wavefunction [7], the prodigious Laughlin wavefunction, in an attempt to explain the unusual transport properties at the "magic" electron densities observed in the experiment. It lead to our current picture of the fractional quantum Hall effect – an incompressible ground state at the magic electron densities separated by a gap from the excitations – and paved the way for many recent developments [8, 9, 10, 11].

The concept of the *composite fermions*, proposed by J. Jain [12, 13, 14], opened a new way for the theoretical study, of both the fractional quantum Hall effect, Ref. [15], and the effects near an electron density corresponding to a half filled lowest Landau level [16], and gave a new possibility to interpret the experimental results. The evidence for these composite particles, consisting of an electron and several quanta of the magnetic flux, was realised experimentally in the beginning of the 90's by many experiments, among them Ref. [17]. Since then, much attention from both experimentalists and theorists has been devoted to understand the physical properties and even the definition of these composite particles. A part of the success in explaining the experiments and the remaining theoretical questions in the field of composite fermions or the fractional quantum Hall effect in general, have been well summarised in Refs. [18, 19, 20, 10].

1.2 Physical nature of the quantum Hall effects

A quantum Hall system consists of charged particles confined to a two dimensional plane moving in a strong magnetic field perpendicular to the plane. The system can be characterised by the density of the charged particles. The defining property of the quantum Hall effect is that at some magnetic field strength the conductivity tensor strictly takes the form

$$\sigma \;=\; \begin{pmatrix} 0 & -\nu\, e^2/h \\ +\nu\, e^2/h & 0 \end{pmatrix} . \tag{1.1}$$

Here, the diagonal elements are zero and ν is an integer in the integer quantum Hall effect and a rational number in the fractional quantum Hall effect. Normally, the electronic conductivity is always a material dependent quantity and also depends on measurement details including sample size and geometry and the nature of the contacts. But that does not seem to be the case here. The exactness and insensitivity to type and location of impurities [21, 22] suggest that, according to Laughlin [4], the effect might be ultimately due to a fundamental principle. The integer or "normal" quantum Hall effect occurs when the Fermi level lies between two Landau levels of the sample [23]. It is, according to Laughlin's argument [4], due to the *"long–range phase rigidity characteristic of a supercurrent"*, and *"the quantisation can be derived from*

gauge invariance and the existence of a mobility gap". The fractional or "anomalous" quantum Hall effect, on the other hand, occurs only in clean samples with very high mobility, at very low temperature and very high magnetic field. This indicates that the electron–electron interaction plays a central role [23]. Laughlin argued that *"this can be understood as a condensation of electrons moving in two dimensions in a high magnetic field into a quantum liquid which has a finite energy gap above its ground state"* [7, 24]. Laughlin describes in Ref. [7] the ground state as an *incompressible state*. To put this incompressibility of the ground state into context, we quote from the abstract of one of the foundation papers of the field written by B. I. Halperin [23] here:

"*... Recently, however, "anomalous" Hall conductance plateaus have been discovered at certain simple fractions* ν *of the unit* e^2/h*, in a situation where a Landau level is partially filled. Explanation of this effect requires that the electrons form a new type of correlated quantum liquid with a commensurate locking term (i. e., a down–ward cusp) in the energy at the corresponding filling fractions. ...*"

A pedagogical introduction into the physics of the quantum Hall effect can be found in Ref. [25] and references therein.

1.3 Ground state and thermodynamic properties

Most of the effort in theoretical studies of the fractional quantum Hall system so far is devoted to zero temperature properties. There are very few finite temperature studies, e.g., Ref. [26, 27, 28, 29]. Here, we shall mention briefly some works, first for zero temperature and then for the finite temperature regime.

The methods which have been used to study the ground state properties of the fractional quantum Hall system are, most of all, numerical methods, the finite–size numerical exact diagonalisation method and Monte Carlo methods. These numerical methods, especially the finite–size numerical exact diagonalisation method, e.g., Ref. [30, 31, 32], have been very useful in the study of the fractional quantum Hall system. They allow to determine the overlap between the true ground state and Laughlin's trial wavefunction. Prior to the proposal of the Laughlin wavefunction [7], the ground state energy of the Wigner crystal, once a candidate of the true ground state of the fractional quantum Hall system, was calculated and there was no singular feature observed at $\nu = 1/3$ [30, 31]. Thus, from this, one is led to suppose that the true ground state of the fractional quantum Hall system is not a Wigner crystal. Moreover, these methods have been very effective in determining whether the fractional quantum Hall effect should occur at some particular particle densities for some particular electron–electron interactions, e.g., see Ref. [33]. The finite–size numerical exact diagonalisation studies indicate clearly that the effect should occur at $\nu = 1/3$ and $\nu = 1/5$ for realistic interactions. However, one of the most important features which has been demonstrated by the

studies of the ground state is the existence of the energy gap above the ground state. The energy gaps calculated by three methods, finite–size numerical exact diagonalisation [32], the single–mode approximation [34] and Monte Carlo method [35] all yield a value of the same magnitude. Another important study on the ground state energy of a zero–range interaction system was performed by C. Gros and A. H. MacDonald using a numerical method [36]. Together with the energy, the chemical potential has also been examined. The most interesting and most important argument given in Ref. [36] is that for this zero–range interaction *"the fractional quantum Hall effect occurs only when* $\nu = \nu_n = n/(2n+1)$ *(or when* $\nu = 1 - \nu_n$*) and at no other fractional filling factors with odd denominators"*. The discontinuity of the chemical potential at $\nu = \nu_n$ is also demonstrated.

There are a few studies on the effect of the temperature. The earliest work that known to us is by Yu. A. Bychkov [26, 27]. In both references, the method of quantum field theory was used to study the effect of the interaction. One of the main results of these studies is that the properties of the total vertex part of the grand canonical thermodynamic potential are related to the Laughlin wavefunction [27].

The energy at finite temperatures was examined by L. Zheng and A. H. MacDonald [28] using the high–temperature expansion method. They succeed in calculating the high–temperature expansion up to the third order of the interaction. With only three orders of the expansion, they observed no clear development of the ground state.

The thermodynamics of the system including the spin degree of freedom has been studied by T. Chakraborty and P. Pietiläinen in Ref. [37, 38]; their work shows the decrease of the polarisation as the temperature increases.

Other thermodynamic properties such as entropy and heat capacity have been examined in Ref. [39, 29]. In Ref. [39], the combined effects of interaction and disorder on the entropy and specific heat have been studied within the Hartree–Fock approximation for the integer quantum Hall effect density. The results were mapped onto the fractional quantum Hall effect density of the lowest Landau level based on the hierarchy picture of the fractional quantum Hall effect [23, 40, 41]. One important prediction is the change in the behaviour of the specific heat from having a maximum at $\nu = 1/3$ to having a minimum at $\nu = 1/3$ as the temperature is lowered. In Ref. [29], the Virial expansion was used to calculate, analytically up to the second order in the electron density and numerically up to the fifth order, the grand canonical thermodynamic potential of the fractional quantum Hall system with a model interaction for which the Laughlin state at $\nu = 1/m$ is the exact ground state. The interaction was considered in two limits: (i) when the interaction becomes infinity (or an infinite hard core model), (ii) when the interaction is still finite (or a hard core model). For an infinite hard core model for which the calculation can be done analytically and is exact, the grand canonical thermodynamic potential and the chemical potential diverge logarithmically as ν approaches $1/m$. For a special hard core model which yields the ($\nu = 1/3$)–Laughlin

state, the chemical potential is discontinuous at $\nu = 1/3$, the specific heat, which should be zero without the electron–electron interaction, becomes finite for the range $0 < \nu < 1/3$ and the thermodynamic density of states vanishes at zero temperature at $\nu = 1/3$.

1.4 Present status of our understanding

In the following, a list of theoretical concepts which have been established and developed in order to explain the observed phenomena will be given. However, the complete theory is still to come. Thus, some concepts still need a better foundation.

Odd denominators in the lowest Landau level

The Laughlin wavefunction yields a description of the system only at $\nu = 1/(2n + 1), n = 1, 2, \ldots$. However, the experiments show that there are many more fractions for which the fractional quantum Hall effect has also been observed, the most prominent set of fractions is called the principal series in which $\nu_n = n/(2n + 1)$. There are two different approaches proposed to explain the effect at these ν_n for $n \neq 1$. The first approach is the hierarchical picture [23, 40, 41]. In this picture, the quasiparticles above the ground state at $\nu = 1/3$ form again a Laughlin state and thus a new "daughter" state at $\nu = 2/5$ and $\nu = 2/7$ is created. Then, the construction is repeated with $\nu = 2/5$ and $\nu = 2/7$ as starting points. After repeating the process several times, the state at $\nu = 6/13$ is created through $\nu = 1/3 \to 2/5 \to 3/7 \to 4/9 \to 5/11 \to 6/13$, but then many quasiparticles should have been created and may already exceed the number of electrons.

A competing explanation has been proposed by J. Jain [12, 42, 14, 43]. The essential idea is that the fractional quantum Hall effect at $\nu = \nu_n$ is related to the integer quantum Hall effect at $\nu = n$. But there is no obvious explanation for the discontinuity of the chemical potential at a fixed particle density which is essentially required for the fractional quantum Hall effect.

There remains a question on the ground states of the ($\nu = 2/3$) and ($\nu = 2/5$)–fractional quantum Hall states whether they are spin polarised states [44, 45, 37]. Experimental evidence suggests the change of the magnitude of the energy gap above the ($\nu = 2/3$)–fractional quantum Hall ground state in tilted magnetic fields [46, 47]. This change may be interpreted as a signal of the unpolarised ($\nu = 2/3$)–fractional quantum Hall ground state at a moderate magnetic field. A number of numerical studies also suggest that in the absence of the Zeeman energy, the ground state at $\nu = 2/3$ might be unpolarised [44, 45].

Recent experiments by S. Kronmüller et. al. [48, 49] reveal a new strange behaviour of the longitudinal resistivity ρ_{xx} at $\nu = 2/3$ and $\nu = 3/5$. The diagonal resistivity shows sharp and strong maxima in an experiment where the magnetic field is increased

extremely slow at 0.002 Tesla/minute; but the diagonal resistivity finds the usual minimum at these particle densities when the magnetic field is increased with normal speed at 0.7 Tesla/minute. So far, this effect is unexplained.

Even denominators – Compressible states

At and around the particle density corresponding to a half filled lowest Landau level, $\nu = 1/2$, is the area where the studies of composite fermion dominates. The composite fermion picture proposed by J. Jain [12] was generalised in a quantum field description by A. Lopez and E. Fradkin [15]. It has been developed and applied to the problem of the $\nu = 1/2$ in 1993 by B. I. Halperin, P. A. Lee and N. Read [16]. In Ref. [16], the energy and self–energy have been calculated, and most important is the prediction of the Fermi surface which have been observed experimentally later. But it proves to be very hard to get beyond the mean field approximation of RPA–type at these even denominator particle densities. Other even denominators in the lowest Landau level are also getting more attention such as the $\nu = 1/4$ [50, 51, 52].

Even denominators in the higher Landau levels

The studies of even denominator states in the higher Landau levels receive much attention recently, experimentally and theoretically. There are many questions. The oldest one might be the fractional quantum Hall effect at $\nu = 5/2$, first observed in 1988 [53], which until today is still an enigma. The first theoretical studies by F. D. M. Haldane and E. H. Rezayi suggested that the state might be unpolarised and incompressible [54]. The second suggestion by G. Moore and N. Read is that the state is polarised [55]. The numerical study by R. H. Morf supports that the ground state at $\nu = 5/2$ is polarised but incompressible [56] and suggested also a new way to interpret the experimental results. E. H. Rezayi and F. D. M. Haldane then confirmed Morf's results and interpreted the compressible state of a weak zero–range interaction as a striped state [57]. The experiment also do not come easily to an agreement. Eisenstein et. al. in Ref. [58] reported that the state at $\nu = 5/2$ collapsed very rapidly in a tilted magnetic field, thus they argued that the state is not a polarised state. But in the recent experiment [59], the strength of the energy gap above the ($\nu = 5/2$)–FQHS has been examined as a function of the magnetic field. It was found that the energy gap varies smoothly with the magnetic field and this has been interpreted as a strong evidence for a spin-polarised ground state at $\nu = 5/2$. The ($\nu = 7/2$)–FQHS is believed to be similar to the ($\nu = 5/2$)–fqhs. There are a number of experimental reports recently on the anisotropy of the ground states of the half filling of the higher Landau levels such as $\nu = 9/2$ and $\nu = 11/2$ [60]. These experimental observations lead to the studies of the striped state as a candidate for the observed anisotropic states [61, 62].

Chapter 2

Motivation

In two decades since the discovery of the fractional quantum Hall effect, many studies have been done – many questioned have been answered. Most of the time, however, the focus of the experimental studies was on the transport properties, and the focus of the theoretical studies was on the ground state properties. Not so many studies dealt with the thermodynamic, or finite temperature properties. It is the energy spectrum of the fractional quantum Hall system that is responsible for the unusual behaviour in the transport properties, and the incompressible ground state of the fractional quantum Hall system is the theoretical explanation of the fractional quantum Hall effect phenomena. This energy spectrum should also be visible and can be studied through the thermodynamic properties as well.

In this work, we should like to investigate the thermodynamic properties, in particular, the energy and the compressibility, of the fractional quantum Hall system at finite temperature. The motivation of this work comprises both conceptual and technical aspects as they will be explained in the following.

It is generally assumed that the electron–electron interaction plays a central role in the fractional quantum Hall effect [23] and is responsible for the unusual, transport and thermodynamic, behaviours of the fractional quantum Hall systems. These unusual behaviours occur at particular values of the electron densities n_{el}. Thus, the assumption of the existence of a link between the interaction and the corresponding selected densities is justified. However, the most successful approach to an explanation of the fractional quantum Hall effect, the Laughlin wavefunction [7], does not illustrate this link properly. This is perhaps due to the unusual character of the wavefunction itself. The Laughlin wavefunction can be defined for a set of densities of the form $n_{el} \sim 1/m$ where m is an odd integer. There is no free parameter at a fixed density. Furthermore, this wavefunction contains no interaction dependent term. Because the electron density is restricted, studies of any property as a smooth function of the density become impossible. The generalisation in the sense of the hierarchical theory [40] does not improve the situation, since neighbouring densities may belong to a different order of the hierarchy. Moreover, in order to obtain the energy as a continuous function

of n_{el}, one needs to go through the infinite order of the hierarchy.

But in the experiments, the fractional quantum Hall states appear as the density (or the magnetic field, correspondingly) is continuously varied. Therefore, I propose another way to approach the problem of the fractional quantum Hall state: Instead of starting with the ground state, we shall *start from the high temperature limit* where there are no preferred states in the thermodynamic ensemble, and *approach the ground state from above*. The advantage of this is that in the high temperature limit, there are no preferred states in the statistical ensemble, thus there is no need to assume a preferred state. Then, we can lower the temperature until we reach a temperature limit given by the order of the expansion. (The higher the order we obtain in the expansion, the lower the temperature we can reach.) While the temperature is being lowered, one can study developments of the thermodynamic properties including how the fractional quantum Hall system develops or approaches its ground state. It is also possible that one may be able to observe indications of the unusual behaviours of the fractional quantum Hall system when the temperature is low enough. And by analysing the energy as a function of the density and the temperature, one may be able to prove the existence of the energy gap above the ground state at a particular density which is required for the incompressibility of the ground state [7, 23] *without any prior assumption*. This way of approaching the ground state is possible because this is a two dimensional system where no second order phase transition is expected to interfere at finite temperatures.

These are the advantages of coming from high temperatures: The density is a variable, thus we can study any thermodynamic property as a function of the density. The interaction will be used explicitly in the calculation and appears in the result as a parameter. Thus, its influence can be studied easily and systematically. Other technical advantages of this new approach are as follows: The interaction divided by the temperature provides a small parameter for systematic expansions. Such a small parameter is desired but absent in the zero temperature studies, where it is, hence, impossible to apply perturbative methods. As opposed to the exact diagonalisation studies of finite system, here the thermodynamic limit is trivial.

Part II

Model

Chapter 3

Model

3.1 Introduction

There is a general agreement that in a quantum Hall system at special magnetic fields, the electron–electron interaction is responsible for the unusual properties of the ground state and for the gap between the ground state and the excited states, and that this gap leads to the *fractional quantum Hall effect*. Thus, we consider in this work interacting electrons moving in two dimensions in a strong magnetic field. Before we set up the description of the interacting many body system, we first review briefly the non–interacting system. This is elementary but necessary since the quantum Hall regime is defined by the Landau quantisation of the kinetic energy. We then consider two interacting particles in order to parameterise the electron–electron interaction. Finally, we shall calculate the interaction matrix element for the many–body system.

3.2 Noninteracting system

The Hamiltonian for an electron of charge $e < 0$ and mass m moving in two dimensions in a perpendicular magnetic field B is given by

$$H_{(0)} \;=\; \frac{1}{2m}\,\left(\vec{p} - \frac{e}{c}\vec{A}\right)^2 \;. \tag{3.1}$$

The operator $\vec{\pi} = \vec{p} - \frac{e}{c}\vec{A}$ is the kinetic momentum operator of a charged particle in a magnetic field (c is the velocity of light). The magnetic field is oriented in $\hat{z}$–direction, $\vec{B} = \nabla \times \vec{A} = B\ \hat{z}, B > 0$, and supposed to be uniform, so that $\vec{A}$ is linear in the coordinates $\vec{x} = (x, y)$. Thus, $H_{(0)}$ is a general two–dimensional harmonic oscillator Hamiltonian, quadratic in space ($\vec{x}$) and in momentum ($\vec{p}$). The eigenstates and eigenenergies can be obtained by an algebraic method, similar to the one used in solving the one–dimensional harmonic oscillator [63]. We start from observing that the

two components of the kinetic momentum are canonically conjugate

$$[\pi_x, \pi_y] \;=\; \frac{i\hbar e}{c}\;\hat{z}\cdot(\nabla\times\vec{A}) \;=\; -\frac{i\hbar^2}{{l_B}^2}\,. \tag{3.2}$$

The magnetic length, ${l_B}^2 = \hbar c/|eB|$, sets the length scale in the presence of a strong magnetic field. The magnetic flux quantum $\phi_0 = 2\pi\ \hbar\ c/|e|$ is related to the magnetic length by $\phi_0 = 2\ \pi\ {l_B}^2\ B$. We define now a first set of ladder operators as follows:

$$b^\dagger \equiv \frac{i\ l_B/\hbar}{\sqrt{2}}\ \ (\pi_x + i\ \pi_y)\ , \qquad\qquad b \equiv \frac{-i\ l_B/\hbar}{\sqrt{2}}\ \ (\pi_x - i\ \pi_y)\ , \tag{3.3}$$

with the commutation relation $[b, b^\dagger] = 1$. Then, the Hamiltonian $H_{(0)}$ can be expressed as

$$H_{(0)} \;=\; \frac{\hbar\ \omega_c}{2}\ (b\ b^\dagger + b^\dagger b)\ , \tag{3.4}$$

where $\omega_c = |eB|/(mc)$ is the cyclotron frequency. Thus, the eigenenergies in the Schrödinger equation become $\hbar\omega_c(n+1/2)$, where $n = 0, 1, 2, \ldots$ is an integer quantum number. Since we have used only two operators out of four in expressing $H_{(0)}$, we can expect these eigenenergies to be degenerate. We define the magnetic translation operator as

$$\vec{\mathcal{T}} \;=\; \vec{\pi} - \frac{\hbar}{{l_B}^2}\ \hat{z}\times\vec{x} \tag{3.5}$$

where $\hat{z}\times\vec{x} = (-y, x)$. The two components of the magnetic translation operator are canonically conjugate:

$$[\mathcal{T}_x, \mathcal{T}_y] = i\hbar^2/{l_B}^2\ , \tag{3.6}$$

and $\vec{\mathcal{T}}$ commutes with $\vec{\pi}$ and hence with the Hamiltonian $[\vec{\mathcal{T}}, H_{(0)}] = 0$.

The second set of ladder operators is then defined by $\vec{\mathcal{T}}$ as follows:

$$a^\dagger \equiv \frac{-i\ l_B/\hbar}{\sqrt{2}}\ \ (\mathcal{T}_x - i\mathcal{T}_y)\ , \qquad\qquad a \equiv \frac{i\ l_B/\hbar}{\sqrt{2}}\ \ (\mathcal{T}_x + i\mathcal{T}_y) \tag{3.7}$$

and the corresponding commutation relations for these ladder operators and with the ladder operators $b,\ b^\dagger$ defined above are $[a, a^\dagger] = 1$ and $[a, b] = [a^\dagger, b] = 0$.

The set of all eigenstates with given kinetic energy is called a Landau level. Here and from now on, the states with "$n = 0$" will be addressed as the "lowest Landau level" and the states with "$n = 1$" will be addressed as the "first Landau level".

Due to the degeneracy of the Landau levels, we have various ways of forming a basis in which $H_{(0)}$ is diagonal.

3.2.1 Symmetric gauge, $\vec{A} = \frac{B}{2}(-y, x, 0)$

In case of this, the symmetric gauge, the Hamiltonian is rotational invariant. Therefore, it commutes with the angular momentum operator $L_z \equiv xp_y - yp_x$:

$$L_z \;=\; -\hbar\ (a^\dagger\ a - b^\dagger\ b)\ , \tag{3.8}$$

and the eigenvalues of this label the degenerate state of the Landau levels. We choose the eigenfunction of $H_{(0)}$ and L_z as our basis. Then, the eigenvalue equations for the Hamiltonian and the angular momentum read

$$H_{(0)} \mid n,m> = \hbar\,\omega_c\,(n+\frac{1}{2}) \mid n,m> \tag{3.9}$$

and

$$L_z \mid n,m> = -\hbar\,(m-n) \mid n,m> \tag{3.10}$$

where $n = 0,1,2,\ldots$ and $m = 0,1,2,\ldots$. All eigenstates can be generated by applying the raising operators $a^\dagger$ and $b^\dagger$ to the ground state $|0,0>$,

$$<\vec{x} \mid n,m> = \frac{1}{\sqrt{n!m!}}\;(b^\dagger)^n\,(a^\dagger)^m\;<\vec{x} \mid 0,0>\,, \tag{3.11}$$

where the ground state is defined by $a \mid 0,0>= b \mid 0,0>= 0$.

The ladder operators, written in the coordinate representation, are (we use $z = x - iy$)

$$a^\dagger = -\sqrt{2}\,l_B\left(\frac{\partial}{\partial z^*} - \frac{1}{4{l_B}^2}\,z\right) \tag{3.12}$$

$$b^\dagger = \sqrt{2}\,l_B\left(\frac{\partial}{\partial z} - \frac{1}{4{l_B}^2}\,z^*\right)\,. \tag{3.13}$$

Then, the normalised ground state wave function is

$$<\vec{x} \mid 0,0> = \frac{1}{\sqrt{2\pi{l_B}^2}}\,e^{-\frac{1}{4{l_B}^2}\,|z|^2}\,, \tag{3.14}$$

From Eq. (3.14) and Eq. (3.12), we note that the wave functions for states in the lowest Landau level in the symmetric gauge with angular momentum m are

$$<\vec{x} \mid 0,m> = \frac{1}{\sqrt{2\pi{l_B}^2}}\,\frac{z^m}{\sqrt{2^m m!{l_B}^{2m}}}\,e^{-\frac{1}{4{l_B}^2}\,|z|^2}\,. \tag{3.15}$$

The complex coordinates can be expressed in terms of ladder operators as

$$\begin{aligned} z &= \sqrt{2}\,l_B\,(\,a^\dagger - b\,)\,, \\ z^* &= \sqrt{2}\,l_B\,(\,a - b^\dagger\,) \end{aligned} \tag{3.16}$$

and hence it follows that

$$\pi\;<n,m \mid z^*\,z \mid n,m> = 2\,\pi\,{l_B}^2\,(n+m+1)\,. \tag{3.17}$$

For large m, these orbitals are strongly localised within a ring of radius $l_B\,\sqrt{2\,(n+m+1)}$ and thickness $\sim l_B/\sqrt{2m}$.

3.2.2 Landau gauge, $\vec{A} = B(0, x, 0)$

In this gauge, the charged particle moves freely along the y–direction. Therefore, the use of eigenfunctions of $H_{(0)}$ and of the translation in y–direction, $\mathcal{T}_y = p_y$, as the basis becomes appropriate. The eigenvalue equations for the Hamiltonian and the magnetic translation operator read

$$H_{(0)} \mid n, k > = \hbar\, \omega_c\, (n + \frac{1}{2}) \mid n, k > \tag{3.18}$$

and

$$\mathcal{T}_y \mid n, k > = \hbar\, k \mid n, k > \ . \tag{3.19}$$

The corresponding wave functions are

$$< \vec{x} \mid n, k > = \varphi_{n,k}(x, y) \ = \ (2^n\, n!\, \sqrt{\pi}\, l_B\, L_y)^{-\frac{1}{2}}\ e^{iky}\, \chi_n \left(x + k{l_B}^2\right) \tag{3.20}$$

where

$$\chi_n(x) \ = \ e^{-\frac{x^2}{2{l_B}^2}}\ H_n\left(\frac{x}{l_B}\right) \tag{3.21}$$

in which $H_n(x)$ is the Hermite polynomial of order n and $n = 0, 1, 2, \ldots$. The momentum eigenvalues k are discrete $k = 2\pi n_y / L_y$ where $n_y = 0, \pm 1, \pm 2, \ldots$ and L_y is the length of the system in y–direction. For further reference, we quote the single particle wave functions in the lowest Landau level in the Landau gauge :

$$< \vec{x} \mid 0, k > = \varphi_{0,k}(x, y) \ = \ \frac{1}{\sqrt{L_y\, l_B}}\ \frac{1}{\pi^{1/4}}\ e^{iky - \frac{1}{2{l_B}^2}\,(x + k{l_B}^2)^2} \ . \tag{3.22}$$

Finally, the expectation value $< x >_{n,k}$ follows from Eq. (3.20):

$$\begin{aligned} < x >_{n,k} \ &= \ \int d^2x\ \varphi^*_{n,k}(x, y)\ x\ \varphi_{n,k}(x, y) \\ &= \ \int dx' \int dy\ \varphi^*_{n,k}(x' - k{l_B}^2, y)\ \left[x' - k{l_B}^2\right]\ \varphi_{n,k}(x' - k{l_B}^2, y) \\ &= \ -k{l_B}^2 \ . \end{aligned} \tag{3.23}$$

$< x >_{n,k}$ is independent of n. In a finite system, $< x >_{n,k}$ should be limited by the confinement, i. e., $x_{min} \leq -k{l_B}^2 \leq x_{max}$, where $x_{max} - x_{min} = L_x$ defines the length of the system in x–direction. We get for $x_{min} = -x_{max}$

$$0 \leq |n_y| \ \leq \ \frac{1}{2}\ \frac{L_x\, L_y}{2\, \pi\, {l_B}^2} \ . \tag{3.24}$$

Thus, the number of single particle states is equal to $L_x L_y / (2\pi {l_B}^2) = L_x L_y |B| / \phi_0 = N_\phi$, the number of flux quanta through the system. This consideration is valid for any Landau level.

3.3 Interacting two–particle system

In this section, we shall discuss two interacting particles in the lowest Landau level. We derive the eigenstates and eigenenergies of such a system. The eigenenergies play an important role in this work as they characterise the interaction.

The Hamiltonian of the interacting two–body system is

$$H_{(2)} = \frac{1}{2m}\left(\vec{p}_1 - \frac{e}{c}\vec{A}_1\right)^2 + \frac{1}{2m}\left(\vec{p}_2 - \frac{e}{c}\vec{A}_2\right)^2 + W(|\vec{x}_1 - \vec{x}_2|)\ . \tag{3.25}$$

To solve the interacting two–body problem, it is useful to separate $H_{(2)}$ by transforming from the representation of individual coordinates $\vec{r}_1$ and $\vec{r}_2$ to the representation of centre–of–mass and relative coordinates. We use capital letters for quantities associated with the centre–of–mass degree of freedom and small letters for quantities associated with the relative degree of freedom.

$$(\vec{R},\ \vec{r}) = \left(\frac{\vec{x}_1 + \vec{x}_2}{2},\ \ \vec{x}_1 - \vec{x}_2\right)\ , \tag{3.26}$$

$$(\vec{P},\ \vec{p}) = \left(\vec{p}_1 + \vec{p}_2,\ \ \frac{\vec{p}_1 - \vec{p}_2}{2}\right)\ . \tag{3.27}$$

The centre–of–mass motion is that of a particle in a magnetic field B with mass $2m$ and charge $2e$. Thus, a magnetic length $l_{B,R}^2 = \frac{1}{2}{l_B}^2$ and a cyclotron frequency $\omega_{c,R} = \omega_c$ can be defined. The relative motion is that of a particle in a magnetic field B and a potential $W(r)$ with mass $m/2$ and charge $e/2$. Thus, a magnetic length $l_{B,r}^2 = 2{l_B}^2$ and a cyclotron frequency $\omega_{c,r} = \omega_c$ can be defined. In the new representation, the ladder operators are defined as

$$b_{R,r}^\dagger = \frac{1}{\sqrt{2}}\left(b_1^\dagger \pm b_2^\dagger\right)\ , \tag{3.28}$$

$$a_{R,r}^\dagger = \frac{1}{\sqrt{2}}\left(a_1^\dagger \pm a_2^\dagger\right)\ . \tag{3.29}$$

Their commutation relations are $[b_r,\ b_r^\dagger] = [b_R,\ b_R^\dagger] = [a_r,\ a_r^\dagger] = [a_R,\ a_R^\dagger] = 1$ and all the other commutators are zero. In the following, we consider the projection of $H_{(2)}$ in the lowest Landau level. The lowest Landau level of the individual particles is also the lowest Landau level of the transformed centre–of–mass and relative particles; i. e., if $b_1|0>=b_2|0>=0$, then, $b_R|0>=b_r|0>=0$. The two–body eigenstates in the lowest Landau level with angular momenta M of the centre–of–mass motion and m of the relative motion factorise, because of the Gaussian form of the exponent, cf. Eq. (3.14): $\mid n_1 = n_2 = 0, M\ m> = \mid M> \mid m>$,

$$<\vec{R} \mid M><\vec{r} \mid m> = \frac{\left(a_R^\dagger\right)^M}{\sqrt{M!}}\ \frac{\left(a_r^\dagger\right)^m}{\sqrt{m!}}\ <\vec{R} \mid 0><\vec{r} \mid 0>\ . \tag{3.30}$$

It is clear that a_r involves only the coordinate $\vec{r}$, and the corresponding momentum, and we can use the result obtained from the non–interacting problem for the centre–of–mass problem with replacement of the magnetic length as mentioned.

In the absence of an interaction, each eigenstate would have an eigenenergy $\hbar\,\omega_c$ and there will be $\binom{N_\phi}{2} = \frac{N_\phi\,(N_\phi-1)}{2}$ states in an area occupied by N_ϕ flux quanta. The interaction in the Hamiltonian then lifts the degeneracy of the two–body eigenstates. The projection of the Hamiltonian Eq. (3.25) onto the lowest Landau level is diagonal in the representation Eq. (3.30) due to the rotational invariance of the interaction $W(r)$ and can be written as

$$H^{(0)}_{(2)} \;=\; \hbar\,\omega_c \sum_{M,m} |M\;m\rangle\;\langle M\;m| + \sum_{M,m} |M\;m\rangle\;W_m\;\langle M\;m| \tag{3.31}$$

where the eigenenergies W_m are

$$W_m \;=\; \langle m \mid W(|\vec{r}|) \mid m\rangle \;=\; \frac{1}{m!}\int_0^\infty dr \left(\frac{r}{2}\right)^{2m+1} W(r)\;e^{-\frac{1}{4}\,r^2}\;. \tag{3.32}$$

From here and now on, we shall work in the thermodynamic limit and use the dimensionless units for which $\hbar = 1$ and ${l_B}^2 = 1$.

3.4 Interacting many–body system

Now, we consider N particles in a Landau level and we define a new variable, the filling factor ν. The "filling factor" is the ratio of the number of particles to the number of single particle states in a given Landau level. Since the number of single particle states is equal to N_ϕ, the number of the flux quanta through the system, see Eq. (3.24),

$$\nu \equiv \frac{N}{N_\phi}\;. \tag{3.33}$$

The filling factor is related to the electron density n_{el} by $\nu = 2\pi {l_B}^2 n_{el}$. ν is the all–important variable in a quantum Hall system. It determines the state of the system which can be quite different as a quantum Hall state at, e. g., $\nu = 1/3$, or a metallic at $\nu = 1/2$, or a Wigner crystal for $\nu < 1/7$ [64].

In this work, we study a regime in which the temperature may be large compared to the interaction characterised by the W_m, but is still much lower than the cyclotron energy. Thus, $n-1$ Landau levels are completely filled and the last, n^{th} Landau level is partially occupied. Then, the projection of the Hamiltonian onto the n^{th} Landau level gives (we measure the energy from the energy of the n^{th} Landau level)

$$H \;=\; \frac{1}{2}\sum_{k_1,k_2,k_3,k_4} W^{(n)}_{k_1k_2k_3k_4}\;c^\dagger_{k_1}c^\dagger_{k_2}c_{k_3}c_{k_4}\;. \tag{3.34}$$

Here, $c_k^\dagger$ and c_k is the creation and annihilation operator, respectively, of a single particle state in the Landau gauge (see Eq. (3.20)). The linear momentum k takes the values $k = 2\pi n_y/L_y$ where $|n_y| = 0, 1, 2, \ldots, (N_\phi - 1)/2$. The interaction matrix element of the effective electron–electron interaction, $W^{(n)}_{k_1k_2k_3k_4}$ can be parameterised by the eigenvalues, W_m, of the two particle Hamiltonian as will be shown below.

The interaction matrix element $W^{(n)}_{k_1k_2k_3k_4}$ for a translational and rotational invariant interaction $W(|\vec{x} - \vec{x}'|)$ between two particles at positions $\vec{x}$ and $\vec{x}'$ is given by

$$\begin{aligned} W^{(n)}_{k_1k_2k_3k_4} &= \int_{-\infty}^{\infty} dx \int_0^{L_y} dy \int_{-\infty}^{\infty} dx' \int_0^{L_y} dy' \\ &\varphi^*_{n,k_1}(x,y)\, \varphi^*_{n,k_2}(x',y')\, W(|\vec{x} - \vec{x}'|)\, \varphi_{n,k_3}(x',y')\, \varphi_{n,k_4}(x,y)\ . \end{aligned} \tag{3.35}$$

In the following, we shall derive the effective electron–electron interaction matrix element of the system we study for the case $n = 0$ and $n = 1$. Here and from now on, the expressions belong to the lowest Landau level, if the upper indices are not indicated explicitly.

3.4.1 Interaction matrix element in the lowest Landau level

We convert the integrand of Eq. (3.35) to relative and centre–of–mass coordinates as in the two–particle calculation. Performing the integrals over the centre–of–mass coordinate yields

$$\begin{aligned} W_{k_1k_2k_3k_4} &= \tfrac{1}{L_y} \left(\tfrac{1}{2\pi}\right)^{1/2} \delta_{k_1+k_2,k_3+k_4}\ e^{-\frac{1}{4}\left[\, q^2+p^2 \,\right]} \\ &\int d^2r\ e^{-\frac{1}{2}\, x^2 - \frac{i}{2}\,(q-p)\, y - \frac{1}{2}\,(q+p)\, x}\ W(|\vec{r}|) \end{aligned} \tag{3.36}$$

where we use the abbreviations $q = k_1 - k_2$ and $p = k_4 - k_3$. Next, we symmetrise the integrand by inserting unity, in the form of two Gaussian integrals, into the expression:

$$\begin{aligned} W_{k_1k_2k_3k_4} &= \tfrac{1}{L_y} \left(\tfrac{1}{2\pi}\right)^{1/2} \delta_{k_1+k_2,k_3+k_4}\ e^{-\frac{1}{4}\left[\, q^2+p^2 \,\right]} \\ &\tfrac{1}{4\pi} \int d^2r \int_{-\infty}^{\infty} du \int_{-\infty}^{\infty} dv\ \ e^{-\frac{1}{4}\left[(u+ix)^2+(v-y)^2\right]}\ e^{-\frac{1}{2}\, x^2}\ e^{-\frac{i}{2}\,(q-p)\, y - \frac{1}{2}\,(q+p)\, x}\ W(|\vec{r}|)\ . \end{aligned} \tag{3.37}$$

Now, we can perform the angular part of the spatial integral. That will bring the expression into a form for which the radial integral of $W(r)$ is similar to that in Eq. (3.32).

Then, we express the radial integral by W_m and find

$$W_{k_1k_2k_3k_4} = \frac{1}{L_y}\left(\frac{1}{2\,\pi}\right)^{1/2} \delta_{k_1+k_2\,,\,k_3+k_4}\;\; e^{-\frac{1}{4}\,[\,q^2+p^2\,]} \sum_{m=0}^{\infty} \frac{W_m}{m!} \int_{-\infty}^{\infty} du \int_{-\infty}^{\infty} dv \left[\frac{(q+p+iu)^2-(q-p+iv)^2}{4}\right]^m e^{-\frac{1}{4}\,(u^2+v^2)}\,. \tag{3.38}$$

These coefficients W_m, the eigenvalues of the two–body system, are known as the Haldane pseudopotential coefficients [33]. Only the *odd part* of $W_{k_1k_2k_3k_4}$ under exchange of k_1 and k_2 (or k_3 and k_4) enters the Hamiltonian, H, in Eq. (3.34). This exchange corresponds to the change of q from $q \rightarrow -q$ (or $p \rightarrow -p$). Only *odd* m yield this fermion–symmetry. Therefore, only *odd eigenvalues* W_{2m+1} yield the required antisymmetric behaviour $W_{k_1k_2k_3k_4} = -W_{k_2k_1k_3k_4} = -W_{k_1k_2k_4k_3}$. *In this work, we restrict the interaction matrix elements* $W_{k_1k_2k_3k_4}$ *to its odd part.* This can be done by subtracting the part of $W(r)$ which corresponds to the even part of the interaction matrix elements, as it is shown in the work of Yu. A. Bychkov [27, 65]. For the sake of clarity, the resulting interaction in real space (which results only in odd interaction matrix elements) will be denoted by $W^F(r)$.

We can classify the two–body interactions into three types according to their (effective) ranges. The first is the infinite–range interaction; the Coulomb interaction ($\sim 1/r$) is an example. For this interaction, $W_m = \sqrt{\frac{\pi}{4}}\;(2m-1)!!/(2^m\;m!)$ falls off very slowly as $\sim 1/(2\sqrt{m})$. For a consideration of the Coulomb interaction, we would need to include a positively charged background. Thus, the method of this study would have to be generalised to become applicable to this type of interaction.

The second type can be called a finite–range interaction; a screened Coulomb interaction ($\sim \exp(-\beta r)/r$) or a Gaussian interaction ($\sim \exp(-\alpha r^2)$) are examples. W_m for this type of interactions decay exponentially, for $W(r) = \exp(-\alpha r^2)$, one get $W_m = 1/(1+4\;\alpha)^{m+1}$.

The third type is the zero–range interaction which will be the main interaction in this study. In this case, W_m contains only s small number of non–zero elements $W_m = W_1\;\delta_{1,m} + W_3\;\delta_{3,m} + \ldots$. In real space, this can be written as (cf. [66, 67, 68]),

$$W(|\vec{r}|) = 4\pi W_1\;(1+\Delta)\;\delta(\vec{r}) + 4\pi W_3\;\left(1+3\;\Delta+\tfrac{3}{2}\;\Delta^2+\tfrac{1}{6}\;\Delta^3\right)\delta(\vec{r}) + \ldots\,. \tag{3.39}$$

The corresponding interaction matrix element can be best derived from Eq. (3.38) with the result

$$W_{k_1k_2k_3k_4} = \frac{2\pi}{L_y}\left(\frac{2}{\pi}\right)^{1/2} \delta_{k_1+k_2,k_3+k_4}\;(k_1-k_2)(k_4-k_3)\;e^{-\frac{1}{4}\left[(k_1-k_2)^2+(k_4-k_3)^2\right]} \left[W_1 + \frac{1}{6}\;W_3\;\left((k_1-k_2)^2-3\right)\;\left((k_4-k_3)^2-3\right)+\ldots\right]\,. \tag{3.40}$$

In the future, we shall refer to an interaction as a one–component interaction if its interaction matrix elements contain only a single pseudopotential coefficient. On the other hand, an interaction in which its interaction matrix elements contain more than one pseudopotential coefficient will be referred to as a multi–component interaction. We shall call a one–component interaction which yields non–zero W_m a W_m–interaction and a multi–component interaction which yields non–zero $W_i, W_j, \cdots$ a $(W_i+W_j+\cdots)$–interaction.

Differential form of $W_{k_1k_2k_3k_4}$

The interaction matrix elements, which have been derived in the previous section, will be used very extensively in the next steps, in Chapter 4 and Chapter 5, for the evaluation of the coefficients of the high–temperature expansion. The form of the interaction matrix elements as shown in Eq. (3.38) or Eq. (3.40) looks quite complicated and leads to many difficulties when used to evaluate the final result. To reduce the effort in the calculation, we shall write the interaction matrix elements in a new form, the differential form.

Starting out with the expression of the interaction matrix elements given in Eq. (3.38), we see that the integrand of the u, v integrals can be written differently:

$$\begin{aligned}
&\int_{-\infty}^{\infty} du \int_{-\infty}^{\infty} dv \left[\frac{(q+p+iu)^2-(q-p+iv)^2}{4}\right]^{2m+1} e^{-\frac{1}{4}(u^2+v^2)} \\
&= \int_{-\infty}^{\infty} du \int_{-\infty}^{\infty} dv\, \partial_\alpha^{2m+1}\, e^{\alpha\,[p+i(u-v)/2]}\, \partial_\beta^{2m+1}\, e^{\beta\,[q+i(u+v)/2]}\, e^{-\frac{1}{4}(u^2+v^2)} \Big|_{\alpha=\beta=0} \\
&= 4\,\pi\, \partial_\alpha^{2m+1}\, \partial_\beta^{2m+1}\, e^{\alpha\,p+\beta\,q}\, e^{-\frac{1}{2}(\alpha^2+\beta^2)} \Big|_{\alpha=\beta=0}\,, \qquad (3.41)
\end{aligned}$$

where α and β are auxiliary variables.

Replacing the u, v integrals in Eq. (3.38) yields the following compact form of the interaction matrix element (only odd relative angular momenta m are taken into account)

$$\begin{aligned}
W_{k_1k_2k_3k_4} &= \frac{2\pi}{L_y}\left(\frac{2}{\pi}\right)^{1/2} \delta_{k_1+k_2,k_3+k_4}\, e^{-\frac{1}{4}\left[\,(k_1-k_2)^2+(k_4-k_3)^2\,\right]} \\
&\quad \sum_{m=0}^{\infty} \frac{W_{2m+1}}{(2m+1)!}\, \partial_\alpha^{2m+1}\, \partial_\beta^{2m+1}\, e^{\beta\,(k_1-k_2)+\alpha\,(k_4-k_3)}\, e^{-\frac{1}{2}(\alpha^2+\beta^2)} \Big|_{\alpha=\beta=0} \qquad (3.42)
\end{aligned}$$

This representation of the interaction matrix elements shall be the basis for our explicit evaluation of the momentum sums in Chapter 4 and Chapter 5. This form of the interaction matrix elements proves to be much easier to use in practical calculation than Eq. (3.40).

3.4.2 Interaction matrix element in the first Landau level

The interaction matrix elements in the first Landau level can be calculated directly, in the same manner as the interaction matrix elements in the lowest Landau level. The full derivation is given in Appendix A, Also, there is another method. Due to the equivalence of the Hilbert spaces of the Landau levels, we can map the Hamiltonian of the system in a given Landau level to the lowest Landau level. Vice versa, one can lift a Landau level just by applying the operator $b_j^\dagger$ for each particle j to the states [69]. Generally, the relation between the pseudopotential coefficients in the lowest Landau level and the pseudopotential coefficients in the first Landau level, Eq. (A.15), is

$$\begin{aligned} W_m^{(1)} &= \frac{1}{4}m(m-1)W_{m-2}^{(0)} - m(m-1)W_{m-1}^{(0)} + \frac{1}{2}\left(3m^2-m+1\right)W_m^{(0)} \\ &\quad -m(m+1)W_{m+1}^{(0)} + \frac{1}{4}(m+1)(m+2)W_{m+2}^{(0)} \,. \end{aligned} \tag{3.43}$$

The first three pseudopotential coefficients in the first Landau level are explicitly:

$$W_1^{(1)} = \frac{3}{2}\,W_1 + \frac{3}{2}\,W_3 \,, \tag{3.44}$$

$$W_3^{(1)} = \frac{3}{2}\,W_1 + \frac{25}{2}W_3 + 5\,W_5 \,, \tag{3.45}$$

$$W_5^{(1)} = 5\,W_3 + \frac{71}{2}\,W_5 + \frac{21}{2}\,W_7 \,. \tag{3.46}$$

We want to emphasise here that the zero–range interaction $W^F(\vec{r}) = 4\pi W_1\,(1+\Delta)\delta(\vec{r})$, which yields $W_m^{(0)} = W_1\,\delta_{m,1}$ in the lowest Landau level[1], leads to two components, $W_1^{(1)}$ and $W_3^{(1)}$, in the first Landau level. Thus, the study of the interaction $W_1 + W_3$ in the lowest Landau level would be equivalent to the study of the one–component interaction (where only $W_1^{(1)}$ is non zero) in the first Landau level.

Generally, one can study the effect of a general zero–range interaction in the first Landau level of the quantum Hall system by studying the corresponding interaction in the lowest Landau level. But, we should not expect that a given interaction $W(r)$ may yield the same effects in different Landau levels. Thus, the characteristic behaviour of the system in the lowest Landau level at the filling factor ν_c due to a specific zero–range interaction may not be visible at the filling factor $1+\nu_c$ when one studies the same interaction in the first Landau level.

[1] $W_m^{(n)}$ denotes the Haldane pseudopotential coefficient in the n^{th} Landau level if m is an integer number, otherwise it denotes a pattern, see below.

Part III

Method

In this part, we shall develop the high–temperature expansion method for the problem of the fractional quantum Hall effect.

In Chapter 4, we give the first part of the calculations which is valid for a general interaction. We start by forming the high–temperature expansion for the grand canonical thermodynamic potential. We then analyse the expectation values of the Hamiltonian to the n^{th} power $< H^n >$, and finally transform from the grand canonical ensemble to the canonical ensemble. The result of this calculation is the high–temperature expansion series of the energy in which each coefficient is written as a function of the filling factor of the form $\nu^{2n-p}\,(1-\nu)^p$ multiplied with momentum sums involving the interaction which we call *patterns*. Next, we discuss how to evaluate the patterns for an arbitrary interaction. We shall see in this consideration that the calculation for the infinite–range interaction cannot be carried out without a neutralising background due to a divergency in the first terms of the expansion series. We finally show the equivalence of the present high–temperature expansion method with the traditional perturbative treatment up to the third order in the interaction.

In Chapter 5, we specialise the calculations to the case of the zero–range interactions by evaluating the patterns for a general zero–range interaction. We also show that the results obtained from the high–temperature expansion method coincide in the lowest order of the density with the results obtained from the first order of the Virial expansion.

Chapter 4

High–temperature expansion for general interaction

In this chapter, we shall develop the high–temperature expansion method for the quantum Hall system. The results obtained here are valid for a general interaction. We shall study the grand canonical thermodynamic potential $\Omega(T, N_\phi, \mu)$. We express $\Omega(T, N_\phi, \mu)$ as a power series in the inverse temperature $\beta = 1/T$. Here, N_ϕ, the number of flux quanta through the system stands for the volume, $N_\phi = L_x L_y/(2\pi {l_B}^2)$. The high–temperature expansion coefficients $\Omega_n(N_\phi, \mu)$ are the cumulant averages of the Hamiltonian H. These are calculated with a diagrammatic method. From the high–temperature expansion series for $\Omega(T, N_\phi, \mu)$, we derive the energy $E(T, N_\phi, \mu)$ and the particle number $N(T, N_\phi, \mu)$ up to a given order in the inverse temperature β. Having the particle number expressed as a function of the chemical potential, μ, we reverse the relation and find μ, i. e., the fugacity, $z = e^{\beta\mu}$ or the Fermi factor, $f = z/(1+z)$, as functions of N. Substituting μ, or z, or f by the density, or equivalently by the filling factor $\nu = N/N_\phi$, in the energy $E(T, N_\phi, \mu)$, we find the energy $E(T, N_\phi, \nu)$ up to the given order in β where the coefficients are given in terms of diagrams. The result then is the energy as a function of temperature and filling factor, the main result of this chapter. In the last part of the chapter, we shall show how to evaluate in principle the coefficients obtained in the previous section for an arbitrary interaction. Also, we shall demonstrate the equivalence of the present high–temperature expansion method with the traditional perturbative theory [28].

4.1 The high–temperature expansion series for the grand canonical thermodynamic potential

We start by expanding the grand canonical thermodynamic potential

$$\Omega(T, N_\phi, \mu) \equiv -T \ln \left\{ \mathrm{Tr} \left[e^{-\beta(H-\mu N)} \right] \right\} \tag{4.1}$$

with respect to the interaction Hamiltonian H (cf. Eq. (3.34)) above). The temperature is measured in units of energy, i. e., $k_B = 1,\ \beta = 1/T$.

Since here, there is no kinetic energy, the unperturbed part of the grand canonical Hamiltonian is μN and commutes with the interaction H. Thus, use of the interaction representation in a perturbative treatment is unnecessary. Therefore, a diagrammatic expansion can be performed without calculation of frequency sums. In this respect, the high–temperature expansion, here, is more similar to a high–temperature expansion in spin systems [70]. However, there is an important difference. In spin systems, a diagrammatic perturbation theory is performed in real space where the interaction is short–range, while in this work, long–range momentum sums need to be calculated, cf. the form of the matrix elements $W_{k_1k_2k_3k_4}$, Eq. (3.40), of the Hamiltonian. In the end, the calculation here will be technically restricted to lower orders than those one can reach in spin systems. The expansion reads

$$\begin{aligned}\Omega(T, N_\phi, \mu) &= -\frac{1}{\beta}\,\ln\left[\mathrm{Tr}\,\left\{e^{\beta\mu N}\right\}\,\cdot\,\left(1-\beta<H>+\frac{1}{2!}\beta^2<H^2>-\ldots\right)\right] \\ &=: N_\phi\sum_{n=0}^{\infty}\beta^{n-1}\,\Omega_n(e^{\beta\mu})\,. \end{aligned} \tag{4.2}$$

We denote the expectation value of the non–interacting system by $<\cdots>=\frac{\mathrm{Tr}\{e^{\beta\mu N\ldots}\}}{\mathrm{Tr}\{e^{\beta\mu N}\}}$. Below, we shall use the fugacity, $z = e^{\beta\mu}$, instead of the chemical potential, μ. The first high–temperature expansion coefficients of $\Omega(T, N_\phi, \mu)$ are

$$\begin{aligned}\Omega_0(z) &= -\ln(1+z) \\ \Omega_1(z) &= \frac{1}{N_\phi}<H> \\ \Omega_2(z) &= -\frac{1}{N_\phi}\,\frac{1}{2!}\,\left[<H^2>-<H>^2\right] \\ \Omega_3(z) &= \frac{1}{N_\phi}\,\frac{1}{3!}\,\left[<H^3>-3<H><H^2>+2<H>^3\right]\,. \end{aligned} \tag{4.3}$$

The square brackets in the last equations define cumulant averages which will be denoted as $<\cdots>_c$ in the future. In the expressions for $\Omega_n(z)$, the thermodynamic limit $N_\phi \to \infty$ is implied. $\Omega_n(z)$ involves only averages of powers of the Hamiltonian $<H^j>$ up to a maximum power of n. Each of these is straight–forwardly calculated by application of Wick's theorem.

Any thermodynamic quantity can be derived from the grand canonical thermodynamic potential. The thermodynamic quantities of interest expressed by a power series in β and the relations of their coefficients to the coefficients $\Omega_n(z)$ are given explicitly in the Appendix B.

4.2 Calculation of the expectation values $< H^n >$

In this section, the procedure used to calculate the $\Omega_n(z)$ will be explained. The new terms and concepts introduced will be discussed in general; however, the calculation of the second order $n = 2$ will be used to demonstrate the idea.

Let's first look at the general form of $< H^n >$,

$$< H^n > = \left(\frac{1}{2}\right)^n \sum_{k_1 \ldots k_{4n}} \underbrace{W_{\cdot\cdot} W_{\cdot\cdot} \ldots W_{\cdot\cdot}}_{n \text{ interactions}} < \underbrace{c^\dagger c^\dagger c\, c}_{1} \ \underbrace{c^\dagger c^\dagger c\, c}_{2} \ \ldots \ \underbrace{c^\dagger c^\dagger c\, c}_{n} > \ . \tag{4.4}$$

A calculation of this expression involves calculation of the average and then evaluation of the summations. The calculation for the average can be done with the aid of Wick's theorem. The general result for such an average will be the sum of all contractions

$$< \underbrace{c^\dagger c^\dagger c\, c}_{1} \ \ldots \ \underbrace{c^\dagger c^\dagger c\, c}_{n} > = \sum_{\substack{\text{all possible} \\ \text{contractions}}} \text{prefactor } f^m (1-f)^{2n-m} \ \underbrace{\delta_{\cdot,\cdot}}_{1} \ \ldots \ \underbrace{\delta_{\cdot,\cdot}}_{2n} \tag{4.5}$$

The prefactor is given by the symmetry of the particular contraction, the Fermi factors, f, come from the averages $< c^\dagger c >$, and the delta functions come from the pairing of c and $c^\dagger$. There is no single particle energy term in the Hamiltonian, therefore, the Fermi factors are independent of the momentum k and this leads to a significant simplification: The products of the Fermi factors, f, can be taken out of the k–summations. Then, the general form of $< H^n >$ is

$$< H^n > = \sum_{\substack{\text{all possible} \\ \text{contractions}}} \underbrace{\text{prefactor } f^m (1-f)^{2n-m} \ \underbrace{\sum_{k_1 \ldots k_{4n}} \overbrace{W_{\cdot,\cdot} W_{\cdot,\cdot} \ldots W_{\cdot,\cdot}}^{n} \ \overbrace{\delta_{\cdot,\cdot} \delta_{\cdot,\cdot} \ldots \delta_{\cdot,\cdot}}^{2n}}_{\text{“pattern”}}}_{\text{“diagram”}} \tag{4.6}$$

We call a given contraction a *diagram* and its momentum sums with the interaction matrix elements a *pattern*. As it turns out, several diagrams will contain the same pattern. Generally, a pattern p of order "n" can be written as

$$W_p^{(n)} = \lim_{N_\phi \to \infty} \tfrac{1}{N_\phi} \sum_{k_1 \ldots k_{4n}} \underbrace{W_{k_1 k_2 k_3 k_4} W_{k_5 k_6 k_7 k_8} \ldots W_{k_{4n-3} k_{4n-2} k_{4n-1} k_{4n}}}_{n} \ \underbrace{\delta_{\cdot,\cdot} \delta_{\cdot,\cdot} \ldots \delta_{\cdot,\cdot}}_{2n} \ . \tag{4.7}$$

Now, we demonstrate our method using the second order "$n = 2$" as an example.

There are three possible contractions for "$n = 2$", one is disconnected and the other two are connected.

$$\sum_{\substack{k_1k_2k_3k_4\\k_5k_6k_7k_8}} W_{k_1k_2k_3k_4}\, W_{k_5k_6k_7k_8} \; < \underbrace{c^\dagger\ \underbrace{c^\dagger c}\ c}\quad \underbrace{c^\dagger\ \underbrace{c^\dagger c}\ c} > \qquad \Longrightarrow$$

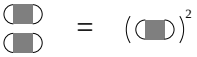

$$\sum_{\substack{k_1k_2k_3k_4\\k_5k_6k_7k_8}} W_{k_1k_2k_3k_4}\, W_{k_5k_6k_7k_8} \; < \underbrace{c^\dagger\ \underbrace{c^\dagger\ c\ \overbrace{c\quad c^\dagger}\ c^\dagger c}\ c} > \qquad \Longrightarrow$$

$$\sum_{\substack{k_1k_2k_3k_4\\k_5k_6k_7k_8}} W_{k_1k_2k_3k_4}\, W_{k_5k_6k_7k_8} \; < \underbrace{c^\dagger\ \underbrace{c^\dagger c}\ \overbrace{c\quad c^\dagger}\ \underbrace{c^\dagger c}\ c} > \qquad \Longrightarrow$$

A *box* represents the interaction vertex $W_{k_1k_2k_3k_4}$; the momentum sums $\sum_{k_1,k_2,k_3,k_4}$ are implied. Only the contributions of the connected diagrams enter $\Omega_2(z)$:

$$\Omega_2(z) \;=\; \lim_{N_\phi\to\infty} -\frac{1}{2\,N_\phi} < H^2 >_c = -\frac{1}{2}\, f^2\,(1-f)^2\, W_a^{(2)} - 2f^3\,(1-f)\, W_b^{(2)}\ . \quad (4.8)$$

Here, the fugacity z enters the Fermi factor $f = z/(1+z)$, and the patterns $W_{a,b}^{(2)}$ are constants given by the following momentum sums:

$$W_a^{(2)} \;=\; \lim_{N_\phi\to\infty} \tfrac{1}{N_\phi} \sum_{k_1,k_2,k_3,k_4} W_{k_2k_1k_3k_4}\, W_{k_4k_3k_1k_2}\ , \quad (4.9)$$

$$W_b^{(2)} \;=\; \lim_{N_\phi\to\infty} \tfrac{1}{N_\phi} \sum_{k_1,k_2,k_3,k_4} W_{k_2k_1k_1k_3}\, W_{k_4k_3k_2k_4}\ . \quad (4.10)$$

Generally, the cumulant averages $< H^n >_c$ are given by a sum of connected diagrams as in Eq. (4.8). Each diagram is given by a prefactor (integer/$n!$), a polynomial of the form $f^m\,(1-f)^{2n-m}$, $m = 2, 3, \ldots, 2n-1$ and a pattern as $W_a^{(2)}$ or $W_b^{(2)}$.

In order to evaluate the expansion for higher n, we implemented Wick's theorem in a computer program which determines for fixed order n the list of connected diagrams containing for each diagram prefactor, polynomial, and pattern. Here, most of the computation time is needed for an identification of diagrams which are mere permutations of the n Hamiltonians. Inevitably, all those diagrams appear in such an evaluation of Wick's theorem. (The calculation of the order $n = 8$ uses about 2 GB memory and takes 48 hours CPU time on a workstation.) In Table 4.1, we show for all orders up to $n = 8$ the total number of diagrams, the number of connected diagrams, and the number of patterns; the term *proper patterns* will be explained below. Note that the number of patterns is much smaller than the number of connected diagrams, since each pattern can appear with about n different polynomial prefactors. The advantage of the present method as compared with the traditional perturbative method is that only the patterns need to be calculated.

4.3 Transformation to the canonical ensemble

In this section, we transform to the canonical ensemble. Energy and filling factor are given by

$$E(T, N_\phi, \mu) \;=\; N_\phi \sum_{n=1}^{\infty} \beta^{n-1} \;\; n \;\; \Omega_n(z) \tag{4.11}$$

and

$$\nu \;=\; \frac{N(T, N_\phi, \mu)}{N_\phi} \;=\; f - \sum_{n=1}^{\infty} \beta^n \;\; z \;\; \partial_z \, \Omega_n(z) \; . \tag{4.12}$$

We need to eliminate the fugacity z in favour of the filling factor ν. Here, Eq. (4.12) and Eq. (4.11) contain z only in the combination $f = z/(1+z)$. Thus, we solve Eq. (4.12) for f term by term in the expansion in β and insert this into Eq. (4.11). Again, we demonstrate this in the second order $n = 2$: With $\Omega_1(z) = f^2 \; W_a^{(1)}$ and $\Omega_2(z)$ from Eq. (4.8), we can solve Eq. (4.12) for f

$$\begin{aligned} f(\nu) = \nu + 2 \, \beta \, W_a^{(1)} \, \nu^2 \, (1-\nu) + \beta^2 \; \Big[& 4 \left(W_a^{(1)} \right)^2 \nu^3 \, (1-\nu) \, (2-3\nu) \\ & - W_a^{(2)} \, \nu^2 \, (1-\nu)^2 \, (1-2\nu) - 2 \, W_b^{(2)} \, \nu^3 \, (1-\nu) \, (3-4\nu) \Big] \\ & + \mathcal{O}(\beta^3 W^3) \; . \end{aligned} \tag{4.13}$$

Substituting this now into Eq. (4.11), we find the following expression for the energy up to the second order in the interaction

$$\begin{aligned} E(T, N_\phi, \nu) \;\; = \;\; & N_\phi \; \Big[W_a^{(1)} \, \nu^2 - \beta \, W_a^{(2)} \, \nu^2 \, (1-\nu)^2 \\ & - 4 \, \beta \; \left\{ W_b^{(2)} - (W_a^{(1)})^2 \right\} \; \nu^3 \, (1-\nu) \Big] + \mathcal{O}(\beta^2 \, W^3) \; . \end{aligned} \tag{4.14}$$

In the lowest order, there is only the pattern

$$W_a^{(1)} \;=\; \text{  } \;=\; \lim_{N_\phi \to \infty} \frac{1}{N_\phi} \sum_{k_1, k_2} W_{k_2 k_1 k_1 k_2} \tag{4.15}$$

order n	1	2	3	4	5	6	7	8
diagrams	1	3	11	50	242	1555	11088	95051
connected diagrams	1	2	8	36	176	1202	8920	79836
patterns	1	2	5	14	50	265	1601	11984
proper patterns	1	1	2	4	10	42	198	1400

Table 4.1: The total number of diagrams, the number of connected diagrams, patterns and proper patterns from first up to eighth order.

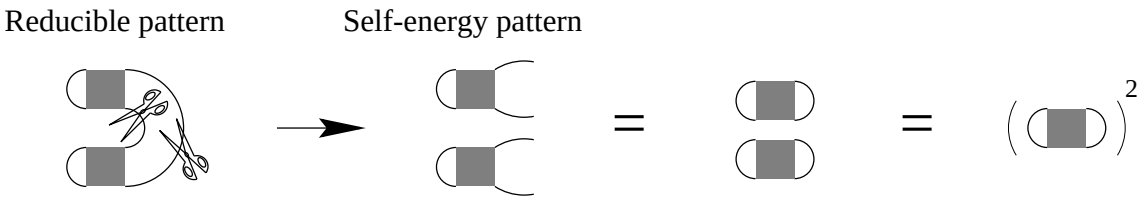

Figure 4.1: The self–energy pattern in the second order

which is given by the energy of the completely filled Landau level. We find explicitly $W_a^{(1)} = \int_0^\infty dr\ r\ W(r)$ (see Eq. (4.31) below). The ν–dependence of this term is such that particle–hole symmetry is fulfilled in this order: Interchanging of c and $c^\dagger$ leads, after normal ordering, to two additional terms in H and thus, the particle–hole symmetry relation for the energy reads

$$E(T, N_\phi, 1-\nu) \;=\; N_\phi\ (1-2\nu)\ W_a^{(1)} + E(T, N_\phi, \nu)\ . \tag{4.16}$$

In the next order β^1 in Eq. (4.14), the first term $\nu^2\ (1-\nu)^2$ obeys the particle–hole symmetry, but the second term $\nu^3\ (1-\nu)$ seems to violate the particle–hole symmetry. But as it turns out, the pattern $W_b^{(2)}$ is reducible in the following sense: One can cut two lines in $W_b^{(2)}$ in such a way that $W_b^{(2)}$ decays into two non–connected parts, see Fig. 4.1. Thus, $W_b^{(2)}$ contains a self–energy insertion. One finds $W_b^{(2)} = \left(W_a^{(1)}\right)^2$ and the term violating the particle–hole symmetry cancelled out.

Generally, a pattern as $W_b^{(2)}$ which decays into two pieces after two lines are cut, is called a *reducible pattern*. Thus, a reducible pattern contains *self–energy patterns*, see Fig. 4.1. The value of such a pattern is just simply the product of both parts, as we shall see now. Using the interaction matrix element which can be obtained easily from Eq. (3.36), we have for the lowest order self–energy pattern

$$\begin{aligned}
\text{  } \;&=\; \lim_{L_y\to\infty} \sum_{k_1 k_4} W_{k_1 k_2 k_3 k_4}\ \delta_{k_1,k_4} \\
&=\; \lim_{L_y\to\infty} \frac{1}{L_y}\ \left(\frac{1}{2\pi}\right)^{1/2} \int d^2r\ W^F(r)\ e^{-\frac{1}{2}\,x^2} \sum_{k_1\ k_4} \delta_{k_1+k_2,k_3+k_4}\ \delta_{k_1,k_4} \\
&\qquad e^{-\frac{1}{4}\left[(k_1-k_2)^2+(k_4-k_3)^2\right]-\frac{i}{2}\ y\ [(k_1-k_2)-(k_4-k_3)]-\frac{1}{2}\ x\ [(k_1-k_2)+(k_4-k_3)]} \\
&=\; \delta_{k_2,\,k_3}\ \frac{1}{2\pi} \int d^2r\ W^F(r) \;=\; \delta_{k_2,\,k_3}\ W_a^{(1)}
\end{aligned} \tag{4.17}$$

We see here that the self–energy pattern in this order is diagonal in its momentum indices, k_2 and k_3, and independent of them, where k_2 and k_3 denote the momentum of the incoming and outgoing lines. This is true in any order. The diagonality results

from the translational symmetry in y–direction ($[\mathcal{T}_y, H] = 0$). The independence is due to the translational symmetry in x–direction ($[\mathcal{T}_x, H] = 0$). This symmetry allows to shift all momenta k_j by a constant amount; $W_{k_1 k_2 k_3 k_4}$ depends only on momentum differences between the k_j, cf. Eq. (3.38) or Eq. (3.40). Therefore, we can just simply *glue* the two remaining unconnected lines together as in Fig. 4.1.

We shall call a non–reducible pattern a *proper pattern*. We implemented the elimination of the fugacity in Eq. (4.12) and Eq. (4.11) and the replacement of the reducible patterns by a product of proper patterns of lower order as in $W_b^{(2)} \Rightarrow (W_a^{(1)})^2$ in a symbolic computer program. The result of this is then the exact series of the energy as a function of the inverse temperature and the filling factor. It contains prefactors, polynomials of the form $\nu^m \ (1-\nu)^{2n-m}$, $m = 2, 3, \ldots, 2n-2$, and only the proper patterns. The proper patterns up to the fifth order are shown in Fig. 4.2. We determine the form of *all* proper patterns up to the eighth order of the high–temperature expansion. So far, we have analysed the structure of the high–temperature expansion series for the energy as a function of the filling factor and temperature. We find

$$E(T, N_\phi, \nu) \ = \ N_\phi \ \left(\nu^2 \, \mathcal{C}^{(1)} + \sum_{n=2}^{\infty} \ \beta^{n-1} \ \sum_{m=-n+2}^{n-2} \ \nu^{n+m} \ (1-\nu)^{n-m} \ \ \mathcal{C}_m^{(n)} \right) \qquad (4.18)$$

and $\mathcal{C}_m^{(n)} = \mathcal{C}_{-m}^{(n)}$. The coefficients $\mathcal{C}_m^{(n)}$ depend on the interaction and are given by the prefactors and proper patterns mentioned above. Comparing this equation with Eq. (4.14), we can identify the first two terms in the high–temperature expansion series for the energy: The *Hartree–Fock energy* which is independent of the temperature, is equal to $\mathcal{C}^{(1)} = W_a^{(1)} = \int_0^\infty \ dr \ r \ W^F(r)$ (see Eq. (4.32) below). The next coefficient in the series is $\mathcal{C}_0^{(2)} = -W_a^{(2)}$. Thus, the evaluation of the high–temperature expansion series for the energy is reduced to the calculation of proper patterns for a given interaction.

An elimination of the reducible diagrams (or reducible patterns) was also very successfully used by Zheng and MacDonald [28]. They uncovered the relation between the cancellation of the reducible diagrams containing the lowest order self–energy pattern and the restoration of the particle–hole symmetry in the energy up to the third order. With our calculation, we confirm the observation of Zheng and MacDonald and extend it up to the eighth order. Zheng and MacDonald also found that the restriction to non–self–energy diagrams leads to a great reduction of the number of terms to be calculated in their perturbation series. The same is observed here, as can be seen in Table 4.1. The number of the proper patterns is smaller than the number of the patterns by almost an order of magnitude in the eighth order. Moreover, comparing the number of the connected diagrams with the number of the proper patterns, we can see a great reduction, too. By the present method there are much less proper patterns to be calculated than connected diagrams in the traditional perturbative treatment.

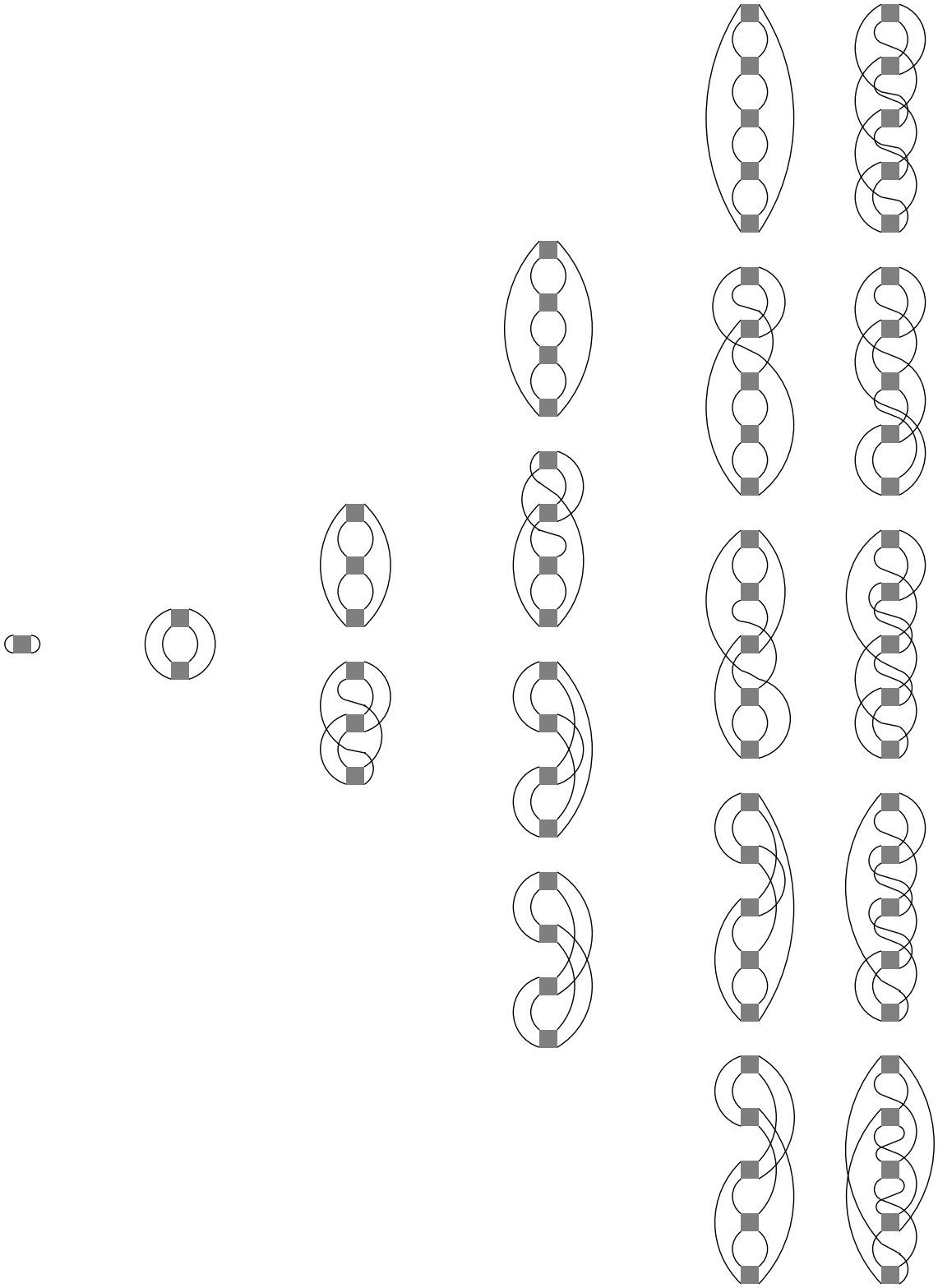

Figure 4.2: The proper patterns from the first up to the fifth order.

4.4 The high–temperature expansion for an arbitrary interaction: real space

In this section, we shall develop a method to evaluate the proper patterns of the high–temperature expansion series. This method will be used extensively in both cases, arbitrary interactions and zero–range interactions. As we have seen in Section 4.2, a pattern of order "n" results from the application of Wick's theorem and describes connections between the "n" vertices which constitute the pattern, cf. Eq. (4.7). It is given by a multiple summation of "$4n$" dimensions on all momentum indices of the product of "n" interaction matrix elements with a set of "$2n$" the Kronecker deltas which come from the lines (Green's functions). Each interaction matrix element also carries a Kronecker delta which ensures the conservation of the momentum at each vertex, see Eq. (3.36). Thus, for the entire "$4n$" summations there are "$3n$" Kronecker deltas which means that we shall have to evaluate actually just "n" summations. Due to the form of the interaction matrix element, the last "n" summations can be evaluated exactly as we want to show now. In the end, each proper pattern will be expressed as a "$2n$" dimensional spatial integral of a product of "n" interactions in real space with a Gaussian factor. Let's first consider the general form of the expression of a proper pattern of order "n" which can be obtained easily from Eq. (4.7) and Eq. (3.36):

$$
\begin{aligned}
W_p^{(n)} = & \lim_{N_\phi \to \infty} \frac{1}{N_\phi} \left(\frac{1}{L_y} \sqrt{\frac{1}{2\pi}} \right)^n \prod_{j=1}^{n} \left(\int d^2 r_j \; W(r_j) \; e^{-\frac{1}{2} x_j^2} \right) \\
& \sum_{k_1 \ldots k_{4n}} \underbrace{\delta_{k_{..},k_{..}} \cdots \delta_{k_{..},k_{..}}}_{2n} \prod_{j=1}^{n} \left(\delta_{k_{4j-3}+k_{4j-2},\, k_{4j-1}+k_{4j}} \right) \prod_{j=1}^{n} \left(e^{-\frac{1}{4} \left[(k_{4j-3}-k_{4j-2})^2 + (k_{4j}-k_{4j-1})^2 \right]} \right) \\
& \prod_{j=1}^{n} \left(e^{-\frac{i}{2} \left[(k_{4j-3}-k_{4j-2}) - (k_{4j}-k_{4j-1}) \right] y_j - \frac{1}{2} \left[(k_{4j-3}-k_{4j-2}) + (k_{4j}-k_{4j-1}) \right] x_j} \right)
\end{aligned}
\tag{4.19}
$$

We transform to *relative* and *centre–of–mass* coordinates at each vertex which we define in the following way ($j = 1, \ldots, n$ numbers the interaction vertex)

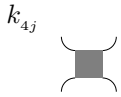

$$
(p_j \; , \; s_j) \;=\; (k_{4j} - k_{4j-1} \; , \; k_{4j} + k_{4j-1}) \tag{4.20}
$$

$$
(q_j \; , \; t_j) \;=\; (k_{4j-3} - k_{4j-2} \; , \; k_{4j-3} + k_{4j-2}) \tag{4.21}
$$

The Jacobian determinant for the transformation $\left| \frac{\partial(k_1,k_2)}{\partial(q_1,t_1)} \right| = \frac{1}{2}$ enters twice at each interaction vertex. The system of the $2n$ Kronecker deltas will be transformed to products of the form $\delta_{\frac{1}{2}(\pm p_i + s_i), \frac{1}{2}(\pm q_j + t_j)}$.

$$W_p^{(n)} = \lim_{N_\phi \to \infty} \frac{1}{N_\phi} \left(\frac{1}{L_y} \sqrt{\frac{1}{2\pi}} \right)^n \prod_{j=1}^{n} \left(\int d^2 r_j \; W(r_j) \; e^{-\frac{1}{2} x_j^2} \right)$$

$$\sum_{\substack{q_1 \ldots q_n \, , \, p_1 \ldots p_n \\ t_1 \ldots t_n \, , \, s_1 \ldots s_n}} \left(\frac{1}{2} \right)^{2n} \; \tilde{\Delta}^{(2n)}(\vec{p}, \vec{q}, \vec{t}, \vec{s}) \; \prod_{j=1}^{n} \left(\; \delta_{t_j, s_j} \; e^{-\frac{1}{4} \left(q_j^2 + p_j^2 \right) - \frac{i}{2} \, (q_j - p_j) \, y_j - \frac{1}{2} \, (q_j + p_j) \, x_j} \right) \; . \tag{4.22}$$

Here, $\tilde{\Delta}^{(2n)}(\vec{p}, \vec{q}, \vec{t}, \vec{s})$ denotes the set of the $2n$ Kronecker deltas which describe the way the interaction vertices are connected. In this section, we use for brevity $\vec{u} = (u_1, u_2, \ldots, u_n)$ for $u = p, q, t, s, x, y$ (unless noticed explicitly, here $\vec{x} \neq (x, y)$).

Evaluating the summations on s_j with the aid of the momentum conservations at each vertex, δ_{t_j, s_j}, we replace s_j by t_j, and $\tilde{\Delta}^{(2n)}(\vec{p}, \vec{q}, \vec{t}, \vec{t})$ becomes $\Delta^{(2n)}(\vec{p}, \vec{q}, \vec{t})$. Only $2n - 1$ Kronecker deltas of the $2n$ Kronecker deltas in $\Delta^{(2n)}(\vec{p}, \vec{q}, \vec{t})$ are independent, since the last momentum conservation is automatically fulfilled. Also, the expression is invariant against a shift of all momenta (cf. Eq. (3.36)). Therefore, there is one summation on t_j, say t_n, which can be performed immediately. Performing this unconnected summation on t_n results in a factor of 2 N_ϕ. Then, the summations (second line in Eq. (4.22)) become

$$N_\phi \sum_{\substack{q_1 .. q_n \, , \, p_1 .. p_n \\ t_1 \, \ldots \, t_{n-1}}} \left(\frac{1}{2} \right)^{2n-1} \; \Delta^{(2n-1)}(\vec{p}, \vec{q}, \vec{t}) \; \; e^{-\frac{1}{4} \left(\vec{q}^2 + \vec{p}^2 \right) - \frac{i}{2} \, (\vec{q} - \vec{p}) \, \vec{y} - \frac{1}{2} \, (\vec{q} + \vec{p}) \, \vec{x}} \; . \tag{4.23}$$

In the next step, we replace the momentum sums on $\vec{p}, \vec{q}$ and $\vec{t}$ by integrals in the limit $L_y \to \infty$ and transform the Kronecker deltas of the form $\frac{L_y}{2\pi} \cdot \frac{1}{2} \cdot \delta_{\frac{1}{2}(\pm p_i + t_i), \frac{1}{2}(\pm q_j + t_j)}$ entering $\Delta^{(2n-1)}(\vec{p}, \vec{q}, \vec{t})$ to delta functions $\delta((\pm p_i + t_i) - (\pm q_j + t_j))$:

$$\left(\frac{L_y}{2\pi} \cdot \frac{1}{2} \right)^{2n-1} \Delta^{(2n-1)}(\vec{p}, \vec{q}, \vec{t}) \; = \; \vec{\delta} \left(\hat{Q}_p^{(n)} \cdot \begin{pmatrix} \vec{p} \\ \vec{t} \end{pmatrix} - \hat{F}_p^{(n)} \cdot \vec{q} \right) \tag{4.24}$$

where $\vec{\delta}$ represents a set of $(2n-1)$ delta functions. $\hat{Q}_p^{(n)}$, is a square $(2n-1) \times (2n-1)$ matrix; $\hat{F}_p^{(n)}$, is a rectangular $(2n-1) \times (n)$ matrix. They describe the contractions in the pattern (given by the above Kronecker deltas). Therefore, the elements of both matrices $\hat{F}_p^{(n)}, \hat{Q}_p^{(n)}$ can be only 0 or ± 1.

We get after performing the transformations

$$W_p^{(n)} = \left(\frac{1}{2\pi} \right)^{n/2} \prod_{j=1}^{n} \left(\int d^2 r_j \; W(r_j) \; e^{-\frac{1}{2} x_j^2} \right)$$

$$\prod_{j=1}^{n} \left(\int_{-\infty}^{\infty} \frac{dq_j}{2\pi} \right) \prod_{j=1}^{n} \left(\frac{1}{2} \, \frac{L_y}{2\pi} \int_{-\infty}^{\infty} dp_j \right) \prod_{j=1}^{n-1} \left(\frac{1}{2} \, \frac{L_y}{2\pi} \int_{-\infty}^{\infty} dt_j \right)$$

$$\left\{ \left(\frac{2\pi}{L_y} \cdot 2 \right)^{2n-1} \vec{\delta} \left(\hat{Q}_p^{(n)} \cdot \begin{pmatrix} \vec{p} \\ \vec{t} \end{pmatrix} - \hat{F}_p^{(n)} \cdot \vec{q} \right) \right\} \; e^{-\frac{1}{4} \left(\vec{q}^2 + \vec{p}^2 \right) - \frac{i}{2} \, (\vec{q} - \vec{p}) \, \vec{y} - \frac{1}{2} \, (\vec{q} + \vec{p}) \, \vec{x}} \; . \tag{4.25}$$

We note that

$$\vec{\delta}\left(\hat{Q}_p^{(n)}\cdot\begin{pmatrix}\vec{p}\\ \vec{t}\end{pmatrix}-\hat{F}_p^{(n)}\cdot\vec{q}\right)=\frac{1}{\left|\det\hat{Q}_p^{(n)}\right|}\,\vec{\delta}\left(\begin{pmatrix}\vec{p}\\ \vec{t}\end{pmatrix}-\hat{Q}_p^{(n)^{-1}}\cdot\hat{F}_p^{(n)}\cdot\vec{q}\right)\;; \tag{4.26}$$

thus, inverting $\hat{Q}_p^{(n)}$, we solve the remaining $2n-1$ equations in $\vec{\delta}$ for p_j and t_j as functions of q_j:

$$\begin{pmatrix}\vec{p}\\ \vec{t}\end{pmatrix}\;=\;\hat{Q}_p^{(n)^{-1}}\cdot\hat{F}_p^{(n)}\cdot\vec{q}\;=:\;\begin{pmatrix}\hat{M}_p^{(n)}\\ \hat{O}_p^{(n)}\end{pmatrix}\cdot\vec{q} \tag{4.27}$$

or $\vec{p}=\hat{M}_p^{(n)}\cdot\vec{q}$ and $\vec{t}=\hat{O}_p^{(n)}\cdot\vec{q}$. The matrix $\hat{M}_p^{(n)}$ describes the relation between the relative in–coming momenta at vertex i, (q_i), and the relative out–going momenta at vertex j, (p_j), for a pattern p of order n.

Before we continue the evaluation of $W_p^{(n)}$, we need to derive an important property of $\hat{M}_p^{(n)}$. After transforming the original variables k_j to the new variables p_j, q_j, s_j and t_j defined in Eq. (4.20) and Eq. (4.21), and replacing $\vec{s}$ by $\vec{t}$, the momentum conservation for a line between vertex i and vertex j becomes $\frac{1}{2}(\pm p_i+t_i)=\frac{1}{2}(\pm q_j+t_j)$. Summing the square of this over all lines of the pattern, we get

$$\sum_{i=1}^{n}\left[(p_i+t_i)^2+(-p_i+t_i)^2\right]=\sum_{j=1}^{n}\left[(q_j+t_j)^2+(-q_j+t_j)^2\right], \tag{4.28}$$

or $\vec{p}^{\,2}=\vec{q}^{\,2}$. Therefore, the transformations between $\vec{q}$ and $\vec{p}$ must be orthogonal, hence $\hat{M}_p^{(n)^T}\cdot\hat{M}_p^{(n)}=1$.

Evaluating now the integrations on $\vec{p}$ and $\vec{t}$, we get

$$\begin{aligned}W_p^{(n)}\;&=\;\frac{1}{\left|\det\hat{Q}_p^{(n)}\right|}\left(\frac{1}{2\pi}\right)^{n/2}\prod_{j=1}^{n}\left(\int d^2r_j\;W(r_j)\;e^{-\frac{1}{2}x_j^2}\right)\\ &\quad\prod_{j=1}^{n}\left(\int_{-\infty}^{\infty}\frac{dq_j}{2\pi}\right)\;e^{-\frac{1}{4}\left(\vec{q}^{\,2}+(\hat{M}_p^{(n)}\cdot\vec{q})^2\right)-\frac{i}{2}\left(\vec{q}-\hat{M}_p^{(n)}\cdot\vec{q}\right)^T\vec{y}-\frac{1}{2}\left(\vec{q}+\hat{M}_p^{(n)}\cdot\vec{q}\right)^T\vec{x}}\\ &=\;\frac{1}{\left|\det\hat{Q}_p^{(n)}\right|}\prod_{j=1}^{n}\left(\int\frac{d^2r_j}{2\,\pi}\;W(r_j)\right)\;e^{-\frac{1}{4}\left[\vec{x}^2+\vec{y}^2-(\vec{x}-i\vec{y})\cdot\hat{M}_p^{(n)}\cdot(\vec{x}+i\vec{y})\right]}.\end{aligned} \tag{4.29}$$

This is the final result which allows to calculate the pattern $W_p^{(n)}$ for an arbitrary interaction $W(r)$. The pattern enters the expression via the matrices $\hat{Q}_p^{(n)}$ and $\hat{M}_p^{(n)}$ which describes its connectivity. For a given pattern, it is straightforward to obtain these matrices. For higher order patterns from the second up to the fourth order, the matrices $\hat{Q}_p^{(n)}$ and $\hat{M}_p^{(n)}$ can be found in Appendix C. While $W_p^{(n)}$ is real, the exponent

in its integrand will be real only if the matrix $\hat{M}_p^{(n)}$ is symmetric; on the other hand, if $\hat{M}_p^{(n)}$ is not symmetric, the exponent will become complex.

Below, we illustrate this general procedure by calculating the proper pattern in the first order and a proper pattern in the third order as examples.

4.4.1 Calculation of the proper pattern of the first order

In the first order, there is only one proper pattern,

$$\begin{aligned} W_a^{(1)} &= \lim_{N_\phi \to \infty} \tfrac{1}{N_\phi} \sum_{k_1 k_2 k_3 k_4} W_{k_1 k_2 k_3 k_4}\, \delta_{k_1,k_4}\, \delta_{k_2,k_3} \\ &= \lim_{N_\phi \to \infty} \tfrac{1}{N_\phi}\, \tfrac{1}{L_y}\, \sqrt{\tfrac{1}{2\,\pi}} \int d^2r\; W^F(r)\; e^{-\frac{1}{2}x^2} \\ &\quad \sum_{p\,q\,t\,s} \left(\tfrac{1}{2}\right)^2 \delta_{\frac{1}{2}\,(q+t),\frac{1}{2}\,(p+s)}\; \delta_{\frac{1}{2}\,(-q+t),\frac{1}{2}\,(-p+s)}\; \delta_{t,s}\; e^{-\frac{1}{4}\left[q^2+p^2\right]-\frac{i}{2}[q-p]\,y-\frac{1}{2}[q+p]\,x} \end{aligned} \tag{4.30}$$

where, $(q,t) = k_1 \mp k_2$ and $(p,s) = k_4 \mp k_3$. Performing the summation on s first, we see that the two remaining Kronecker deltas are identical; that was meant earlier by the statement *only "$2n-1$" Kronecker deltas are independent*. No part in the expression depends on t, therefore, the summation on t together with factor $1/2$ just gives the number of states, $1/2 \sum_t = N_\phi$. Further, we have $\hat{Q}_a^{(1)} = 1$ and $\hat{M}_a^{(1)} = 1$. The expression corresponding to Eq. (4.29) becomes

$$\begin{aligned} W_a^{(1)} &= \sqrt{\tfrac{1}{2\,\pi}} \int d^2r\; W^F(r)\; e^{-\frac{1}{2}x^2}\; \tfrac{1}{2\,\pi} \int_{-\infty}^{\infty} dq\; e^{-\frac{1}{2}\,q^2 - q\,x} \\ &= \tfrac{1}{2\,\pi} \int d^2r\; W^F(r)\;. \end{aligned} \tag{4.31}$$

$W_a^{(1)}$ will diverge, if $W^F(r)$ is an infinite–range interaction, if the interaction does not decay faster than r^{-2}. The method developed here will be useful only for interactions which decay fast enough, i. e., for any finite–range interaction. An infinite–range interaction, such as the Coulomb interaction needs consideration a positive background. We note here that the first coefficient in Eq. (4.18) is

$$\mathcal{C}^{(1)} \;=\; W_a^{(1)} \;=\; \int_0^\infty dr\; r\; W^F(r) \tag{4.32}$$

4.4.2 Calculation of a proper pattern of the third order

In the third order, we choose to demonstrate the calculation for the proper pattern $W_a^{(3)}$, because for this pattern, the exponent in Eq. (4.29) becomes complex due to the

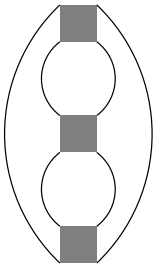

Figure 4.3: A proper pattern of the third order $W_a^{(3)}$

non–symmetry of the matrix $\hat{M}_a^{(3)}$.

$$W_a^{(3)} = \lim_{N_\phi \to \infty} \frac{1}{N_\phi} \sum_{k_1,\ldots,k_{12}} W_{k_1k_2k_3k_4}\, W_{k_5k_6k_7k_8}\, W_{k_9k_{10}k_{11}k_{12}} \delta_{k_1,k_{12}}\ \delta_{k_2,k_{11}}\ \delta_{k_3,k_6}\ \delta_{k_4,k_5}\ \delta_{k_7,k_{10}}\ \delta_{k_8,k_9}\ . \tag{4.33}$$

Using the transformation set up above and replacing the interaction matrix elements with the aid of Eq. (3.36), we get

$$\begin{aligned} W_a^{(3)} = {} & \lim_{N_\phi\to\infty} \frac{1}{N_\phi} \left(\frac{1}{L_y}\right)^3 \left(\frac{1}{2\,\pi}\right)^{3/2} \prod_{j=1}^{3} \left(\int d^2r_j\ W^F(r_j)\ e^{-\frac{1}{2}\,x_j^2} \right) \\ & \sum_{\{q_j,p_j,t_j,s_j\}} \left(\tfrac{1}{2}\right)^6\ \delta_{\frac{1}{2}(p_3+s_3),\frac{1}{2}(q_1+t_1)}\ \delta_{\frac{1}{2}(-p_3+s_3),\frac{1}{2}(-q_1+t_1)}\ \delta_{\frac{1}{2}(-p_1+s_1),\frac{1}{2}(-q_2+t_2)} \\ & \delta_{\frac{1}{2}(p_1+s_1),\frac{1}{2}(q_2+t_2)}\ \delta_{\frac{1}{2}(-p_2+s_2),\frac{1}{2}(-q_3+t_3)}\ \delta_{\frac{1}{2}(p_2+s_2),\frac{1}{2}(q_3+t_3)} \\ & \delta_{t_1,s_1}\ \delta_{t_2,s_2}\ \delta_{t_3,s_3} \prod_{j=1}^{3} \left(e^{-\frac{1}{4}\left[q_j^2+p_j^2\right] - \frac{i}{2}\,(q_j-p_j)\,y_j + \frac{1}{2}\,(q_j+p_j)\,x_j} \right) \end{aligned} \tag{4.34}$$

where q_j, p_j, t_j and s_j are defined as in Eq. (4.21) and Eq. (4.20). The calculation proceeds in the same manner as in the lower order. We first evaluate the summations on s_j and then shift $t_{1,2}$ by t_3. t_3 then drops out and the summation on t_3 becomes $2N_\phi$. After the shift, we shall find that the last Kronecker delta follows from the others. Thus, we omit the last Kronecker delta. The matrices are given by

$$\hat{Q}_a^{(3)} = \begin{pmatrix} 0 & 0 & 1 & -1 & 0 \\ 0 & 0 & -1 & -1 & 0 \\ -1 & 0 & 0 & 1 & -1 \\ 1 & 0 & 0 & 1 & -1 \\ 0 & -1 & 0 & 0 & 1 \end{pmatrix} \quad \text{and} \quad \hat{F}_a^{(3)} = \begin{pmatrix} 1 & 0 & 0 \\ -1 & 0 & 0 \\ 0 & -1 & 0 \\ 0 & 1 & 0 \\ 0 & 0 & -1 \end{pmatrix} \tag{4.35}$$

Thus, solving the remaining Kronecker deltas, we find as solutions $t_1 = t_2 = 0$ and $(p_1, p_2, p_3) = (q_2, q_3, q_1)$,

$$\hat{M}_a^{(3)} \;=\; \begin{pmatrix} 0 & 1 & 0 \\ 0 & 0 & 1 \\ 1 & 0 & 0 \end{pmatrix} \;. \tag{4.36}$$

Using the solutions in evaluating the summations on p_j and t_j, we get

$$\begin{aligned} W_a^{(3)} \;&=\; \left(\tfrac{1}{2}\right)^2 \left(\tfrac{1}{2\,\pi}\right)^{9/2} \prod_{j=1}^{3} \left(\int d^2 r_j \; W^F(r_j) \; e^{-\frac{1}{2}\, x_j^2} \right) \\ &\quad \int_{-\infty}^{\infty} dq_1 \int_{-\infty}^{\infty} dq_2 \int_{-\infty}^{\infty} dq_3 \; e^{-\frac{1}{2}\left(q_1^2+q_2^2+q_3^2\right)} \\ &\quad e^{-\frac{i}{2}[(q_1-q_2)\, y_1+(q_2-q_3)\, y_2+(q_3-q_1)\, y_3]-\frac{1}{2}[(q_1+q_2)\, x_1+(q_2+q_3)\, x_2+(q_3+q_1)\, x_3]} \\ &=\; \frac{1}{4} \prod_{j=1}^{3} \left(\int \frac{d^2 r_j}{2\pi} \; W^F(r_j) \right) e^{-\frac{1}{4}\left[\vec{x}^2+\vec{y}^2-(\vec{x}-i\,\vec{y})\; \hat{M}_a^{(3)}\; (\vec{x}+i\,\vec{y})\right]} \;. \end{aligned} \tag{4.37}$$

We note here that the coefficient in Eq. (4.18) containing $W_a^{(3)}$ is

$$\mathcal{C}_1^{(3)} \;=\; \frac{1}{2}\, W_a^{(3)} \;. \tag{4.38}$$

In this section, we have demonstrated how to evaluate the proper patterns for an arbitrary interaction. It is clear, though, that for a given interaction $W^F(r)$, the calculation of the integrals is a complex task which cannot be performed in higher orders.

4.5 Equivalence of the present method to the traditional perturbative treatment

In this section, we shall prove the equivalence of the high–temperature expansion method presented here to the high–temperature expansion within the framework of the traditional perturbative method which was used by L. Zheng and A. H. MacDonald [28]. We refer our reader to their original work. In Fig. 4.4, the connected diagrams studied in Ref. [28] are shown. As we have emphasised in Section 4.2, a *connected diagram* of order n here can be described as a linear combination of *proper patterns* with polynomial prefactors of the form $f^m\,(1-f)^{2n-m}$ and integer prefactors, cf. Eq. (4.6). In fact, the factors $f^m\,(1-f)^{2n-m}$ result from the frequency sum evaluations of the diagrams in Fig. 4.4.

The diagrams in Fig. 4.4 are grouped in such a way that all diagrams in a column have the same frequency sum results, possibly up to a factor of -1. Explicit calculations of the frequency sums of the connected diagrams from the first order up to the third order can be found in the Appendix D.

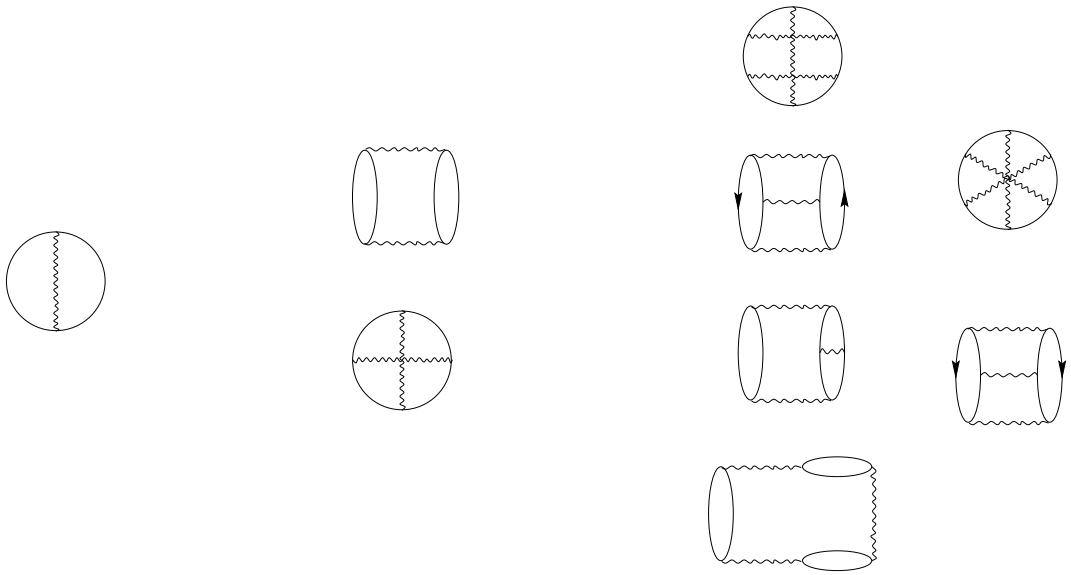

Figure 4.4: The connected diagrams from the first up to the third orders.

It was shown by A. V. Andreev and Yu. A. Bychkov [65] that topological different diagrams (diagrams in the same group) may be equal up to a minus sign. They also trace the physical reason for this back to the symmetry of the Hamiltonian. Here, we can observe that property easily and directly: Consider the interaction matrix element of the two–body interaction in the lowest Landau level, for example Eq. (3.40). Then, it is obvious that interchanging indices *only* of the annihilation operators (or *only* of the creation operators) will result in a minus sign:

$$W_{k_1k_2k_3k_4} \;=\; -W_{k_1k_2k_4k_3} \;=\; -W_{k_2k_1k_3k_4} \;=\; W_{k_2k_1k_4k_3}\;. \tag{4.39}$$

On the other hand, interchanging of two annihilation operators at an interaction relates two diagrams in the same column. Here, we shall use the connected diagrams in the second order, the second column in Fig. 4.4, to demonstrate this statement.

The two connected diagrams can be expressed as following:

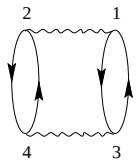

$$\Longrightarrow \quad \underbrace{f^2(1-f)^2}_{\omega\text{–sums}} \sum_{\substack{k_1k_2k_1'k_2' \\ k_3k_4k_3'k_4'}} W_{k_1k_2k_2'k_1'}\, W_{k_3k_4k_4'k_3'}\, \delta_{k_1',k_3}\, \delta_{k_2',k_4}\, \underline{\delta_{k_3',k_1}\, \delta_{k_4',k_2}}$$

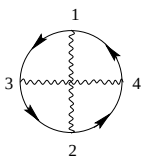

$$\Longrightarrow \quad \underbrace{f^2(1-f)^2}_{\omega\text{–sums}} \sum_{\substack{k_1k_2k_1'k_2' \\ k_3k_4k_3'k_4'}} W_{k_1k_2k_2'k_1'}\, W_{k_3k_4k_4'k_3'}\, \delta_{k_1',k_3}\, \delta_{k_2',k_4}\, \underline{\delta_{k_3',k_2}\, \delta_{k_4',k_1}}$$

The topological differences between the two connected diagrams appear in the underlined terms. We now discuss the reason why connected diagrams of the same group

have the same frequency sums. This is because those connected diagrams are restricted by the same energy conservation constraints at each interaction and no k–dependent ϵ_k appears in the Green's function. Hence, the ω–sums can be pulled out of the remaining k–sums. For example in the second order, we have $\omega_1+\omega_2=\omega_3+\omega_4$ at the interactions in both diagrams. After performing the momentum sums over all annihilation operator indices $(k_1^{'},k_2^{'},k_3^{'},k_4^{'})$, both second order diagrams

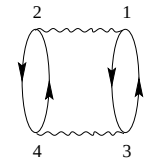

$$\Longrightarrow \qquad f^2(1-f)^2 \underbrace{\sum_{k_1k_2k_3k_4} W_{k_1k_2k_4k_3}\, W_{k_3k_4k_2k_1}}_{N_\phi\, W_a^{(2)}} \tag{4.40}$$

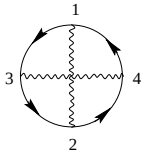

$$\Longrightarrow \qquad f^2(1-f)^2 \underbrace{\sum_{k_1k_2k_3k_4} W_{k_1k_2k_4k_3}\, W_{k_3k_4k_1k_2}}_{-N_\phi\, W_a^{(2)}} \tag{4.41}$$

differ only by a minus sign according to Eq. (4.39). We also see that there is only *one* group of diagrams and this corresponds in our language to *one* proper pattern instead of to *two* connected diagrams.

In the third order, we can group *six* connected diagrams into *two* groups which means we have *two* proper patterns in the third order instead of *six* connected diagrams. The groupings and the corresponding proper patterns in the second and third orders are shown in Fig. 4.5.

We can now compare the free energy of Ref. [28] with the result of our approach. After Eq. (4) of Ref. [28], the free energy is written as

$$F(\nu) \;=\; F_{\rm HF}(\nu) + \alpha^{(2)}(\nu)\;\beta + \alpha^{(3)}(\nu)\;\beta^2 + \mathcal{O}(\beta^3)\;. \tag{4.42}$$

Note that the expansion coefficients for the free energy $\alpha^{(n)}(\nu)$ of Ref. [28] are different from those for the energy, $\alpha_n(\nu)$ which we use in this work. Using the results of the frequency sums given in Appendix D together with the symmetry factors given in Ref. [28], the coefficients $\alpha^{(2)}(\nu)$, and $\alpha^{(3)}(\nu)$ for an arbitrary interaction $W^F(r)$ are

$$F_{\rm HF}(\nu) \;=\; N_\phi \left\{ T\left[\nu\;\ln\nu + (1-\nu)\;\ln(1-\nu)\right] + \nu^2\, W_a^{(1)} \right\}, \tag{4.43}$$

$$\alpha^{(2)}(\nu) \;=\; \frac{1}{4}\left\{ \quad - \quad \right\} \;=\; -\frac{1}{2}\, N_\phi\, \nu^2\, (1-\nu)^2\, W_a^{(2)}\;, \tag{4.44}$$

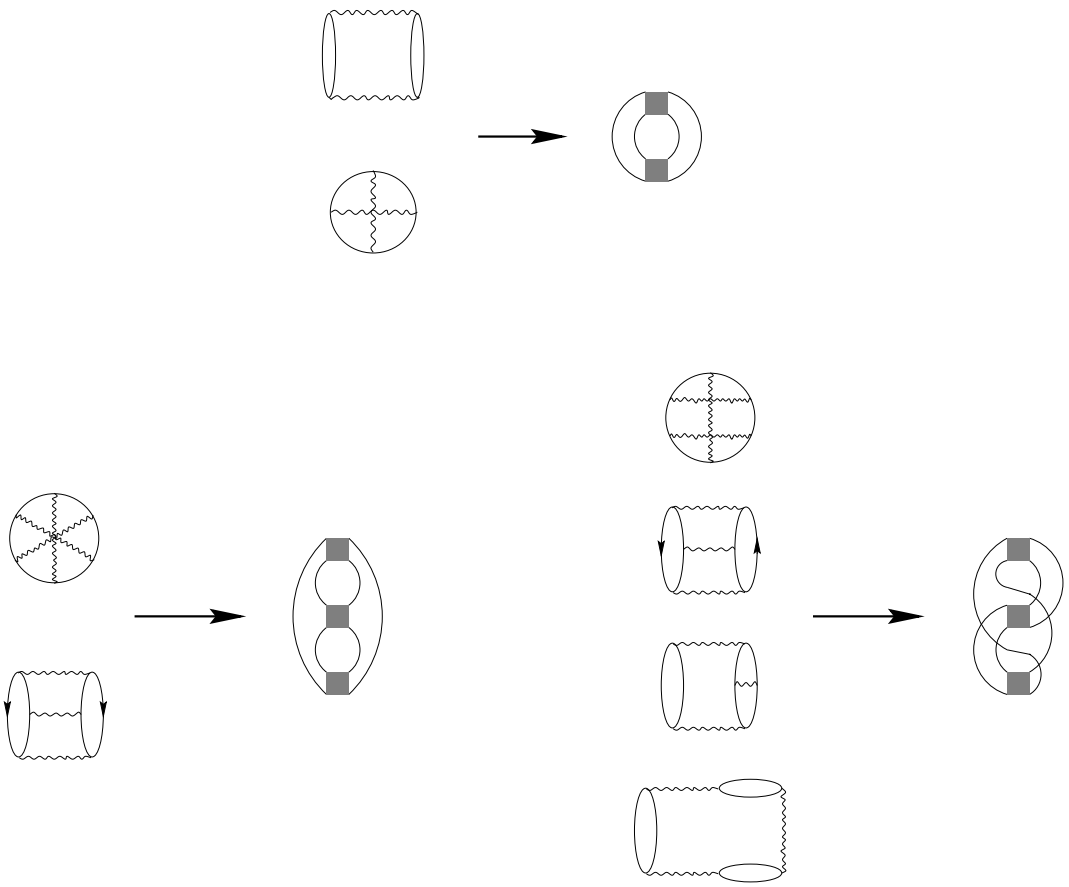

Figure 4.5: The connected diagrams and the corresponding proper patterns in the second order and the third order.

$$\alpha^{(3)}(\nu) = \frac{1}{6}\left\{ \quad - \quad + \; 3 \quad - \quad + \quad - \; 3 \quad \right\}$$

$$= \frac{1}{6}\, N_\phi \, \left[\left(\nu^4\,(1-\nu)^2 + \nu^2\,(1-\nu)^4\right)\, W_a^{(3)} + 8\,\nu^3\,(1-\nu)^3\, W_b^{(3)}\right] . \qquad (4.45)$$

In comparison, the free energy derived from Eq. (B.7) and Eq. (B.9) together with Eq. (4.18) and Eq. (6.3) can be written as

$$F(T, N_\phi, \nu) = N_\phi \left\{ T\,\left[\nu\,\ln\nu + (1-\nu)\,\ln(1-\nu)\right] + \nu^2\,\mathcal{C}^{(1)} + \frac{1}{2}\beta\,\nu^2\,(1-\nu)^2\,\mathcal{C}_1^{(2)} \right.$$

$$\left. + \frac{1}{3}\,\beta^2\,\left[\left(\nu^4\,(1-\nu)^2 + \nu^2\,(1-\nu)^4\right)\,\mathcal{C}_1^{(3)} + \nu^3\,(1-\nu)^3\,\mathcal{C}_0^{(3)}\right] + \mathcal{O}(\beta^3) \right\} . \qquad (4.46)$$

We get from the high–temperature expansion $\mathcal{C}^{(1)} = W_a^{(1)}$, $\mathcal{C}_0^{(2)} = -W_a^{(2)}$, $\mathcal{C}_1^{(3)} = \frac{1}{2}W_a^{(3)}$,

and $\mathcal{C}_0^{(3)} = 4W_b^{(3)}$. Thus, Eq. (4.42) and Eq. (4.46) coincide. and we have shown explicitly up to the third order, the equivalence of the present method to the traditional perturbative treatment used in the work of L. Zheng and A. H. MacDonald in Ref. [28].

To conclude this section, we write down the main result, the energy, up to the third order

$$E(T,N_\phi,\nu) \;=\; N_\phi \left\{ \nu^2\, W_a^{(1)} - \beta\, \nu^2\, (1-\nu)^2\, W_a^{(2)} \right.$$
$$\left. +\frac{1}{2}\,\beta^2\, \left[\left(\nu^4\,(1-\nu)^2 + \nu^2\,(1-\nu)^4 \right)\, W_a^{(3)} + 8\,\nu^3\,(1-\nu)^3\, W_b^{(3)} \right] + \mathcal{O}(\beta^3) \right\}, \tag{4.47}$$

where the patterns needed in evaluating Eq. (4.47) for an arbitrary interaction are as follows

$$W_a^{(1)} \;=\; \frac{1}{2\pi} \int d^2r\; W^F(r) \tag{4.48}$$

$$W_a^{(2)} \;=\; \frac{1}{2} \prod_{j=1}^{2} \left(\frac{1}{2\pi} \int d^2r_j\; W^F(r_j) \right)\; e^{-\frac{1}{4}\left[(x_1+x_2)^2+(y_1+y_2)^2\right]} \tag{4.49}$$

$$W_a^{(3)} \;=\; \frac{1}{4} \prod_{j=1}^{3} \left(\frac{1}{2\pi} \int d^2r_j\; W^F(r_j) \right) e^{-\frac{1}{4}\left[\vec{x}^2+\vec{y}^2-(\vec{x}-i\,\vec{y})\;\hat{M}_a^{(3)}\;(\vec{x}+i\,\vec{y})\right]} \tag{4.50}$$

$$W_b^{(3)} \;=\; \frac{1}{3} \prod_{j=1}^{3} \left(\frac{1}{2\pi} \int d^2r_j\; W^F(r_j) \right) e^{-\frac{1}{6}\left[(x_1+x_2+x_3)^2+(y_1+y_2+y_3)^2\right]} \tag{4.51}$$

where $\hat{M}_a^{(3)}$ is given in Eq. (4.36) and $\vec{x} = (x_1, x_2, x_3)$ and similarly for $\vec{y}$ and $\vec{r}_j = (x_j, y_j)$. This result generalises the third order result of L. Zheng and A. H. MacDonald [28] to the case of an arbitrary interaction up to this order of the high–temperature expansion.

Chapter 5

Evaluation of the high–temperature expansion for zero–range interaction

In this chapter, we first evaluate the proper patterns $W_p^{(n)}$ specifically for zero–range interactions. These interactions have been introduced in Section 3.4. We shall see that the calculation of $W_p^{(n)}$ for these interactions is greatly simplified by the differential representation of the interaction matrix elements which was introduced in Section 3.4.1.

In the second part of the chapter, we shall check the result of the high–temperature expansion with the Virial expansion up to the lowest order in ν.

5.1 Calculation of a proper pattern of order n for arbitrary zero–range interaction

The general expression of a proper pattern of order n is taken from the first equality in Eq. (4.29)

$$W_p^{(n)} = \frac{1}{\left|\det \hat{Q}_p^{(n)}\right|} \left(\frac{1}{2\pi}\right)^{n/2} \prod_{j=1}^{n} \left(\int_{-\infty}^{\infty} \frac{dq_j}{2\pi} \right) e^{-\frac{1}{4}\left(\vec{q}^2 + (\hat{M}_p^{(n)}\vec{q})^2\right)} \prod_{j=1}^{n} \left(\int d^2 r_j \, W(r_j) \, e^{-\frac{1}{2}x_j^2 - \frac{i}{2}\left(\vec{q} - \hat{M}_p^{(n)}\vec{q}\right)_j y_j - \frac{1}{2}\left(\vec{q} + \hat{M}_p^{(n)}\vec{q}\right)_j x_j} \right) . \quad (5.1)$$

Bearing in mind that $\hat{M}_p^{(n)}\vec{q}$ is nothing but the former variable $\vec{p}$, we then identify the spatial integrals in the above expression with the spatial integrals in Eq. (3.36). Thus, we can make use of the result of the integrals from Eq. (3.42). By comparing Eq. (3.36) with Eq. (3.42), we see that the above equation can be written in differential form as

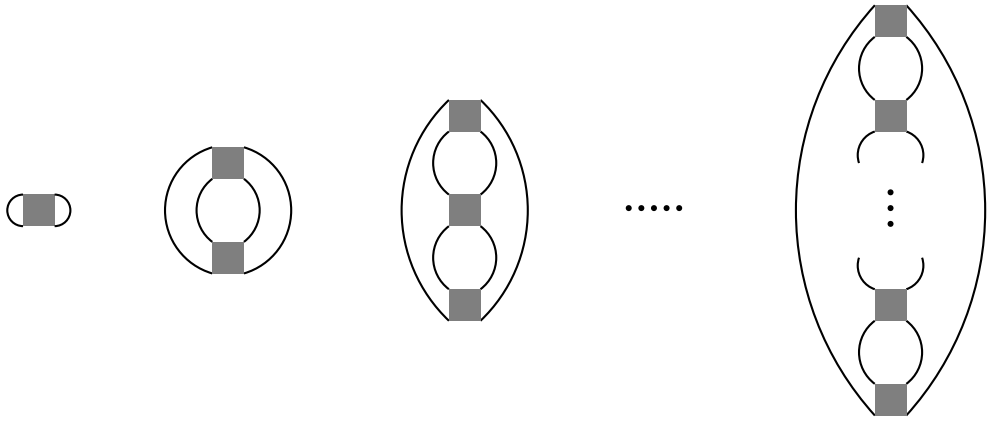

Figure 5.1: The proper patterns $W_a^{(n)}$.

$$W_p^{(n)} = \frac{1}{\left|\det \hat{Q}_p^{(n)}\right|} \left(\frac{2}{\pi}\right)^{n/2} \prod_{j=1}^{n} \left(\sum_{m_j=0}^{\infty} \frac{W_{2m_j+1}}{(2m_j+1)!} \, \partial_{\alpha_j}^{2m_j+1} \, \partial_{\beta_j}^{2m_j+1} \right) e^{-\frac{1}{2}(\vec{\alpha}^2+\vec{\beta}^2)}$$
$$\prod_{j=1}^{n} \left(\int_{-\infty}^{\infty} dq_j \right) e^{-\frac{1}{2}\,\vec{q}^2+\vec{\alpha}\,\hat{M}_p^{(n)}\vec{q}+\vec{\beta}\,\vec{q}} \Big|_{\vec{\alpha}=\vec{\beta}=0} . \tag{5.2}$$

At this point, the integrals on q_j can be performed immediately, and we get

$$W_p^{(n)} = \frac{2^n}{\left|\det \hat{Q}_p^{(n)}\right|} \prod_{j=1}^{n} \left(\sum_{m_j=0}^{\infty} \frac{W_{2m_j+1}}{(2m_j+1)!} \, \partial_{\alpha_j}^{2m_j+1} \, \partial_{\beta_j}^{2m_j+1} \right) e^{\vec{\alpha}\,\hat{M}_p^{(n)}\,\vec{\beta}} \Big|_{\vec{\alpha}=\vec{\beta}=0} \tag{5.3}$$

Thus, we have reduced the evaluation of a proper pattern to differentiations which are performed by a symbolic computer program. This program determines for a given proper pattern the matrices $\hat{Q}_p^{(n)}$ and $\hat{M}_p^{(n)}$ and then performs the differentiations for a given interaction model. The matrices $\hat{Q}_p^{(n)}$ and $\hat{M}_p^{(n)}$ characterise a given pattern and need to be determined only once for all interactions. For $n = 1, \ldots, 4$, they are listed in Appendix C.

5.1.1 The special patterns $W_a^{(n)}$

In this section, we shall evaluate the special patterns, $W_a^{(n)}$ which have the structure as shown in Fig. 5.1. Patterns of this type are interesting because they, and only they, yield the prefactors of the *lowest power* in ν, proportional to ν^2, in the energy. Therefore, if we can calculate $W_a^{(n)}$, we can check our method for arbitrary order of the temperature with the second order result of the Virial expansion which we shall derive in Section 5.2.

We consider a cumulant average $< H^n >_c$ and its evaluation with Wick's theorem. In order to get the lowest power of ν, one needs to have the highest power of $(1-\nu)$, i. e., one has to contract each annihilation operator to its nearest neighbour creation operator of the next two–body Hamiltonian on the right. Thus, there is only *one* way to contract all operators to get the lowest power of ν:

$$\Big\langle \underbrace{c^\dagger \; \overbrace{c^\dagger \; c \; \overbrace{c \quad c^\dagger}} \; c^\dagger \; \overbrace{c \; \overbrace{c \quad c^\dagger} \; c^\dagger} \; c \; c \quad \cdots \quad c^\dagger \; c^\dagger \; c}_{} \; c \Big\rangle \tag{5.4}$$

At each Hamiltonian, the operators $c^\dagger$ can be permuted, and this cancels the prefactors of 1/2. This leads to $\Omega_n(z) \; = \; \frac{(-1)^{n-1}}{n!} \left[f^2 \; W_a^{(n)} + \mathcal{O}(f^3) \right]$.

The matrices $M_a^{(n)}$ which correspond to the patterns $W_a^{(n)}$ (or the above contraction) can be written as

$$\hat{M}_a^{(n)} = \begin{pmatrix} 0 & 0 & 0 & \cdots & 0 & 1 \\ 1 & 0 & 0 & \cdots & 0 & 0 \\ 0 & 1 & 0 & \cdots & 0 & 0 \\ 0 & 0 & 1 & \cdots & 0 & 0 \\ \vdots & \vdots & \vdots & \ddots & \vdots & \vdots \\ 0 & 0 & 0 & \cdots & 1 & 0 \end{pmatrix}_{n,n} \; . \tag{5.5}$$

The evaluation of Eq. (5.3) for these $M_a^{(n)}$ can be done very easily. The exponent in Eq. (5.3) becomes

$$e^{\vec{\alpha} \; \hat{M}_a^{(n)} \; \vec{\beta}} = e^{\alpha_2 \; \beta_1 + \alpha_3 \; \beta_2 + \cdots + \alpha_n \; \beta_{n-1} + \alpha_1 \; \beta_n} \; . \tag{5.6}$$

Then, we differentiate this exponential function with respect to each variable (α_i, β_i) and finally take the limit $\vec{\alpha} = \vec{\beta} = 0$. We observe that the differentiations of the above exponential function will lead to zero after taking the limits, unless all differentiations appear in the same order m, i. e.,

$$\begin{aligned} & \partial_{\alpha_1}^{2m_1+1} \cdots \partial_{\alpha_n}^{2m_n+1} \quad \partial_{\beta_1}^{2m_1+1} \cdots \partial_{\beta_n}^{2m_n+1} \; e^{\alpha_2 \; \beta_1 + \alpha_3 \; \beta_2 + \cdots + \alpha_n \; \beta_{n-1} + \alpha_1 \; \beta_n} \quad \Big|_{\vec{\alpha}=\vec{\beta}=0} \\ = \; & \partial_{\alpha_1}^{2m_1+1} \cdots \partial_{\alpha_n}^{2m_n+1} \; \alpha_1^{2m_n+1} \; \alpha_2^{2m_1+1} \cdots \alpha_n^{2m_{n-1}+1} \quad \Big|_{\vec{\alpha}=0} \\ = \; & \sum_m \prod_{j=1}^{n} \Big((2m_j+1)! \;\; \delta_{m_j,m} \Big) \; . \end{aligned} \tag{5.7}$$

Thus, we have in total

$$\prod_{j=1}^{n} \left(\sum_{m_j=0}^{\infty} \frac{W_{2m_j+1}}{(2m_j+1)!} \; \partial_{\alpha_j}^{2m_j+1} \; \partial_{\beta_j}^{2m_j+1} \right) \quad e^{\vec{\alpha} \; \hat{M}_a^{(n)} \; \vec{\beta}} \quad \Big|_{\vec{\alpha}=\vec{\beta}=0} = \sum_{m=0}^{\infty} \Big(W_{2m+1} \Big)^n \; . \tag{5.8}$$

The matrices $Q_a^{(n)}$ have a special structure too, see Appendix C. We find in the order $n \geq 1$, $\left|\det \hat{Q}_a^{(n)}\right| = 2^{n-1}$. Thus, we have $W_a^{(n)} = 2 \sum_{m=0}^{\infty} \left(W_{2m+1}\right)^n$ and

$$\Omega_n(z) = \frac{(-1)^{n-1}}{n!} \left(2\, f^2 \sum_{m=0}^{\infty} \left(W_{2m+1}\right)^n + \mathcal{O}(f^3) \right) . \tag{5.9}$$

From the relation between $E(T, N_\phi, \mu)$ and $\Omega(T, N_\phi, \mu)$ in Eq. (B.4) (in the lowest power in ν, we can simply replace f by ν), we can express our result in terms of the coefficients $\mathcal{C}_{n-2}^{(n)}$, defined in Eq. (4.18):

$$\mathcal{C}_{n-2}^{(n)} = \frac{(-1)^{n-1}}{(n-1)!} \sum_{m=0}^{\infty} 2 \left(W_{2m+1}\right)^n . \tag{5.10}$$

5.2 Low density limit, Virial expansion

In this section, we shall calculate the grand canonical thermodynamic potential of the quantum Hall system in the Virial expansion. The Virial expansion has been used before by K. Tevosyan and A. H. MacDonald [29] to study the system for the W_1–interaction. Here, we shall generalise their method to an arbitrary zero–range interaction. We shall calculate the grand canonical thermodynamic potential up to the second order in the electron density. Then we shall proceed to calculate the energy as a function of the electron density, and compare with the result of the previous section.

We start with the general expression of the grand canonical thermodynamic potential $\Omega(T, N_\phi, z)$ for the lowest Landau level with N_ϕ states. The Virial expansion is an expansion in the fugacity $z = e^{\beta\,\mu}$. Hamiltonian and particle number are commutative. The zero–energy level is fixed at the lowest Landau level, thus there is no one–body energy in the consideration. We get up to second order in z

$$\begin{aligned} \Omega(T, N_\phi, \mu) &\equiv -T \ln \left\{ \sum_{N=0}^{\infty} \mathrm{Tr}_{(N)} \left[e^{-\beta\,(H_{(N)} - \mu N)} \right] \right\} \\ &= -T \ln \left\{ \mathrm{Tr}_{(0)}\,[1] + \mathrm{Tr}_{(1)} \left[e^{\beta\,\mu} \right] + \mathrm{Tr}_{(2)} \left[e^{-\beta\, H_{(2)} + 2\,\beta\,\mu} \right] + \mathcal{O}(e^{3\,\beta\,\mu}) \right\} , \end{aligned} \tag{5.11}$$

where $\mathrm{Tr}_{(N)}$ denotes the sum over all possible states of N particles. Thus, $\mathrm{Tr}_{(0)}\,[1] = 1$, and $\mathrm{Tr}_{(1)} \left[e^{\beta\,\mu} \right] = z\, N_\phi$.

The two–particle trace can be evaluated, since we know all the eigenvalues of the two–body problem, see Section 3.3. Using the degeneracy of the states that have energy W_{2m+1} (calculated in Ref. [29]) we have

$$
\begin{aligned}
&\mathrm{Tr}_{(2)}\left[e^{-\beta\,H_{(2)}+2\,\beta\,\mu)}\right] = \\
&\quad \left\{\tfrac{N_\phi\,(N_\phi-1)-(N_\phi-2)\,(N_\phi-3)}{2}\,e^{-\beta\,W_1} + \tfrac{(N_\phi-2)\,(N_\phi-3)-(N_\phi-4)\,(N_\phi-5)}{2}\,e^{-\beta\,W_3}+\cdots\right\}\,e^{2\,\beta\,\mu} \\
&= \frac{z^2}{2}\sum_{m=0}\left\{[N_\phi-2m][N_\phi-(2m+1)]-[N_\phi-(2m+2)][N_\phi-(2m+3)]\right\}\,e^{-\beta\,W_{2m+1}}
\end{aligned}
\tag{5.12}
$$

Then, we get (cutting the summation off at the highest possible relative angular momentum, $2m+1=N_\phi$)

$$
\Omega(T,N_\phi,\mu) = -T\ln\left\{1+z\;N_\phi+z^2\sum_{m=0}^{(N_\phi-1)/2}(2N_\phi-4m-3)\;e^{-\beta\,W_{2m+1}}+\mathcal{O}(z^3)\right\}\,. \tag{5.13}
$$

Next, we expand the logarithm to get the final form of $\Omega(T,N_\phi,\mu)$ up to the second order in the fugacity z. In the thermodynamic limit, we get:

$$
\Omega(T,N_\phi,\mu) = -\frac{N_\phi}{\beta}\,\left\{z-\frac{z^2}{2}\,\left[1-4\sum_{m=0}^{\infty}\left(e^{-\beta\,W_{2m+1}}-1\right)\right]+\mathcal{O}(z^3)\right\}\,. \tag{5.14}
$$

Then, the energy and the filling factor are

$$
E(T,N_\phi,\mu) = N_\phi\;2\;z^2\sum_{m=0}^{\infty}W_{2m+1}\;e^{-\beta\,W_{2m+1}}+\mathcal{O}(z^3)\,, \tag{5.15}
$$

$$
\nu(z,T) = z-z^2\left[1-4\sum_{m=0}^{\infty}\left(e^{-\beta\,W_{2m+1}}-1\right)\right]+\mathcal{O}(z^3)\,. \tag{5.16}
$$

In this order, we can simply replace z by ν since the energy in this second order contains only one term, already of the second order in the fugacity. Thus, the energy becomes after expanding in β

$$
E(T,N_\phi,\nu) = N_\phi\;\nu^2\sum_{n=1}^{\infty}(-\beta)^{n-1}\,\frac{2}{(n-1)!}\sum_{m=0}^{\infty}\left(W_{2m+1}\right)^n+\mathcal{O}(\nu^3)\,. \tag{5.17}
$$

The coefficients $\mathcal{C}_{n-2}^{(n)}$ read off from Eq. (5.17) are equivalent to those derived from the high–temperature expansion given in Eq. (5.10). Thus, we have proven explicitly the equivalence of the high–temperature expansion series in the second order in the electron density with the Virial expansion method.

Part IV

Results

Chapter 6

Energy and compressibility in the lowest Landau level: Exact high–temperature expansion results

In this chapter, we shall present the results obtained from the calculation set up in the chapters two to five. There will be two thermodynamic properties studied here, the energy and the compressibility. We shall give the direct, exact results obtained from the high–temperature expansion at finite temperature in this chapter and show extrapolations to zero temperature in the next chapter.

The interaction matrix elements as given in Eq. (3.42) contain an infinite number of parameters, the pseudopotential coefficients W_{2m+1}, Eq. (3.32), [71, 33]. Here, we shall study only those interactions for which the first two of the pseudopotential coefficients are non–zero. We have two purposes in mind for using such an interaction.

First, we check our method by applying it to a known case: An interaction with just *one* non–zero pseudopotential coefficient , (*one–component interactions*), say W_{2m+1}–interaction, is known to have the Laughlin state with an exponent $2m+3,\ m \geq 0$ [7] as ground states at $\nu = \nu_m = 1/(2m+3)$. It is an incompressible state, thus, the energy per particle has a cusp [23], the chemical potential jumps, and the inverse compressibility becomes infinity at ν_m at zero temperature. The magnitude of this interaction, W_{2m+1}, sets the energy scale. The size of the energy gap above the ground state is also proportional to the magnitude of the interaction. Thus, studying the one–component interactions, we can analyse how much of this we can see in a high–temperature expansion up to the order considered here.

Second, we use our method, after realising its validity and applicability, to study a more general interaction for which there are more than one pseudopotential coefficients in the interaction matrix elements (*multi–component interaction*). The above picture, quite clear in the case of the one–component interaction, is not longer so clear in the case of multi–component interactions because, for the $(W_1 + W_3)$–interaction, there are at least two (competitive) energy scales, W_1 and W_3. Here, it is strictly unknown how

the energy or any thermodynamic quantity should behave, in particular, between the filling factors $\nu = 1/5$ and $\nu = 1/3$. We characterise a multi–component interaction by the ratios between the components. Here, we have the ratio $R = W_1/W_3$. The multi–component $(W_1 + W_3)$–interaction will be considered as a W_1 dominant interaction when $R >> 1$. Physical interactions such as the Coulomb interaction which decay with increasing distance have $R > 1$ ($R = 1.6$ in case of the Coulomb interaction), but here we shall study both $R > 1$ and $R < 1$ because we would like to study the transition between two pure cases, $W_1 \neq 0, W_3 = 0$ and $W_1 = 0, W_3 \neq 0$.

The energy will be the first quantity we study and then we shall proceed to the compressibility. Our variables here are the filling factor $\nu = N/N_\phi$, and the temperature T. First, we wish to study the effect of the temperature, or the development into the fractional quantum Hall states as the temperature is lowered. By analysing the inverse compressibility, we shall find and develop a tool to indicate the transition. Second, we wish to study how the transition is influenced by the interaction and how the picture changes as the interaction is varied.

We should like to note that the previous finite temperature study of Ref. [29] summarised "the thermodynamic signature of the fractional quantum Hall effect is completely absent when the temperature reaches half of the gap temperature". We shall see below that, in the order considered here, there are already indications of a development of the fractional quantum Hall ground state as T approaches half of the value of the interaction.

Temperature scale

In the presentations of our results, we shall use a scaled temperature. The only energy scale of the system comes from the interaction. To have a clear understanding of the temperature or energy scale used below, we should like to have here a brief discussion.

1. We shall use τ as a dimensionless measure of the temperature,

$$\tau = \frac{T}{W_{tot}} \; . \tag{6.1}$$

   Here, the total interaction W_{tot} is defined as half of the energy per particle of the completely filled lowest Landau level. For example, $W_{tot} = W_1$ for the W_1–interaction and $W_{tot} = W_1 + W_3$ for the $(W_1 + W_3)$–interaction.

2. The total interaction will be used as the scale of the energy,

$$W_{tot} = 1 \; . \tag{6.2}$$

Thus, the energy per particle of the completely filled lowest Landau level is always 2 in our dimensionless units. Comparing two different interactions characterised by W_1

and $W_1 + W_3 > W_1$, we see that for $\tau_{W_1} = \tau_{(W_1+W_3)}$, the real temperatures are related by $T_{W_1}(\tau) < T_{(W_1+W_3)}(\tau)$. Similarly, for $T_{W_1} = T_{(W_1+W_3)}$, the scaled temperatures are related by $\tau_{W_1}(T) > \tau_{(W_1+W_3)}(T)$. We assume the strength of the phenomena of the fractional quantum Hall effect at $\nu = 1/(2m+3)$ to increase with the ratio W_{2m+1}/T. Consequently, we must study for multi–component interactions a lower scaled temperature τ than for the one–component interaction in order to observe phenomena of the same strength.

6.1 Energy

We have derived the energy $E(T, N_\phi, \nu)$ from the grand canonical thermodynamic potential in Section 4.3; there its structure has also been discussed, cf. Eq. (4.18). Here, we define the coefficients of the expansion of the energy, $\alpha_n(\nu)$, for $n \geq 2$ as

$$\alpha_n(\nu) = \sum_{m=-n+2}^{n-2} \nu^{n+m} \, (1-\nu)^{n-m} \, \mathcal{C}_m^{(n)} \; , \tag{6.3}$$

and for $n = 1$

$$\alpha_1(\nu) \; = \; \nu^2 \, \mathcal{C}^{(1)} \; = \; \nu^2 \, W_a^{(1)} \; = \; 2 \, \nu^2 \, \sum_{m=0}^{\infty} \, W_{2m+1} \; . \tag{6.4}$$

Since the Hamiltonian contains just a two–body interaction, at least two particles are required for the energy to become non–zero, therefore, the coefficients $\alpha_n(\nu)$ all start with ν^2. Then, the particle–hole symmetry requires its counter part $(1-\nu)$ to appear at least in the second power, too (see Section 4.3).

In the following, we analyse the energy per particle $\mathcal{E}(T, \nu)$,

$$\mathcal{E}(T, \nu) := \frac{E(T, N_\phi, \nu)}{N} = \frac{1}{\nu} \, \sum_{n=1}^{\infty} \, \beta^{n-1} \, \alpha_n(\nu) \; . \tag{6.5}$$

6.1.1 Energy of the one–component interaction system

In this section, we shall present results of the energy for the W_1–interactions and W_3–interactions. For the W_1–interaction interaction, we expect to see a cusp in the plot of $\mathcal{E}(T, \nu)$ as a function of ν developing around $\nu = 1/3$ as we come from high temperatures to lower temperatures, and for $\nu < 1/3$, $\mathcal{E}(T, \nu)$ should decrease to zero as $T \to 0$. We also expect the same behaviour for the W_3–interaction, but at $\nu = 1/5$. We show the results down to the lowest possible temperature where the expansion of the considered order is still valid, i. e., energy and specific heat are positive, unless it is explicitly mentioned.

W_1–interaction

Here, we study the energy of the W_1–interaction. The first coefficient functions for the W_1–interaction are given by

$$\begin{aligned}
\alpha_1(\nu) &= 2\,\nu^2\,W_1\,, \\
\alpha_2(\nu) &= -2\,(1-\nu)^2\,\nu^2\,W_1^2\,, \\
\alpha_3(\nu) &= \left[(1-\nu)^4\,\nu^2 - \tfrac{32}{27}\,(1-\nu)^3\,\nu^3 + (1-\nu)^2\,\nu^4\right]\,W_1^3\,. \qquad (6.6)
\end{aligned}$$

The numerical coefficients $\mathcal{C}_m^{(n)}$ up to $n = 8$ are given in Table 6.1 for $W_1 = 1$. They are exact fractions of very large integers (278 digits for the numerator of $\mathcal{C}_0^{(8)}$); for $n > 4$, we give only the leading 10 digits of the coefficients.

Fig. 6.1 shows the energy per particle as a function of the filling factor for various temperatures. The high–temperature result (dash–dotted straight line) is identical to the *Hartree–Fock approximation*, $\mathcal{E}^{HF}(T,\nu) = 2\,\nu$. As the temperature is lowered, it can be seen clearly how the expected cusp in $\mathcal{E}(T,\nu)$ develops around $\nu = 1/3$.

The plot (a) is the result up to the seventh order and the other plot (b) is the result up to the eighth order. We see that there is not a big change observed as we go up an order at this range of the temperature which is about half of the interaction. One change worth mentioning here concerns the approach to the origin of the energy per particle: The solid lines ($\tau = 0.5$) in both plots are very similar outside the region $\nu \leq 1/3$ but they approach the origin differently. The solid line in (a), the seventh order, approaches the origin with a finite slope of 0.311; the solid line in (b), the eighth order, approaches the origin with a slope of 0.260. This is to be compared with the exact slope 0.271 at $\tau = 0.5$ resulting from the Virial expansion derived below, see Eq. (5.17). If we lower the temperature a little bit more to $\tau = 0.45$, we see that the curve in (a) starts to oscillate and crosses the curve of $\tau = 0.5$. This shows, since the specific heat $C_v = \frac{\partial E}{\partial T} < 0$, that we leave the region of applicability of the high–

$n\backslash m$	0	1	2	3	4	5	6
3	$-\frac{32}{27}$	1					
4	$-\frac{548284}{253125}$	$\frac{352696}{253125}$	$-\frac{1}{3}$				
5	−2.010001778	3.319570883	−0.730235026	$\frac{1}{12}$			
6	−5.121609632	3.490438330	−3.274027914	0.186460176	$-\frac{1}{60}$		
7	−6.234653674	6.225558336	−6.163032602	2.259167774	0.0101135932	$\frac{1}{360}$	
8	−7.669623737	8.107220838	−12.60225176	7.387509731	−1.223529718	−0.033101824	$-\frac{1}{2520}$

Table 6.1: The coefficients $\mathcal{C}_m^{(n)}$ for the zero–range interaction $W_1 = 1$ for $n = 3, \ldots, 8$ and $m \geq 0$. For $n = 2$, the coefficient is $\mathcal{C}_0^{(2)} = -2$. For $m < 0$, $\mathcal{C}_m^{(n)}$ can be found from the particle–hole symmetry : $\mathcal{C}_m^{(n)} = \mathcal{C}_{-m}^{(n)}$.

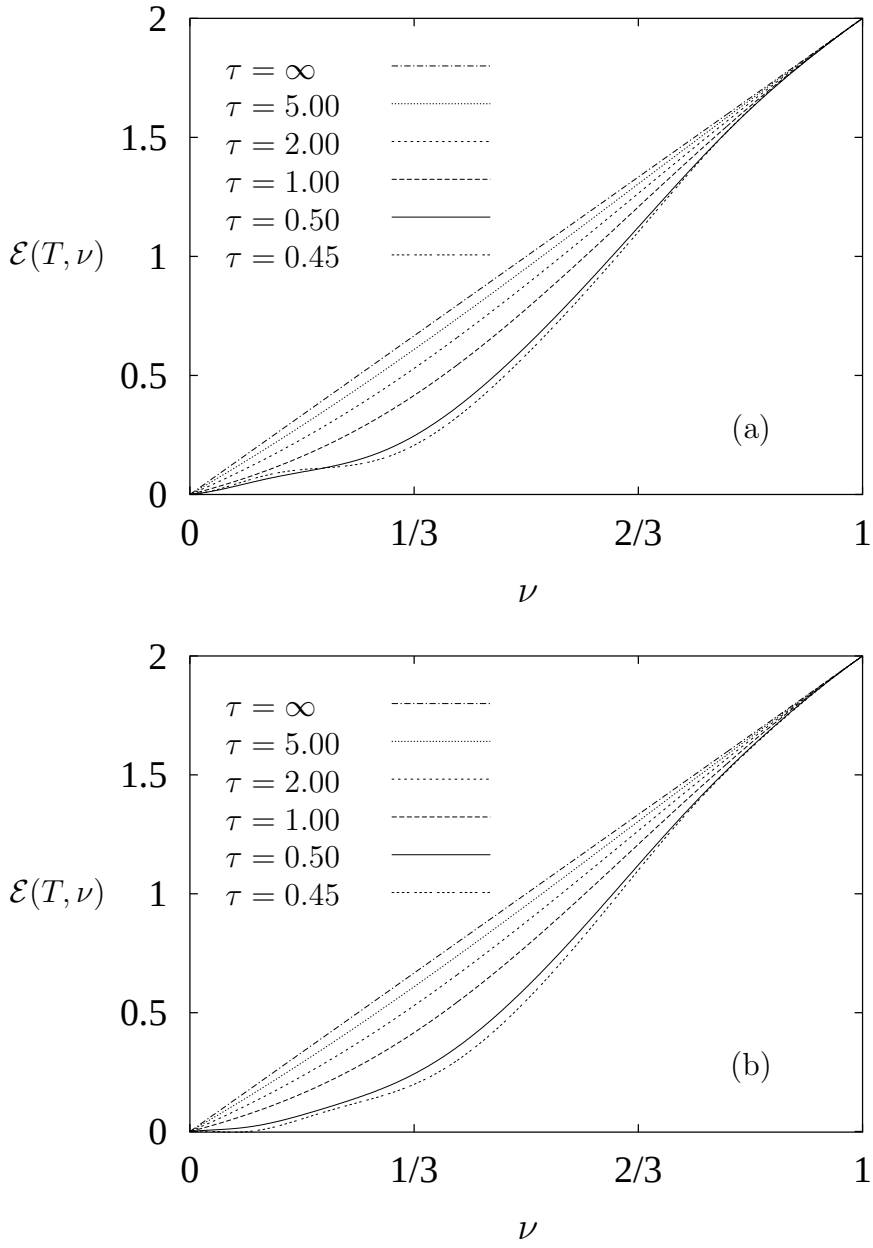

Figure 6.1: The energy per particle resulting from the high–temperature expansion up to (a) the *seventh* order and (b) the *eighth* order of the interaction for various temperatures for W_1–interaction; $\tau = T/W_1$.

temperature expansion in this order and at this temperature. However, the curve for the same temperature of the eighth order result still behaves correctly. It approaches the origin with approximately a zero slope for a longer range of ν than that of the higher temperature at $\tau = 0.5$. This is the improvement we expect to see when higher orders of the expansion are included. In Fig. 6.2 (a), we show how the results develop as we increase the order of the high–temperature expansion. We note that the result up to the fifth order, the upper line in Fig. 6.2 (a), behaves quite differently from other orders for the W_1–interaction. We found no reason for this exceptional behaviour of the fifth order result in the case of the W_1–interaction. We also note that the energies per particle of all orders are quite close (except that of the fifth order) as the filling factor increases beyond $\nu = 1/3$.

W_3–interaction

In the following, we study the energy of the W_3–interaction. The first coefficient functions for the W_3–interaction are given by

$$\begin{aligned} \alpha_1(\nu) &= 2\,\nu^2\,W_3\,, \\ \alpha_2(\nu) &= -2\,(1-\nu)^2\,\nu^2\,W_3^2\,, \\ \alpha_3(\nu) &= \left[(1-\nu)^4\,\nu^2 - \tfrac{16928}{19683}\,(1-\nu)^3\,\nu^3 + (1-\nu)^2\,\nu^4\right]\,W_3^3\,. \end{aligned} \tag{6.7}$$

The numerical coefficients $\mathcal{C}_m^{(n)}$ for the W_3–interaction up to $n = 8$ are given in Table 6.2 for $W_3 = 1$. They are exact fractions of very large integers (774 digits for the numerator of $\mathcal{C}_0^{(8)}$); for $n > 4$, we give only the leading 10 digits of the coefficients.

Fig. 6.3 shows the energy per particle as a function of the filling factor resulting from the high–temperature expansion series, up to (a) the fifth order, (b) the sixth order, (c) the seventh order and (d) the eighth order, for various temperatures. The straight line is the high temperature result and is identical to the Hartree–Fock energy

$n\backslash m$	0	1	2	3	4	5	6
3	$-\frac{16928}{19683}$	1					
4	$-\frac{5799768306163}{5766503906250}$	$\frac{6199729889464}{2883251953125}$	$-\frac{1}{3}$				
5	−0.963985143	−0.4295061834	−2.047214229	$\frac{1}{12}$			
6	-7.070002838	-6.888597076	-3.573818607	1.202422704	$-\frac{1}{60}$		
7	13.40613937	9.810730586	8.401506170	5.841265933	-0.516258970	$\frac{1}{360}$	
8	13.31554536	23.75605622	11.07580399	2.153473457	-5.019934738	0.176240420	$-\frac{1}{2520}$

Table 6.2: The coefficients $\mathcal{C}_m^{(n)}$ for the zero–range interaction $W_3 = 1$ for $n = 3, \ldots, 8$ and $m \geq 0$. For $n = 2$, the coefficient is $\mathcal{C}_0^{(2)} = -2$. For $m < 0$, $\mathcal{C}_m^{(n)}$ can be found from the particle–hole symmetry : $\mathcal{C}_m^{(n)} = \mathcal{C}_{-m}^{(n)}$.

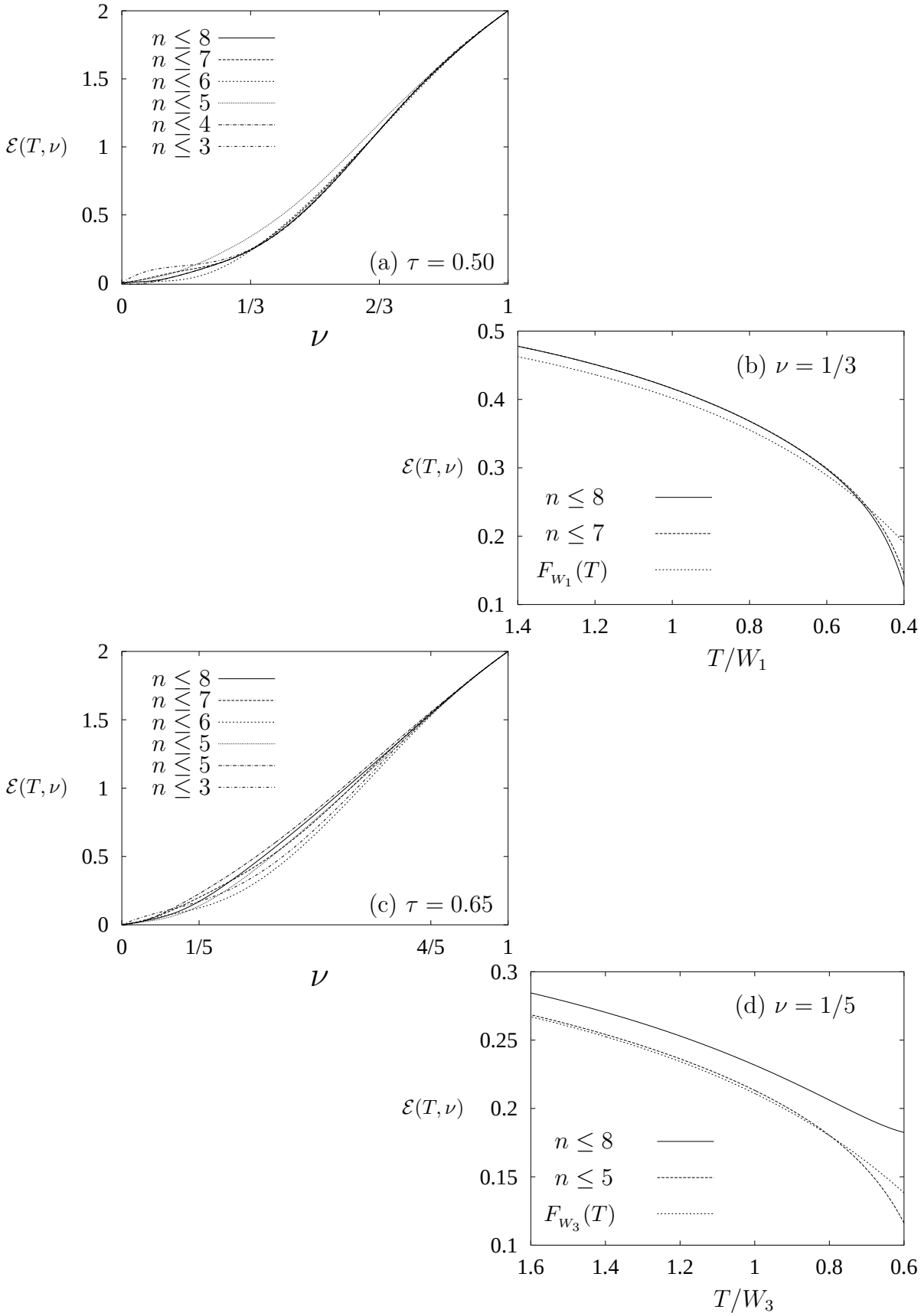

Figure 6.2: Energy per particle as a function of ν and T. W_1–interaction, (a) at $\tau = 0.50$ and (b) at $\nu = 1/3$ with a trial function $F_{W_1}(T) = 2/3\ e^{-0.480 W_1/T}$. W_3–interaction, (c) at $\tau = 0.65$ and (d) at $\nu = 1/5$ with a trial function $F_{W_3}(T) = 2/5\ e^{-0.615 W_3/T}$

as in the case of the W_1–interaction. There is a *weak* indication of a developing cusp in the energy per particle as the temperature approaches 0.65 in the neighbourhood of $\nu = 1/5$; $T = 0.65$ is the lowest temperature can be reached by the high–temperature expansion series up to the eighth order (the corresponding value is 0.45 for the W_1–interaction). There appear unphysical behaviours in the energy per particle when the temperature is lower than 0.65. As an example, we plot the energy per particle at $T = 0.55$, the short–dashed line in the plots in Fig. 6.3. For the result up to the fifth order, the energy per particle illustrates a clearer cusp at $\nu = 1/5$ but there is no improvement shown in any other higher order up to the eighth order. In the sixth order, the cusp appears to move away from $\nu = 1/5$. We see that the high–temperature expansion result for energy per particle up to the sixth order at $T = 0.55$ begins to oscillate in the small ν regime which shows that the temperature has become too low for the application of the high–temperature expansion result up to this order. In the seventh and the eighth orders, the energy per particle at $T = 0.55$ crosses the energy at higher temperatures at some filling factors which indicates that the specific heat becomes negative which is unphysical.

We can also see from Fig. 6.2(c) that at $T = 0.65$, the energy per particle still varies with the order, much more than in the corresponding case Fig. 6.2(a) of the W_1–interaction.

In Fig. 6.2(b) and Fig. 6.2(d), we fit the energy per particle at $\nu = 1/3$ for the W_1–interaction and at $\nu = 1/5$ for the W_3–interaction, respectively, with an exponential function of the form $A_{W_{2m+1}}\, e^{-\beta\, \Delta_{W_{2m+1}}}$. Very roughly, we determine the magnitude of the parameters $A_{W_{2m+1}}$ and $\Delta_{W_{2m+1}}$ which results in $A_{W_1} = 2/3$ and $\Delta_{W_1} = 0.480 W_1$, and $A_{W_3} = 2/5$ and $\Delta_{W_3} = 0.615 W_3$. If we interprete $\Delta_{W_{2m+1}}$ as the (approximated) size of the energy gap above the $\nu = 1/(2m+3)$–fractional quantum Hall state, we can reach the temperature of the magnitude of the energy gap by the high–temperature expansion result up to the eighth order. However, while we can reach a temperature just below the energy gap in case of the W_1–interaction, we cannot get to such low temperatures in the case of the W_3–interaction. (Note that we cannot compare quantitatively our estimates $\Delta_{W_{1,3}}$ for the zero–range interaction with the results for the gaps $\Delta_{1/3}$ and $\Delta_{1/5}$ for the Coulomb interaction. With a ratio $W_1/W_3 = 1.6$ for the Coulomb interaction, we find $\Delta_{W_1}/\Delta_{W_3} \sim 1.25$, while the numerical result is $\Delta_{1/3}/\Delta_{1/5} \sim 4$ from Refs. [7, 34].)

6.1.2 Energy of multi–component interaction system

Here, we study the energy per particle of the $(W_1{+}W_3)$–interaction system as a function of the filling factor and temperature with a parameter $R = W_1/W_3$ which marks the strength of the W_1–interaction compared to that of the W_3–interaction.

In Fig. 6.4, we show the energy per particle as function of the filling factor for various ratios R. We note that we do not show the curve of $\tau = 0.45$ and $\tau = 0.50$ in

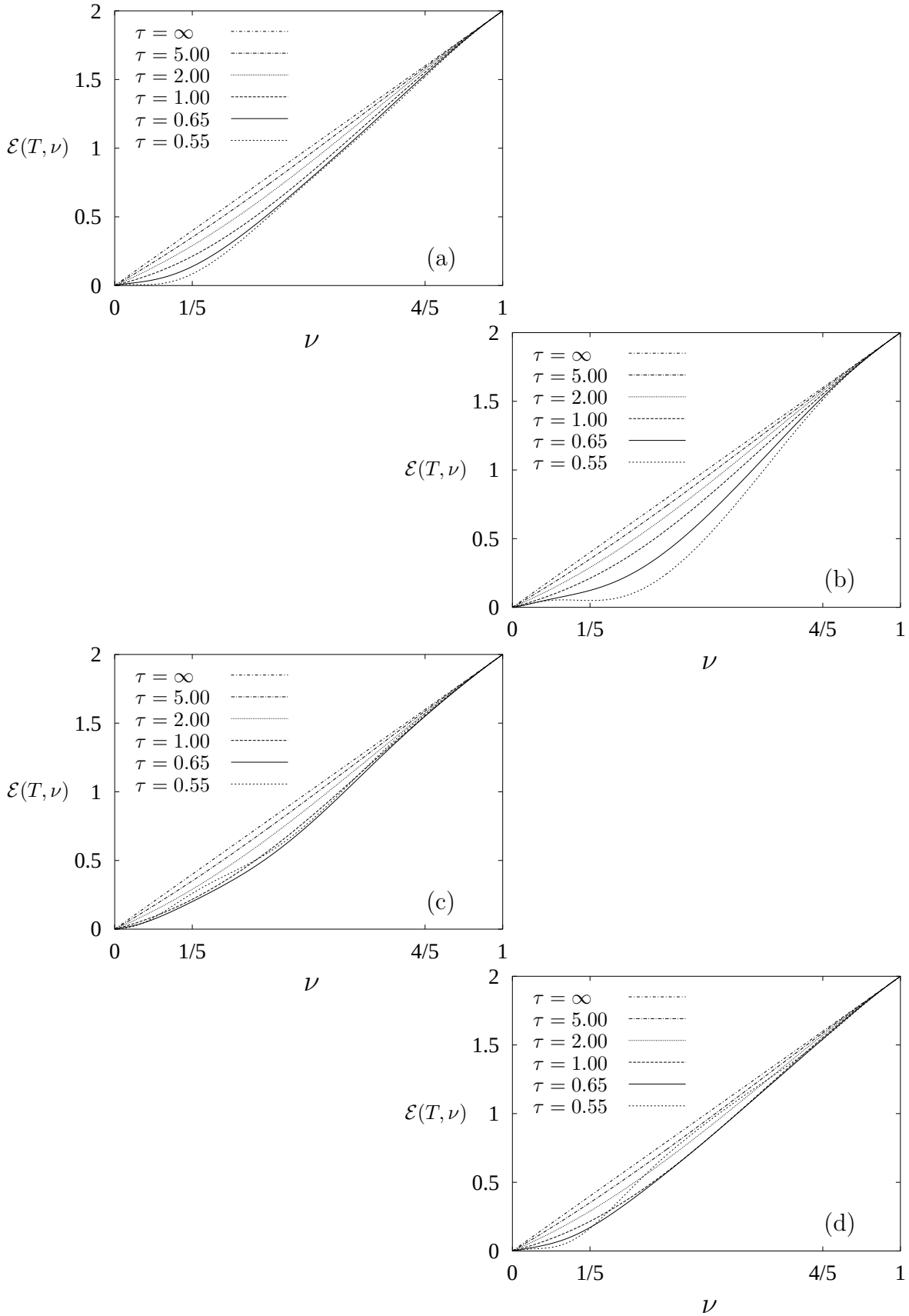

Figure 6.3: The energy per particle resulting from the high–temperature expansion up to (a) the *fifth* order, (b) the *sixth* order, (c) the *seventh* order and (d) the *eighth* order of the interaction for various temperatures for the W_3–interaction; $\tau = T/W_3$.

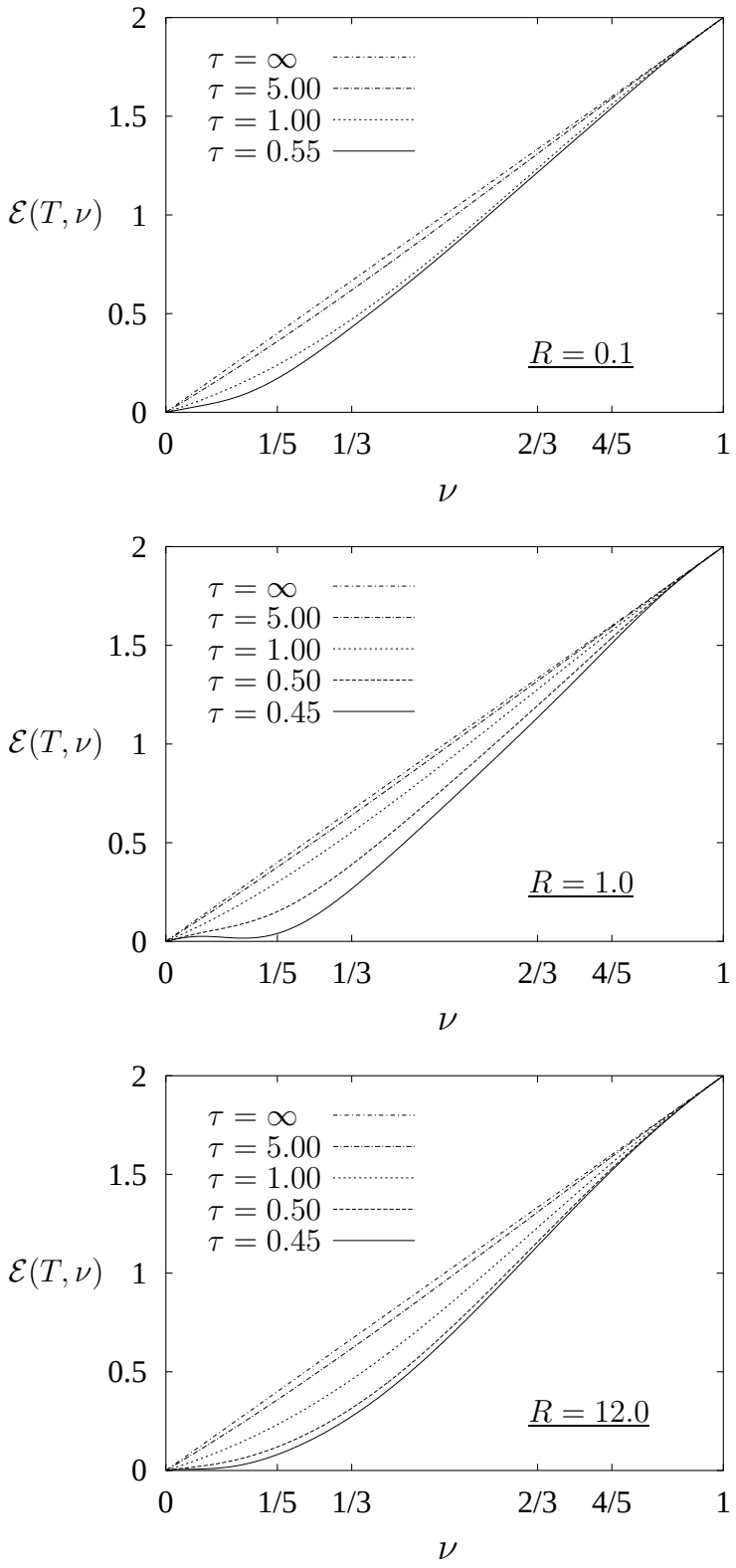

Figure 6.4: The energy per particle resulting from the high–temperature expansion up to the *eighth* order of the $(W_1 + W_3)$–interaction as a function of ν for various ratios $R = W_1/W_3$ and temperatures T, $\tau = T/(W_1 + W_3)$.

the plots of $R = 0.1$ (curves of these two temperatures are shown in plots of other R). The omitted curves, if included, would cross curves of higher temperatures at some filling factors indicating that these temperatures are too low for the application of the high–temperature expansion of this order for this R. One common behaviour of the three plots is how the energy develops in response to the decreasing of the temperature: The energy in the whole range of ν decreases with decreasing temperature and begins to develop a cusp at a particular filling factor.

Comparing the three plots, we can see that the location on the ν axis, where this cusp in the energy seems to develop, moves with the ratio R. It moves away from $\nu = 1/3$ towards $\nu = 1/5$ as R decreases. For the extreme cases, for very large and very small R, the energy per particle and the cusp behave similar to that of the corresponding one–component interaction. We note that adding a small perturbation of W_3 to the W_1–interaction lifts the energy per particle a little higher and adding a small perturbation of W_1 to the W_3–interaction smooths the energy per particle below $\nu = 1/3$.

In order to systematically study the development of the cusp in $\mathcal{E}(T, \nu)$, we need to extract the position of the cusp on the filling factor axis. According to the picture of the energy per particle described above, the first derivative, or the slope of $\mathcal{E}(T, \nu)$ with respect to ν, would become zero for $0 < \nu < \nu_{cusp}$ (ν_{cusp} denotes the filling factor where the cusp is found) and stay finite for $\nu > \nu_{cusp}$ as $T \to 0$. The slope for $0 < \nu < \nu_{cusp}$ would decrease with decreasing temperature, but for $\nu > \nu_{cusp}$ the slope would increase or stay constant with decreasing temperature. Thus, we solve numerically the following equation for ν

$$\frac{\partial}{\partial T} \frac{\partial \mathcal{E}(T, \nu)}{\partial \nu} = 0 , \tag{6.8}$$

and its smallest solution ν determines where the cusp develops. The solutions, $\nu_{cusp}(R, T)$, for given temperatures $T = 0.55, 0.65$, and 0.75 for ratios $10^{-4} < R < 10^4$ are plotted in Fig. 6.5. There is another solution at $1 - \nu_{cusp}(R, T)$; we show only the first half of the filling factor axis. R increases from top to bottom, from a W_3–dominant interaction to a W_1–dominant interaction.

There are various features in Fig. 6.5.

1. For *small* R, $R < 0.1$, ν_{cusp} is in the neighbourhood and on the left of $\nu = 1/5$.

2. ν_{cusp} varies strongly with R in the region $0.1 < R < 10$.

3. For *large* R, $R > 10$, ν_{cusp} is in the neighbourhood and on the right of $\nu = 1/3$.

The solution ν_{cusp} moves as the interaction changes. However, it appears to be very stable against a perturbation of the other component of the interaction; ν_{cusp} changes very little over a two orders of magnitude change of R, $10^{-4} < R < 10^{-2}$ and $10^2 < R < 10^4$.

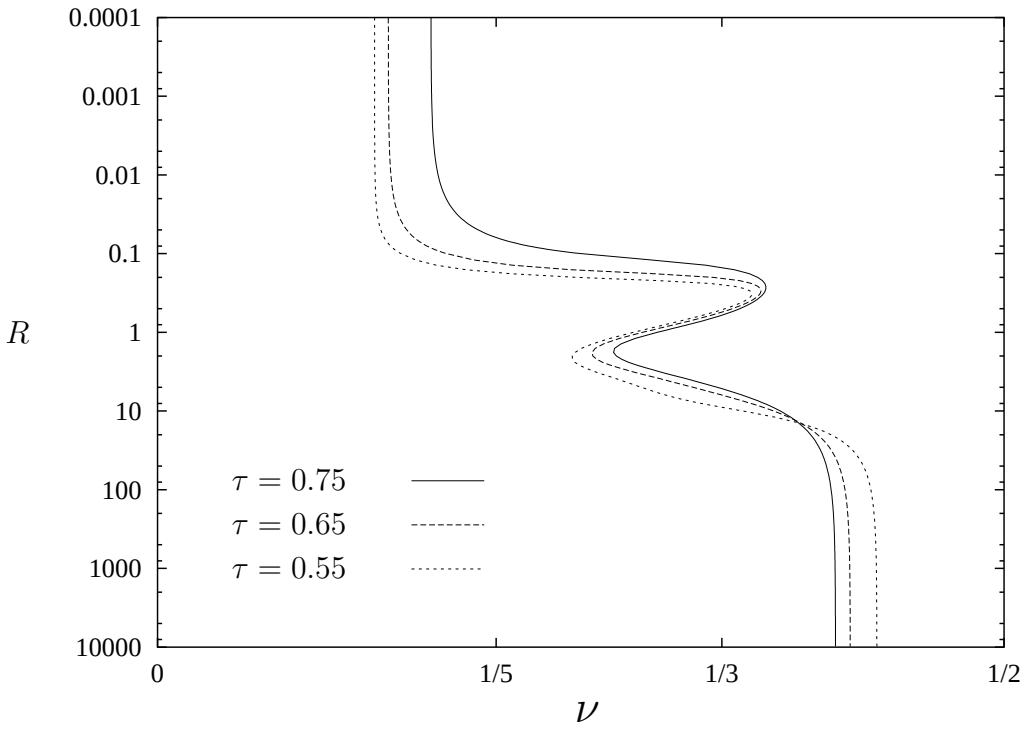

Figure 6.5: The smallest solution $\nu_{cusp}(R,T)$ of the equation $\frac{\partial^2 \mathcal{E}(T,\nu)}{\partial T\, \partial \nu} = 0$ for various ratios and temperature.

We conclude that the filling factor where the cusp in the energy per particle appears, ν_{cusp}, is related to the interaction but does not change much with the perturbation from the undominant component of the interaction.

6.2 Inverse compressibility

In this section, we shall study the inverse compressibility $\kappa_{_T}^{-1}(T,\nu)$ of the fractional quantum Hall system for various interactions. We note that the compressibility is a many–body quantity and reflects many–body properties. In studies of non–interacting systems (one–body problems), the compressibility is related to the single–particle density of states. In the present work, the Hamiltonian consists of only the interaction. Therefore, the inverse compressibility here cannot be simply interpreted by a density of states.

Our discussion shall start with the derivation of the high–temperature expansion series for the inverse compressibility. An intriguing feature in the results, *crossing points* will require special examination. Thus, we shall study the conditions under which these *crossing points* become possible. After finishing this general discussion, we shall present the results obtained by the high–temperature expansion calculation in the same manner as in the case of the energy.

6.2.1 The high–temperature expansion series for the inverse compressibility

In this section, we shall derive the high–temperature series for the inverse compressibility $\kappa_{_T}^{-1}(T,\nu)$ from the free energy, $F(T,N_\phi,\nu)$. The canonical free energy $F(T,N_\phi,\nu)$ is most conveniently derived from the energy $E(T,N_\phi,\nu)$ by integration as shown in Appendix B. From $F(T,N_\phi,\nu)$, we can find any thermodynamic quantity as a power series in the inverse temperature; the corresponding coefficients are related to the coefficients of the energy, $\alpha_n(\nu)$. These relations are also given in Appendix B for the thermodynamic quantities of interest.

The inverse compressibility $\kappa_{_T}^{-1}(T,\nu)$ is defined as

$$\kappa_{_T}^{-1}(T,\nu) \;\equiv\; -V\,\left(\frac{\partial P}{\partial V}\right)_{T,N} \tag{6.9}$$

where P and V are pressure and (two dimensional) volume, respectively.

Deriving P from the free energy, we write

$$\kappa_{_T}^{-1}(T,\nu) = \nu\,\left(\frac{\partial P}{\partial \nu}\right)_{T} = \frac{\nu^2}{2\pi}\left(\frac{\partial^2 (F/N_\phi)}{\partial \nu^2}\right)_{T}\,. \tag{6.10}$$

(Note that $\nu = 2\pi {l_B}^2 n_{el}$ and we use units in which the magnetic length, $l_B = \sqrt{\hbar c/|eB|}$, is unity.) Then, we write the high–temperature expansion series for $\kappa_{_T}^{-1}(T,\nu)$ (see Eq. (B.10)),

$$\kappa_{_T}^{-1}(T,\nu) = \frac{T}{2\pi}\;\frac{\nu}{1-\nu} + \frac{1}{2\pi}\;\sum_{n=1}^{\infty}\,\beta^{n-1}\,\frac{1}{n}\,\nu^2\;\frac{\partial^2\alpha_n(\nu)}{\partial\nu^2}\,. \tag{6.11}$$

The first part in the expression for $\kappa_{_T}^{-1}(T,\nu)$ in Eq. (6.11) is given by the non–interacting system; we define the second term as the *interacting part* of the inverse compressibility (for brevity, we shall call this quantity *interacting inverse compressibility*):

$$\kappa_{_{T,W}}^{-1}(T,\nu) \equiv \kappa_{_T}^{-1}(T,\nu) - \frac{T}{2\pi}\;\frac{\nu}{1-\nu} = \frac{1}{2\pi}\;\sum_{n=1}^{\infty}\,\beta^{n-1}\,\frac{1}{n}\,\nu^2\;\frac{\partial^2\alpha_n(\nu)}{\partial\nu^2}\,. \tag{6.12}$$

This quantity reflects *exclusively* the influence of the interaction on the inverse compressibility. From the particle–hole symmetry relation in the energy (cf. Eq. (4.18) and Eq. (B.6)), we see that $\alpha_n(\nu) = \alpha_n(1-\nu)$, for $n > 1$. Thus,

$$\frac{\partial^2\alpha_n(\nu)}{\partial\nu^2} = \frac{\partial^2\alpha_n(1-\nu)}{\partial(1-\nu)^2}\,. \tag{6.13}$$

Thus, we define the quantity

$$\kappa_{T,S}^{-1}(T,\nu) = \frac{1}{\nu^2}\ \kappa_T^{-1}(T,\nu)\ . \tag{6.14}$$

as particle–hole symmetric inverse compressibility.

A criterion for the inverse compressibility at small filling factors

The thermodynamic potential has been obtained in Eq. (5.14) in the lowest order of the Virial expansion. We calculate the pressure and then the inverse compressibility with the general result

$$\kappa_T^{-1}(T,\nu) = \frac{\nu\ T}{2\ \pi}\ \left\{1+\nu\ \left[1-4\ \sum_{m=0}^{\infty}\ \left(e^{-\beta W_{2m+1}}-1\right)\right]\right\} + \mathcal{O}\left(\nu^3\right)\ . \tag{6.15}$$

In case of the W_1–interaction, we get

$$\kappa_T^{-1}(T,\nu) = \frac{\nu\ T}{2\ \pi}\ \left[1+5\ \nu-4\ \nu\ e^{-\beta W_1}\right] + \mathcal{O}\left(\nu^3\right)\ . \tag{6.16}$$

This result is valid for all temperatures at small filling factor. The interacting part of the inverse compressibility is

$$\kappa_{T,W}^{-1}(T,\nu) = \frac{2\ \nu^2\ T}{\pi}\ \left[1-e^{-\beta W_1}\right] + \mathcal{O}\left(\nu^3\right)\ >\ 0\ , \tag{6.17}$$

and

$$\frac{\partial\kappa_{T,W}^{-1}(T,\nu)}{\partial T} = \frac{2\ \nu^2}{\pi}\ \left[1-(1+\beta W_1)\ e^{-\beta W_1}\right] + \mathcal{O}\left(\nu^3\right)\ >\ 0\ . \tag{6.18}$$

Thus, $\kappa_{T,W}^{-1}(T,\nu)$ must increase with the temperature near $\nu = 0$. We shall use this inequality as an criterion to check the validity of our results. Due to the particle–hole symmetry, the above considerations are valid correspondingly near $\nu = 1$.

6.2.2 Crossing points in the inverse compressibility: Sum rules for the pressure of the completely filled lowest Landau level

One of the common features seen in the plots of the inverse compressibility, Fig. 6.9–Fig. 6.16 below, for any interaction and order is *crossings* of the curves of different temperature at some filling factors. We shall address these crossings in the curves of the inverse compressibility as *crossing points*. Such a crossing point indicates that the inverse compressibility depends very weakly on the temperature at that particular filling factor for a narrow range of the temperature. These crossing points may move in the filling factor as the temperature changes from one region to the other, but there will be crossing points in the inverse compressibility if the temperature is not

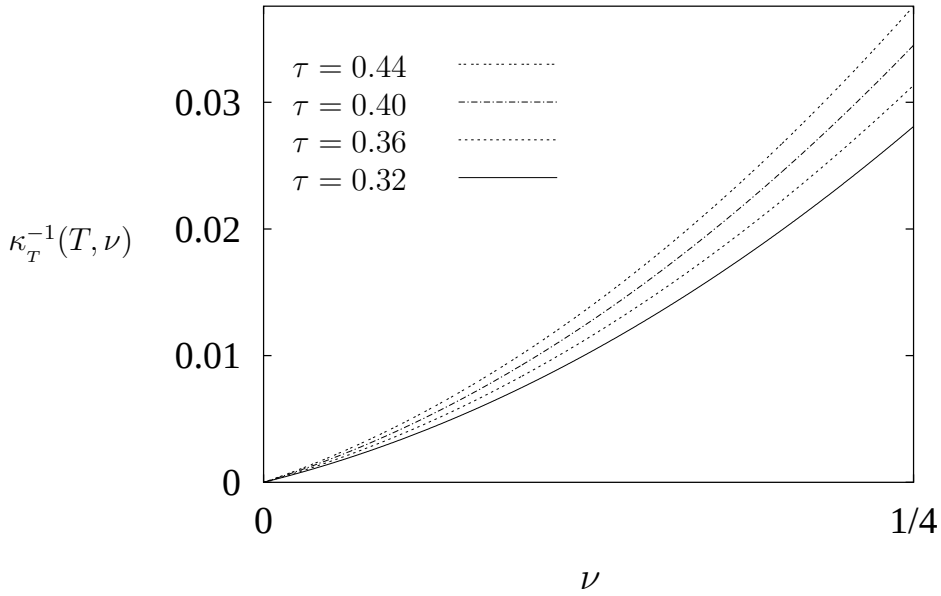

Figure 6.6: Dependency of the inverse compressibility on the filling factor and temperature in the neighbourhood of $\nu = 0$.

too high. Further more, in the interacting inverse compressibility, crossing points will always occur in the whole range of temperature. In order to understand the appearance of such crossings, we show below the derivation of integral relations, *sum rules*. These ensure the existence of at least two crossing points in the interacting inverse compressibility. Here, the work of Vollhardt [72] on similar crossing points in the specific heat of correlated systems has been very useful for our study of the crossing points.

Existence of crossing points

We integrate $\kappa_T^{-1}(T,\nu)$ in Eq. (6.10) and get with $P(T,\nu=0)=0$

$$P(T,\nu') = \int_0^{\nu'} d\nu \; \frac{\kappa_T^{-1}(T,\nu)}{\nu} \; . \tag{6.19}$$

Using $\kappa_T^{-1}(T,\nu)$ from Eq. (6.11) and integrating the derivatives of the energy coefficients by part, we get explicitly

$$\begin{aligned} P(T,\nu) &= -\frac{T}{2\pi} \; \ln(1-\nu) + \frac{1}{2\pi} \; \nu^2 \; W_a^{(1)} \\ &\quad + \frac{1}{2\pi} \; \sum_{n=2}^{\infty} \; \beta^{n-1} \; \frac{1}{n} \left(\nu \; \partial_\nu \alpha_n(\nu) - \alpha_n(\nu) \right) . \end{aligned} \tag{6.20}$$

It follows from Eq. (6.3) that all $\alpha_n(\nu)$ for $n \geq 2$ contain the factor $(1-\nu)$ at least to the second power. Therefore, the sum in Eq. (6.20) vanishes as $\nu \to 1$.

Thus, $P(T,\nu)$ becomes linear in T as $\nu \to 1$ and the second temperature derivative of $P(T,\nu)$ vanishes as $\nu \to 1$:

$$\lim_{\nu\to 1} \frac{\partial^2 P(T,\nu)}{\partial T^2} = \int_0^1 d\nu \; \frac{1}{\nu} \; \frac{\partial^2 \kappa_{_T}^{-1}(T,\nu)}{\partial T^2} = 0 \; . \tag{6.21}$$

We call the relation Eq. (6.21) a sum rule for the inverse compressibility of the quantum Hall system. We conclude that $\partial_{_T}^2 \kappa_{_T}^{-1}(T,\nu)$ must be zero for given temperature at some particular filling factor $\nu_c(T)$ as ν moves from the area where $\partial_T^2 \kappa_{_T}^{-1}(T,\nu)$ is positive to the area where its value becomes negative. As in Ref. [72], the dependence of $\nu_c(T)$ on T, i. e., how sharp a crossing point is defined, needs further consideration. Also, for a proof of the existence of crossing points in $\kappa_{_T}^{-1}(T,\nu)$ we would need the *first* derivative to be zero at some filling factor, $\partial_{_T} \kappa_{_T}^{-1}(T,\nu) = 0$. However, we can still expect a crossing point in $\kappa_{_T}^{-1}(T,\nu)$ when the temperature is not too high, i. e., when the first term in Eq. (6.20) becomes weak enough. This is actually the case in the cases we study, see below.

In the same manner, we consider now the *interacting part of the pressure* $P_{_W}(T,\nu) = P(T,\nu) + \frac{T}{2\pi} \; \ln(1-\nu)$. Then,

$$\lim_{\nu\to 1} \; P_{_W}(T,\nu) = \frac{1}{2\pi} \; W_a^{(1)} \; . \tag{6.22}$$

Here, the first temperature derivative is sufficient to derive a sum rule:

$$\lim_{\nu\to 1} \frac{\partial \; P_{_W}(T,\nu)}{\partial T} = \int_0^1 d\nu \; \frac{1}{\nu} \; \frac{\partial \; \kappa_{_{T,W}}^{-1}(T,\nu)}{\partial T} = 0 \; . \tag{6.23}$$

This relation is a sum rule for the interacting inverse compressibility. By the same argument used above, we conclude now that $\kappa_{_{T,W}}^{-1}(T,\nu)$ becomes independent of the temperature at particular filling factors. Therefore, there will always be at least one crossing point in the plot of the interacting inverse compressibility for a narrow range of temperature.

The derivation shows that the sum rules follow from the vanishing of the coefficients $\alpha_n(\nu)$ in the limit in which all single–particle states are occupied, $\nu = 1$. The energy coefficients $\alpha_n(\nu)$ originate from the interaction. Thus, the sum rules are due to the interaction and not due to the finiteness of the band. That is shown in Appendix F where we calculate the pressure of a non–interacting system with a finite band. We find there that no temperature derivative of $P(T,\nu)$ vanishes, cf. Eq. (F.11). Thus, a sum rule as in Eq. (6.21) or Eq. (6.23) cannot be derived for such a system. We conclude that the sum rules and, thus, the existence of the crossing points is exclusively due to the interaction. We shall present below evidence which show that the location of the

crossing points is related to the form of the interaction. To this end, it is useful to ask how the inverse compressibility of the quantum Hall system should look like.

We would like to give a short remark concerning the other crossings which appear in the plots of the inverse compressibility as a function of the filling factor for a fixed temperature when the ratios between components of the combined interaction vary. A sum rule for these crossings can also be derived as for the crossing points which appear at a fixed set of the ratios when the temperature varies (see Fig. 6.7).

The first two terms in Eq. (6.20), $-\frac{T}{2\pi}\ \ln(1-\nu)+\frac{1}{2\pi}\ \nu^2\ W_a^{(1)}$, are independent of the interaction ($W_a^{(1)}=2$ because we can always normalise the total energy). Thus, we have a sum rule (let W denote the interaction)

$$\lim_{\nu\to 1}\ \frac{\partial\ P(T,\nu)}{\partial W}\ \ =\ \ \int_0^1 d\nu\ \ \frac{1}{\nu}\ \ \frac{\partial\ \kappa_{_T}^{-1}(T,\nu)}{\partial W}\ \ =\ 0\ . \tag{6.24}$$

By the same argument used above, we conclude that inverse compressibility becomes independent of the interaction at particular filling factors.

There are two possible kinds of crossing points. However in the following, we shall concentrate on only one kind, the one which appears at a fixed ratio when the temperature varies.

Location of crossing points

We consider a one–component interaction W_{2m+1}–interaction and a corresponding Laughlin state with $\nu=\nu_m=1/(2m+3)$. Then, there is an energy gap above this ground state, the size of this energy gap is proportional to the interaction. According to the incompressibility of the Laughlin state, we expect to see the following scenario: At finite temperature, the inverse compressibility is zero at $\nu=0$, finite for all $\nu<1$ and infinity at $\nu=1$. In the limit $T\to 0$, the inverse compressibility becomes zero for $\nu<\nu_m$ and diverges at $\nu=\nu_m$ for the W_{2m+1}–interaction. Thus, the slope of $\kappa_{_T}^{-1}(T,\nu)$ with respect to ν would become infinity at $\nu=\nu_m$ at $T=0$. From this and from the limit obtained in the Virial expansion cf. Fig. 6.6, we expect the behaviour of $\kappa_{_T}^{-1}(T,\nu)$ for finite temperatures $T_1<T_2$ and $\nu\le\nu_m$ as follows:

1. $\kappa_{_T}^{-1}(T_1,\nu)\ \ <\ \ \kappa_{_T}^{-1}(T_2,\nu)$
2. $\partial_\nu\ \kappa_{_T}^{-1}(T_1,\nu)\Big|_{\nu=\nu_m}\ \ >\ \ \partial_\nu\ \kappa_{_T}^{-1}(T_2,\nu)\Big|_{\nu=\nu_m}$

The inverse compressibility must decrease with decreasing temperature as ν approaches 0. But, its slope has to increase with decreasing temperature as ν approaches ν_m. Thus, there should be a crossing point $\nu_{crossing}$ near $\nu=\nu_m$ which moves towards $\nu=\nu_m$ as $T\to 0$. We conclude that we should expect at least one crossing points at small ν where $\kappa_{_T}^{-1}(T,\nu)\to\infty$ for a given interaction.

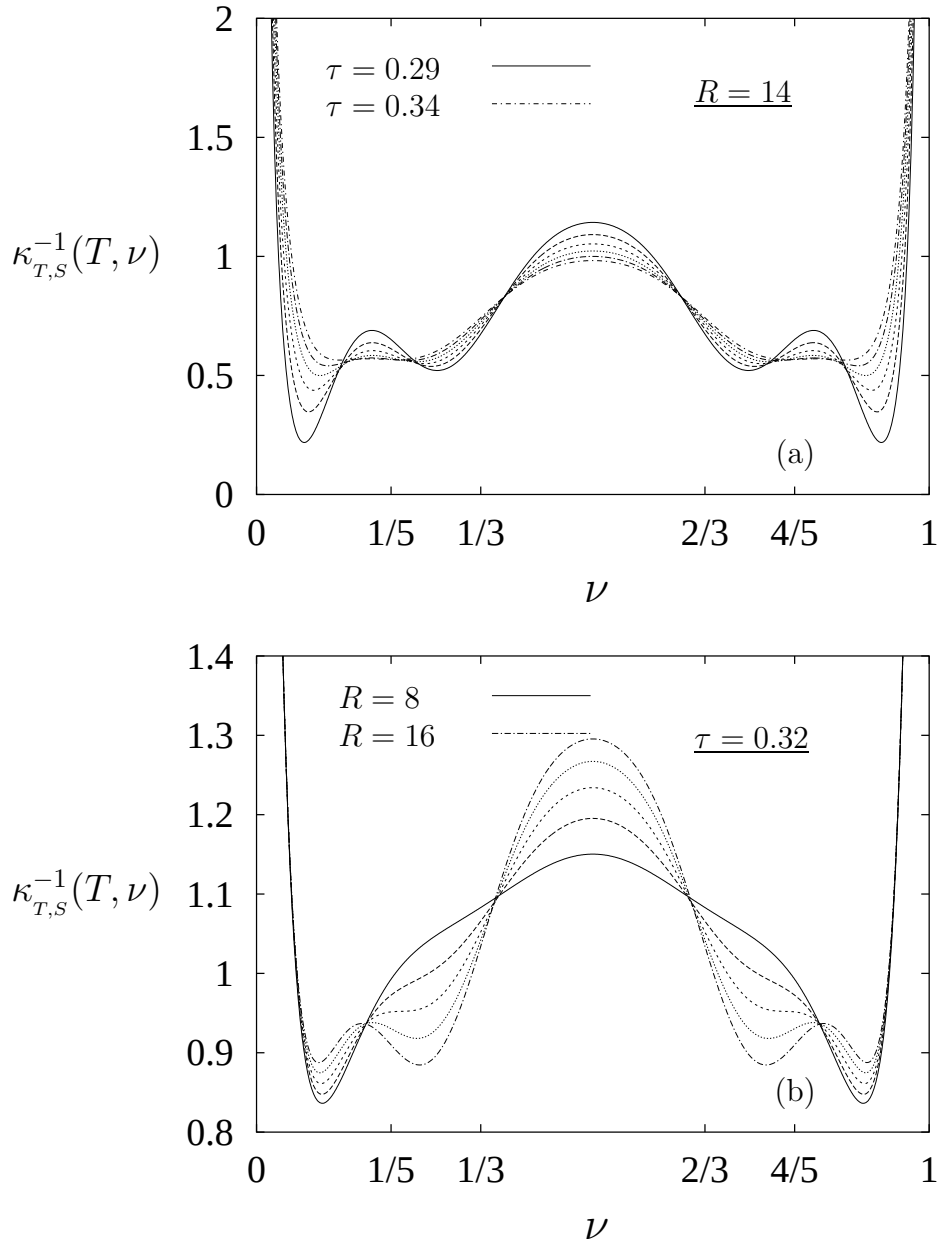

Figure 6.7: The inverse compressibility as a function of the filling factor (a) for a given interaction ratio $R = W_1/W_3 = 14$ for various temperature (b) for a given temperature $\tau = T/(W_1 + W_3) = 0.32$ for various interaction ratios $R = W_1/W_3$.

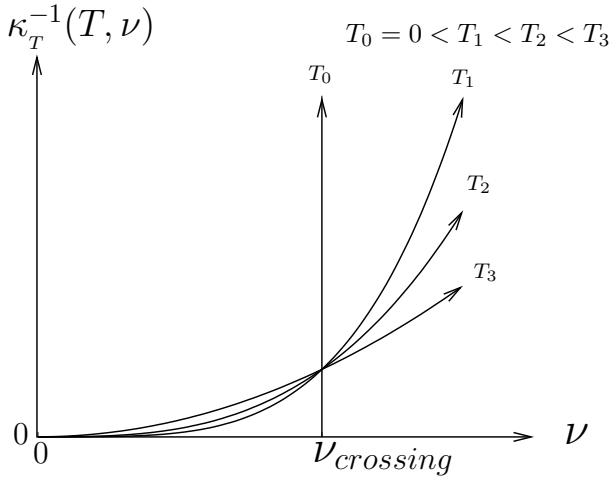

Figure 6.8: Schematic behaviour of the inverse compressibility as a function of ν for various T.

We note that even though the inverse compressibility will also diverge at $\nu = 1$, there is no crossing point due to this divergency. The origin and nature of the divergencies at the *magic* filling factors ($\nu = \nu_m$ and $\nu = 1 - \nu_m$) and at $\nu = 1$ are different. The divergency at $\nu = 1$, $\kappa_T^{-1}(\nu = 1, T) = \infty$, comes from the non–interacting part of the inverse compressibility, the first term in Eq. (6.11); it will occur at any temperature. On the other hand, the divergencies at $\nu = \nu_m$ and $\nu = 1 - \nu_m$ will occur only at zero temperature and as we argue above, they are caused by the interaction.

6.2.3 Inverse compressibility of the one–component interaction systems

In this study, we obtain eight terms of the high–temperature expansion series of the inverse compressibility, therefore, we are limited to study finite temperatures above the ground state and cannot expect to see a divergency in the inverse compressibility. Nevertheless, we should be able to study the development of the divergency as a temperature is lowered, and also the filling factor dependence within our limited results.

W_1–interaction

The results of the high–temperature expansion series up to the seventh and eighth order for the W_1–interaction ($W_1 = 1$) are shown in Fig. 6.9 and Fig. 6.10, respectively. The first of the three plots in each figure is the (complete) inverse compressibility $\kappa_T^{-1}(T, \nu)$, the second plot is the particle–hole symmetric inverse compressibility $\kappa_{T,S}^{-1}(T, \nu)$, and the third plot is the interacting part of the inverse compressibility $\kappa_{T,W}^{-1}(T, \nu)$.

There are various features in Fig. 6.9 and Fig. 6.10.

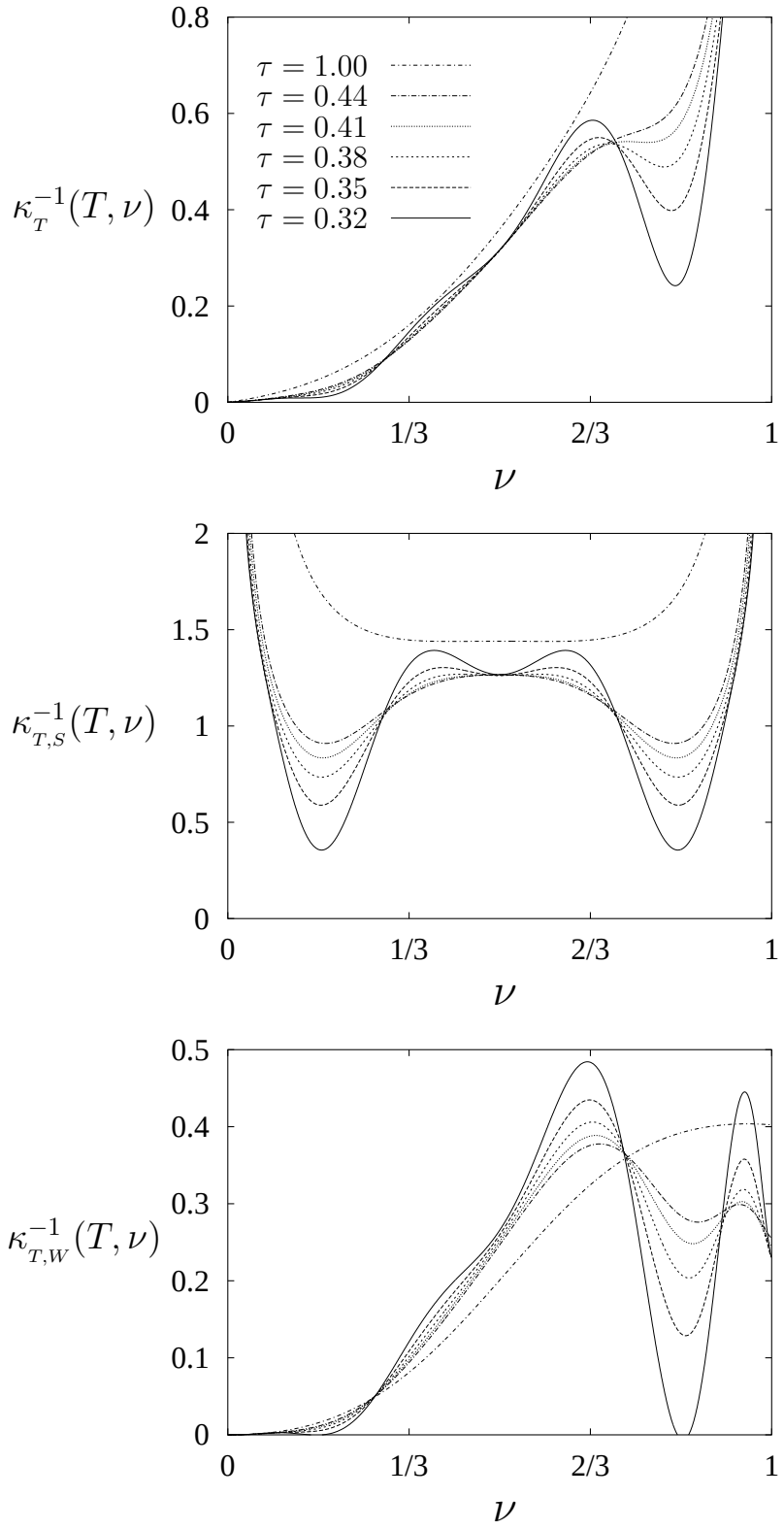

Figure 6.9: The inverse compressibility, its particle–hole symmetric version and the interacting inverse compressibility resulting from the high–temperature expansion up to the *seventh* order of the W_1–interaction for various temperatures. Corresponding line types in the three plots belong to the same temperature $\tau = T/W_1$.

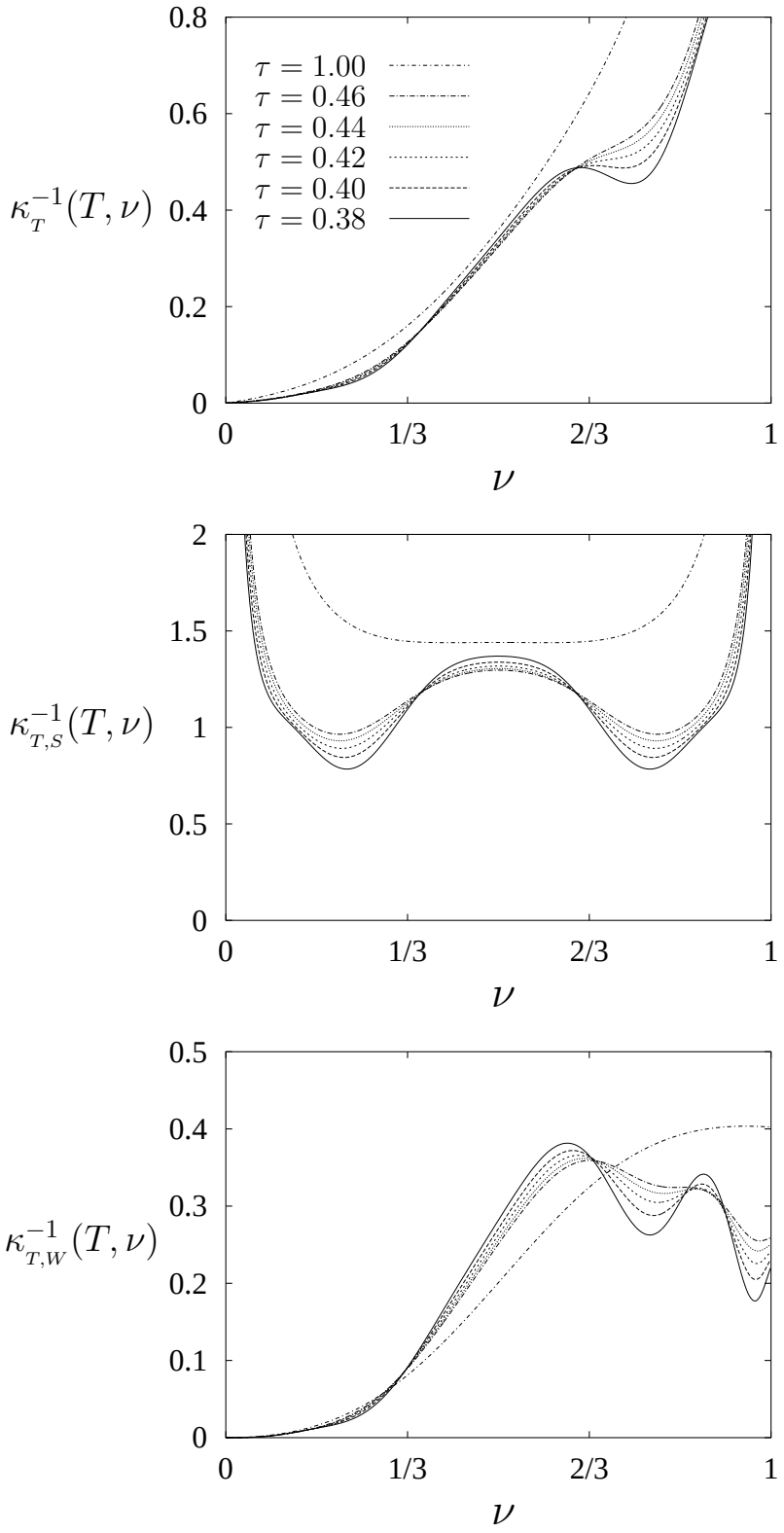

Figure 6.10: The inverse compressibility, its particle–hole symmetric version and the interacting inverse compressibility resulting from the high–temperature expansion up to the *eighth* order of the W_1–interaction for various temperatures. Corresponding line types in the three plots belong to the same temperature $\tau = T/W_1$.

1. There are *two* crossing points as they are discussed in Section 6.2.2 near the filling factors $\nu = 1/3$ and $\nu = 2/3$ in any plot in Fig. 6.9 and Fig. 6.10.

2. There are *two* peaks in $\kappa_{T,S}^{-1}(T,\nu)$ and *one* peak and *one* shoulder in $\kappa_{T}^{-1}(T,\nu)$ and $\kappa_{T,W}^{-1}(T,\nu)$ developing near the filling factors $\nu = 2/3$ and $\nu = 1/3$ in the seventh order result in Fig. 6.9.

3. There are oscillations beyond $\nu = 2/3$ in the plot of $\kappa_{T,W}^{-1}(T,\nu)$.

The general behaviour of the results in the seventh and eighth orders away from $\nu = 1/2$ are similar, in particular the crossing points near $\nu = 1/3$ and $\nu = 2/3$. However, the behaviour in the neighbourhood of $\nu = 1/2$ and the developing of the peaks near $\nu = 1/3$ and $\nu = 2/3$ change with the order. Here, we shall discuss briefly the oscillations in the regime $2/3 < \nu < 1$ of the interacting inverse compressibility. The oscillations appear strongly in $\kappa_{T,W}^{-1}(T,\nu)$ because the non–interacting term has been subtracted. In $\kappa_{T}^{-1}(T,\nu)$ and $\kappa_{T,S}^{-1}(T,\nu)$, this term dominates more and more as ν approaches 1; thus, it can, when included, smooth the oscillations caused by the high order polynomial in ν. The oscillations, therefore, are just the effect of the increasing of the order of the polynomial in ν of the inverse compressibility. As can be seen clearly, the number of oscillations increases as the order increases. As $T \to 0$, the exact result for $\kappa_{T}^{-1}(T,\nu)$ vanishes for $2/3 < \nu < 1$. Thus, this is how we expect this oscillating behaviour of the interacting inverse compressibility to develop with the order of the expansion and with the temperature: At finite temperature and for finite orders, the number of the oscillations will be finite. As the order approaches infinity, the number of the oscillations also approaches infinity, and the interacting part of inverse compressibility becomes a smooth function with a finite value. As the temperature of the infinite order approaches zero, this smooth function will approach zero in the whole regime $2/3 < \nu < 1$.

W_3–interaction

The results for the inverse compressibility for the W_3–interaction ($W_3 = 1$) are shown in Fig. 6.11 and Fig. 6.12. We show the result in the fifth and the eighth orders here because of the behaviour seen earlier in the discussion of the energy of this interaction.

There are various features in Fig. 6.11 and Fig. 6.12.

1. There are *four* crossing points. One pair of these crossing points are on the left and right sides of the filling factor $\nu = 1/5$ and the other pair are on the left and right sides of the filling factor $\nu = 4/5$.

2. There are *two* peaks developing between a pair of crossing points near $\nu = 1/5$ and $\nu = 4/5$ in each plot in both orders.

3. There are oscillations beyond $\nu = 4/5$ in the plot of $\kappa_{T,W}^{-1}(T,\nu)$.

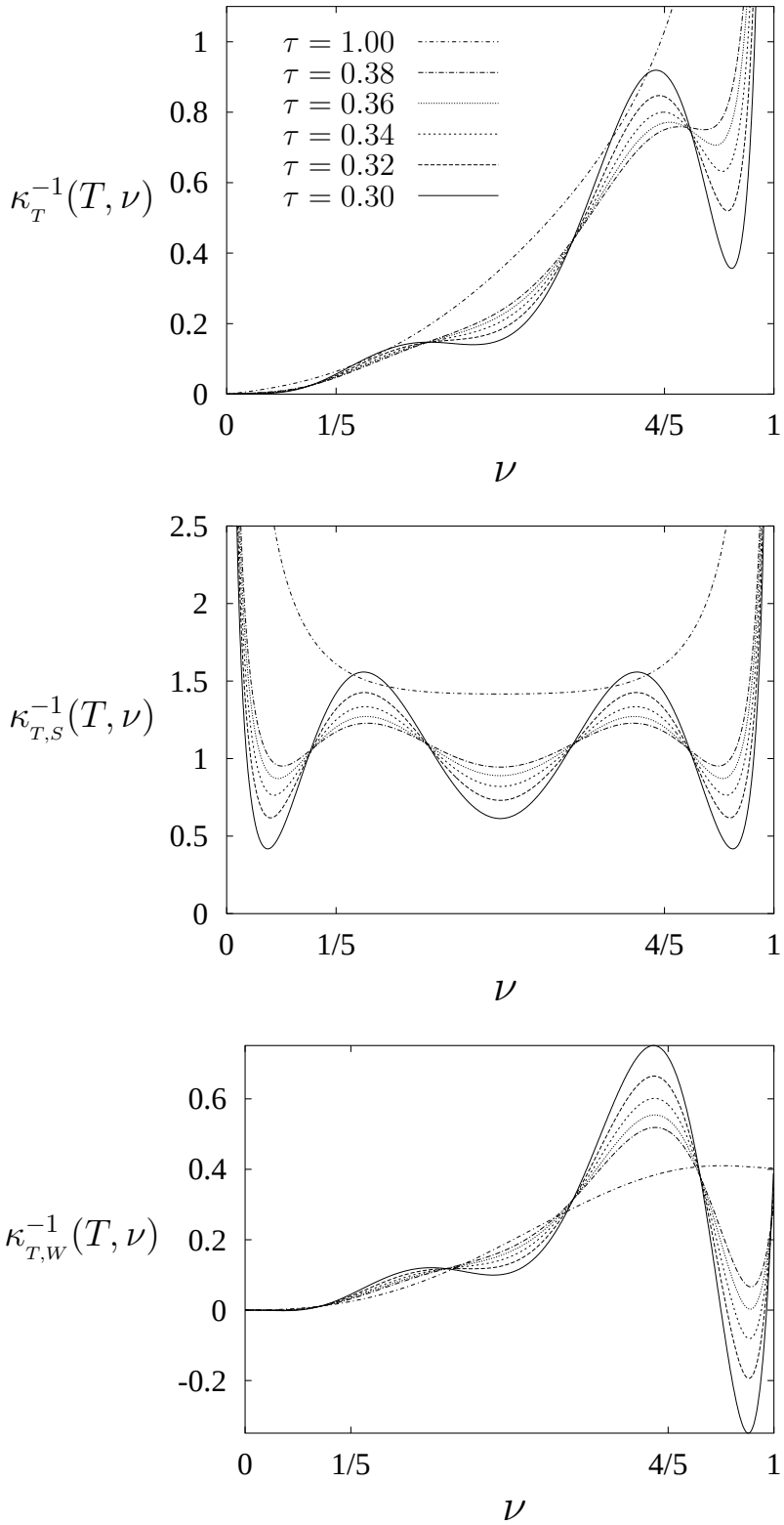

Figure 6.11: The inverse compressibility, its particle–hole symmetric version and the interacting part of the inverse compressibility resulting from the high–temperature expansion up to the *fifth* order of the W_3–interaction for various temperatures. Corresponding line types in the three plots belong to the same temperature $\tau = T/W_3$.

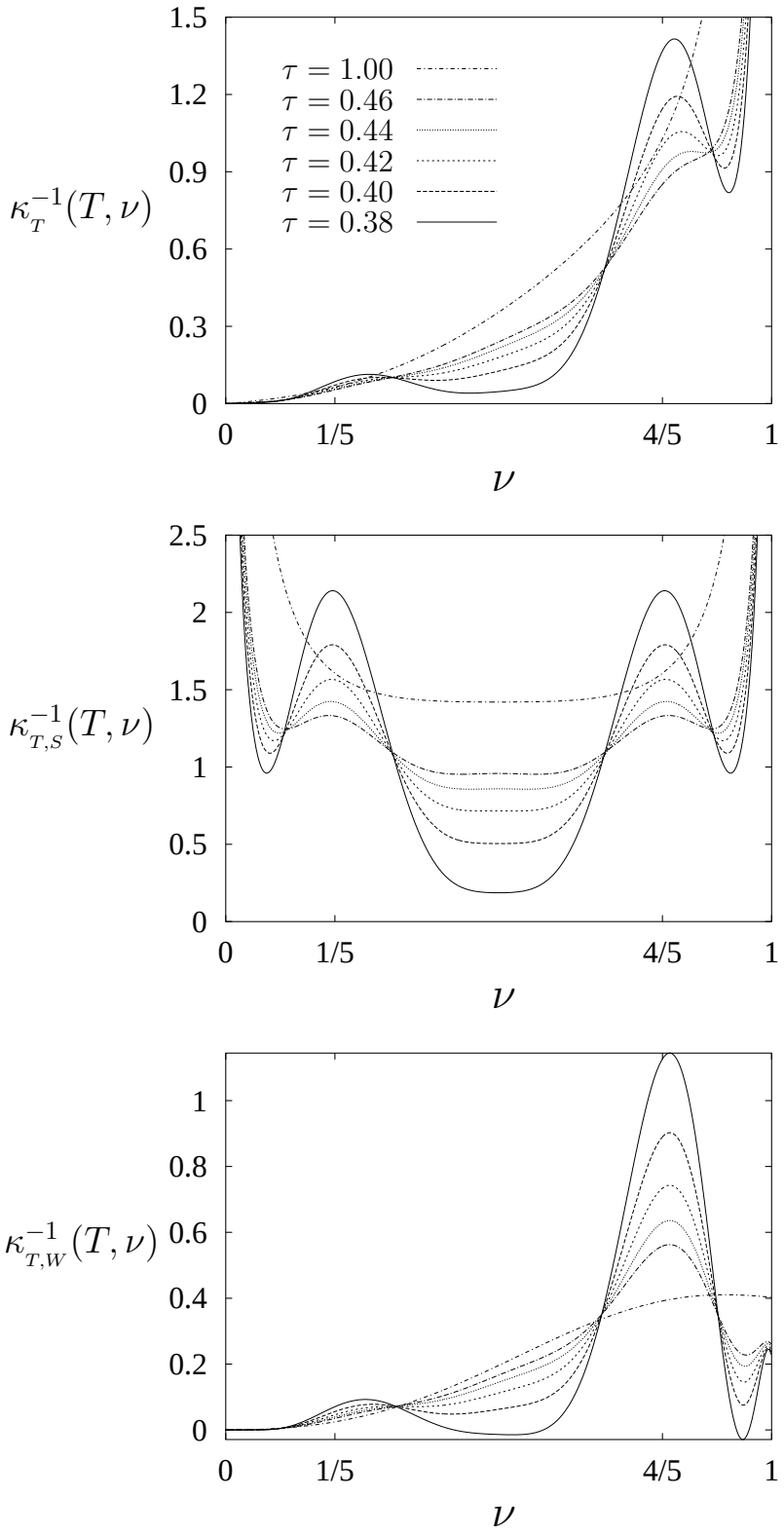

Figure 6.12: The inverse compressibility, its particle–hole symmetric version and the interacting part of the inverse compressibility resulting from the high–temperature expansion up to the *eighth* order of the W_3–interaction for various temperatures. Corresponding line types in the three plots belong to the same temperature $\tau = T/W_3$.

One observation which may be worth mentioning here is the similarity of inverse compressibility resulting from the *fifth* order and from the *eighth* order of the high–temperature expansion. As the expansion goes *three* orders higher (or *six* orders higher in the order of the polynomial in ν), we still have the same number of crossings. Thus, if we try to interprete the crossings in the inverse compressibility as oscillations, their number would be independent of the order of the result. This is in contrast to the *true* oscillation of $\kappa^{-1}_{T,W}(T,\nu)$ in the case of the W_1–interaction for $2/3 < \nu < 1$. Therefore, the above interpretation cannot be right and the crossing points are characteristic for the interaction, independent of the order. This observation is true in the case of W_1–interaction as well, but it is clearer visible in the result of W_3–interaction.

Summary and discussion

We see various features in the plots of the inverse compressibility of the W_1–interaction and W_3–interaction. There are similarities as well as differences. Thus, we should like to summarise the characteristic behaviour of the crossing points of the inverse compressibility of these one–component interactions.

1. Similarities between the cases of the W_1–interaction and the W_3–interaction:

   (a) Response to changing of the temperature : With decreasing temperature, the inverse compressibility decreases for $0 < \nu < \nu_{crossing}$ where $\nu_{crossing}$ is the smallest crossing point (or correspondingly in the region related through the particle–hole symmetry).

   (b) Peaks : The inverse compressibility peaks between two crossing points.

   (c) Oscillations : There are oscillations in the interacting inverse compressibility in the region beyond the expected characteristic filling factors.

2. Difference – number of crossing points : The properties of the compressibility for a one–component interaction, see discussion in connection with Fig. 6.8, allows to expect at least two crossing points, one near ν_m and the other near $1 - \nu_m$ where ν_m is the crucial filling factor. Nevertheless, except from oscillations, there are *two* crossing points in the case of W_1–interaction but *four* in the case of W_3–interaction. We have an intuitive suggestion to explain why the case of the W_1–interaction may be special: The concept of a one–component W_m interaction is singular in the sense that only a relative angular momentum m of a pair yields a finite interaction. Now, $m = 1$ is the lowest possible angular momentum. Thus, the W_1–interaction can be considered as different from all the other one–component interactions which react only to a higher angular momentum but not to $m = 1$. The W_1–interaction has the Laughlin state at $\nu = 1/3$ as ground state. Fig. 6.13 shows the filling factors at which the Laughlin states are expected for

the various one–component interactions. In this sense, the W_1–interaction is a border case.

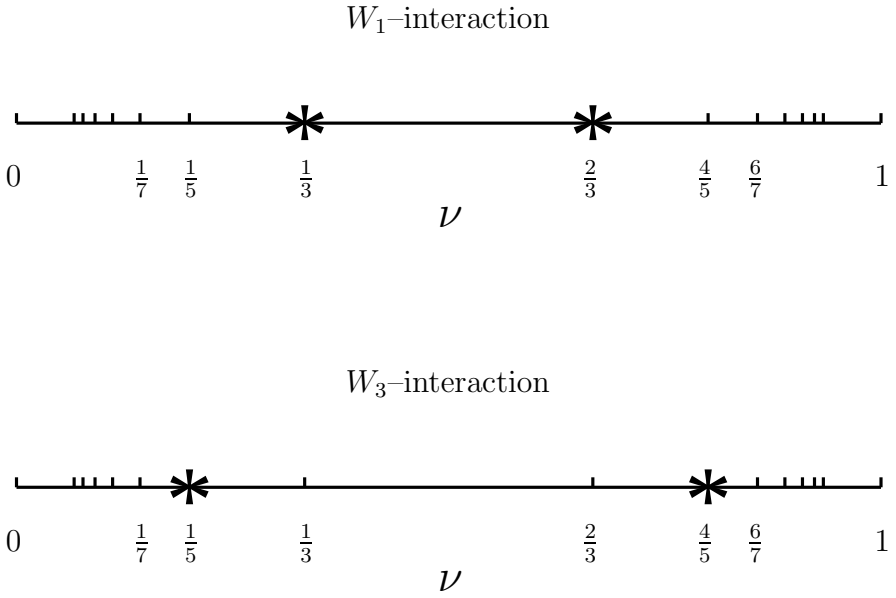

Figure 6.13: Schematic picture : Filling factors for which the Laughlin states are exact ground states (∗).

We conclude that the locations where the crossing points in the inverse compressibility appear are related to the interactions which are responsible for the fractional quantum Hall ground states at $\nu = 1/3$ and at $\nu = 1/5$, respectively. Therefore, we shall use these crossing points as indications which signal the existence of the fractional quantum Hall ground states already at finite temperatures. In our analysis of the more complicated interaction below we shall regard the two crossing points near $\nu = 1/3$ and $\nu = 2/3$, such as those in Fig. 6.9 and Fig. 6.10, as the crossing points belonging to the ($\nu = 1/3$)–fractional quantum Hall ground state and the four crossing points near $\nu = 1/5$ and ($\nu = 4/5$), such as those in Fig. 6.11 and Fig. 6.12, as the crossing points belonging to the ($\nu = 1/5$)–fractional quantum Hall state.

6.2.4 Inverse compressibility of a multi–component interaction system, $(W_1 + W_3)$–interaction

The study of the inverse compressibilities of the one–component interactions in the last section shew us that the appearance of crossing points is interaction dependent. Here, we want to investigate a combined interaction which contains both, the W_1 and the W_3 pseudopotential coefficients. The question here is whether there is a parameter regime where the features of both one–component interactions appear simultaneously in the

results of the multi–component interaction. Moreover, we shall study the transition between the one–component regimes dominated by the W_1–interaction and the W_3–interaction, respectively.

Map of our expectation in the (interaction, temperature)–plane

We define the ratio $R = W_1/W_3$. In all plots for this interaction, $W_1 + W_3 = 1$ as discussed in the beginning of the chapter; and thus

$$W_1 \;=\; \frac{R}{1+R} \qquad \text{and} \qquad W_3 \;=\; \frac{1}{1+R}\,.$$

For the time being, we assume that the energy gaps at $\nu = 1/3$ and $\nu = 1/5$ are given by W_1 and W_3, respectively, and consider in Fig. 6.14, the (interaction, temperature)–plane, (R, τ)–plane.

For any fixed R, there are three regions along the temperature axis. The first region is where the temperature is lower than both energy gaps. In the second region, the temperature lies between the larger and smaller energy gap. The third region is where the temperature is higher than both energy gaps. We expect to see a singular behaviour of the inverse compressibility developing in any regions where $T < W_1$ or $T < W_3$ or both, however, we must also keep in mind the influence of the finite temperature which can weaken any signal of the singular behaviour.

In the region where $T < W_1$ and $T < W_3$, we may expect to see a signal of the development of the coexistence of two fractional quantum Hall states in the form of the existence of *six* crossing points. Two of these crossing points should be in the neighbourhood of $\nu = 1/3$ and $\nu = 2/3$ and the other four should be in the neighbourhood of $\nu = 1/5$ and $\nu = 4/5$ at some (low enough) temperatures, lower than both energy gaps, and for some intermediate R.

Six crossing points significant for two fractional quantum Hall states

The inverse compressibilities in the eighth order of the high–temperature expansion are plotted for a fixed ratio $R = 12$ and for various temperatures in Fig. 6.15. We show three plots in the same way as they were plotted in the previous discussion of the one–component interactions. We choose to show the result for the ratio $R = 12$ because at this parameter, the inverse compressibility shows both influences of the W_1–interaction and W_3–interaction, *two* crossing points near $\nu = 1/3$ and $\nu = 2/3$, and *four* crossing points on the left and right of $\nu = 1/5$ and $\nu = 4/5$, respectively. This is best seen in the particle–hole symmetric version $\kappa^{-1}_{T,S}(T, \nu)$. The six crossing points, discussed above, exist in the neighbourhood of the expected filling factors. Thus, this is an interaction for which one can expect transitions into quantum Hall states at both filling factors, $\nu = 1/3$ and $\nu = 1/5$. In the following, we discuss the effects of the ratio R and the temperature T on the behaviour of the inverse compressibility.

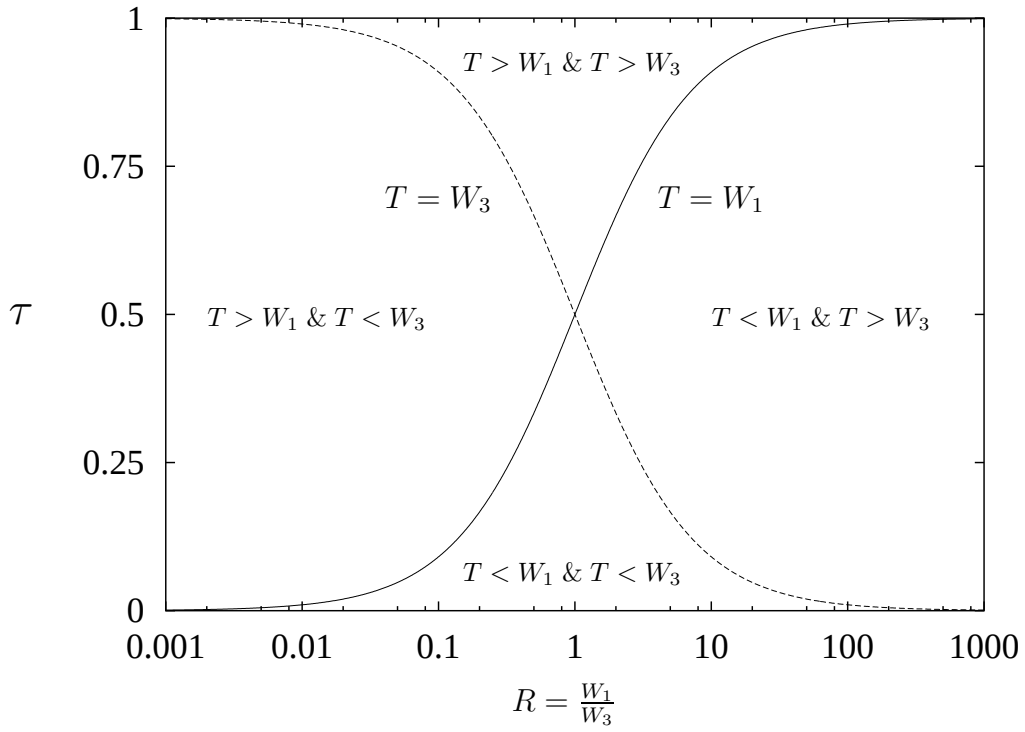

Figure 6.14: The area in the (R, τ)–plane can be divided into four parts according to the relation between the temperature T and the interactions W_1 and W_3.

Effects of the ratio R on the appearance of the crossing points

In Fig. 6.16, we show a series of plots of the particle–hole symmetric inverse compressibility as a function of the filling factor resulting from the high–temperature expansion up to the eighth order. In each plot, different temperatures are shown at a fixed ratio of R. The two scaled temperatures, τ, given in each plot are the lowest and the highest temperatures of the curves in the plot. The temperature difference between adjacent curves is 0.01. Here, the temperatures have been selected in such a way that the inverse compressibility remains positive. We also want to keep the temperature range constant for the widest possible range of R for the benefit of the comparison of the results of different R.

The ratio R increases from top left to bottom right. The top left plot has the lowest R, $R = 10^{-4}, (W_1 \sim 0)$, and the bottom right plot has the highest R, $R = 10^4, (W_3 \sim 0)$. One can see the gradual change of the form of the inverse compressibility due to the change in the interaction from the W_3–dominant interaction to the W_1–dominant interaction.

For small ratios $R \leq 0.1$ where W_3 dominates the interaction, we see *four* crossing points and *two* peaks in the neighbourhood of $\nu = 1/5$ and $\nu = 4/5$ and there is no indication of any development at $\nu = 1/3$ and $\nu = 2/3$.

For intermediate ratios $0.1 \leq R \leq 10$ where neither W_1 nor W_3 dominates the

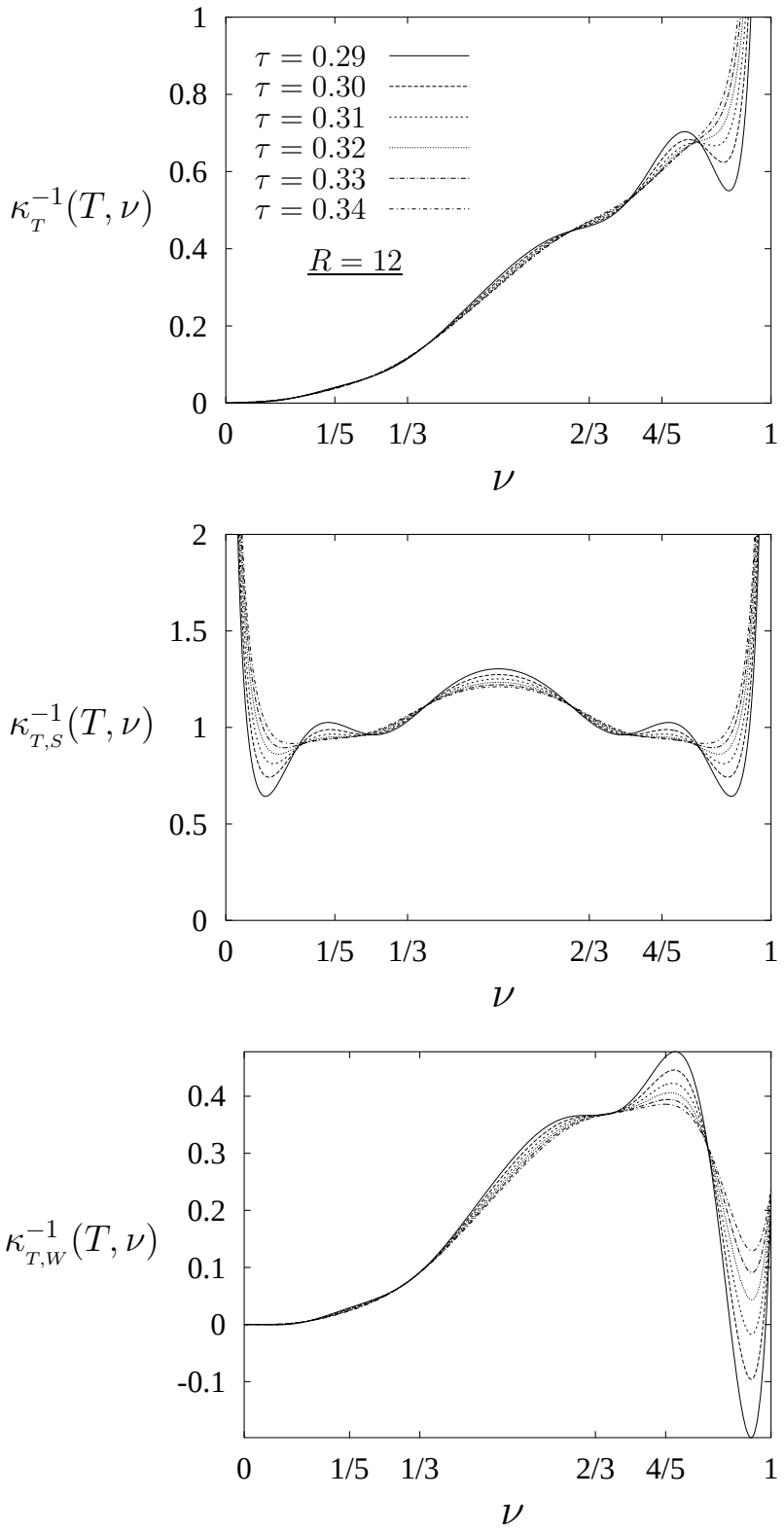

Figure 6.15: The inverse compressibility, its particle–hole symmetric version and the interacting inverse compressibility resulting from the high–temperature expansion up to the *eighth* of the $(W_1 + W_3)$–interaction for $R = 12$ for various temperatures. The corresponding line types in the three plots belong to the same temperature $\tau = T/(W_1 + W_3)$.

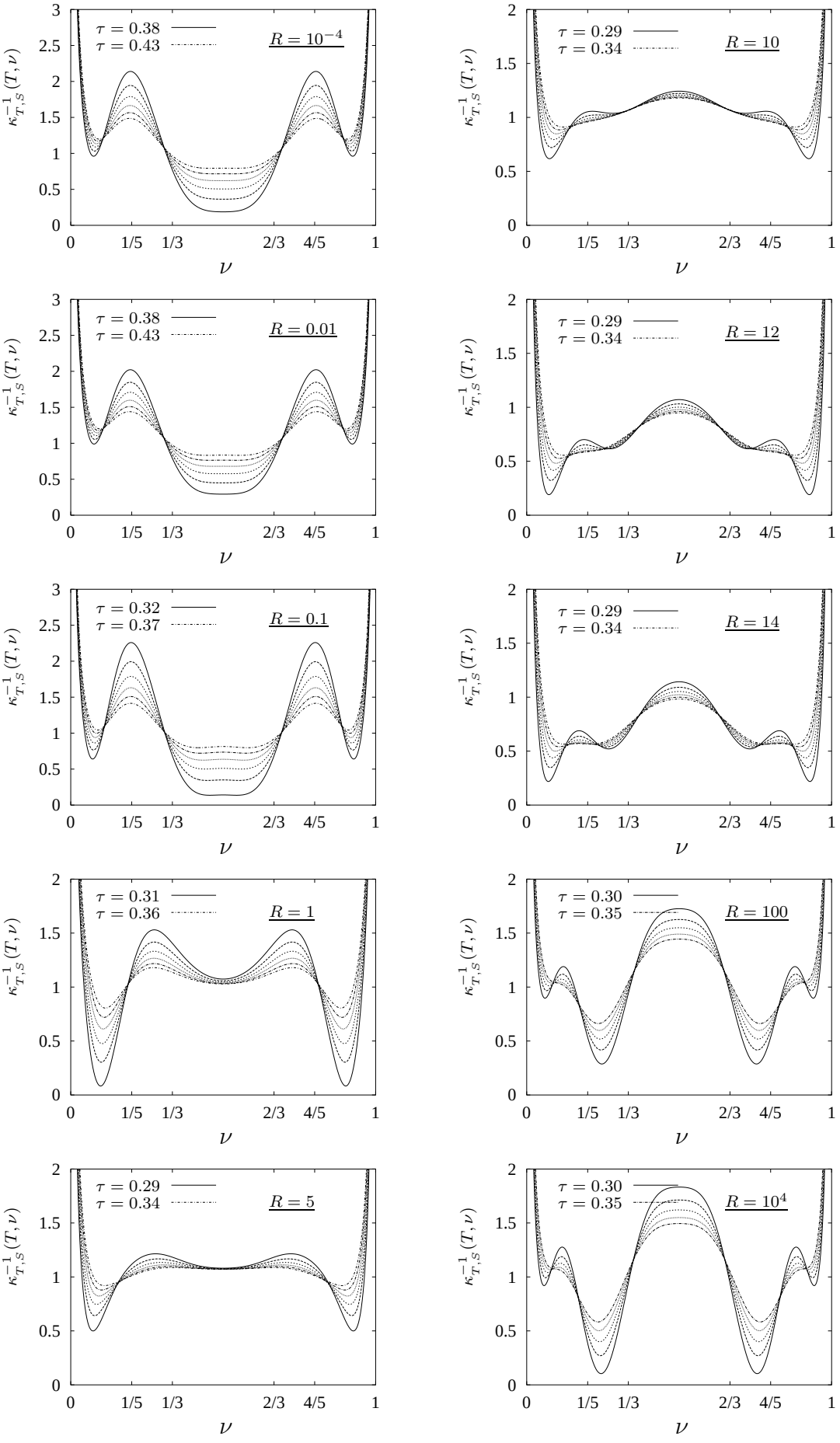

Figure 6.16: Effect of $R = W_1/W_3$ on $\kappa_{T,S}^{-1}(T,\nu)$, $\tau = T/(W_1 + W_3)$.

interaction, we observe changes in the plots of the inverse compressibilities: As R approaches 1, two crossing points, one on the right of $\nu = 1/5$ and one on the left of $\nu = 4/5$, disappear. As R approaches 5, the minimum at $\nu = 1/2$ becomes weaker. As R approaches 10, the weak minimum at $\nu = 1/2$ becomes a maximum and simultaneously, *fours* more crossing points begin to develop, each two on the left and right of $\nu = 1/3$ and $\nu = 2/3$. Now, we enter the area in the R, T–plane where the effects at both filling factors appear simultaneously. The four new crossing points can be seen clearly in the plot of $R = 12$. The magnitude of the slopes of the inverse compressibilities near $\nu = 1/3$ and $\nu = 2/3$ also becomes stronger.

If we increase R further to 100 and beyond, we shall enter the W_1 dominant region where the effect at $\nu = 1/5$ should be weak and should be weaker as R becomes larger. The plots in this region of R seems to contradict this picture. But, if we compare with the case of the W_1–interaction (Fig. 6.10), we have to conclude that the crossings near $\nu = 1/3$ and $\nu = 2/3$ are the crossing points in the W_1–interaction. Further, the positions of the two crossing points with the smallest ν and largest ν in these two plots move beyond $\nu = 1/5$ and $\nu = 4/5$, respectively. This is another indication that these crossings in the plot of $R = 100$ and $R = 10^4$ are not real crossing points in our sense but rather describe oscillations, because the temperature becomes too low. We shall discuss this point again below in connection with of Fig. 6.17.

However, we argue that the six crossing points observed in the region of $R \sim 12$ are real crossing points in the sense that they indicate for this interaction the coexistence of the two fractional quantum Hall states, the ($\nu = 1/3$)–fractional quantum Hall ground state and the ($\nu = 1/5$)–fractional quantum Hall state.

In order to provide support for our above claim, we study now the location of the crossing points in the (ν, τ)–plane for a wider range of temperatures than it is possible in plots at fixed temperatures. This is best done by considering the first temperature derivative of the inverse compressibility and of the interacting inverse compressibility which should be zero at the crossing points:

$$\frac{\partial \kappa_{_T}^{-1}(T,\nu)}{\partial T} \;=\; 0 \qquad\qquad \text{and} \qquad\qquad \frac{\partial \kappa_{_{T,W}}^{-1}(T,\nu)}{\partial T} = \; 0\;. \tag{6.25}$$

The numerical solutions of these two equations are displayed in Fig. 6.17–Fig. 6.19. The solutions are symmetric around $\nu = 1/2$, we show only the region $\nu > 1/2$.

In Fig. 6.17, each point or curve indicates the locations in the (ν, τ)–plane where the crossing points, the solutions of the first equation can be found for a given R.

We shall start with the two limiting cases, $R = \infty$ and $R = 0$ which correspond to the W_1–interaction and W_3–interaction, respectively. We expect that the solutions of the whole range $0 < R < \infty$ should lie in the area bounded by the solutions of $R = \infty$ and $R = 0$. And this seems to be the case.

For $R = \infty$ and $\nu > 1/2$, there exist *one* crossing point for temperatures $0.3726 \leq \tau \leq 0.5209$. The solution starts out from $\nu = 1/2$ at $\tau = 0.5209$ and moves to the

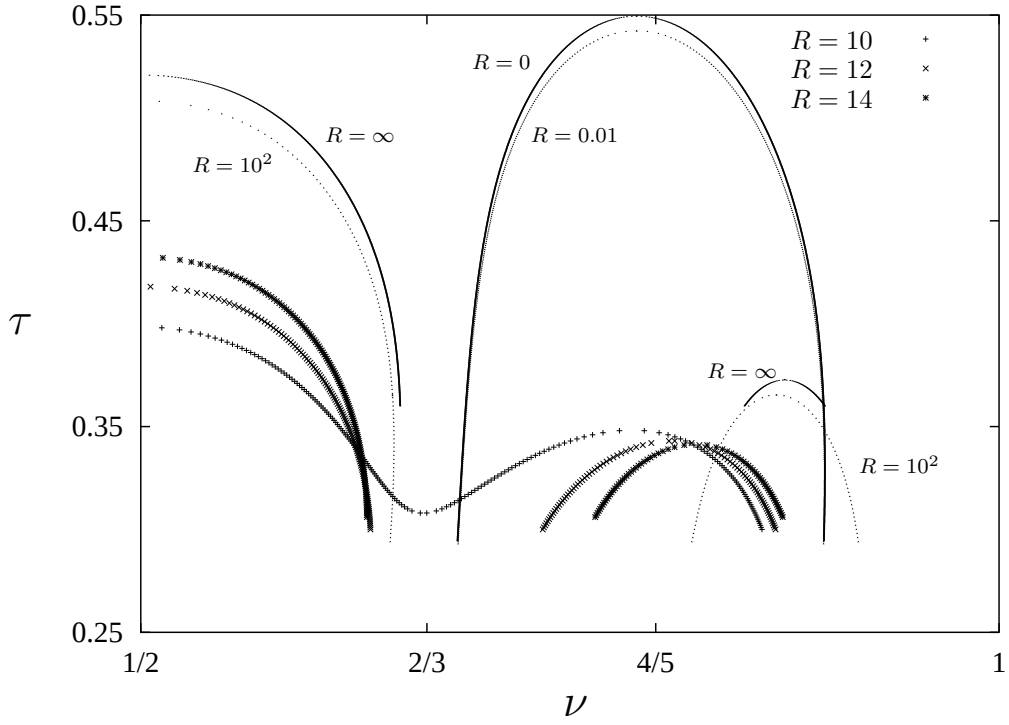

Figure 6.17: The crossing points in the inverse compressibility $\kappa_{_T}^{-1}(T,\nu)$ for various ratios $R = W_1/W_3$ and temperature $\tau = T/(W_1 + W_3)$.

neighbourhood of $\nu = 2/3$ as τ approaches 0.3726 There is no solution for $\tau > 0.5209$. For $\tau < 0.3726$, *two more* candidates for crossing points appear (three crossing points in total). These two crossing points lie beyond $\nu = 4/5$ and we have to consider them as corresponding to oscillations which signal that the temperature becomes too low: we are leaving the area of validity of the high–temperature expansion in the considered order.

For $R = 0$ and in the same range of ν, there exist *two* crossing points for temperatures $0.2944 \leq \tau \leq 0.5495$ and there is no solution for the first equation in the range of $\tau > 0.5495$. The two crossing points start out from the neighbourhood of $\nu = 4/5$ at high temperature and each one moves to the left and right of $\nu = 4/5$ as τ becomes lower.

So, we have *two* separated regions on the ν–axis marked by the solutions of the limiting case where the solutions can be found. We shall use this as an criterion to judge which component of the $(W_1 + W_3)$–interaction yields the shown up effect.

Next, we shall move from the two borders towards the area where R is finite. We first arrive at the very large R, for example $R = 10^2$, and very small R, for example $R = 10^{-2}$. The solutions of these two cases are very close to those of $R = \infty$ and $R = 0$ and lie inside the marked area. For $R = 10^2$, there exist *three* solutions: *One* of them starts out from the neighbourhood of $\nu = 1/2$ at high temperature and moves towards

$\nu = 2/3$ as T becomes lower. The other *two* are beyond $\nu = 4/5$ in the area where the oscillations were found in case of $R = \infty$ when the temperature becomes too low. At this point, we can support our claim above that the crossings which appear beyond $\nu = 4/5$ in the plots of finite R for $R > 14$ are due to oscillations. They are not real crossing points in the sense considered here. For $R = 10^{-2}$, there exist *two* crossing points in the same area of the solutions of $R = 0$. These solutions behave very similar to those of $R = 0$ as a function of T. We conclude here that for a finite but very large or very small R, the solutions exist only in one region of ν either on the side of the solution of $R = \infty$, or on the side of the solution of $R = 0$.

We move further with R to the inner part of the R scale, or to the neighbourhood of $R \sim 12$, where, from Fig. 6.15, we expect that the combined influences of the W_1–interaction and W_3–interaction will lead to simultaneous appearance of features at $\nu = 2/3$ and $\nu = 4/5$. We present in Fig. 6.17 three curves which represent the solutions of the first of Eqs. (6.25) for $R = 10$, the plus symbol (+), for $R = 12$, the times symbol ($\times$), and for $R = 14$, the star symbol ($*$). The solutions for values of these R exist simultaneously in *two* regions on the ν–axis, where the solutions occur separately in the limiting case, for a given temperature inside the range of T where solutions can be found. We observe that the maximum temperature, where the crossing point related too $\nu = 2/3$ can exist, *decreases* with decreasing R. Oppositely, the maximum temperature where the crossing points corresponding to the $\nu = 4/5$ exist *increases* with decreasing R. These two effects together give quite a clear picture of the development of the two fractional quantum Hall states with decreasing R. The second effect also supports our above claim. The maximum temperature where the crossing points corresponding to $\nu = 4/5$ can be observed should decreases with increasing R. But as shown in Fig. 6.17, the maximum temperature of the trace at $\nu > 4/5$ for $R = 10^2$ is much higher than that of $R = 10$. Thus this trace does not represent real crossing points which would develop out of the real crossing points at $\nu \sim 4/5$ for $R \sim 12$.

In Fig. 6.18 and Fig. 6.19, we plot the solutions of the first and second equation in Eqs. (6.25), respectively, in the (R, ν)–plane for the range of, $10^{-4} \leq R \leq 10^4$ at various temperatures. The temperature difference between adjacent curves is 0.02.

We observe various features of the solution of the first equation of Eqs. (6.25) in Fig. 6.18.

1. Dependence on R: The solutions, the crossing points, appear symmetric around $\nu = 4/5$ when $R << 1$. As R increases, the location where the solutions exist moves towards the neighbourhood of $\nu = 2/3$. The crossing points beyond $\nu = 4/5$ for $R >> 1$ correspond to the oscillations discussed above.

2. Transition region: There is no clear behaviour of the solution in the transition region of R where $0.1 < R < 20$. The region in R and T where six crossing points can be seen is very narrow (cf. Fig. 6.17) and cannot be easily seen in Fig. 6.18.

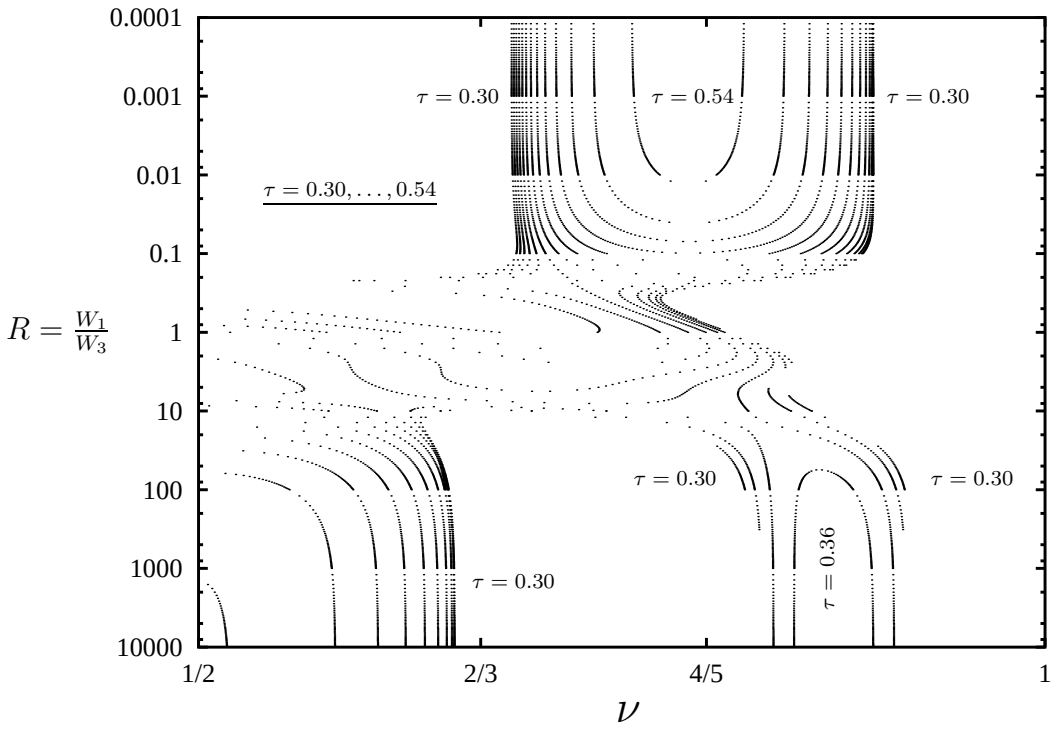

Figure 6.18: The crossing points in the inverse compressibility $\kappa_{_T}^{-1}(T, \nu)$ for $1/2 \leq \nu \leq 1$ as a function of the ratio R.

3. Dependence on τ: As the temperature increases, the crossing points corresponding to $\nu = 4/5$ move towards $\nu = 4/5$ until they merge and disappear. For higher T, we need smaller R in order to observe the crossing points. The crossing point corresponding to $\nu = 2/3$ moves towards $\nu = 1/2$ as T increases. For higher T, we need larger R in order to observe the crossing point.

The solutions of the second equation in Eqs. (6.25) shown in Fig. 6.19 behave in general similar to the solutions of the first equation with the exception of the behaviour with respect to the change in T, especially for large T. This can be expected since the non–interacting term which has been taken out is linear in T. This term will be also very large as ν approaches 1 since it has $(1 - \nu)$ in the denominator.

Here, we list only differences.

1. Crossing over: It is much easier in Fig. 6.19 to follow the solutions of a given T for varying R than it is in Fig. 6.18. As R increases from small values, one of the crossing points corresponding to $\nu = 4/5$, the one on the left, disappears at $\nu = 1/2$ and the other crosses over to become the crossing point corresponding to $\nu = 2/3$ (cf. $\tau = 0.6$).

2. Temperature dependence : The solutions of the second equation depend much weaker on temperature than the solutions of the first equation. In the low temper-

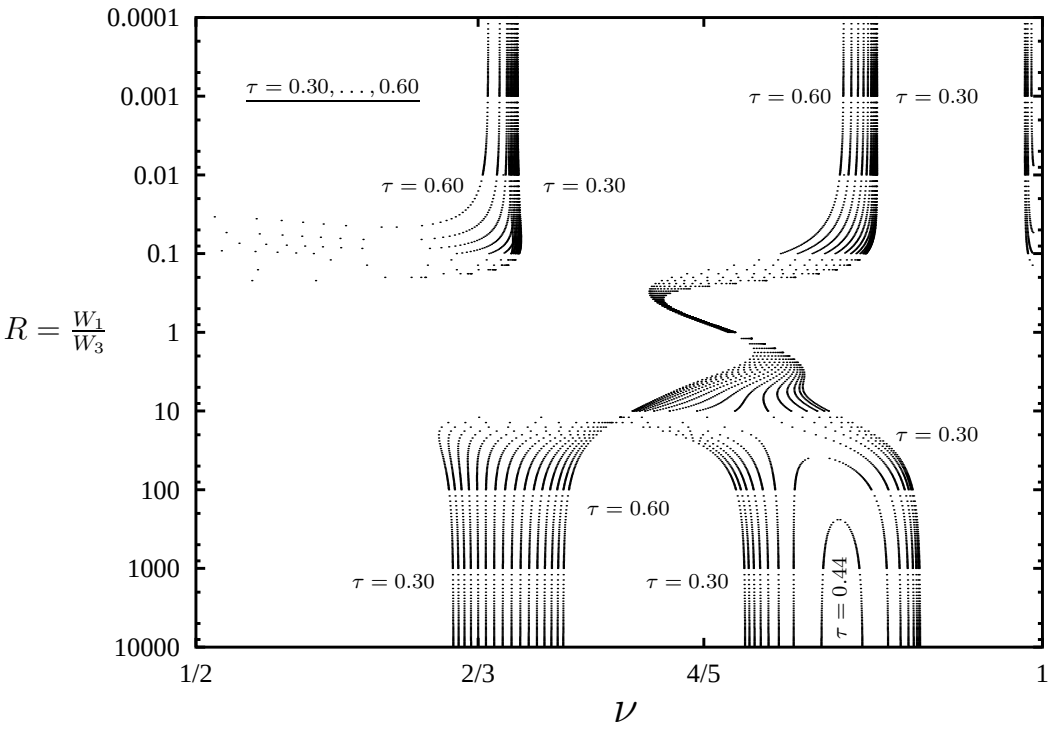

Figure 6.19: The crossover of the crossing points in the interacting part of the inverse compressibility $\kappa^{-1}_{T,W}(T,\nu)$ from $\nu = \frac{4}{5}$ to $\nu = \frac{2}{3}$ as the ratio R increases.

ature regime, the solutions of both equations are very close (compare the curves for $\tau = 0.3$ in both figures.). However, as the temperature is increased, both crossing points for $R < 0.1$ in Fig. 6.19 move towards smaller ν, while the corresponding curves in Fig. 6.18 move towards $\nu = 4/5$. For $R > 10$, the solutions shift to larger ν (it shifts to smaller ν in the other case).

3. Behaviour in the transition region: The solutions vary very rapidly with R in the transition region, but the varying of the solutions of different T is similar.

We would like to emphasise that the most interesting and may be the most important feature observed here is the crossing over of the solutions symmetric around $\nu = 4/5$ for small $R \sim 10^{-4}$ to $\nu = 2/3$ for large $R \sim 10^4$. This feature appears in both Fig. 6.18 and Fig. 6.19 but it can be seen clearer in the latter. This behaviour illustrates our statement that the form of the interaction is responsible for the location of the crossing points of the inverse compressibility on the filling factor axis.

Effects of the temperature T on the appearance of the crossing points

Next, we study the effect of the temperature. In Fig. 6.20, we show a series of plots, from three values of R, of the particle–hole symmetric inverse compressibility as a

function of the filling factor with the scaled temperature τ as a parameter. Plots in the same row belong to a given R; R increases from from top to bottom. The temperatures in the right plots are higher than the temperatures of the left plots. The two (scaled) temperatures given in each plot are the lowest and highest temperatures of the curves in the plot. The temperature difference between the nearest neighbour curves is 0.01.

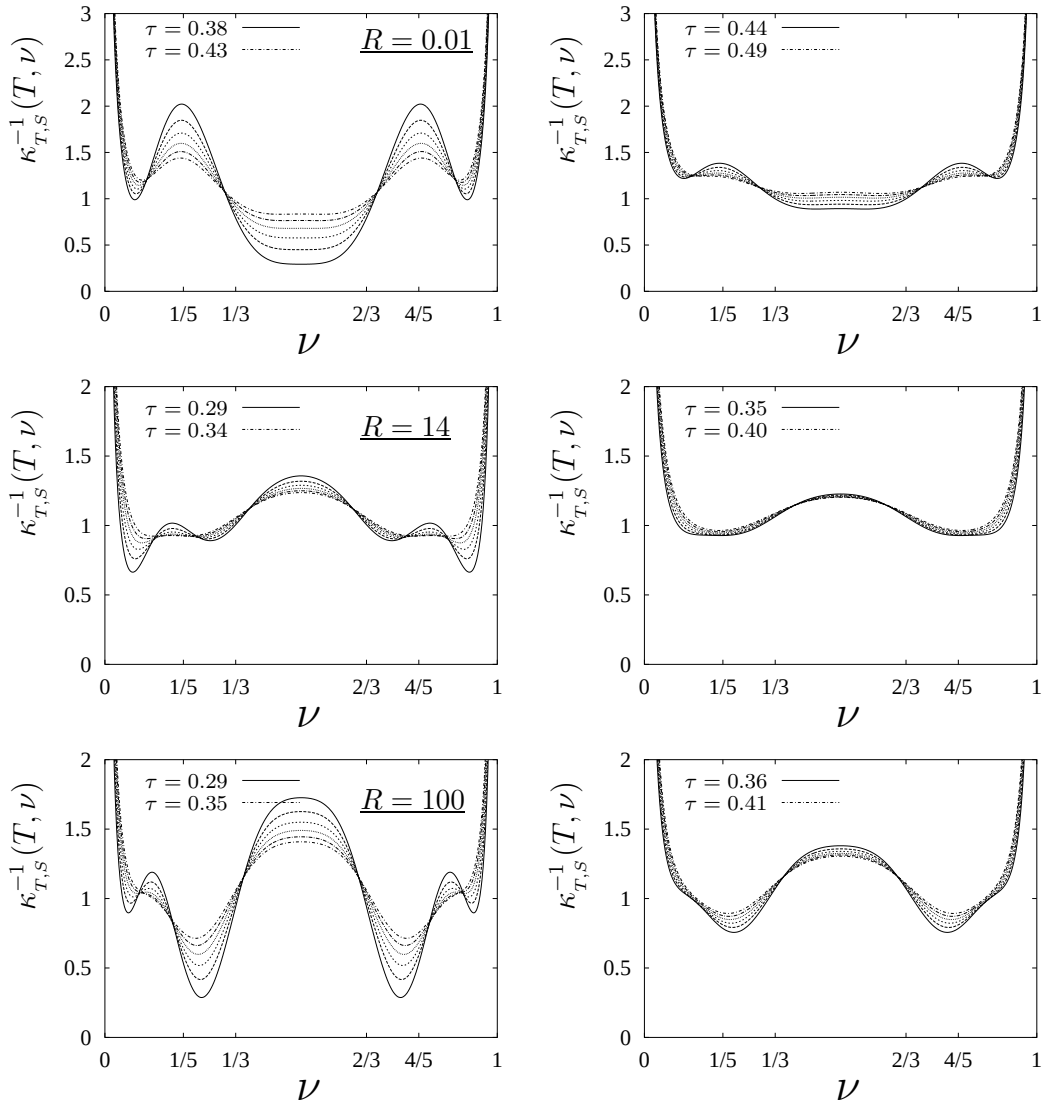

Figure 6.20: Effect of the temperature on the inverse compressibility for three values of the ratios $R = W_1/W_3$.

In any plot in Fig. 6.20, we see that increasing of the temperature reduces the magnitude of the slopes of $\kappa_{T,S}^{-1}(T,\nu)$ [or $\kappa_{T}^{-1}(T,\nu)$] in the neighbourhood of the crossing points. In case of $R = 100$, for which we observe the oscillations (for $0 < \nu < 1/5$ and $4/5 < \nu < 1$) at lower temperatures, these oscillations are weakened or removed as the temperature becomes higher.

When the temperature is raised, it weakens the singular behaviours observed in the lower temperature regimes. The singular behaviours corresponding to a particular fractional quantum Hall ground state will disappear when the temperature is high enough to overcomes the energy gap above that particular state. Considering the plots for $R = 14$, we see that by raising the temperature, we weaken the effect of the fractional quantum Hall ground state at $\nu = 1/3$ and $\nu = 2/3$ and remove any indication of the fractional quantum Hall ground state at $\nu = 1/5$ and $\nu = 4/5$ in $\kappa_{_T}^{-1}(T, \nu)$. That means that at the temperature shown in the right plots the temperature is already higher than the energy gap above the $(\nu = 1/5)$–fractional quantum Hall state, therefore, no signature of the $(\nu = 1/5)$–fractional quantum Hall ground state will be observed in $\kappa_{_T}^{-1}(T, \nu)$.

"Phase diagram" of the inverse compressibility for the (W_1+W_3)–interaction

In the following, we try to interprete the results of the high–temperature expansion in terms of a diagram similar to Fig. 6.14. As an indicator for the *phase*, we use the number of the crossing points (for $\nu > 1/2$). The Fig. 6.21 shows the resulting diagram in the (R, τ)–plane.

For high temperature, the structure of this map is similar to the schematic map of Fig. 6.14. However, we cannot reliably fill the area of the map at lower temperatures since the results are limited to finite temperature.

There are areas along the R axis as described before in the discussion of Fig. 6.14. The first area, part of it is now shaded in grey, is where $T > W_1$ and $T < W_3$. In this area, $R < 0.2$. The second area, part of it is now shaded in light grey, grey and black, is where $T < W_1$ and $T < W_3$. In this area, $0.2 < R < 20$. The third area, part of it is now shaded in light grey and black, is where $T < W_1$ and $T > W_3$. In this area, $R > 20$.

We see that the map looks complicated in the second area but it looks simpler in the first and the third areas. In the first area, the W_3–interaction dominates the interaction and there, we find two crossing points in the neighbourhood of $\nu = 4/5$. The third area is where the W_1–interaction dominates the interaction and where we find one crossing point in the neighbourhood of $\nu = 2/3$. The structure of the intermediate region, the second area, is complicated. The narrow region, where there are crossing points corresponding to both $\nu = 2/3$ and $\nu = 4/5$, is near $R \sim 10$ and $\tau \sim 0.35$. It is clear, that one needs higher orders in the high–temperature expansion, before one can hope to obtain more reliable results here.

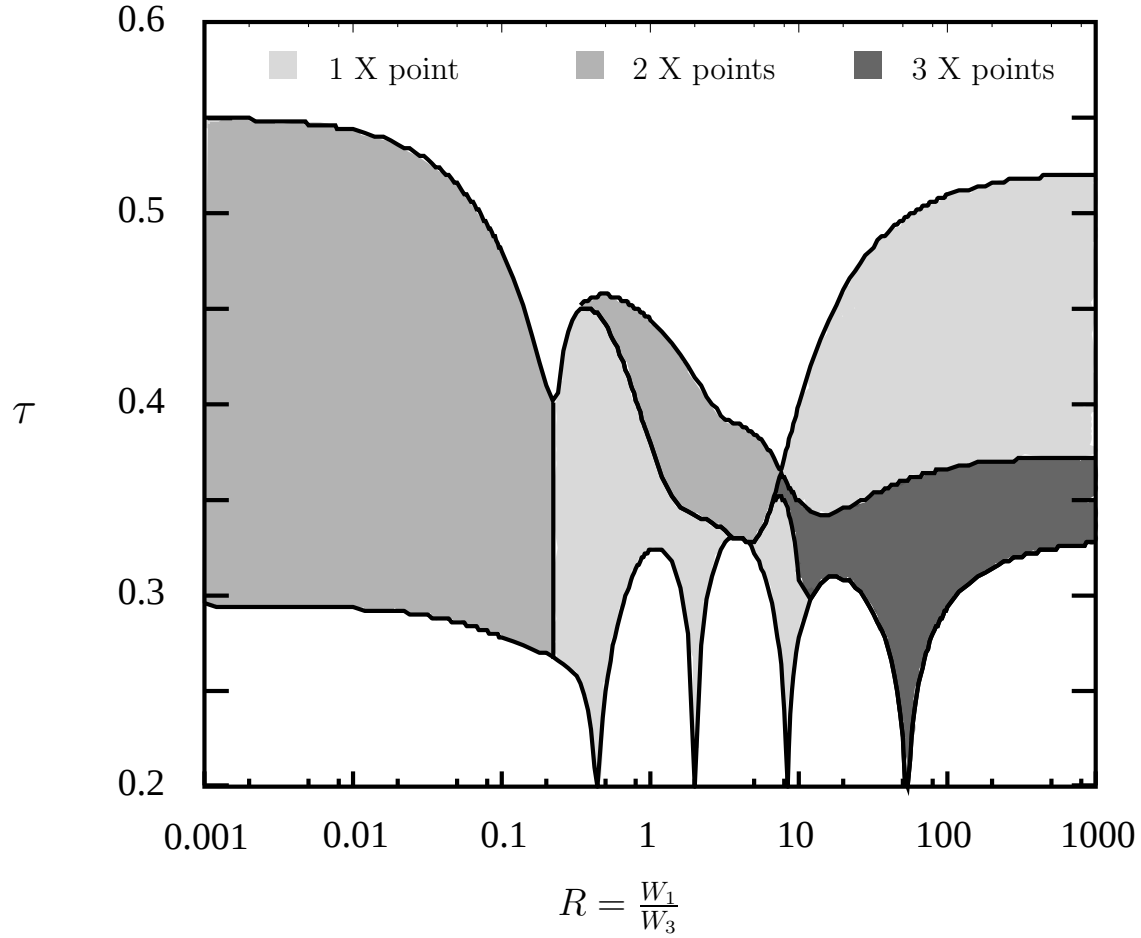

Figure 6.21: Phase diagram of the crossing points for $\nu > 1/2$.

Chapter 7

Energy and compressibility in the lowest Landau level: Extrapolated results

In Chapter 6, the exact results of the high–temperature expansion for the energy and the inverse compressibility were presented. The singular behaviour predicted by the Laughlin theory is characteristic only for the ground state. In order to reach ground state, one would need infinite orders of the high–temperature expansion. Therefore, in this chapter, we shall study three different extrapolation schemes which may help to extend our exact finite–temperature results to lower temperatures (since the zero temperature limit cannot be reached by our limited results). The aim of this chapter is to confirm the results and the tendencies observed at (high) finite temperature in the previous chapter within the limitations of the extrapolating schemes. As in the previous chapter, we shall start with the discussion on the energy which will be followed by the discussion on the inverse compressibility.

7.1 Extrapolation of the energy

We start again with the expression of the exact high–temperature expansion series of the energy

$$E(T, N_\phi, \nu) = N_\phi \sum_{n=1}^{\infty} \beta^{n-1} \alpha_n(\nu) \,, \tag{7.1}$$

where the coefficients of the expansion of the energy, $\alpha_n(\nu)$, defined in Eq. (6.3) have the dimension of T^n.

The general character of the energy per particle $\mathcal{E}(T, \nu)$ at zero temperature as expected for a zero–range interaction is as follows. The energy per particle is zero as long as the electron density, or the filling factor ν is smaller than a characteristic value,

ν_c, depending on the form of the electron–electron interaction and becomes finite as soon as the filling factor exceeds ν_c. This would give a down–ward cusp at ν_c. However, we do not expect a sharp cusp at finite temperature but a smooth behaviour. This smooth transition may appear as a bending of the curve of the energy per particle around ν_c. This bending should increase as the temperature is decreased.

In the following, we discuss three procedures of extrapolating the finite temperature energy to the ground state, $\mathcal{E}_0^{ext}(\nu)$ and to finite but lower temperatures, $\mathcal{E}^{ext}(T,\nu)$.

7.1.1 Padé approximants

The first extrapolation scheme is the well–known Padé approximants. A detailed discussion of the approximants we use here is given in Appendix G. For extrapolating the energy, we use the equal order $[k,k]$–Padé approximant. Within the order we can reach in the high–temperature expansion, we can calculate the approximants for $k = 1, 2, 3$. The $[k,k]$–Padé approximants are characterised by k poles in the T plane. For $k = 1$, the pole is at negative T for all ν, so we can approach the zero–temperature limit by this approximant. However, the energy $\mathcal{E}_0^{[1,1]}(\nu)$ becomes negative in a wide range of ν. This feature of the result is unphysical since the energy of the Hamiltonian, Eq. (3.34), is strictly positive for our zero–range interaction model which does not contain any interaction with a positive background. The $[1,1]$–Padé approximant is shown in the comparison of various approximations later in this section in Fig. 7.5. For $k = 2$, one of the poles is located at large positive T; thus, this approximant cannot be used for an extrapolation to low temperature. For $k = 3$, two poles are complex conjugate and one is negative for all ν. Thus, for $k = 3$ (as for $k = 1$) the finite temperature approximant approaches its zero–temperature limit smoothly (and uniformly in ν) as T is lowered. The approximant shows a clear indication of a cusp developing at the corresponding filling factor.

Below, we show series of plots of the $[3,3]$–Padé approximation of the energy per particle for the W_1–interaction, the W_3–interaction and the $(W_1 + W_3)$–interaction, respectively.

One–component interactions

Fig. 7.1 shows the extrapolated energy per particle plotted as a function of the filling factor for various temperatures. The results for the W_1–interaction and for the W_3–interaction is given in the top and bottom plot, respectively. In the top plot, for the W_1–interaction $\mathcal{E}^{[3,3]}(T,\nu)$ shows a clear indication of a cusp developing at $\nu = 1/3$ which is expected. In the other plot, for the W_3–interaction, $\mathcal{E}^{[3,3]}(\tau,\nu)$ shows, as in the exact results, no clear indication for a cusp at $\nu = 1/5$, but shows an improvement compared to the exact results.

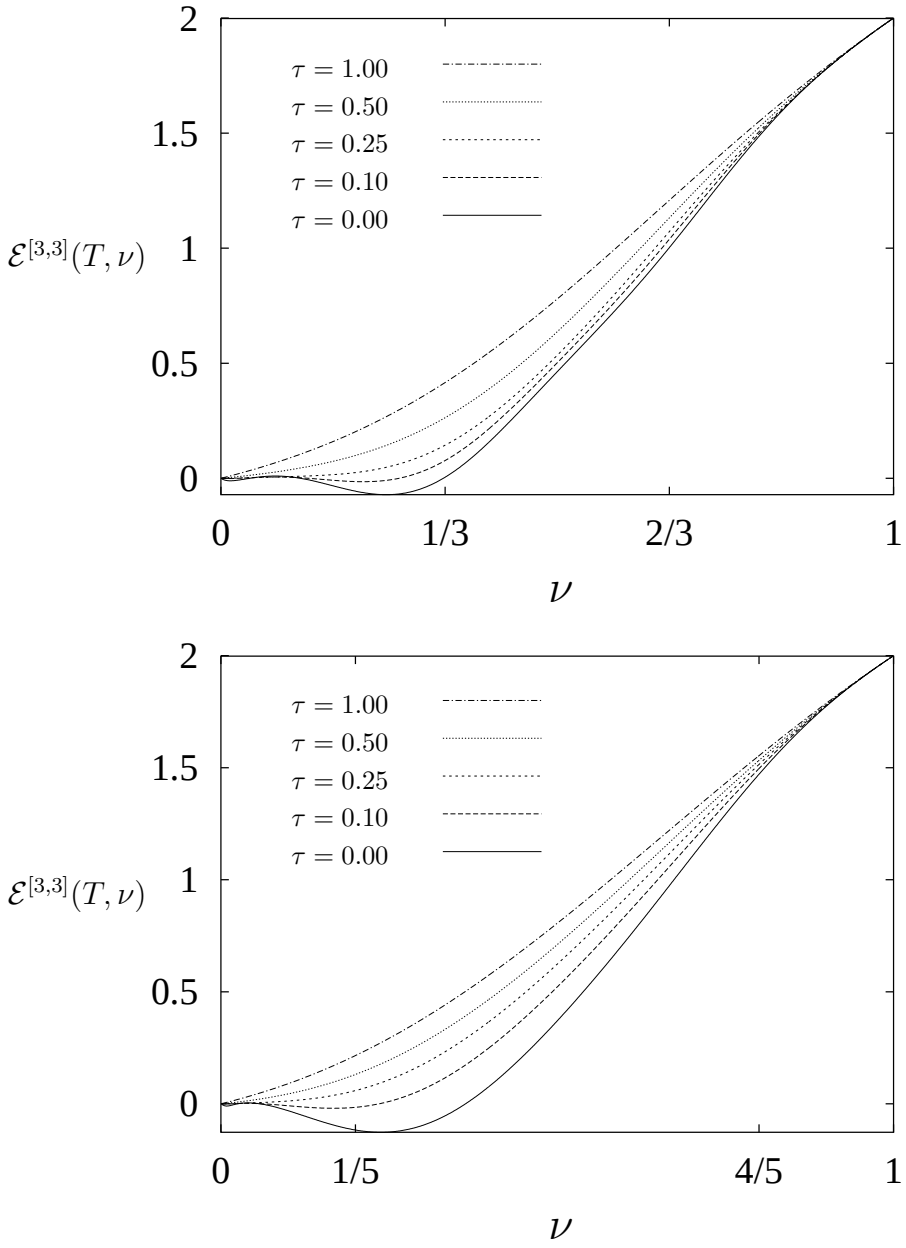

Figure 7.1: The $[3,3]$–Padé extrapolation for the energy per particle of two one–component interactions: W_1–interaction (above) and W_3–interaction (below).

Two–component interaction

Fig. 7.2 shows the extrapolated energy per particle plotted for $(W_1 + W_3)$–interaction as a function of the filling factor for various temperatures. The energy per particle is plotted for a given R in the top ($R = 4.5$) and the middle ($R = 12$) plots. It can be seen clearly that a cusp develops as the temperature is lowered, and the location where the cusp is found moves from $\nu = 1/5$ towards $\nu = 1/3$ as the the ratio R increases. In the bottom plot, the energy per particle is plotted for a given scaled temperature $\tau = 0.20$. Here, again, we see a movements toward $\nu = 1/3$ from $\nu = 1/5$ as R increases.

We do not see an indication of two cusps.

7.1.2 Exponential ansatz

In an attempt to avoid the unphysical divergencies in the rational Padé approximants, we try a new *ad hoc* ansatz function with an exponential dependence on temperature

$$E^{exp-fit}(T, N_\phi, \nu) = E_a(\nu) + E_b(\nu)\, e^{-\beta\Delta(\nu)} \,. \tag{7.2}$$

Here, positivity of ground state energy and specific heat would demand the positivity of all parameters $E_a(\nu)$, $E_b(\nu)$ and $\Delta(\nu)$. By comparing the high–temperature expansion of this function with the series Eq. (6.5) up to third order, we find as the ground state energy per particle

$$\mathcal{E}_0^{exp-fit}(\nu) = \frac{1}{\nu}\,\alpha_1(\nu) - \frac{1}{\nu}\,\frac{\alpha_2^2(\nu)}{2\alpha_3(\nu)} \,. \tag{7.3}$$

One–component interactions

There is again a range of negative energy in the small filling factor regime which is, however, a little smaller than in the case of the $[1,1]$–Padé approximant cf., Fig. 7.5. The major difference between the extrapolated results of this *exponential–fit* and the $[1,1]$–*Padé approximation* is that here, the asymptotic behaviour of the ground state energy per particle starts out with zero slope at $\nu = 0$.

We do not see much features within this extrapolation scheme due to the low order of the expansion it can account for. The $[3,3]$–Padé approximant extrapolates the exact series by taking seven order of the expansion into account, while the *exponential–fit* takes only three order of the expansion into account. We have tried to improve the model by using a different exponent and prefactor but no convincing extrapolated result could be obtained. In Fig. 7.3, we show the results of two extrapolation schemes for two one–component interaction studied here, W_1–interaction and W_3–interaction. We see that the curves belonging to the W_1–interaction are to the right of those of the W_3–interaction as expected.

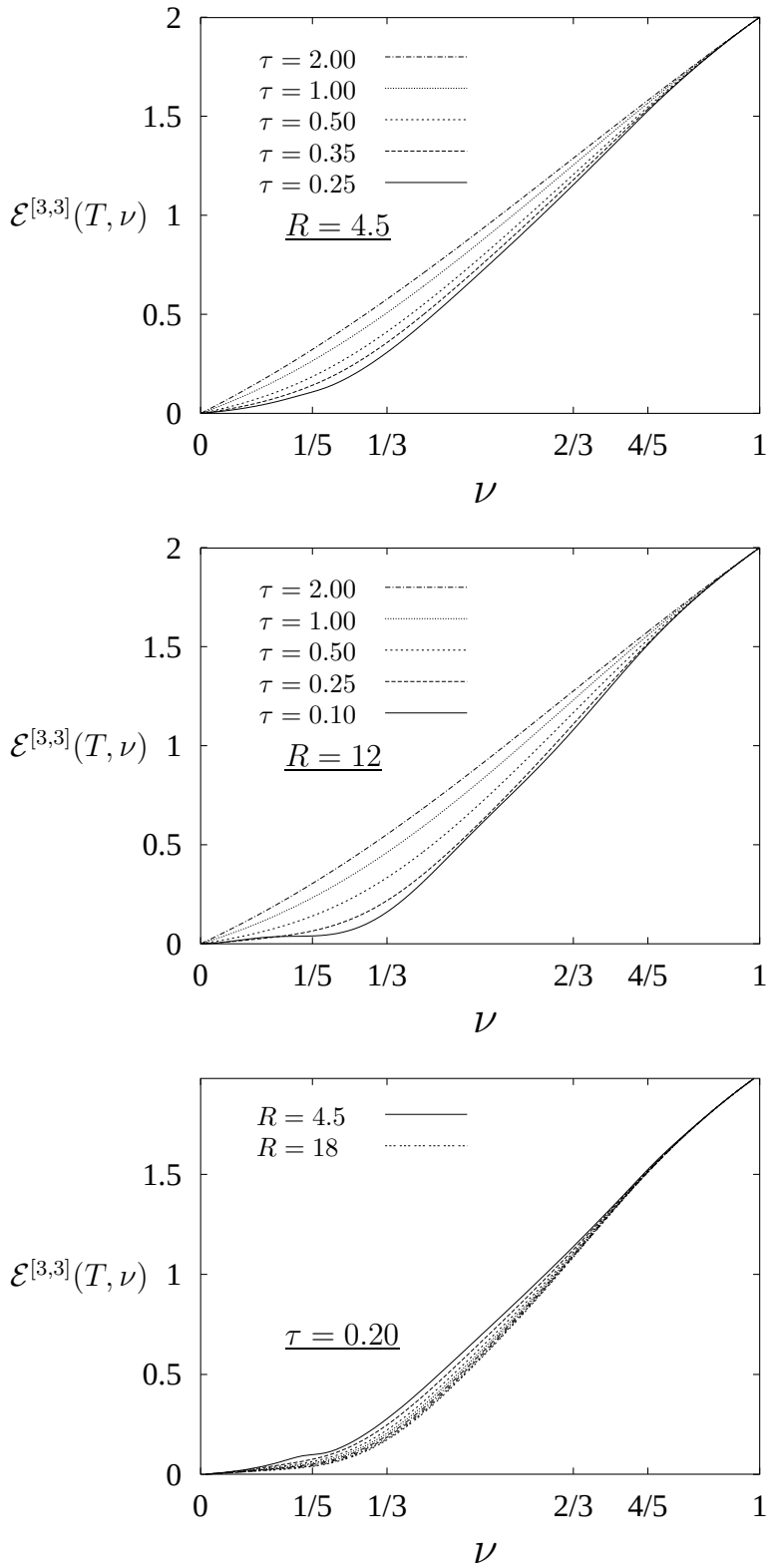

Figure 7.2: The $[3,3]$–Padé extrapolated energy per particle of a multi–component interaction $(W_1 + W_3)$–interaction, the ratio $R = W_1/W_3$. The R difference between two adjacent curves is 2, except for the upper most pair in which $R = 4.5$ and $R = 6$.

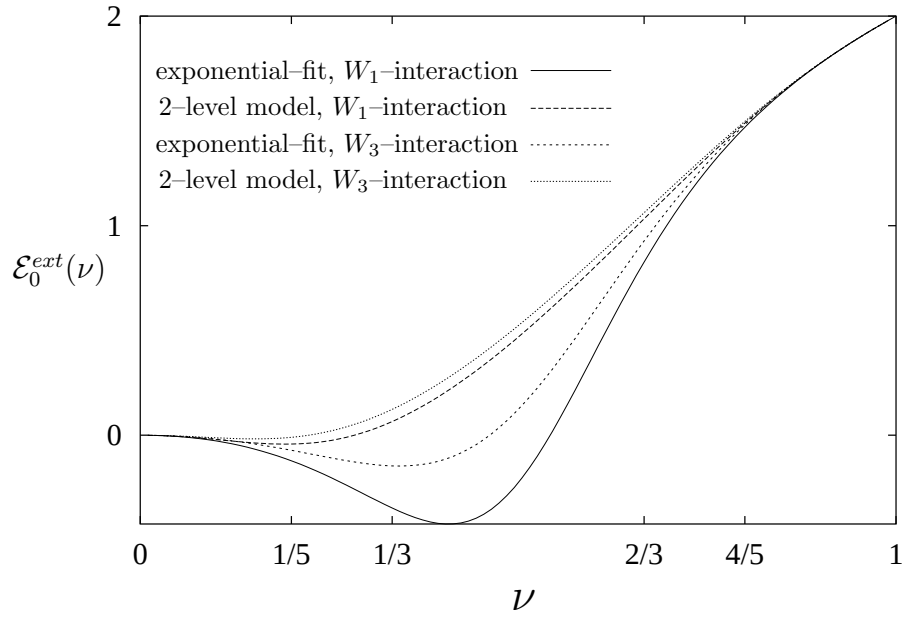

Figure 7.3: Extrapolated ground state energy per particle of the W_1–interaction and W_3–interaction as a function of the filling factor from two extrapolation schemes : the *exponential–fit* and the *2–level model*.

Two–component interaction

It has not been possible to extrapolate the exact high–temperature expansion series of the energy of the $(W_1 + W_3)$–interaction by the exponential ansatz.

7.1.3 N_L–level ansatz

Motivated by the *exponential–fit* scheme, we now study a different ansatz. This approximates the exact many–body density of states by concentrating the levels into only N_L levels, at an energy $E_j(\nu)$. The levels are degenerate with degeneracy $n_j(\nu)$. This yields

$$E^{N_L-level}(T, N_\phi, \nu) = N_\phi \, \frac{\sum_{j=1}^{N_L} E_j(\nu)\; n_j(\nu)\; e^{-\beta E_j(\nu)}}{\sum_{j=1}^{N_L} n_j(\nu)\; e^{-\beta E_j(\nu)}} \; . \tag{7.4}$$

The parameters $n_j(\nu)$ and $E_j(\nu)$ are to be determined. In the N_L^{th} order of this approximation we need $(2N_L - 1)$ terms of the high–temperature expansion (we rescale the $n_j(\nu)$ to fulfil the normalisation condition $\sum_{j=1}^{N_L} n_j(\nu) = 1$). In the lowest order, $N_L = 2$, we get the ground state energy per particle as

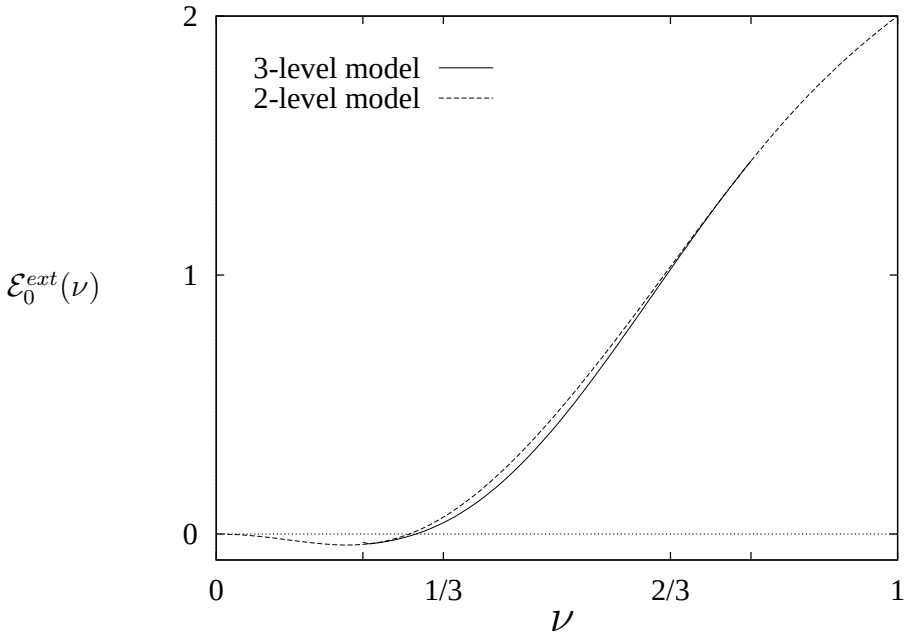

Figure 7.4: The ground state energy of the three–level model compared to that of the two–level model for the W_1–interaction. ν_c and $1-\nu_c$ are the critical filling factors where the three–level model collapses to the two–level model.

$$\mathcal{E}_0^{2-level}(\nu) = \frac{1}{\nu}\,\alpha_1(\nu) - \frac{1}{\nu}\,\frac{\alpha_2^2(\nu)}{\alpha_3(\nu) + \sqrt{\alpha_3^2(\nu) - \alpha_2^3(\nu)}}\,. \tag{7.5}$$

Details for the calculation of $N_L = 3$ are given in Appendix H.

One–component interactions

The two–level model, Fig. 7.3, shows clear indication of a cusp developing in the energy per particle at $\nu = 1/3$ for the W_1–interaction and at $\nu = 1/5$ for the W_3–interaction in the limit of zero temperature.

The three–level model shows a small improvement toward the expected solution. But there are difficulties in applying this extrapolation scheme to any other interaction except the W_1–interaction. These difficulties also exist in the case of the W_1–interaction but not for the wide range of ν. However, they exist in the wide range or the whole range of ν in cases of other interactions. Thus, we shall discuss the application of the three–level model only to the case of the W_1–interaction.

The ground state energy of the three–level model is shown in Fig. 7.4. We compare the ground state energy of this three–level model with that of the two–level model. From that figure, we can clearly see that the ground state energy of the three–level model merges into that of the two–level model at both ν_c and $1-\nu_c$.

In conclusion, the analysis of the three–level model shows that the deviation of the

ground state energy of the three–level model from that of the two–level model is small, even at its maximum. Nevertheless, the three–level model represents an improvement toward the exact solution.

It may be useful to note that the model given in the N_L–level model may not fit to the nature of the system we study. In this model, we assume that the energy spectrum of the system can be separated into N_L–degenerate energy levels. As it turns out clearly in the case of W_1–interaction discussed above, two of three energy levels merge and become twofold degenerate–energy–level–system.

Two–component interaction

It has not been possible to extrapolate the exact high–temperature expansion series of the energy of the $(W_1 + W_3)$–interaction by the N_L–model.

Comparison of the extrapolated results:

In Fig. 7.5, we show the results of three extrapolation schemes. The results point in the same direction: The down–ward cusp in the energy per particle develops at the corresponding filling factor.

Note that in Ref. [28] the free energy is extrapolated while we extrapolate the energy. Thus, our result appears to be different from their Fig. 3 in Ref. [28], yet both curves have the same form. However, calculating the free energy from our result, Eq. (6.5), and extrapolating the free energy, we have precisely reproduced the result Fig. 3 of Ref. [28]. The transformation between the canonical free energy and energy is shown in Appendix B.

7.2 Extrapolation of the inverse compressibility

We start with the expression of the exact high–temperature expansion series of the inverse compressibility taken from Eq. (6.11)

$$\kappa_{_T}^{-1}(T,\nu) \;=\; \frac{T}{2\pi}\;\frac{\nu}{1-\nu} + \frac{1}{2\pi}\;\sum_{n=1}^{\infty}\;\beta^{n-1}\;k_n(\nu)\;, \tag{7.6}$$

where, we define coefficients of $\kappa_{_T}^{-1}(T,\nu)$ as

$$k_n(\nu) \;=\; \frac{1}{n}\;\nu^2\;\frac{\partial^2\alpha_n(\nu)}{\partial\nu^2}\;. \tag{7.7}$$

From the Laughlin theory, the ground state of the fractional quantum Hall system is an incompressible state which means that the inverse compressibility diverges as $T \to 0$.

The inverse compressibility changes very rapidly as a function of the filling factor, especially at the ground state, i. e., the inverse compressibility decreases with the

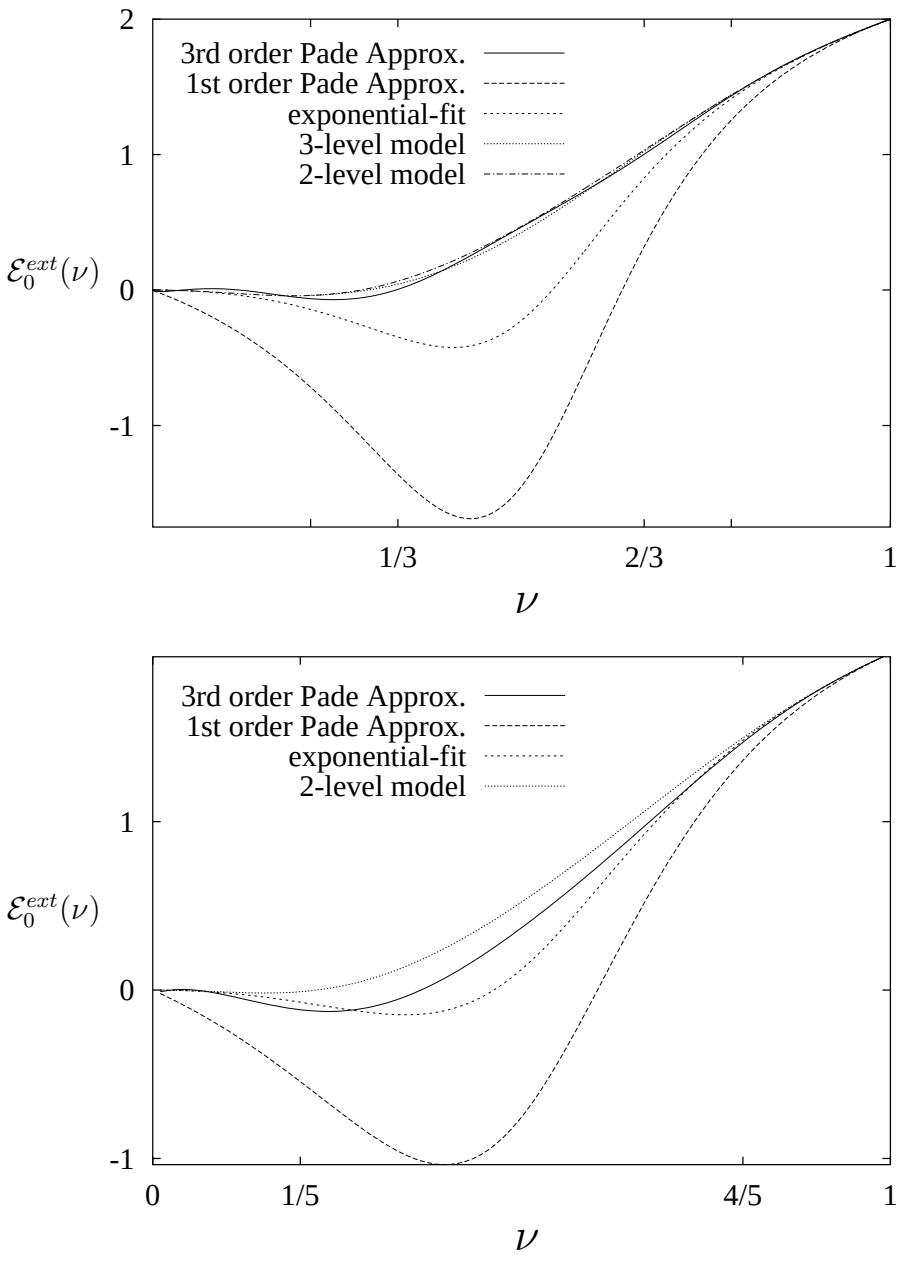

Figure 7.5: Comparison of the extrapolated ground state energy per particle from 3 different schemes described in the text. The top plot is of the W_1–interaction and the bottom plot is of the W_3–interaction.

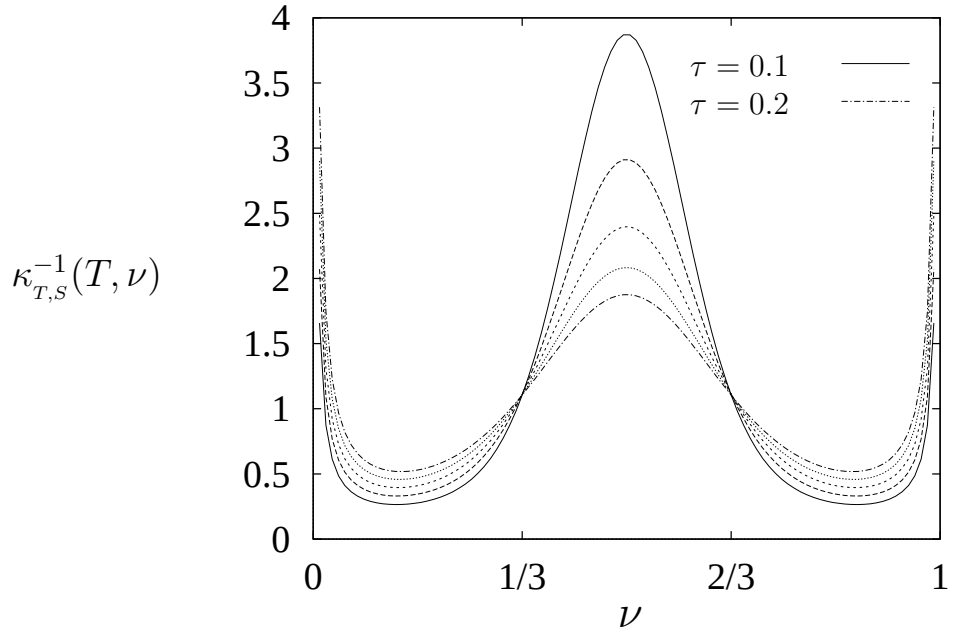

Figure 7.6: The extrapolated inverse compressibility for the W_1–interaction as a function of the filling factor. The extrapolation function conatians four parameters $a(\nu), b(\nu), c(\nu)$, and $d(\nu)$ and is defined as $\kappa_T^{-1}(T,\nu) = T\left[a(\nu) + \left(b(\nu) + \frac{1}{T}c(\nu)\right)\, e^{-\frac{1}{T}d(\nu)}\right]$. The temperature difference between the adjacent curves is 0.025.

decreasing of the temperature below a critical filling factor and diverges as the temperature decreases at the critical filling factor. To extrapolate such a quantity which behaves extremely is a difficult task even though, in our case, we have a suggestion from the result of the Virial expansion that the inverse compressibility should start out from the origin ($\nu = 0$) exponentially in the inverse temperature.

We have tried several extrapolation schemes including those used for extrapolating the energy. However, we found finite temperature singularities in any scheme except those which take only a few coefficients, $k_n(\nu), n \leq 3$, into account. This low order extrapolation results, one scheme of them is shown in Fig. 7.6, cannot and should not provide insightful result, therefore we shall not discuss those schemes here. The Padé approximants which provide good result in the extrapolation of the energy also have unphysical singularities in the extrapolation of the inverse compressibility, however, they deserve some consideration. We shall briefly discuss these Padé extrapolated results.

7.2.1 Padé approximants

One–component interaction, W_1–interaction

The $[4,3]$–Padé extrapolated inverse compressibility is shown in Fig. 7.7 for the W_1–interaction. We see that there are singularities on the left and right of the plot.

We see the crossing points similar to those appearing in the exact high–temperature expansion results. Unfortunately, up to this order of the approximant, $[4,3]$, only $k_n(\nu),\ n = 1,\ldots,7$ are taken into consideration. This means that it is unlikely that the application of this approximant to the W_3–interaction would be fruitful because up to this order, the results for the W_3–interaction vary strangely with the order.

Two–component interaction, $(W_1 + W_3)$–interaction

The $[4,3]$–Padé extrapolated inverse compressibility is shown in Fig. 7.8 for the $(W_1 + W_3)$–interaction. We see that there are singularities on the left and right of the plot. We would like to mention only two points which are clearly observed from the plots: First, there are crossing points appearing in the top plot. They appear in the same manner as those in the exact high–temperature expansion result but we observe two weak crossing point between $\nu = 1/5$ and $\nu = 1/3$ and between $\nu = 2/3$ and $\nu = 4/5$ which are not seen in the exact high–temperature expansion result. Second, we observe in the bottom plot that magnitudes of peaks of the extrapolated inverse compressibility change according to the interaction parameter R. The magnitude of peaks at $\nu = 1/3$ and $\nu = 2/3$ increases as R increase while the magnitude of peaks at $\nu = 1/5$ and $\nu = 2/5$ decreases accordingly. This behaviour is as expected.

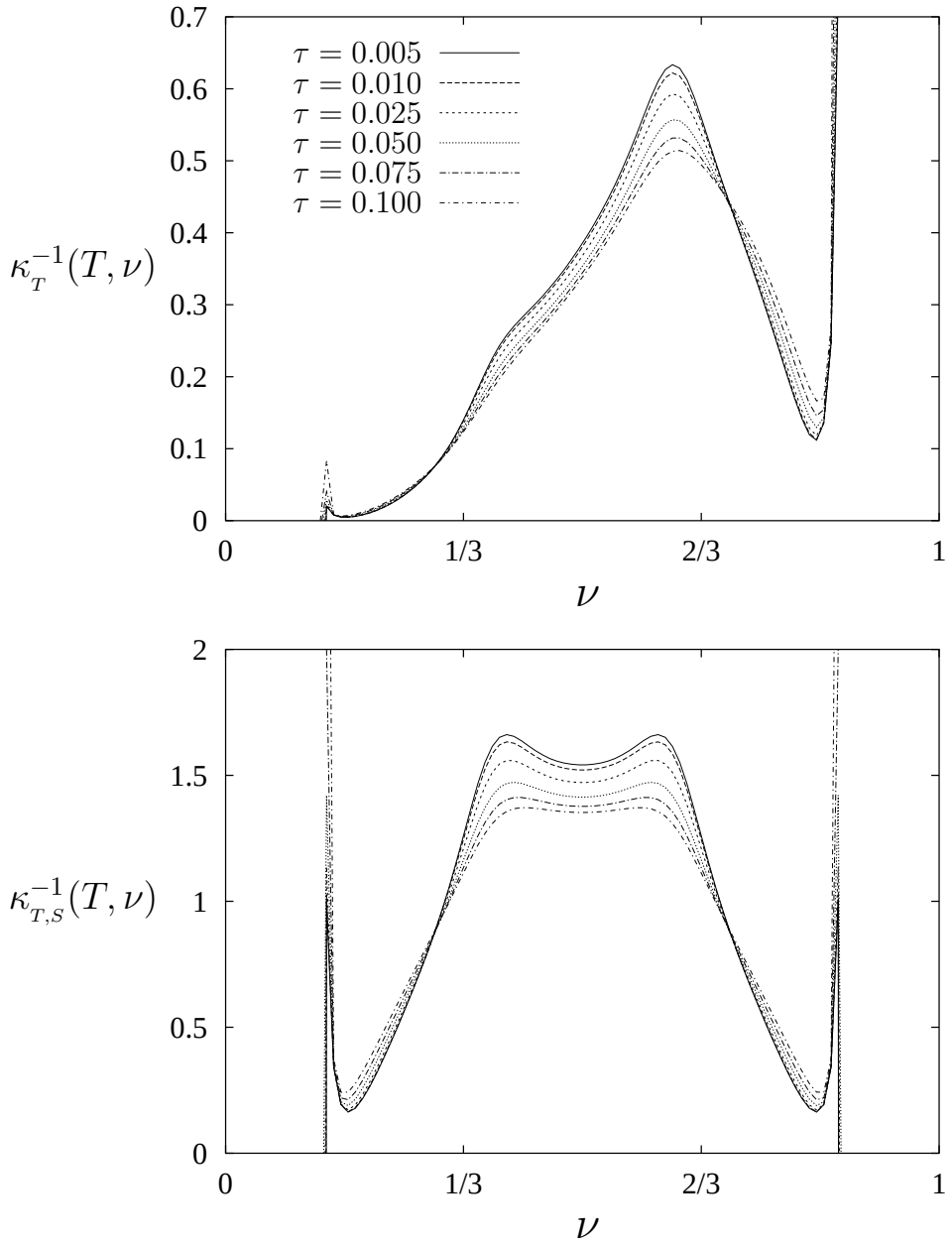

Figure 7.7: The inverse compressibility extrapolated by the $[4,3]$–Padé approximant. The top plot is the actual extrapolated inverse compressibility while the bottom plot is its particle–hole symmetric part. Curves of the same line types are plotted for the same temperature.

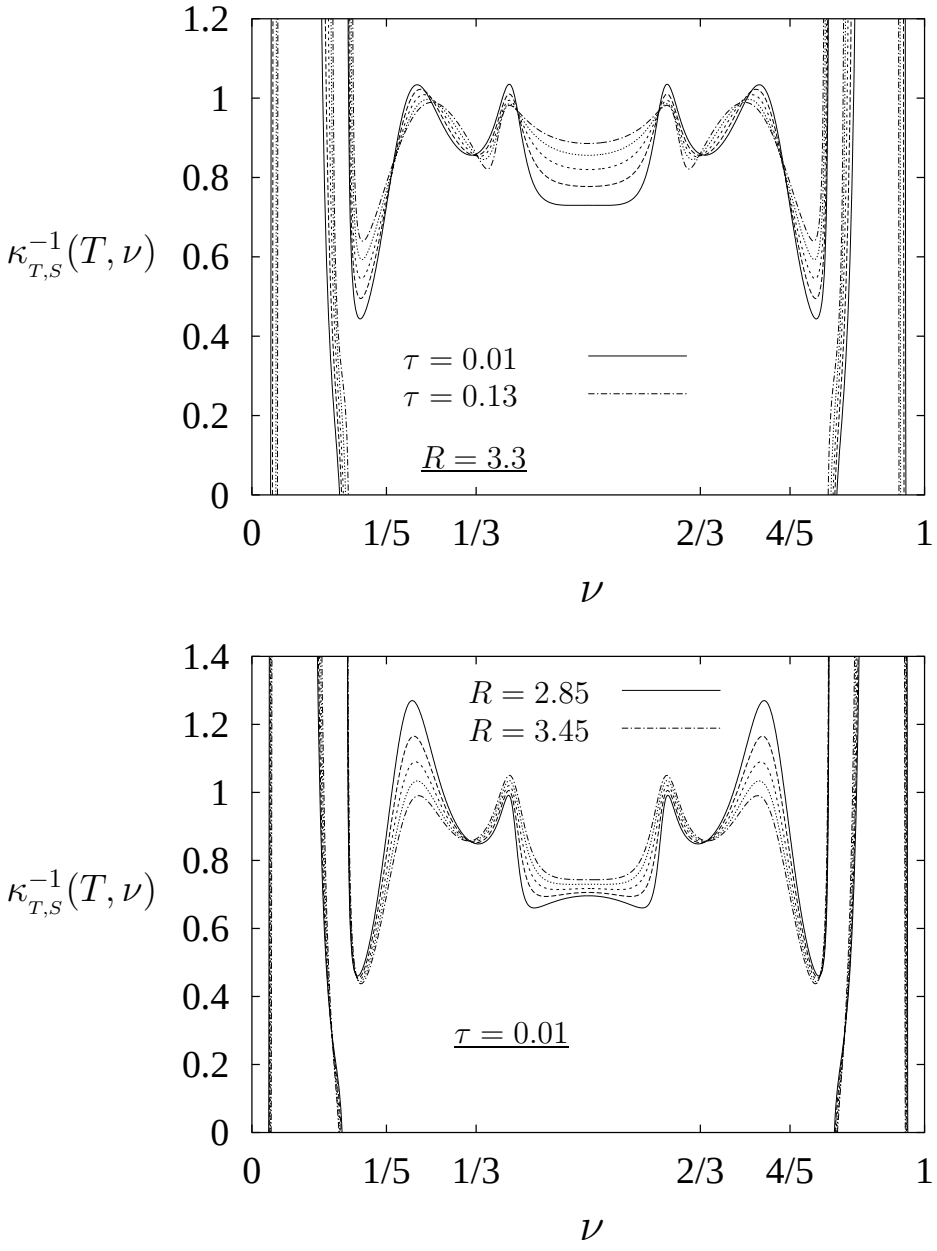

Figure 7.8: The particle–hole symmetric Padé extrapolated inverse compressibility of the $(W_1 + W_3)$–interaction: The extrapolated inverse compressibility is plotted for constant $R = 3.3$ in the top plot. The temperature difference between the adjacent curves, in this plot, is 0.03. In the bottom plot, the extrapolated inverse compressibility is plotted for a constant temperature $\tau = 0.01$. The R difference between the adjacent curves is 0.15.

Part V

Conclusions and Outlook

Chapter 8

Conclusions

The grand canonical thermodynamic potential of the fractional quantum Hall system – electrons moving in two dimensions in a strong magnetic field and at low temperature – in the limit where only states in the lowest Landau level are occupied, has been calculated with the high–temperature expansion method up to the eighth order of the expansion in the interaction. The method considered here is applicable in the region where the temperature is finite but much lower than the cyclotron energy which separates two Landau levels. The grand canonical thermodynamic potential is written as a power series in the inverse temperature with the coefficients expressed as a sum of *patterns* with prefactors which are polynomial in the Fermi function. Patterns are defined as common factors in the *connected diagrams* which yield the same frequency sums. The definition of the patterns is possible due to the degeneracy of the Landau level. From the grand canonical thermodynamic potential, the energy and the particle number, or the particle density, have been derived as a function of the chemical potential. Inverting the expression of the particle density as a function of the chemical potential results in the chemical potential as a function of the particle density or the *filling factor*. Thus, the energy can be written as a function of the filling factor. (For a fixed particle number, the filling factor can be varied through the change of the magnetic field; this magnetic field sets the number of the single particle states in a Landau level.) Under the Legende transformation from the grand canonical ensemble to the canonical ensemble, the *reducible patterns* which contain a *self–energy insertion* of the *first order* are subtracted. Due to the translation symmetries in x– and y–directions, a pattern which contains a self–energy insertion of any order can be replaced by the product of *proper patterns*. Thus, the energy can be written as a power series in the inverse temperature where the coefficients are expressed as sums of proper patterns with polynomial prefactors of the filling factor. A proper pattern is characterised by two matrices which describe the connectivity of the diagram and are independent of the interaction. From the energy, the canonical free energy has been derived.

The proper patterns up to the third order, and thus the energy of an arbitrary interaction up to this order have been evaluated. This result has been checked with the

known result from the traditional perturbative method and is found to be identical. Also, the energy of the lowest order in the filling factor has been obtained for all temperature in an arbitrary interaction and has been compared with the result from the second order Virial expansion. The comparison shows the equivalence.

The study carried out here is confined to the lowest Landau level. However, as have been shown, the interaction matrix element of the higher Landau level can be written as a linear combination of the interaction matrix element of the lowest Landau level due to the equivalence of the Hilbert space of different Landau levels. Thus, a study of the $(W_1 + W_3)$–interaction for the special ratio $R = W_1/W_3 = 1$ in the lowest Landau level is identical with the study of the zero–range interaction with $W(r) = W4\pi(1+\Delta)\delta^2(r)$ in the first Landau level.

The proper patterns up to the eighth order have been evaluated for three zero–range interactions, i. e., the W_1–interaction, the W_3–interaction, and the $(W_1 + W_3)$–interaction. Thus, the energy, the canonical free energy, and, thus, the compressibility for the zero–range interactions have been obtained up to the eighth order. The energy and the compressibility have been studied as functions of the interaction and the temperature.

The ground state energy per particle of the fractional quantum Hall system of the W_{2m+1}–interaction is known to have a cusp at a filling factor of $\nu = \nu_m = 1/(2m + 3)$. Thus, an appearance of a cusp is used as an indication of the existence of the fractional quantum Hall state. At high temperature, the energy shows always the result of the Hartree–Fock calculation. If the temperature decreases, the energy per particle up to the eighth order of the expansion in the *one–component* interactions, i. e., the W_1–interaction and the W_3–interaction, develops a cusp at the expected filling factor corresponding to the interaction. However, the indication of the cusp in the energy per particle of the W_1–interaction is stronger than the that of the W_3–interaction. Up to the order considered here, the energy per particle of the *mixed* interactions or the *two–component* interaction, the $(W_1 + W_3)$–interaction, develops only one cusp. The location of the cusp is defined as a filling factor where the slope of the energy per particle with respect to the filling factor changes its behaviour as the temperature is lowered. The study of this cusp shows that the cusp moves smoothly between the limits given by the one–component interactions.

The curves of the inverse compressibility of a given interaction for different temperatures *cross* at certain filling factors. These *crossing points* are shown to be an indication of a fractional quantum Hall state. Two *sum rules* which ensure the existence of the crossing points are derived. They indicate that the existence of the crossing points is *due to* the interaction. There will be *at least two* crossing points in any plot of the inverse compressibility as long as the temperature is not too high and there will always be at least two crossing points in the plots of the interacting part of the inverse compressibility.

The filling factors of the crossing points are determined numerically as filling factors

where the first temperature derivative of the inverse compressibility vanishes. For the one–component interactions, the W_1–interaction and the W_3–interaction, the crossing points in the inverse compressibility appear in the neighbourhood of the expected filling factor corresponding to the interaction. Two and four crossing points are observed in case of the W_1–interaction and the W_3–interaction, respectively. In the case of the $(W_1 + W_3)$–interaction, *six* crossing points can be observed for a narrow range of the ratio between W_1 and W_3. These six crossing points can be identified with the crossing points existing in the two one–component interactions. Thus, the appearance of these six crossing points indicates that two fractional quantum Hall states exist simultaneously. The study of the crossing points as a function of the interaction shows that their location is interaction dependent. The crossing points are weakened by the increase of the temperature.

Chapter 9

Outlook

The field of the fractional quantum Hall effect is very rich. There are many open questions and many new questions may arise at any time. In the following, we shall list some extensions which can be made to the present work in order to answer or verify some open questions.

Remaining unattended crossing point

We have pointed out that there is a second kind of crossing points in the inverse compressibility. These are crossing points between curves at the same temperature, but for different interaction. This kind of crossing point needs to be critically examined because it seems to emphasise the characteristic behaviour of the inverse compressibility. One knows that without an interaction, there will be no such a crossing point. However, the crossing points of this kind indicate that the inverse compressibility is interaction independent at some filling factors. One may try to interpret this crossing point also as a signal of the fractional quantum Hall state.

Higher orders of the expansion

The eighth order results provide qualitative pictures but cannot provide any quantitative information. This is also the lowest order for which the qualitative pictures start to appear. One can see that the results provide clearer pictures for the W_1–interaction compared to those of the more complicated interactions such as the W_3–interaction and the $(W_1 + W_3)$–interaction. Thus, higher order results are desirable in order to confirm and to quantify the observations made here. When higher order terms are included, the temperature can be lowered, thus the effects can be studied in more details with more accuracy.

Longer range interaction

The result up to the eighth order has been evaluated only for the zero–range interaction. It would be desirable to evaluate this result for other interactions which are more realistic, or have longer range, for two reasons. First, the result may provide the information of how the fractional quantum Hall states depend on the range of the interaction or whether the long–range interaction yields stable fractional quantum Hall states. Second, the comparison of the result of the present method to results of other theoretical studies or the experimental studies might become possible. This may also enable us to study the hierarchical states observed in experiments and other theoretical model studies which have longer range interactions.

Higher–Landau Levels

As the interaction matrix element of the higher Landau level can be written as a linear combination of the interaction matrix element of the lowest Landau level, one may be able to study the fractional quantum Hall states in the higher Landau levels by the results obtained here. However, the proper patterns have to be evaluated with the corresponding interaction. There is no Laughlin type of state, which is the exact ground state of a zero–range interaction, in the higher Landau levels, but fractional quantum Hall states such as $\nu = 4/3, 5/3$, and $\nu = 7/3$ are observed experimentally. Thus, it might be interesting to examine in the higher Landau level the effects of the interactions for which the Laughlin states are the exact ground states in the lowest Landau level.

Spin properties

The calculation which has been performed here is for a spin polarised system; the spin dependence is excluded. It will be very interesting to generalise the present method to include the spin. Then, one may be able to reconsider the states such as the $\nu = 2/3$ where it is still unclear whether it is a spin polarised state or a spin unpolarised state.

Comparison to the experiment: crossing points

There is one experiment on the inverse compressibility of the fractional quantum Hall system which is known to us [73]. The experiment was performed in order to measure the compressibility signature d_t which is proportional to the inverse compressibility. The experimental result is shown below in Fig. 9.1. Qualitatively, one can say that one sees similar features in the experimental result and our theoretical result, cf. Fig. 6.15. Note that d_t is direct proportional to $\kappa^{-1}_{T,S}(T,\nu)$ and the filling factor axes in the experimental plot and our plots are different. However, there appear two crossing points near $\nu = 1/3$ in the experiment but one in the theory.

Here, we have the following working hypothesis: We discuss only the crossing points in the first half of the filling factor axis $0 < \nu < 1/2$. The crossing point of the left on the expected filling factor, i. e., left of ν_m for the W_{2m+1}–interaction, appears necessarily but the crossing point on the right on the expected filling factor is due to the possible existence of a quantum Hall state at a larger filling factor. Thus, we interpret the crossing point on the right of $\nu = 1/5$ as a W_3–interaction also leads to a suppression of relative angular momentum 1 in the wavefunction. This means that if particles avoid to have a relative angular momentum m, they should avoid also any angular momentum smaller than m.

Our argument yields a possible explanation for the appearance of the crossing point right of $\nu = 1/3$ in the experiment. It appears because of the existence of the fractional quantum Hall state at $\nu = 2/5$. However, we do not see the crossing point on the right of $\nu = 1/3$ in our theoretical plots, e. g. Fig. 6.9, Fig. 6.10 and Fig. 6.15. This requires a consideration of the effect of the temperature. We argue that the temperature we can study in the eighth order result is still to high for an existence the fractional quantum Hall state at $\nu = 2/5$. Thus, the crossing point on the right of $\nu = 1/3$ does not appear in our plots. In the experiment, however, the temperature is low enough for the existence of the fractional quantum Hall state at $\nu = 2/5$, thus the crossing point right of $\nu = 1/3$ appears.

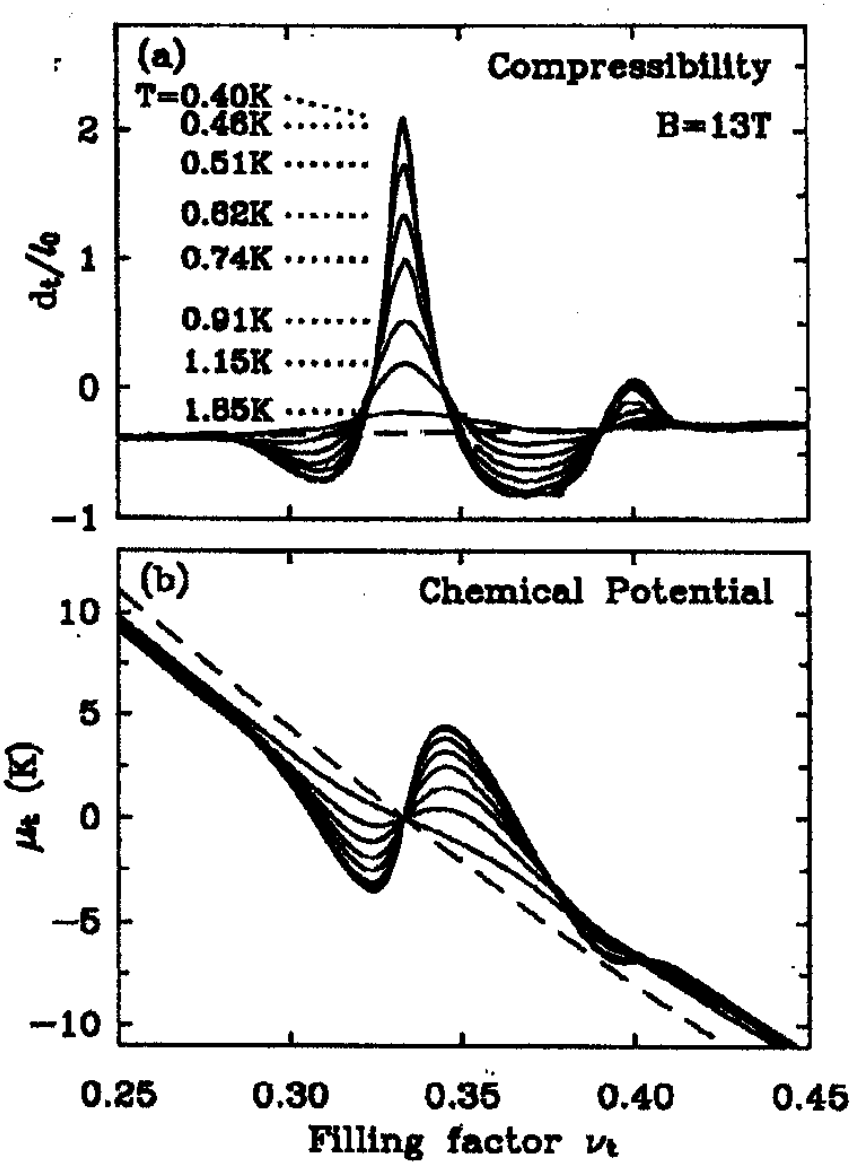

Figure 9.1: Experimental result of the compressibility signature $d_t \equiv (\epsilon/e^2)(\partial\mu/\partial N)$ which is proportional to the inverse compressibility (l_0 is the magnetic length). After Fig. 9 of J. P. Eisenstein, L. N. Pfeiffer, and K. W. West, Phys. Rev. B **50**, 1760 (1994): *(a) Temperature dependence of $\nu_t = \frac{1}{3}$ FQHE compressibility signature at $B = 13$ T. The nearly horizontal dashed line is a fit to the high–temperature background compressibility. (b) Chemical potential around the $\nu_t = \frac{1}{3}$ FQHE obtained by integrating the compressibility data in (a). Dashed line is the integral of the background compressibility.*

Part VI

Appendix

Appendix A

Interaction matrix element in the first Landau level

There are two calculation to be discussed in this section. The first calculation is a direct derivation, as we have done in Section 3.4.1, of the interaction matrix element in the first Landau level as a function of the momentum difference and the pseudo potential coefficients, W_{2m+1}. The second calculation is an indirect derivation where we consider how the pseudo potential coefficients of the first Landau level $W_m^{(1)}$ can be expressed as linear combinations of the pseudo potential coefficients of the lowest Landau level W_{2m+1}. As expected, these two calculations lead to the same result.

A.1 The first consideration

The single particle wave function for particle in the first Landau level takes the form

$$\varphi_{1,k}(x,y) = \left(\tfrac{2}{L_y}\right)^{1/2} \tfrac{1}{\pi^{1/4}} \, (x+k) \, e^{iky - \frac{1}{2}(x+k)^2} \, . \tag{A.1}$$

Using the above wave function and following the calculation of the preceding section, the interaction matrix element in Eq. (3.35) becomes

$$\begin{aligned} W^{(1)}_{k_1k_2k_3k_4} = \tfrac{1}{L_y^2} \, \tfrac{1}{\pi} \int d^2r \int d^2R \; & e^{-\frac{i}{2}\left[(k_1+k_2)-(k_3+k_4)\right] R_y} \; e^{-\frac{i}{2}\left[(k_1-k_2)+(k_3-k_4)\right] r_y} \\ & W(r) \; e^{-\frac{1}{2}\left(k_1^2+k_2^2+k_3^2+k_4^2\right)} \; e^{-\frac{1}{2}R_x^2 - \frac{1}{2}(k_1+k_2+k_3+k_4)\, R_x} \; e^{-\frac{1}{2}r_x^2 - (k_1-k_2-k_3+k_4)\, r_x} \\ & \left(\prod_{j=1}^{4} \partial_{\alpha_j} e^{\alpha_j \, k_j} \right) \; e^{+\frac{1}{2}(\alpha_1+\alpha_2+\alpha_3+\alpha_4)\, R_x} \; e^{+\frac{1}{2}(\alpha_1-\alpha_2-\alpha_3+\alpha_4)\, r_x} \; \Big|_{\alpha_i=0} \, , \end{aligned} \tag{A.2}$$

where $\vec{R}$ and $\vec{r}$ are the centre of mass and the relative coordinates, respectively; $(\vec{r}, \vec{R}) = (\vec{x} \mp \vec{x}')$.

First, we can integrate on R_y which results a delta function $L_y 2\delta_{(k_1+k_2=k_3+k_4)}$. Then we do the integral on R_x which results $\sqrt{2\pi}\ e^{\frac{1}{8}(\vec{k}-\vec{\alpha})^2}$ with $\vec{k} = (k_1, k_2, k_3, k_4)$ and correspondingly for $\vec{\alpha}$.

Considering the exponent $\vec{\alpha}\cdot\vec{k}+\frac{1}{8}(\vec{k}-\vec{\alpha})^2$ with the aid of the momentum conservation–delta function, we get

$$\left(\vec{\alpha}\cdot\vec{k}+\frac{1}{8}(\vec{k}-\vec{\alpha})^2\right)\delta(k_1+k_2=k_3+k_4)$$
$$= \frac{1}{2}(\alpha_1-\alpha_2)q+\frac{1}{2}(\alpha_4-\alpha_3)p+\frac{1}{8}(\vec{k})^2+\frac{1}{8}(\vec{\alpha})^2$$

and

$$\delta(k_1+k_2=k_3+k_4)\left(-\frac{1}{2}\vec{k}^2+\frac{1}{8}(\vec{k})^2\right) = -\frac{1}{4}\left(q^2+p^2\right)$$

where $(q,p) = (k_1-k_2, k_4-k_3)$. Inserting the unity in form of a double Gaussian integrals, we arrive at

$$W^{(1)}_{k_1k_2k_3k_4} = \frac{2}{L_y}\left(\frac{2}{\pi}\right)^{1/2}\delta_{k_1+k_2,k_3+k_4}\ e^{-\frac{1}{4}\left[\,q^2+p^2\,\right]}\ \sum_{n=0}^{\infty}\frac{W_n}{n!}\int_{-\infty}^{\infty}du\int_{-\infty}^{\infty}dv\ e^{-\frac{1}{4}\left[u^2+v^2\right]}$$
$$\left(\prod_{j=1}^{4}\partial_{\alpha_j}\right)\ e^{\frac{1}{2}[(\alpha_1-\alpha_2)q+(\alpha_4-\alpha_3)p]+\frac{1}{8}(\vec{\alpha})^2}$$
$$\left[\frac{\left((q+p+(\alpha_1-\alpha_2)+(\alpha_4-\alpha_3)+i\,u)^2-(q-p+i\,v)^2\right)}{4}\right]^n . \qquad \text{(A.3)}$$

Now, we shall concentrate in the evaluation of the differentiations. We define a function

$$F(\vec{\alpha};p,q) = e^{\frac{1}{2}[(\alpha_1-\alpha_2)q+(\alpha_4-\alpha_3)p]+\frac{1}{8}(\vec{\alpha})^2}$$
$$\left[\frac{\left((q+p+(\alpha_1-\alpha_2)+(\alpha_4-\alpha_3)+i\,u)^2-(q-p+i\,v)^2\right)}{4}\right]^n$$

and we define a differential operator $\hat{O}(\vec{\alpha}) = \left(\prod_{j=1}^{4}\partial_{\alpha_j}\right)$.

There will be a few transformations to be done in order to simplify the expression. In the following, we shall list these transformations and the corresponding $F(\vec{\alpha};p,q)$ and $\hat{O}(\vec{\alpha})$.

The first transformation $(s,t) = (\alpha_1 \mp \alpha_2)$ and $(s',t') = (\alpha_4 \mp \alpha_3)$ is to simplify the differential operator and the exponent in $F(\vec{\alpha},u,v;p,q)$. In this step $F(\vec{\alpha};p,q)$ and $\hat{O}(\vec{\alpha})$ become

$$F(s,s',t,t';p,q) = e^{-\frac{1}{2}[sq+s'p]+\frac{1}{8}(t+t')^2}\ \left[\frac{\left((q+p+s+s'+i\,u)^2-(q-p+i\,v)^2\right)}{4}\right]^n$$
$$\hat{O}(s,s',t,t') = \left(\partial_t^2-\partial_s^2\right)\left(\partial_{t'}^2-\partial_{s'}^2\right) .$$

Here, one can see that $F(s,s',t,t';p,q)$ contains t and t' only as $t+t'$, thus, the second transformation is $(T,T') = (t \pm t')/2$ and then rescale T again by $t = 2T$. This step results in

$$\begin{aligned} F(s,s',t;p,q) &= e^{-\frac{1}{2}[sq+s'p]+\frac{1}{8}t^2} \left[\frac{\left((q+p+s+s'+i\,u)^2-(q-p+i\,v)^2\right)}{4}\right]^n \\ \hat{O}(s,s',t) &= \left(\partial_t^2-\partial_s^2\right)\left(\partial_t^2-\partial_{s'}^2\right) . \end{aligned}$$

Actually, one can perform the differentiation on t very easily here. Next, we shall do the last transformation in order to simplify one of the remaining differentiations. From the transformation $\alpha = (s+s')/2$ and $\alpha' = s-s'$, one get

$$\begin{aligned} F(\alpha,\alpha',t;p,q) &= e^{-\frac{1}{2}\left(\alpha'(q-p)-\frac{1}{4}\alpha(q+p)\right)+\frac{1}{8}t^2} \left[\frac{\left((q+p+2\alpha+i\,u)^2-(q-p+i\,v)^2\right)}{4}\right]^n \\ \hat{O}(\alpha,\alpha',t) &= \left[\partial_t^4-\partial_t^2\left(\tfrac{1}{2}\partial_\alpha^2+2\partial_{\alpha'}^2\right)+\tfrac{1}{16}\partial_\alpha^4+\partial_{\alpha'}^4-\tfrac{1}{2}\partial_\alpha^4\partial_{\alpha'}^2\right) . \end{aligned}$$

After the last transformation, one can perform all differentiations except that on α. This results in

$$\begin{aligned} W^{(1)}_{k_1k_2k_3k_4} = \tfrac{2}{L_y}\left(\tfrac{2}{\pi}\right)^{1/2}\delta_{k_1+k_2,k_3+k_4}\, e^{-\frac{1}{4}\left[\,q^2+p^2\,\right]} \sum_{n=0}^{\infty}\frac{W_n}{n!}\int_{-\infty}^{\infty}du\int_{-\infty}^{\infty}dv\, e^{-\frac{1}{4}\left[u^2+v^2\right]} \\ \tfrac{1}{16}\left[3-2\left(\partial_\alpha^2+(q-p)^2\right)+\left(\partial_\alpha^2-(q-p)^2\right)^2\right] \\ e^{-\frac{1}{4}\alpha(q+p)}\left[\frac{\left((q+p+2\alpha+i\,u)^2-(q-p+i\,v)^2\right)}{4}\right]^n \Bigg|_{\alpha=0} . \end{aligned} \tag{A.4}$$

This is the differential form of the interaction matrix element of the first Landau level.

The remaining works are to perform the last differentiation on α and to perform the integrals on u and v which are standard.

Now, we specialise the result to the zero–range potential for which $W(r) = 4\pi W_1\,(1+\Delta)\,\delta^2(r)$ and the interaction matrix element take the form

$$\begin{aligned} W^{(1)}_{k_1k_2k_3k_4} = \tfrac{2\pi}{L_y}\left(\tfrac{2}{\pi}\right)^{1/2}\delta_{k_1+k_2,k_3+k_4}\, e^{-\frac{1}{4}\left[(k_1-k_2)^2+(k_4-k_3)^2\right]}\, W_1 \\ \left[\frac{(k_1-k_2)(k_4-k_3)}{4}\left\{(k_1-k_2)^2(k_4-k_3)^2-3\left((k_1-k_2)^2+(k_4-k_3)^2\right)+15\right\}\right. \\ \left.-(k_1-k_2)^2(k_4-k_3)^2+(k_1-k_2)^2+(k_4-k_3)^2-1\right] \end{aligned} \tag{A.5}$$

and only the antisymmetric part that would be relevant, therefore,

$$W^{(1)}_{k_1k_2k_3k_4} \Rightarrow \frac{2\pi}{L_y}\left(\frac{2}{\pi}\right)^{1/2}\delta_{k_1+k_2,k_3+k_4}\,(k_1-k_2)(k_4-k_3)\,e^{-\frac{1}{4}\left[(k_1-k_2)^2+(k_4-k_3)^2\right]} \frac{3}{2}\,W_1\,\left[1+\frac{1}{6}\,\left((k_1-k_2)^2-3\right)\,\left((k_4-k_3)^2-3\right)\right]. \quad (A.6)$$

The interaction matrix element given in Eq.(A.6) is equivalent to the interaction matrix element in the lowest Landau level, Eq. (3.40), for the selection case in which only $W_1 = W_3$ are non zero and have form $W_1 = W_3 := \frac{3}{2}\,W_1$.

A.2 The second consideration

In the following, we shall show the derivation, which is mentioned earlier as the second derivation of the interaction matrix element in the first Landau level. Here, we shall derive the expression of the pseudo potential coefficients in the first Landau level, $W^{(1)}_m$, as a recursive function of the pseudo potential coefficients in the lowest Landau level, W_m. By this, we shall how the selected choice above comes about. We use the symmetric gauge basis to emphasise the derivation.

The single particle wave function for particle in the first Landau level in the symmetric gauge is

$$\mid m,1> = \frac{1}{\sqrt{2\pi(m+1)!2^m}}\,e^{-\frac{1}{4}|z|^2}\,z^m\,\left((m+1)-\frac{1}{2}\,|z|^2\right) \quad (A.7)$$

In general, let $\mid m,n>$ be a single particle wave function of particle in the n^{th} Landau level with angular momentum m.

We then have an identity

$$< n,m_1';n,m_2' \mid e^{i\,\vec{k}\cdot(\vec{r_1}-\vec{r_2})} \mid n,m_1;n,m_2 > = \left\{\,\mathcal{L}^0_n\left(\frac{k^2}{2}\right)\,\right\}^2 < m_1';m_2' \mid e^{i\,\vec{k}\cdot(\vec{r_1}-\vec{r_2})} \mid m_1;m_2 > \quad (A.8)$$

The pseudo potential coefficients in the n^{th} Landau level of the interaction $W(\vec{r})$ is

$$\begin{aligned} W^{(n)}_m &= < n,m\,|W(\vec{r})|\,n,m > \\ &= \frac{1}{(2\pi)^2}\int d^2k\,W(\vec{k})\,< n,m\,|e^{i\,\vec{k}\cdot\vec{r}}|\,n,m > \\ &= \frac{1}{(2\pi)^2}\int d^2k\,\left\{W(\vec{k})\,\left[\mathcal{L}^0_n\left(\frac{k^2}{2}\right)\right]^2\right\}\,< m\,|e^{i\,\vec{k}\cdot\vec{r}}|\,m > . \end{aligned} \quad (A.9)$$

For the special case of the lowest Landau level where $n = 0$,

$$\begin{aligned} W_m^{(0)} &= \frac{1}{(2\pi)^2} \int d^2k\, W(\vec{k}) \; < m \,|e^{i\,\vec{k}\cdot\vec{r}}|\, m > \\ &= \frac{1}{(2\pi)^2} \int d^2k\, W(\vec{k})\, \mathcal{L}_m^0(k^2)\, e^{-k^2} \; . \end{aligned} \tag{A.10}$$

We, then, see that $W(\vec{k})$ in the n^{th} Landau level is equivalent to the interaction $\left\{W(\vec{k}) \; \left[\; \mathcal{L}_n^0 \left(\frac{k^2}{2}\right) \; \right]^2\right\}$ in the lowest Landau level.

From Eq.(A.9), we consider the special case of $n = 1$ and from the second equation in Eq. (A.10), we find

$$W_m^{(1)} = \frac{1}{(2\pi)^2} \int d^2k\, W(\vec{k}) \; \left[1 - \frac{k^2}{2}\right]^2 \mathcal{L}_m^0(k^2)\, e^{-k^2} \tag{A.11}$$

Using the recursion formulae of the Laguare polynomial $\mathcal{L}_m^\alpha$, we find

$$\begin{aligned} x\mathcal{L}_m^{\alpha+1}(x) &= (m+\alpha+1)\mathcal{L}_m^\alpha(x) - (m+1)\mathcal{L}_{m+1}^\alpha(x) \\ &= (m+\alpha)\mathcal{L}_{m-1}^\alpha(x) - (m-x)\mathcal{L}_m^\alpha(x) \; , \\ \mathcal{L}_m^{\alpha+1}(x) &= -\mathcal{L}_{m-1}^\alpha(x) + \mathcal{L}_m^\alpha(x) \; . \end{aligned} \tag{A.12}$$

Thus, the necessary recursion formulae for our consideration become

$$\begin{aligned} k^2\mathcal{L}_m^0(k^2) &= -m\mathcal{L}_{m-1}^0(k^2) + (2m+1)\mathcal{L}_m^0(k^2) - (m+1)\mathcal{L}_{m+1}^0(k^2) \\ k^4\mathcal{L}_m^0(k^2) &= m(m-1)\mathcal{L}_{m-2}^0(k^2) - 4m^2\mathcal{L}_{m-1}^0(k^2) \\ &\quad + \left(m^2 + (m+1)^2 + (2m+1)^2\right)\mathcal{L}_m^0(k^2) \\ &\quad -4(m+1)^2\mathcal{L}_{m+1}^0(k^2) + (m+1)(m+2)\mathcal{L}_{m+2}^0(k^2) \; . \end{aligned} \tag{A.13}$$

Putting the above recursion relations into Eq. (A.11), we find

$$\begin{aligned} W_m^{(1)} = &\frac{1}{(2\pi)^2} \int d^2k\, W(\vec{k})\, \mathcal{L}_m^0(k^2) e^{-k^2} \\ &-\frac{1}{(2\pi)^2} \int d^2k\, W(\vec{k}) \; \left\{(2m+1)\mathcal{L}_m^0(k^2) - m\mathcal{L}_{m-1}^0(k^2) - (m+1)\mathcal{L}_{m+1}^0(k^2)\right\} e^{-k^2} \\ &+\frac{1}{(2\pi)^2} \int d^2k\, W(\vec{k})\, \frac{1}{4} \; \left\{m(m-1)\mathcal{L}_{m-2}^0(k^2) - 4m^2\mathcal{L}_{m-1}^0(k^2)\right. \\ &\qquad + \left(m^2 + (m+1)^2 + (2m+1)^2\right)\mathcal{L}_m^0(k^2) - 4(m+1)^2\mathcal{L}_{m+1}^0(k^2) \\ &\qquad \left. +(m+1)(m+2)\mathcal{L}_{m+2}^0(k^2)\right\} e^{-k^2} \end{aligned} \tag{A.14}$$

Finally, one gets

$$\begin{aligned} W_m^{(1)} &= \frac{1}{4}m(m-1)W_{m-2}^{(0)} - m(m-1)W_{m-1}^{(0)} + \frac{1}{3}\left(3m^2 - m + 1\right)W_m^{(0)} \\ &\quad -m(m+1)W_{m+1}^{(0)} + \frac{1}{4}(m+1)(m+2)W_{m+2}^{(0)} \end{aligned} \tag{A.15}$$

Note that the relation which appeared in the interaction matrix element between the pseudo potential coefficients in the previous section is explicitly reconstructed here.

Appendix B

Thermodynamic relations and free energy

In the following, the thermodynamic quantities we are interested in will be given as power series in β and the coefficients are expressed by the high–temperature expansion coefficients, $\Omega_n(z)$, or the high–temperature expansion coefficients of the energy, $\alpha_n(\nu)$ for the grand canonical and canonical ensemble, respectively.

We also show how one can reconstruct the free energy $F(T, N_\phi, \nu)$ from the high–temperature series of the energy, (6.5).

B.1 Grand canonical emsemble: $\Omega(T, N_\phi, \mu)$

$$d\Omega \;=\; -SdT - PdV - Nd\mu = -SdT - 2\pi l_B^2\; P\; dN_\phi - N_\phi\; \nu\; d\mu \tag{B.1}$$

$$\text{Thermodynamic potential: } \Omega(T, N_\phi, \mu) \;=\; N_\phi \sum_{n=0}^{\infty} \beta^{n-1}\; \Omega_n(z)\;;\; z = e^{\beta\mu} \tag{B.2}$$

$$\text{Filling factor: } \nu \;=\; \frac{N}{N_\phi} \;=\; -\frac{1}{N_\phi}\left(\frac{\partial\Omega(T, N_\phi, \mu)}{\partial\mu}\right)_{T, N_\phi} \;=\; -\sum_{n=0}^{\infty} \beta^n\; z\; \partial_z\Omega_n(z) \tag{B.3}$$

$$\text{Energy: } E(T, N_\phi, \mu) \;=\; \left(\frac{\partial\beta\Omega(T, N_\phi, \mu)}{\partial\beta}\right)_{N_\phi, \beta\mu} \;=\; N_\phi \sum_{n=1}^{\infty}\; \beta^{n-1}\; n\; \Omega_n(z) \tag{B.4}$$

$$\text{Compressibility: } \kappa_T(T,\mu) = -\frac{1}{V}\left(\frac{\partial V}{\partial P}\right)_T = \frac{2\pi l_B^2}{\nu^2}\left(\frac{\partial \nu}{\partial \mu}\right)_T$$
$$= -\frac{2\pi l_B^2}{\nu^2}\sum_{n=0}^{\infty}\beta^{n+1}\, z\,\partial_z\, z\,\partial_z\,\Omega_n(z) \qquad \text{(B.5)}$$

B.2 Canonical ensemble: $F(T, N_\phi, \nu)$

We rewrite the energy in Eq. (4.18) in the form

$$E(T,N_\phi,\nu) = N_\phi \sum_{n=1}^{\infty}\beta^{n-1}\,\alpha_n(\nu)\,. \qquad \text{(B.6)}$$

Note that we use $\alpha_n(\nu)$ for the energy $E(T, N_\phi, \nu)$ while L. Zheng and A. H. MacDonald use $\alpha^{(n)}(\nu)$ for the free energy $F(T, N_\phi, \nu)$.

We integrate the relation (cf. Eq. (6.5))

$$E(T,N_\phi,\nu) = \left.\frac{\partial(\beta F(T,N_\phi,\nu))}{\partial\beta}\right|_{N_\phi,\nu} = N_\phi\sum_{n=1}^{\infty}\beta^{n-1}\,\alpha_n(\nu)\,. \qquad \text{(B.7)}$$

with the boundary condition

$$\beta F(T,N_\phi,\nu)|_{\beta=0} = N_\phi\Big[\nu\,\ln\nu + (1-\nu)\,\ln(1-\nu)\Big]\,. \qquad \text{(B.8)}$$

Thus, the free energy can be written of a power series in β as

$$F(T,N_\phi,\nu) = N_\phi\left\{T\left[\nu\,\ln\nu + (1-\nu)\,\ln(1-\nu)\right] + \sum_{n=1}^{\infty}\frac{1}{n}\,\beta^{n-1}\,\alpha_n(\nu)\right\}\,. \qquad \text{(B.9)}$$

From $F(T, N_\phi, \nu)$ in connection with the results for the $\alpha_n(\nu)$, we can calculate the high–temperature series of any thermodynamic quantity in the canonical ensemble.

Inverse compressibilty

$$\kappa_T^{-1}(T,\nu) = \left[-\frac{1}{V}\left(\frac{\partial V}{\partial P}\right)_T\right]^{-1} = \frac{\nu^2}{2\pi l_B^2}\,\frac{\partial^2[F(T,N_\phi,\nu)/N_\phi]}{\partial\nu^2}$$
$$= \frac{T}{2\pi l_B^2}\left(\frac{\nu}{1-\nu} + \sum_{n=1}^{\infty}\frac{1}{n}\,\beta^n\,\nu^2\,\partial_\nu^2\,\alpha_n(\nu)\right) \qquad \text{(B.10)}$$

Appendix C

The matrices $\hat{Q}$ and $\hat{M}$ used for calculating the proper patterns

In this Appendix, we list the matrices $\hat{Q}_p^{(n)}$ and $\hat{M}_p^{(n)}$ of the proper pattern $W_p^{(n)}$ for $n \leq 4$.

$$\hat{Q}_a^{(1)} = \begin{pmatrix} 1 \end{pmatrix} \qquad \hat{M}_a^{(1)} = \begin{pmatrix} 1 \end{pmatrix}$$

$$\hat{Q}_a^{(2)} = \begin{pmatrix} 0 & 1 & -1 \\ 0 & -1 & -1 \\ 1 & 0 & 1 \end{pmatrix} \qquad \hat{M}_a^{(2)} = \begin{pmatrix} 0 & 1 \\ 1 & 0 \end{pmatrix}$$

$$\hat{Q}_a^{(3)} = \begin{pmatrix} 0 & 1 & 0 & -1 & 1 \\ 0 & -1 & 0 & -1 & 1 \\ 0 & 0 & 1 & 0 & -1 \\ 0 & 0 & -1 & 0 & -1 \\ 1 & 0 & 0 & 1 & 0 \end{pmatrix} \qquad \hat{M}_a^{(3)} = \begin{pmatrix} 0 & 0 & 1 \\ 1 & 0 & 0 \\ 0 & 1 & 0 \end{pmatrix}$$

$$\hat{Q}_b^{(3)} = \begin{pmatrix} 0 & 1 & 0 & -1 & 1 \\ 0 & 0 & 1 & -1 & 0 \\ 1 & 0 & 0 & 1 & -1 \\ 0 & 0 & -1 & 0 & -1 \\ -1 & 0 & 0 & 1 & 0 \end{pmatrix} \qquad \hat{M}_b^{(3)} = \begin{pmatrix} \frac{1}{3} & \frac{2}{3} & -\frac{2}{3} \\ \frac{2}{3} & \frac{1}{3} & \frac{2}{3} \\ -\frac{2}{3} & \frac{2}{3} & \frac{1}{3} \end{pmatrix}$$

$$\hat{Q}_a^{(4)} = \begin{pmatrix} 0 & 1 & 0 & 0 & -1 & 1 & 0 \\ 0 & -1 & 0 & 0 & -1 & 1 & 0 \\ 0 & 0 & 1 & 0 & 0 & -1 & 1 \\ 0 & 0 & -1 & 0 & 0 & -1 & 1 \\ 0 & 0 & 0 & 1 & 0 & 0 & -1 \\ 0 & 0 & 0 & -1 & 0 & 0 & -1 \\ 1 & 0 & 0 & 0 & 1 & 0 & 0 \end{pmatrix} \qquad \hat{M}_a^{(4)} = \begin{pmatrix} 0 & 0 & 0 & 1 \\ 1 & 0 & 0 & 0 \\ 0 & 1 & 0 & 0 \\ 0 & 0 & 1 & 0 \end{pmatrix}$$

$$\hat{Q}_b^{(4)} = \begin{pmatrix} 0 & 1 & 0 & 0 & -1 & 1 & 0 \\ 0 & -1 & 0 & 0 & -1 & 1 & 0 \\ 0 & 0 & 1 & 0 & 0 & -1 & 1 \\ 0 & 0 & 0 & 1 & 0 & -1 & 0 \\ 1 & 0 & 0 & 0 & 1 & 0 & -1 \\ 0 & 0 & 0 & -1 & 0 & 0 & -1 \\ -1 & 0 & 0 & 0 & 1 & 0 & 0 \end{pmatrix} \qquad \hat{M}_b^{(4)} = \begin{pmatrix} 0 & \frac{1}{3} & \frac{2}{3} & -\frac{2}{3} \\ 1 & 0 & 0 & 0 \\ 0 & \frac{2}{3} & \frac{1}{3} & \frac{2}{3} \\ 0 & -\frac{2}{3} & \frac{2}{3} & \frac{1}{3} \end{pmatrix}$$

$$\hat{Q}_c^{(4)} = \begin{pmatrix} 0 & 1 & 0 & 0 & -1 & 1 & 0 \\ 0 & 0 & 1 & 0 & -1 & 0 & 1 \\ 1 & 0 & 0 & 0 & 1 & -1 & 0 \\ 0 & 0 & 0 & 1 & 0 & -1 & 0 \\ -1 & 0 & 0 & 0 & 1 & 0 & -1 \\ 0 & 0 & 0 & -1 & 0 & 0 & -1 \\ 0 & -1 & 0 & 0 & 0 & 1 & 0 \end{pmatrix} \qquad \hat{M}_c^{(4)} = \begin{pmatrix} \frac{1}{2} & \frac{1}{2} & -\frac{1}{2} & \frac{1}{2} \\ \frac{1}{2} & \frac{1}{2} & \frac{1}{2} & -\frac{1}{2} \\ -\frac{1}{2} & \frac{1}{2} & \frac{1}{2} & \frac{1}{2} \\ \frac{1}{2} & -\frac{1}{2} & \frac{1}{2} & \frac{1}{2} \end{pmatrix}$$

$$\hat{Q}_d^{(4)} = \begin{pmatrix} 0 & 1 & 0 & 0 & -1 & 1 & 0 \\ 0 & 0 & 1 & 0 & -1 & 0 & 1 \\ 1 & 0 & 0 & 0 & 1 & -1 & 0 \\ 0 & 0 & 0 & 1 & 0 & -1 & 0 \\ 0 & -1 & 0 & 0 & 0 & 1 & -1 \\ 0 & 0 & 0 & -1 & 0 & 0 & -1 \\ -1 & 0 & 0 & 0 & 1 & 0 & 0 \end{pmatrix} \qquad \hat{M}_d^{(4)} = \begin{pmatrix} \frac{1}{5} & \frac{4}{5} & \frac{2}{5} & -\frac{2}{5} \\ \frac{4}{5} & \frac{1}{5} & -\frac{2}{5} & \frac{2}{5} \\ -\frac{2}{5} & \frac{2}{5} & \frac{1}{5} & \frac{4}{5} \\ \frac{2}{5} & -\frac{2}{5} & \frac{4}{5} & \frac{1}{5} \end{pmatrix}$$

Appendix D

Calculation of the frequency sums for the connected diagrams

In this Appendix, we shall calculate in the standard Matsubara technique the frequency sums of the connected diagrams of the first three orders in order to prove the equivalence between the traditional perturbative technique and the present method. Here $\omega = 2\pi\frac{1}{\beta}(n + 1/2)$ denote the Matsubara frequencies (n integer).

D.1 The first order diagram

There is an only one connected diagram, see Fig. D.1, in this order which can be calculated easily.

$$T \sum_{\omega_1} \frac{e^{i\,\omega_1\,0}}{i\omega_1 - (\epsilon - \mu)}\, T \sum_{\omega_2} \frac{e^{i\,\omega_2\,0}}{i\omega_2 - (\epsilon - \mu)} = f^2 \,, \tag{D.1}$$

where the Fermi function f is the sum over Green's function

$$T \sum_{\omega} \frac{e^{i\,\omega\,0}}{i\omega - (\epsilon - \mu)} = f \,. \tag{D.2}$$

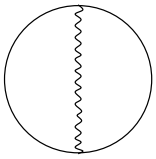

Figure D.1: Connected diagram in the first order

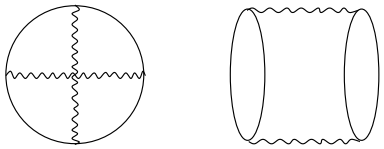

Figure D.2: Connected diagrams in the second order

D.2 The second order diagrams

In the second order, we find two connected diagrams, see Fig. D.2. These two diagrams, however, yield the same value in the frequency sums calculation. The difference of the two diagrams appears only in the momentum indices which do not affect the frequency sum calculation.

$$
\begin{aligned}
& T \sum_{\omega_1} \frac{e^{i\,\omega_1\,0}}{i\omega_1 - (\epsilon-\mu)}\, T \sum_{\omega_2} \frac{e^{i\,\omega_2\,0}}{i\omega_2 - (\epsilon-\mu)} \;\times \\
& T \sum_{\omega_3} \frac{e^{i\,\omega_3\,0}}{i\omega_3 - (\epsilon-\mu)}\; \frac{e^{i\,(\omega_1+\omega_2-\omega_3)\,0}}{i\,(\omega_1+\omega_2-\omega_3) - (\epsilon-\mu)} \\
& \quad = T \sum_{\omega_2} \frac{e^{i\,\omega_2\,0}}{i\omega_2 - (\epsilon-\mu)}\, T \sum_{\omega_3} \frac{1}{i\omega_3 - (\epsilon-\mu)} \\
& \qquad T \sum_{\omega_1} \frac{e^{i\,\omega_1\,0}}{i\omega_1 - (\epsilon-\mu)}\; \frac{1}{i\,(\omega_1+\omega_2-\omega_3) - (\epsilon-\mu)} \\
& \quad = T \sum_{\omega_2} \frac{e^{i\,\omega_2\,0}}{i\omega_2 - (\epsilon-\mu)}\, T \sum_{\omega_3} \frac{1}{i\omega_3 - (\epsilon-\mu)} \;\times \\
& \qquad T \sum_{\omega_1} \frac{e^{i\,\omega_1\,0}}{i\,(\omega_2-\omega_3)} \left[\frac{1}{i\omega_1 - (\epsilon-\mu)} - \frac{1}{i\,(\omega_1+\omega_2-\omega_3) - (\epsilon-\mu)} \right]
\end{aligned}
\tag{D.3}
$$

This yields zero since we can shift ω_1 by $\omega_2 - \omega_3$ in the summation, except for the case of $\omega_2 = \omega_3$ which we have to treat separately. In that case, we rewrite the first line of the above equation as

$$
\begin{aligned}
& T \sum_{\omega_1} \frac{e^{i\,\omega_1\,0}}{i\omega_1 - (\epsilon-\mu)}\, T \sum_{\omega_2} \frac{e^{i\,\omega_2\,0}}{i\omega_2 - (\epsilon-\mu)} \;\times \\
& T \sum_{\omega_3} \frac{e^{i\,\omega_3\,0}}{i\omega_3 - (\epsilon-\mu)}\; \frac{e^{i\,(\omega_1+\omega_2-\omega_3)\,0}\;\delta_{\omega_2,\omega_3}}{i\,(\omega_1+\omega_2-\omega_3) - (\epsilon-\mu)} \\
& \qquad = \; T \left[T \sum_{\omega} \frac{1}{(i\omega - (\epsilon-\mu))^2} \right]^2 \; = \; \beta\, f^2\,(1-f)^2\,,
\end{aligned}
\tag{D.4}
$$

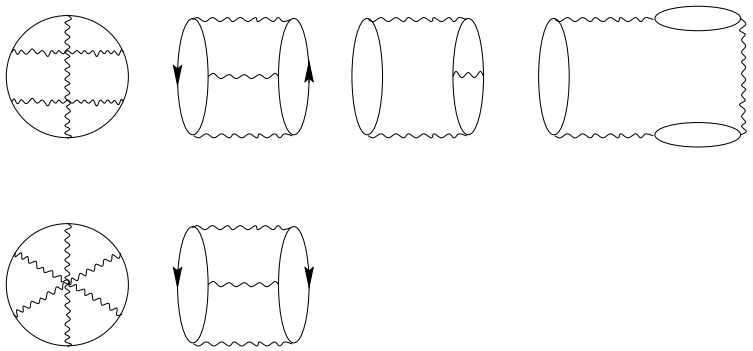

Figure D.3: Connected diagrams in the third order

where we calculated the sum by differentiation of Eq. (D.2) with respect to the chemical potential μ.

$$T\sum_{\omega}\frac{e^{i\,\omega\,0}}{\left(i\omega-(\epsilon-\mu)\right)^2}=-\beta\;f\;(1-f)\;. \tag{D.5}$$

D.3 The third order diagrams

In the third order, we find six connected diagrams, see Fig. D.3. The four diagrams in the first row, however, result in the same value in the frequency sum calculation, and the two diagrams in the second row result the same value in frequency sums calculation, too. The difference between those diagrams which result the same frequency sum appear, as is the case for the second order, only in the momentum indices which does not affect the frequency sum calculation.

First, we calculate the first diagram in the first row in Fig. D.3.

$$\begin{aligned}
&T\;\sum_{\omega_1}\frac{e^{i\,\omega_1\,0}}{i\omega_1-(\epsilon-\mu)}\;T\;\sum_{\omega_2}\frac{e^{i\,\omega_2\,0}}{i\omega_2-(\epsilon-\mu)}\;T\;\sum_{\omega_3}\frac{e^{i\,\omega_3\,0}}{i\omega_3-(\epsilon-\mu)}\;\times\\
&T\;\sum_{\omega_4}\frac{e^{i\,\omega_4\,0}}{i\omega_4-(\epsilon-\mu)}\;\frac{e^{i\,(\omega_1+\omega_2-\omega_3)\,0}}{i\;(\omega_1+\omega_2-\omega_3)-(\epsilon-\mu)}\;\frac{e^{i\,(\omega_3+\omega_4-\omega_1)\,0}}{i\;(\omega_3+\omega_4-\omega_1)-(\epsilon-\mu)}\\
&\quad=T\;\sum_{\omega_1}\frac{e^{i\,\omega_1\,0}}{i\omega_1-(\epsilon-\mu)}\;T\;\sum_{\omega_2}\frac{e^{i\,\omega_2\,0}}{i\omega_2-(\epsilon-\mu)}\;\times\\
&\qquad T\;\sum_{\omega_3}\frac{e^{i\,\omega_3\,0}}{i\omega_3-(\epsilon-\mu)}\;\frac{1}{i\;(\omega_1+\omega_2-\omega_3)-(\epsilon-\mu)}\;\times\\
&\qquad T\;\sum_{\omega_4}\frac{e^{i\,\omega_4\,0}}{i\omega_4-(\epsilon-\mu)}\;\frac{\delta_{\omega_1,\omega_3}}{i\;(\omega_3+\omega_4-\omega_1)-(\epsilon-\mu)}\;\times\\
&\quad=T^2\;\sum_{\omega_1}\frac{e^{i\,\omega_1\,0}}{\Big(i\omega_1-(\epsilon-\mu)\Big)^2}\;T\;\sum_{\omega_2}\frac{e^{i\,\omega_2\,0}}{\Big(i\omega_2-(\epsilon-\mu)\Big)^2}\;T\;\sum_{\omega_4}\frac{e^{i\,\omega_4\,0}}{\Big(i\omega_4-(\epsilon-\mu)\Big)^2}
\end{aligned}$$

$$= T \left[-\beta f \, (1-f) \right]^3 \; = \; -\beta^2 f^3 \, (1-f)^3 \, , \tag{D.6}$$

Here, $\delta_{\omega_1,\omega_3}$ appears in the sum on ω_4 for the same reason as explained below Eq. (D.3).

Then, we go to the second row in Fig. D.3 and calculate the last diagram.

$$\begin{aligned} & T \sum_{\omega_1} \frac{e^{i\,\omega_1\,0}}{i\omega_1 - (\epsilon-\mu)} \; T \sum_{\omega_2} \frac{e^{i\,\omega_2\,0}}{i\omega_2 - (\epsilon-\mu)} \; \times \\ & T \sum_{\omega_3} \frac{e^{i\,\omega_3\,0}}{i\omega_3 - (\epsilon-\mu)} \; \frac{e^{i\,(\omega_1+\omega_2-\omega_3)\,0}}{i\,(\omega_1+\omega_2-\omega_3) - (\epsilon-\mu)} \; \times \\ & T \sum_{\omega_5} \frac{e^{i\,\omega_5\,0}}{i\omega_5 - (\epsilon-\mu)} \; \frac{e^{i\,(\omega_1+\omega_2-\omega_5)\,0}}{i\,(\omega_1+\omega_2-\omega_5) - (\epsilon-\mu)} \, . \end{aligned} \tag{D.7}$$

Here, we can calculate the sums over ω_3 and ω_5 for fixed ω_1 and ω_2.

$$\begin{aligned} T \sum_{\omega} \frac{1}{i\omega - x} \; \frac{1}{i\,(\omega_1+\omega_2-\omega) - x} \; &= \; T \sum_{\omega} \frac{1}{i\,(\omega_1+\omega_2) - 2\,x} \\ & \quad \left[\frac{1}{i\omega - x} + \frac{1}{i\,(\omega_1+\omega_2-\omega) - x} \right] \\ &= \; \frac{1}{i\,(\omega_1+\omega_2) - 2\,x} \; T \sum_{\omega} \frac{e^{i\,\omega\,0}}{i\omega - x} + \frac{e^{i\,\omega\,0}}{-i\,\omega - x} \\ &= \; \frac{1}{i\,(\omega_1+\omega_2) - 2\,x} \; [f + (1-f)] \\ &= \; \frac{1}{i\,(\omega_1+\omega_2) - 2\,x} \; (2\,f-1) \, . \end{aligned} \tag{D.8}$$

Then, Eq. (D.7) becomes

$$\begin{aligned} & (2\,f-1)^2 \, T \sum_{\omega_1} \frac{1}{i\omega_1 - (\epsilon-\mu)} \; T \sum_{\omega_2} \frac{1}{i\omega_2 - (\epsilon-\mu)} \; \frac{1}{\Big(i\,(\omega_1+\omega_2) - 2\,(\epsilon-\mu)\Big)^2} \\ & = (2\,f-1)^2 \, T \sum_{\omega_1} \frac{e^{i\,\omega_1\,0}}{i\omega_1 - (\epsilon-\mu)} \; \times \\ & \quad \left[T \sum_{\omega_2} \frac{1}{\Big(i\omega_1 - (\epsilon-\mu)\Big)^2} \; \left(\frac{1}{i\omega_2 - (\epsilon-\mu)} - \frac{1}{i(\omega_1+\omega_2) - 2\,(\epsilon-\mu)} \right) \right. \\ & \quad \left. - \, T \sum_{\omega_2} \frac{1}{i\omega_1 - (\epsilon-\mu)} \; \frac{1}{\Big(i(\omega_1+\omega_2) - 2\,(\epsilon-\mu)\Big)^2} \right] \end{aligned}$$

$$= (2\ f-1)^2\ \left[\frac{f\ (1-f)}{(1-2\ f)}\ T\ \sum_{\omega_1}\frac{e^{i\ \omega_1\ 0}}{(i\omega_1-(\epsilon-\mu))^3}\right.$$

$$\left.-\beta\ f^2\ (1-f)^2\ T\ \sum_{\omega_1}\frac{e^{i\ \omega_1\ 0}}{(i\omega_1-(\epsilon-\mu))^2}\right]$$

$$= \frac{\beta^2}{2}\ \left[f^4\ (1-f)^2+f^2\ (1-f)^4\right] \tag{D.9}$$

By the results of the frequency sums above, together with the momentum sums result which will be shown in Section 4.5, we can prove the equivalence of the present method, the high–temperature expansion method, to the traditional perturbative method.

Appendix E

The coefficients $\mathcal{C}_m^{(n)}$ for the $(W_1 + W_3)$–interaction

$$\begin{aligned}
\mathcal{C}^{(1)} &= 2\,W_1 + 2\,W_3 \\
\mathcal{C}_0^{(2)} &= -2\,{W_1}^2 - 2\,{W_3}^2
\end{aligned}$$

$$\begin{aligned}
\mathcal{C}_0^{(3)} &= \frac{-32\,{W_1}^3}{27} + \frac{2464\,{W_1}^2\,W_3}{243} - \frac{2144\,W_1\,{W_3}^2}{2187} - \frac{16928\,{W_3}^3}{19683} \\
\mathcal{C}_1^{(3)} &= {W_1}^3 + {W_3}^3
\end{aligned}$$

$$\begin{aligned}
\mathcal{C}_0^{(4)} &= \frac{-548284\,{W_1}^4}{253125} + \frac{640622288\,{W_1}^3\,W_3}{34171875} - \frac{159488316272\,{W_1}^2\,{W_3}^2}{7688671875} \\
&\quad - \frac{153993867248\,W_1\,{W_3}^3}{38443359375} + \frac{5799768306163\,{W_3}^4}{5766503906250} \\
\mathcal{C}_1^{(4)} &= \frac{352696\,{W_1}^4}{253125} - \frac{527843072\,{W_1}^3\,W_3}{34171875} - \frac{14357608432\,{W_1}^2\,{W_3}^2}{7688671875} \\
&\quad - \frac{90149970688\,W_1\,{W_3}^3}{38443359375} + \frac{6199729889464\,{W_3}^4}{2883251953125} \\
\mathcal{C}_2^{(4)} &= \frac{-{W_1}^4}{3} - \frac{{W_3}^4}{3}
\end{aligned}$$

$$\begin{aligned}
\mathcal{C}_0^{(5)} &= -2.01\,{W_1}^5 + 60.0569\,{W_1}^4\,W_3 - 86.7762\,{W_1}^3\,{W_3}^2 + 27.543\,{W_1}^2\,{W_3}^3 \\
&\quad + 17.6793\,W_1\,{W_3}^4 - 0.963985\,{W_3}^5
\end{aligned}$$

$$
\begin{aligned}
\mathcal{C}_1^{(5)} &= 3.31957\,{W_1}^5 - 46.5438\,{W_1}^4\,W_3 + 87.9718\,{W_1}^3\,{W_3}^2 + 1.61281\,{W_1}^2\,{W_3}^3 \\
&\quad +10.7582\,W_1\,{W_3}^4 - 0.429506\,{W_3}^5 \\
\mathcal{C}_2^{(5)} &= -0.730235\,{W_1}^5 + 12.3988\,{W_1}^4\,W_3 + 5.07997\,{W_1}^3\,{W_3}^2 + 0.568715\,{W_1}^2\,{W_3}^3 \\
&\quad +2.94035\,W_1\,{W_3}^4 - 2.04721\,{W_3}^5 \\
\mathcal{C}_3^{(5)} &= 0.0833333\,{W_1}^5 + 0.0833333\,{W_3}^5
\end{aligned}
$$

$$
\begin{aligned}
\mathcal{C}_0^{(6)} &= -5.12161\,{W_1}^6 + 159.118\,{W_1}^5\,W_3 - 630.485\,{W_1}^4\,{W_3}^2 + 229.466\,{W_1}^3\,{W_3}^3 \\
&\quad -53.2719\,{W_1}^2\,{W_3}^4 - 13.7914\,W_1\,{W_3}^5 - 7.07\,{W_3}^6 \\
\mathcal{C}_1^{(6)} &= 3.49044\,{W_1}^6 - 137.465\,{W_1}^5\,W_3 + 457.708\,{W_1}^4\,{W_3}^2 - 271.666\,{W_1}^3\,{W_3}^3 \\
&\quad -20.0463\,{W_1}^2\,{W_3}^4 - 12.0979\,W_1\,{W_3}^5 - 6.8886\,{W_3}^6 \\
\mathcal{C}_2^{(6)} &= -3.27403\,{W_1}^6 + 52.9892\,{W_1}^5\,W_3 - 133.775\,{W_1}^4\,{W_3}^2 - 49.1063\,{W_1}^3\,{W_3}^3 \\
&\quad -13.7953\,{W_1}^2\,{W_3}^4 - 2.54434\,W_1\,{W_3}^5 - 3.57382\,{W_3}^6 \\
\mathcal{C}_3^{(6)} &= 0.18646\,{W_1}^6 - 6.94952\,{W_1}^5\,W_3 - 4.6699\,{W_1}^4\,{W_3}^2 - 1.1259\,{W_1}^3\,{W_3}^3 \\
&\quad -0.646324\,{W_1}^2\,{W_3}^4 - 1.7751\,W_1\,{W_3}^5 + 1.20242\,{W_3}^6 \\
\mathcal{C}_4^{(6)} &= -0.0166667\,{W_1}^6 - 0.0166667\,{W_3}^6
\end{aligned}
$$

$$
\begin{aligned}
\mathcal{C}_0^{(7)} &= -6.23465\,{W_1}^7 + 446.72\,{W_1}^6\,W_3 - 2858.75\,{W_1}^5\,{W_3}^2 + 3507.85\,{W_1}^4\,{W_3}^3 \\
&\quad -529.418\,{W_1}^3\,{W_3}^4 + 177.576\,{W_1}^2\,{W_3}^5 - 21.1243\,W_1\,{W_3}^6 + 13.4061\,{W_3}^7 \\
\mathcal{C}_1^{(7)} &= 6.22556\,{W_1}^7 - 330.281\,{W_1}^6\,W_3 + 2186.98\,{W_1}^5\,{W_3}^2 - 2261.2\,{W_1}^4\,{W_3}^3 \\
&\quad +558.206\,{W_1}^3\,{W_3}^4 + 169.134\,{W_1}^2\,{W_3}^5 - 20.0177\,W_1\,{W_3}^6 + 9.81073\,{W_3}^7 \\
\mathcal{C}_2^{(7)} &= -6.16303\,{W_1}^7 + 197.545\,{W_1}^6\,W_3 - 922.876\,{W_1}^5\,{W_3}^2 + 696.217\,{W_1}^4\,{W_3}^3 \\
&\quad +157.203\,{W_1}^3\,{W_3}^4 + 121.209\,{W_1}^2\,{W_3}^5 - 14.7763\,W_1\,{W_3}^6 + 8.40151\,{W_3}^7 \\
\mathcal{C}_3^{(7)} &= 2.25917\,{W_1}^7 - 37.5967\,{W_1}^6\,W_3 + 128.848\,{W_1}^5\,{W_3}^2 + 100.884\,{W_1}^4\,{W_3}^3 \\
&\quad +25.5508\,{W_1}^3\,{W_3}^4 + 19.3866\,{W_1}^2\,{W_3}^5 - 6.04295\,W_1\,{W_3}^6 + 5.84127\,{W_3}^7 \\
\mathcal{C}_4^{(7)} &= 0.0101136\,{W_1}^7 + 3.04699\,{W_1}^6\,W_3 + 2.74632\,{W_1}^5\,{W_3}^2 + 1.16461\,{W_1}^4\,{W_3}^3 \\
&\quad +0.260552\,{W_1}^3\,{W_3}^4 + 0.442585\,{W_1}^2\,{W_3}^5 + 0.741667\,W_1\,{W_3}^6 - 0.516259\,{W_3}^7 \\
\mathcal{C}_5^{(7)} &= 0.00277778\,{W_1}^7 + 0.00277778\,{W_3}^7
\end{aligned}
$$

$$
\begin{aligned}
\mathcal{C}_0^{(8)} &= -7.66962\,{W_1}^8 + 1015.57\,{W_1}^7\,W_3 - 11188.2\,{W_1}^6\,{W_3}^2 \\
&\quad +24625.4\,{W_1}^5\,{W_3}^3 - 12816.3\,{W_1}^4\,{W_3}^4 + 833.629\,{W_1}^3\,{W_3}^5 \\
&\quad -447.481\,{W_1}^2\,{W_3}^6 - 73.6481\,W_1\,{W_3}^7 + 13.3155\,{W_3}^8 \\
\mathcal{C}_1^{(8)} &= 8.10722\,{W_1}^8 - 877.268\,{W_1}^7\,W_3 + 8654.85\,{W_1}^6\,{W_3}^2 \\
&\quad -18321.9\,{W_1}^5\,{W_3}^3 + 7173.34\,{W_1}^4\,{W_3}^4 - 951.453\,{W_1}^3\,{W_3}^5 \\
&\quad -425.246\,{W_1}^2\,{W_3}^6 - 15.3762\,W_1\,{W_3}^7 + 23.7561\,{W_3}^8 \\
\mathcal{C}_2^{(8)} &= -12.6023\,{W_1}^8 + 536.501\,{W_1}^7\,W_3 - 4587.58\,{W_1}^6\,{W_3}^2 + 7626.59\,{W_1}^5\,{W_3}^3 \\
&\quad -2200.68\,{W_1}^4\,{W_3}^4 - 277.946\,{W_1}^3\,{W_3}^5 - 408.036\,{W_1}^2\,{W_3}^6 \\
&\quad -16.31\,W_1\,{W_3}^7 + 11.0758\,{W_3}^8 \\
\mathcal{C}_3^{(8)} &= 7.38751\,{W_1}^8 - 193.697\,{W_1}^7\,W_3 + 1102.\,{W_1}^6\,{W_3}^2 \\
&\quad -962.771\,{W_1}^5\,{W_3}^3 - 759.8\,{W_1}^4\,{W_3}^4 - 213.705\,{W_1}^3\,{W_3}^5 \\
&\quad -116.13\,{W_1}^2\,{W_3}^6 + 5.88218\,W_1\,{W_3}^7 + 2.15347\,{W_3}^8 \\
\mathcal{C}_4^{(8)} &= -1.22353\,{W_1}^8 + 18.415\,{W_1}^7\,W_3 - 94.5276\,{W_1}^6\,{W_3}^2 \\
&\quad -109.865\,{W_1}^5\,{W_3}^3 - 48.3452\,{W_1}^4\,{W_3}^4 - 17.5436\,{W_1}^3\,{W_3}^5 \\
&\quad -13.1612\,{W_1}^2\,{W_3}^6 + 7.33782\,W_1\,{W_3}^7 - 5.01993\,{W_3}^8 \\
\mathcal{C}_5^{(8)} &= -0.0331018\,{W_1}^8 - 1.10857\,{W_1}^7\,W_3 - 1.22594\,{W_1}^6\,{W_3}^2 \\
&\quad -0.722188\,{W_1}^5\,{W_3}^3 - 0.222406\,{W_1}^4\,{W_3}^4 - 0.093177\,{W_1}^3\,{W_3}^5 \\
&\quad -0.198152\,{W_1}^2\,{W_3}^6 - 0.242325\,W_1\,{W_3}^7 + 0.17624\,{W_3}^8 \\
\mathcal{C}_6^{(8)} &= -0.000396825\,{W_1}^8 - 0.000396825\,{W_3}^8
\end{aligned}
$$

Appendix F

Free electron gas in a flat band

In the high–temperature expansion result, we find crossing points in the inverse compressibility. Is this related to the finiteness of the band that we study? In order to check this, we study a system of free particle in a finite flat band. This appendix is devoted to a discussion of the thermodynamic properties of the system of free particles in a flat band in which $z(\epsilon) = \frac{n_0}{2\,W}$ where $|\epsilon| \leq W$.

The thermodynamic potential of this system is written as

$$\Omega(T, V, \mu) = -\frac{n_0\, T\, V}{2\, W} \int_{-W}^{W} d\epsilon\ \ln(1 + e^{-\beta\,(\epsilon-\mu)}) \tag{F.1}$$

We calculate the number of particle density, n,

$$n = -\frac{1}{V}\ \left(\frac{\partial\Omega}{\partial\mu}\right)_{T,V} = \frac{n_0}{2\, W} \int_{-W}^{W} d\epsilon\ f(\epsilon-\mu) = \frac{n_0\, T}{2\, W}\ \ln\left(\frac{1 + e^{\beta\,(W+\mu)}}{1 + e^{-\beta\,(W-\mu)}}\right) \tag{F.2}$$

where $f(\epsilon - \mu) = 1/(1 + e^{\beta\,(\epsilon-\mu)})$ is the Fermi function.

First, we consider the particle density n in the limit in which $\mu \to \infty$. We find

$$\lim_{\mu\to\infty} n = \frac{n_0\, T}{2\, W}\ \Big(\beta\,(W+\mu) + \beta\,(W-\mu)\Big) = n_0 \tag{F.3}$$

This shows that n_0 is actually the maximum particle density that can be filled in the system.

We invert the relation between μ and N in Eq. (F.2) and find

$$e^{\beta\,\mu} = \frac{e^{2\,\beta\,W\,\nu} - 1}{e^{\beta\,W}\ \left(1 - e^{2\,\beta\,W\,(\nu-1)}\right)}\ , \tag{F.4}$$

where $\nu = n/n_0$ is the filling fraction.

We find for the compressibility, κ_T,

$$\kappa_T = -\frac{1}{V}\ \left(\frac{\partial V}{\partial P}\right)_{T,N} = \frac{V}{N^2}\ \left(\frac{\partial N}{\partial\mu}\right)_{T,V} = -\frac{n_0}{2\, n^2\, W}\ \Big(f(W-\mu) - f(-W-\mu)\Big)\ , \tag{F.5}$$

where $n = N/V$ is particle density.

Using the above expression of $e^{\beta\,\mu}$, we get

$$\kappa_T^{-1}(T,\nu) = 2\;\nu^2\;n_0\;W\;\left(\frac{\sinh(\beta W)}{\cosh(\beta W)-\cosh(\beta W(2\nu-1))}\right) \tag{F.6}$$

This inverse compressibility is a smooth function as long as we are away from $\nu = 0$ and $\nu = 1$. The inverse compressibility shows no crossing point when being plotted against the filling fraction, ν.

Now, we want to study the behaviour of pressure and its second derivative with respect to temperature around $\nu = 1$.

From thermodynamics, we calculate the pressure from $\Omega(T,V,\mu)$

$$P(T,\mu) = -\left(\frac{\partial\Omega}{\partial V}\right)_{T,\mu} = \frac{n_0\;T}{2\;W}\int_{-W}^{W} d\epsilon\;\ln\left(1+e^{-\beta\;(\epsilon-\mu)}\right)\;. \tag{F.7}$$

We are interested only in the limit $\nu \to 1$ in which chemical potential μ diverges. Therefore,

$$\begin{aligned}
\lim_{\mu\to\infty} P(T,\mu) &= \lim_{\mu\to\infty}\frac{n_0\;T}{2\;W}\int_{-W}^{W} d\epsilon\;\ln\left[e^{\beta\;(\mu-\epsilon)}\;\left(1+e^{\beta\;(\epsilon-\mu)}\right)\right] \\
&= \frac{n_0\;T}{2\;W}\int_{-W}^{W} d\epsilon\;\left[\beta\mu+\ln\left(1+e^{\beta\;(\epsilon-\mu)}\right)\right] \\
&= n_0\;T(\beta\mu)+\mathcal{O}(1-\nu)\;.
\end{aligned} \tag{F.8}$$

We find $e^{\beta\,\mu}$ at the same limit from Eq. (F.4)

$$\lim_{\mu\to\infty} e^{\beta\,\mu} \propto \frac{\sinh(\beta\;W)}{\beta\;W\;(1-\nu)}\;. \tag{F.9}$$

Finally, we find

$$\lim_{\nu\to 1} P(T,\nu) \propto -n_0\;T\;\ln\left((1-\nu)\;\frac{\beta\;W}{\sinh(\beta\;W)}\right) \tag{F.10}$$

and the quantity of interest:

$$\begin{aligned}
\lim_{\nu\to 1}\frac{\partial^2 P(T,\nu)}{\partial T^2} &= -n_0\;\partial_T^2\;\left[T\ln\left(\frac{\beta\;W}{\sinh(\beta\;W)}\right)\right] \\
&= \frac{n_0}{T}\;\left[1+\left(\frac{\beta\;W}{\sinh(\beta\;W)}\right)^2\right]+\mathcal{O}(1-\nu) \\
&\neq 0\;.
\end{aligned} \tag{F.11}$$

Here, we shall discuss why we are interested $\partial^2 P(T,\nu)/\partial T^2$. It is related directly to the inverse compressibility as implied in Eq. (F.5) or explicitly,

$$\lim_{\nu\to 1} \frac{\partial^2 P(T,\nu)}{\partial T^2} = \int_0^1 \frac{d\nu}{\nu}\, \frac{\partial^2 \kappa_T^{-1}}{\partial T^2} \ . \tag{F.12}$$

Therefore, the above derivative represents the integral of the temperature derivative of the inverse compressibility with respect to the filling factor. Because of the positiveness of the filling factor, a zero integral, would be the result of the temperature derivative of the inverse compressibility alone. In order for an integral of a finite boundary to become zero, the integrand has to change signs within the boundary, to be able to have a cancellation.

This is what happens in the fractional quantum Hall system. The crossing points appearing in the plots of the inverse compressibility against the filling factor for various temperatures (each curve corresponds to each temperature) means that at some specific filling factors, the inverse compressibility is independent of temperature within a finite range of temperature.

While in case of the fractional quantum Hall system, the left hand side of the equation corresponding to Eq. (F.12) is zero, cf. Eq. (6.21), and that leads to the sum rule, and to the existence of the crossing points. The situation is totally different.

Thus, the existence of the crossing points in the plots of the inverse compressibility of the fractional quantum Hall system against the filling factor is not due to the finiteness of the Landau band.

Appendix G

The Padé approximation

The Padé approximant is a well known function for extrapolating a series. In this work, the Padé approximants are used to extrapolate the high–temperature expansion results, the energy and the inverse compressibility, down to zero temperature or to the regimes where the temperature is lower than that could be reached by the high–temperature expansion results themselves.

In this Appendix, we aim to study the Padé approximants of order $[M, N]$ for two special cases: $M = N$ and $M = N + 1$. The Padé approximant here will have only two variables according to the nature of this study. Thus, the Padé approximant of order $[M, N]$ here can be written as

$$F^{[M,N]}(x, y) = \frac{\sum_{n=0}^{M} \tilde{p}_n(x) y^n}{1 + \sum_{n=1}^{N} \tilde{q}_n(x) y^n} \tag{G.1}$$

where we assume that the function behaves as a power series in y and the coefficient of each power of y is a function of x. Hence, $F^{[M,N]}(x, y)$ has $M + N + 1$ parameters, $\tilde{p}_0(x), \ldots, \tilde{p}_M(x)$ and $\tilde{q}_1(x), \ldots, \tilde{q}_N(x)$. It can be clearly seen that in the limit for which $y \to \infty$, $F^{[M,N]}(x, y)$ would diverge for $M > N$ and become zero for $M < N$. On the other hand, $F^{[M,N]}(x, y)$ can converge to a finite value, $\tilde{p}_N(x)/\tilde{q}_N(x)$, if $M = N$ and $\tilde{q}_N(x) \neq 0$.

Thus, the energy will be extrapolated with the equal order Padé approximants, $F^{[N,N]}(\nu, \beta)$. On the other hand, the inverse compressibility will be extrapolated with the unequal order Padé approximants, $F^{[N+1,N]}(\nu, \beta)$, due to the nature of the quantity itself. (The high–temperature expansion series of the inverse compressibility starts with β^{-1} instead of β^0, see Eq. (6.11).)

G.1 Solving the Padé approximant : $F^{[M,N]}(\nu,\beta)$

In order to solve the Padé approximant $F^{[M,N]}(\nu,\beta)$, which has $M+N+1$ parameters, we need a series of $M+N+1$ coefficients. For convenience, we write the high–temperature expansion series as following

$$G(\nu,\beta) = \sum_{n=0}^{M+N} g_n(\nu)\ \beta^n + \mathcal{O}(\beta^{M+N+1})\ . \tag{G.2}$$

The extrapolating equation for the high–temperature expansion series of the energy by $F^{[M,N]}(\nu,\beta)$ can be written as

$$\sum_{n=0}^{M} \tilde{p}_n(\nu)\beta^n = \left(1+\sum_{n=1}^{N} \tilde{q}_n(\nu)\beta^n\right) \sum_{n=0}^{2N+1} g_n(\nu)\ \beta^n\ . \tag{G.3}$$

Solving this equation order by order, we find the relation between the high–temperature expansion coefficients, $g_n(\nu)$, and the Padé approximant coefficients, $\tilde{p}_n(\nu)$ and $\tilde{q}_n(\nu)$, as follow

$$\begin{aligned} \tilde{p}_n(\nu) &= \sum_{i=0}^{M} g_{n-i}(\nu)\ \tilde{q}_i(\nu)\ , \\ 0 &= \sum_{i=0}^{N} g_{M+j-i}(\nu)\tilde{q}_i(\nu)\ , \qquad\qquad j=1,\ldots,N \end{aligned} \tag{G.4}$$

with $\tilde{q}_0(\nu)=1$.

For further convenience in expressing the result, we introduce a new set of dimensionless parameters $r_n(\nu)$

$$r_n(\nu) = \left(\frac{g_0(\nu)}{g_1(\nu)}\right)^n\ \frac{g_n(\nu)}{g_0(\nu)}\ , \tag{G.5}$$

in which $r_0(\nu)=r_1(\nu)=1$.

With these parameters, the Padé approximant $F^{[M,N]}(\nu,\beta)$ becomes

$$F^{[M,N]}(\nu,\tilde{\beta}) = \frac{g_0(\nu)\ \sum\limits_{n=0}^{M} p_n(\nu)\tilde{\beta}^n}{g_0(\nu)+\sum\limits_{n=1}^{N} q_n(\nu)\tilde{\beta}^n}, \tag{G.6}$$

where

$$\begin{aligned} \Big(p_n(\nu),\ q_n(\nu)\Big) &= \left(\frac{g_0(\nu)}{g_1(\nu)}\right)^n\ (\tilde{p}_n(\nu),\ \tilde{q}_n(\nu)g_0(\nu)) \\ \tilde{\beta} &= \frac{g_1(\nu)}{g_0(\nu)}\ \beta\ , \end{aligned} \tag{G.7}$$

with $q_0(\nu) = g_0(\nu)$. The system of the solutions becomes

$$p_n(\nu) = \sum_{i=0}^{M} q_i(\nu)\, r_{n-i}(\nu) \tag{G.8}$$

$$0 = \sum_{i=0}^{N} q_i(\nu)\, r_{M+j-i}(\nu)\,, \qquad j = 1,\ldots,N \tag{G.9}$$

Solving Eq. (G.8), we find $p_n(\nu)$ as a function of $g_0(\nu), g_1(\nu)$ and $q_j(\nu)$. Solving Eq. (G.9), we find $q_n(\nu)$ as a function of $g_j(\nu)$. Hence, we obtain the coefficients of the Padé approximant, $p_n(\nu)$ and $q_n(\nu)$, expressed by the the coefficients of the power series $g_j(\nu)$.

We denote the extrapolated result by

$$\mathcal{G}^{[M,N]}(\nu,\tilde{\beta}) = F^{[M,N]}(\nu,\tilde{\beta}) \tag{G.10}$$

and the extrapolated to zero temperature result for the case $M = N$ is denoted by

$$\mathcal{G}_0^{[N,N]}(\nu) = g_0(\nu)\,\frac{p_N(\nu)}{q_N(\nu)}\,. \tag{G.11}$$

For simplicity and brevity, the argument (ν) of functions p, q and r will be omitted from here on.

G.1.1 Equal order Padé approximant : $F^{[N,N]}(\nu,\beta)$

Equal order Padé approximant : $N = 1$

For "$N = 1$", we have from Eq. (G.8) and Eq. (G.9)

$$\left.\begin{array}{c} p_0 = q_0 \\ p_1 = q_0 + q_1 \\ 0 = q_0\, r_2 + q_1 \end{array}\right\} \qquad \begin{array}{c} p_0 = g_0(\nu) \\ p_1 = g_0(\nu)\,(1 - r_2) \\ q_1 = -g_0(\nu)\, r_2 \end{array} \tag{G.12}$$

Thus, the extrapolated results in this order $N = 1$ are

$$\mathcal{G}^{[1,1]}(\nu,\tilde{\beta}) = g_0(\nu)\,\left(1 + \frac{\tilde{\beta}}{1 - r_2\,\tilde{\beta}}\right)\,, \tag{G.13}$$

and

$$\mathcal{G}_0^{[1,1]}(\nu) = g_0(\nu)\,\left(1 - \frac{1}{r_2}\right)\,. \tag{G.14}$$

Equal order Padé approximant : $N = 2$

For $N = 2$, we have from Eq. (G.8) and Eq. (G.9) :

$$\begin{aligned} p_0 &= q_0 \ , \\ p_1 &= q_0 + q_1 \ , \\ p_2 &= q_0 \, r_2 + q_1 + q_2 \ , \\ 0 &= q_0 \, r_3 + q_1 \, r_2 + q_2 \ , \\ 0 &= q_0 \, r_4 + q_1 \, r_3 + q_2 \, r_2 \ , \end{aligned} \tag{G.15}$$

which results in

$$\begin{aligned} p_0 &= g_0(\nu) \\ p_1 &= g_0(\nu) \, \frac{r_2^2 - r_3 - r_2 \, r_3 + r_4}{r_2^2 - r_3} \\ p_2 &= g_0(\nu) \, \frac{r_2^3 + r_3^2 + r_4 - r_2 \, (2r_3 + r_4)}{r_2^2 - r_3} \\ q_1 &= -g_0(\nu) \, \frac{r_2 \, r_3 - r_4}{r_2^2 - r_3} \\ q_2 &= g_0(\nu) \, \frac{r_3^2 - r_2 \, r_4}{r_2^2 - r_3} \end{aligned} \tag{G.16}$$

Thus, the extrapolated results in this order $N = 2$ are

$$\mathcal{G}^{[2,2]}(\nu, \tilde{\beta}) = g_0(\nu) \left(1 + \frac{\tilde{\beta} \, (r_2^2 - r_3) + \tilde{\beta}^2 \, (r_2^3 - 2 r_2 r_3 + r_4)}{r_2^2 - r_3 + \tilde{\beta}(r_4 - r_2 r_3) + \tilde{\beta}^2 (r_3^2 - r_2 r_4)} \right) \tag{G.17}$$

and

$$\mathcal{G}_0^{[2,2]}(\nu) = g_0(\nu) \left(1 + \frac{r_2^3 - 2 r_2 r_3 + r_4}{r_3^2 - r_2 r_4} \right) \tag{G.18}$$

Equal order Padé approximant : $N = 3$

For $N = 3$, we have from Eq. (G.8) and Eq. (G.9) :

$$\begin{aligned} p_0 &= q_0 \ , \\ p_1 &= q_0 + q_1 \ , \\ p_2 &= q_0 \, r_2 + q_1 + q_2 \ , \\ p_3 &= q_0 \, r_3 + q_1 \, r_2 + q_2 + q_3 \ , \\ 0 &= q_0 \, r_4 + q_1 \, r_3 + q_2 \, r_2 + q_3 \ , \\ 0 &= q_0 \, r_5 + q_1 \, r_4 + q_2 \, r_3 + q_3 \, r_2 \ , \\ 0 &= q_0 \, r_6 + q_1 \, r_5 + q_2 \, r_4 + q_3 \, r_3 \ , \end{aligned} \tag{G.19}$$

which result

$$
\begin{aligned}
p_0 &= g_0(\nu) \\
p_1 &= \frac{g_0(\nu)}{d_{33}}\Big(r_3^3 - r_3^2 r_4 + (1+r_2)r_4^2 - r_4 r_5 \\
&\quad + r_2^2(r_5 - r_6) + r_3(r_2(r_5 - 2r_4) - r_5 + r_6)\Big) \\
p_2 &= \frac{g_0(\nu)}{d_{33}}\Big(r_2^3 r_5 - r_4 r_5 + r_5^2 - r_3^2(r_4 + r_5) - r_4 r_6 - r_2^2(2r_3 r_4 + r_6) \\
&\quad + r_3(r_4^2 + r_6) + r_2(r_3^3 + r_4(2r_4 - r_5) + r_3 r_6)\Big) \\
p_3 &= \frac{g_0(\nu)}{d_{33}}\Big(r_3^4 + r_2^2 r_4^2 - r_4^3 + r_5^2 - r_2^3 r_6 - r_4 r_6 - r_3^2(3r_2 r_4 + 2r_5 + r_6) \\
&\quad - r_2(2r_4 r_5 + r_5^2 - r_4 r_6) + 2r_3(r_4^2 + r_4 r_5 + r_2(r_2 r_5 + r_6))\Big) \\
q_1 &= -\frac{g_0(\nu)}{d_{33}}\Big(r_3^2 r_4 - r_2 r_4^2 + r_4 r_5 + r_2^2 r_6 - r_3(r_2 r_5 + r_6)\Big) \\
q_2 &= -\frac{g_0(\nu)}{d_{33}}\Big(r_3^2 r_5 + r_2 r_4 r_5 - r_5^2 + r_4 r_6 - r_3(r_4^2 + r_2 r_6)\Big) \\
q_3 &= -\frac{g_0(\nu)}{d_{33}}\Big(r_4^3 + r_2 r_5^2 + r_3^2 r_6 - r_4(2r_3 r_5 + r_2 r_6)\Big) \\
d_{33} &= r_3^3 + r_4^2 + r_2^2 r_5 - r_3(2r_2 r_4 + r_5)
\end{aligned}
\tag{G.20}
$$

From these solutions, we can form the extrapolated result according to Eq. (G.10) and Eq. (G.6). The extrapolated result to $\beta \to \infty$ in this order $N = 3$ is

$$
\mathcal{G}_0^{[3,3]}(\nu) = g_0(\nu)\left(1 - \frac{r_3^4 + r_2^2 r_4^2 - 2r_2 r_4 r_5 + r_5^2 - r_3^2(3r_2 r_4 + 2r_5) - r_2^3 r_6 - r_4 r_6 + 2r_3(r_4^2 + r_2(r_2 r_5 + r_6))}{r_4^3 + r_2 r_5^2 + r_3^2 r_6 - r_4(2r_3 r_5 + r_2 r_6)}\right) \tag{G.21}
$$

G.1.2 Unequal order Padé approximant : $F^{[N+1,N]}(\nu,\beta)$

The procedure in solving the unequal order Padé approximant is much the same to the procedure in solving the equal order Padé approximant. We shall give the solutions, $p_j(\nu)$ and $q_j(\nu)$, of the Padé approximants from $N = 0$ to $N = 3$ directly. From these solutions, we can form the extrapolated results, $\mathcal{G}^{[N+1,N]}(\nu,\tilde{\beta})$ according to Eq. (G.10) and Eq. (G.6).

Unequal order Padé approximant : $N = 0$

$$p_0 = g_0(\nu) , \qquad p_1 = g_0(\nu) \tag{G.22}$$

Thus, the extrapolated inverse compressibility for this order $N = 0$ is trivial

$$\mathcal{G}^{[1,0]}(\nu, \tilde{\beta}) = g_0(\nu)(1 + \tilde{\beta}) . \tag{G.23}$$

Unequal order Padé approximant : $N = 1$

$$\begin{aligned} p_0 &= g_0(\nu) \\ p_1 &= g_0(\nu)(1 - \frac{r_3}{r_2}) \\ p_2 &= g_0(\nu)(r_2 - \frac{r_3}{r_2}) \\ q_1 &= -g_0(\nu) \, \frac{r_3}{r_2} \end{aligned} \tag{G.24}$$

Thus, the extrapolated inverse compressibility for this order $N = 1$ is

$$\mathcal{G}^{[2,1]}(\nu, \tilde{\beta}) = g_0(\nu) \left(1 + \frac{\tilde{\beta} \, r_2 \, + \tilde{\beta}^2 \, (r_2^2 - r_3)}{r_2 - \tilde{\beta} \, r_3} \right) . \tag{G.25}$$

Unequal order Padé approximant : $N = 2$

$$\begin{aligned} p_0 &= g_0(\nu) \\ p_1 &= g_0(\nu) \, \left(1 - \frac{r_3 \, r_4 - r_2 \, r_5}{r_3^2 - r_2 \, r_4} \right) \\ p_2 &= g_0(\nu) \, \left(r_2 - \frac{r_3 \, r_4 - r_2 \, r_5 - r_4^2 + r_3 \, r_5}{r_3^2 - r_2 \, r_4} \right) \\ p_3 &= g_0(\nu) \, \left(r_3 - \frac{2 \, r_2 \, r_3 \, r_4 - r_2^2 \, r_5 - r_4^2 + r_3 \, r_5}{r_3^2 - r_2 \, r_4} \right) \\ q_1 &= -g_0(\nu) \, \left(\frac{r_3 \, r_4 - r_2 \, r_5}{r_3^2 - r_2 \, r_4} \right) \\ q_2 &= g_0(\nu) \, \left(\frac{r_4^2 - r_3 \, r_5}{r_3^2 - r_2 \, r_4} \right) \end{aligned} \tag{G.26}$$

Unequal order Padé approximant : $N = 3$

$$
\begin{aligned}
p_0 &= g_0(\nu) \\
p_1 &= \frac{g_0(\nu)}{d_{43}}\Big(r_4^3 - r_4^2 r_5 + r_2 r_5\,(r_5 - r_6) + r_3\,(r_5^2 + r_3\,(r_6 - r_7)) \\
&\quad + r_4\,(r_3\,(-2r_5 + r_6) + r_2\,(-r_6 + r_7))\Big) \\
p_2 &= \frac{g_0(\nu)}{d_{43}}\Big(r_2^2\,(r_5^2 - r_4 r_6) - r_4^2\,(r_5 + r_6) + r_3\,(r_5^2 - r_5 r_6 - r_3 r_7) \\
&\quad + r_2\,(r_4^3 + r_3^2 r_6 - r_5 r_6 + r_6^2 - r_5 r_7 + r_4\,(r_7 - 2r_3 r_5)) + r_4\,(r_5^2 + r_3\,(r_6 + r_7))\Big) \\
p_3 &= \frac{g_0(\nu)}{d_{43}}\Big(r_4 r_5^2 - r_5^3 + r_3^3 r_6 - r_4^2 r_6 + 2r_4 r_5 r_6 - r_4^2 r_7 - r_3^2\,(2r_4 r_5 + r_2 r_7) \\
&\quad + r_2^2\,(r_4 r_7 - r_5 r_6) + r_2\,(r_6^2 - r_4^2 r_5 - r_5 r_7) \\
&\quad + r_3\,(r_4^3 + 2r_2 r_5^2 - r_5 r_6 - r_6^2 + r_4 r_7 + r_5 r_7)\Big) \\
p_4 &= \frac{g_0(\nu)}{d_{43}}\Big(r_4^4 + r_3^2 r_5^2 - r_5^3 + r_2^2 r_6^2 - r_3^3 r_7 - r_2^2 r_5 r_7 - r_4^2\,(3r_3 r_5 + 2r_2 r_6 + r_7) \\
&\quad - r_3\,(2r_2 r_5 r_6 + r_6^2 - r_5 r_7) + 2r_4\,((r_3^2 + r_5) r_6 + r_2\,(r_5^2 + r_3 r_7))\Big) \\
q_1 &= -\frac{g_0(\nu)}{d_{43}}\Big(r_4^2 r_5 - r_3 r_5^2 + r_2 r_5 r_6 + r_3^2 r_7 - r_4\,(r_3 r_6 + r_2 r_7)\Big) \\
q_2 &= -\frac{g_0(\nu)}{d_{43}}\Big(r_4^2 r_6 + r_3 r_5 r_6 - r_4\,(r_5^2 + r_3 r_7) + r_2\,(r_5 r_7 - r_6^2)\Big) \\
q_3 &= -\frac{g_0(\nu)}{d_{43}}\Big(r_5^3 + r_3 r_6^2 + r_4^2 r_7 - r_5\,(2r_4 r_6 + r_3 r_7)\Big) \\
d_{43} &= r_4^3 + r_2 r_5^2 + r_3^2 r_6 - r_4\,(2r_3 r_5 + r_2 r_6)
\end{aligned}
\tag{G.27}
$$

Appendix H

Three–Level Model

In this Appendix, we shall study the three–level model. We shall first define our parameters which describe the model. Then, we shall calculate the general solution and finally consider the physical condition on the parameters. There are two conditions that need to be checked with the solution. One is the positivity of the degeneracy of each level. The second is the reality of each energy level. Later in this chapter, we shall see that the model cannot be used for too small or too large particle densities, i. e. filling factors. There is a specific range of filling factors in which all conditions are satisfied. At the borders of this range, we shall see that the model collapses from three energy levels into two degenerate energy levels. That defines the regime where the model can be used. Finally, the ground state energy of the model is studied. At the points where the three–level model collapses into two–level model, the ground state energies of both models merge smoothly.

H.1 Parameterisation

We specialise the general expression for the N_L–model to the case $N_L = 3$; then, the energy of our model is written as

$$E^{3-level}(T, N_\phi, \nu) = N_\phi \, \frac{\sum\limits_{j=1}^{3} E_j(\nu)\, n_j(\nu)\, e^{-\beta E_j(\nu)}}{\sum\limits_{j=1}^{3} n_j(\nu)\, e^{-\beta E_j(\nu)}} \, . \tag{H.1}$$

Here, we have five parameters, the energies $E_j(\nu)$ and the degeneracies $n_j(\nu)$ which are normalised according to $\sum_{j=1}^{3} n_j(\nu) = 1$. From the above equation, we can easily see that our parameters are invariant under permutation of the three levels. Thus, we define a new set of parameters which transform according to representations of the permutation group. The first parameter is $E_c(\nu)$ the centre of the energy levels of the model,

$$E_c(\nu) = \frac{1}{3} \sum_{j=1}^{3} E_j(\nu) \ . \tag{H.2}$$

$E_c(\nu)$ is invariant under permutations. The remaining parameters include the distance of each energy level, $\Delta_j(\nu)$, from E_c

$$\Delta_j(\nu) = E_j(\nu) - E_c(\nu) \ . \tag{H.3}$$

We define complex parameters $\Delta(\nu)$, $\Delta^*(\nu)$, $n(\nu)$ and $n^*(\nu)$ which transform according to two–dimensional representation of the permutation group,

$$\Delta(\nu) = \frac{1}{3} \left[\Delta_1(\nu) + q\ \Delta_2(\nu) + q^2\ \Delta_3(\nu)\right] , \tag{H.4}$$

and

$$n(\nu) = n_1(\nu) + q n_2(\nu) + q^2 n_3(\nu) \ , \tag{H.5}$$

where q is the third root of unity, $q = e^{2\pi i/3}$.

By inspecting of the expansion of Eq. (H.1), we observe that there is an only one type of combination of $n_j(\nu)$ and $\Delta_j(\nu)$ which enters the further calculations. Thus, we define the combination, $y_m(\nu)$,

$$y_m(\nu) = \sum_{j=1}^{3} n_j(\nu) \Delta_j(\nu)^m \tag{H.6}$$

in which $n_j(\nu)$ and $\Delta_j(\nu)$ are to be expressed by $n(\nu)$ and $\Delta(\nu)$ with the aid of Eq. (H.2–H.3). Then, Eq. (H.1) becomes

$$\frac{E^{3-level}(T, N_\phi, \nu)}{N_\phi} = E_c(\nu) + \frac{\sum\limits_{n=0}^{\infty} \frac{1}{n!} (-\beta)^n y_{n+1}(\nu)}{\sum\limits_{n=0}^{\infty} \frac{1}{n!} (-\beta)^n y_n(\nu)} \ , \tag{H.7}$$

We now use the first five coefficients $\alpha_n(\nu)$ of the high–temperature series expansion of the energy to determine the parameters $E_c(\nu)$, $\Delta(\nu)$ and $n(\nu)$. Expanding (H.7) up to fourth order in β, we find

$$\left[\sum_{n=1}^{5} \beta^{n-1}\ \alpha_n(\nu) - E_c(\nu)\right] \left[\sum_{n=0}^{4} \frac{1}{n!} (-\beta)^n y_n(\nu)\right] = \sum_{n=1}^{4} \frac{1}{n!} (-\beta)^n y_{n+1}(\nu) + \mathcal{O}[\beta^5] \ . \tag{H.8}$$

In the lowest order in β, we find $\alpha_1(\nu) - E_c(\nu) = y_1(\nu)$. The next four orders give

$$\left[\sum_{n=2}^{5} \beta^{n-1}\ \alpha_n(\nu)\right] \left[\sum_{n=0}^{3} \frac{1}{n!} (-\beta)^n y_n(\nu)\right] = \sum_{n=1}^{4} \frac{1}{n!} (-\beta)^n (y_{n+1}(\nu) - y_1(\nu)\ y_n(\nu)) + \mathcal{O}[\beta^5] \tag{H.9}$$

H.2 General solution

At this point, we have two sets of equations for $y_n(\nu)$. The first relates $y_n(\nu)$ to the high–temperature expansion coefficients, $\alpha_n(\nu)$. That can be derived from equations (H.8–H.9). Explicitly, we have

$$\begin{aligned}
y_1(\nu) &= \alpha_1(\nu) - E_c(\nu) && \text{(H.10)}\\
y_2(\nu) &= -\alpha_2(\nu) + y_1(\nu)^2 && \text{(H.11)}\\
y_3(\nu) &= 2\,\alpha_3(\nu) - 3\,y_1(\nu)\,\alpha_2(\nu) + y_1(\nu)^3 && \text{(H.12)}\\
y_4(\nu) &= -6\,\alpha_4(\nu) + 8\,y_1(\nu)\,\alpha_3(\nu) - 6\,y_1(\nu)^2\,\alpha_2(\nu) + 3\,\alpha_2(\nu)^2 + y_1(\nu)^4 && \text{(H.13)}\\
y_5(\nu) &= 24\,\alpha_5(\nu) - 30\,y_1(\nu)\,\alpha_4(\nu) + 20\,y_1(\nu)^2\,\alpha_3(\nu) - 10\,y_1(\nu)^3\,\alpha_2(\nu) \\
&\quad -20\,\alpha_2(\nu)\,\alpha_3(\nu) + y_1(\nu)^5 && \text{(H.14)}
\end{aligned}$$

The second relates $y_n(\nu)$ via Eq. (H.6) to the parameters $\Delta(\nu)$ and $n(\nu)$ defined in Eq. (H.4–H.5):

$$\begin{aligned}
y_1(\nu) &= \Big(\Delta(\nu)\,n^*(\nu) + \Delta^*(\nu)\,n(\nu)\Big) && \text{(H.15)}\\
y_2(\nu) &= \Big(\Delta(\nu)^2\,n(\nu) + \Delta^*(\nu)^2\,n^*(\nu)\Big) + 2\,|\Delta(\nu)|^2 && \text{(H.16)}\\
y_3(\nu) &= \Big(\Delta(\nu)^3 + \Delta^*(\nu)^3\Big) + 3\,|\Delta(\nu)|^2\,\Big(\Delta(\nu)\,n^*(\nu) + \Delta^*(\nu)\,n(\nu)\Big) && \text{(H.17)}\\
y_4(\nu) &= \Big(\Delta(\nu)^4\,n^*(\nu) + \Delta^*(\nu)^4\,n(\nu)\Big) \\
&\quad +4\,|\Delta(\nu)|^2\,\Big(\Delta(\nu)^2\,n(\nu) + \Delta^*(\nu)^2\,n^*(\nu)\Big) + 6\,|\Delta(\nu)|^4 && \text{(H.18)}\\
y_5(\nu) &= \Big(\Delta(\nu)^5\,n(\nu) + \Delta^*(\nu)^5\,n^*(\nu)\Big) + 5\,|\Delta(\nu)|^2\,\Big(\Delta(\nu)^3 + \Delta^*(\nu)^3\Big) \\
&\quad +10\,|\Delta(\nu)|^4\Big(\Delta(\nu)\,n^*(\nu) + \Delta^*(\nu)\,n(\nu)\Big) && \text{(H.19)}
\end{aligned}$$

Thus, we have five real non–linear equations for five unknown parameters, $x(\nu) = \alpha_1(\nu) - E_c(\nu)$, $\Delta(\nu)$ and $n(\nu)$. We shall first solve for $n(\nu)$ and $n^*(\nu)$ using Eq. (H.15-H.16) and then for $\Delta(\nu)$ and $\Delta^*(\nu)$ using Eq. (H.17–H.18). Then, everything is expressed by $y_2(\nu)$, $y_3(\nu)$, $y_4(\nu)$ and $x(\nu)$. Replacing all $y_n(\nu)$ by those from (H.11–H.13), then, $n(\nu)$, $n^*(\nu)$, $\Delta(\nu)$ and $\Delta^*(\nu)$ are expressed by the high–temperature expansion coefficients, $\alpha_n(\nu)$, and the last unsolved parameter $x(\nu)$. Finally, we solve for $x(\nu)$ which yields $E_c(\nu)$.

First, we solve (H.15) and (H.16) for $n(\nu)$ and $n^*(\nu)$ and get,

$$n(\nu) = \frac{-\Big(\alpha_2(\nu) + x(\nu)^2 + 2\,|\Delta(\nu)|^2\Big)\,\Delta(\nu) - x(\nu)\,\Delta^*(\nu)^2}{\Delta(\nu)^3 - \Delta^*(\nu)^3} \qquad \text{(H.20)}$$

Next, we solve (H.17) and (H.18) for $\Delta(\nu)$ and $\Delta^*(\nu)$ and find,

$$\begin{aligned} |\Delta(\nu)|^2 &= \frac{x(\nu)\, y_3(\nu) - y_4(\nu)}{3\, \alpha_2(\nu)} \\ &= \frac{1}{\alpha_2(\nu)} \left[2 \left(\alpha_4(\nu) - \alpha_3(\nu)\, x(\nu) \right) + \alpha_2(\nu) \left(x(\nu)^2 - \alpha_2(\nu) \right) \right] , \end{aligned} \tag{H.21}$$

and

$$\begin{aligned} \Delta(\nu)^3 + \Delta^*(\nu)^3 &= y_3(\nu) - \frac{x(\nu) \left(y_3(\nu)\, x(\nu) - y_4(\nu) \right)}{\alpha_2(\nu)} \\ &= -2 \left(x(\nu)^3 - \alpha_3(\nu) \right) - \frac{6\, x(\nu)}{\alpha_2(\nu)} \left(\alpha_4(\nu) - \alpha_3(\nu)\, x(\nu) \right) . \end{aligned} \tag{H.22}$$

From now, we shall use the real and imaginary parts of $\Delta(\nu)^3$ as auxiliary variables, $\Delta(\nu)^3 = a(\nu) + i\, b(\nu)$. Then, we find

$$a(\nu) = -x(\nu)^3 + \alpha_3(\nu) - \frac{3\, x(\nu)}{\alpha_2(\nu)} \left(\alpha_4(\nu) - \alpha_3(\nu)\, x(\nu) \right) , \tag{H.23}$$

and $b(\nu) = \{ |\Delta(\nu)|^6 - a(\nu)^2 \}^{\frac{1}{2}}$.

We can replace $\Delta(\nu)$ in the expression (H.20) of $n(\nu)$ by these new parameters $a(\nu)$ and $b(\nu)$,

$$\begin{aligned} n(\nu) &= \frac{i}{2\, b(\nu) \left(a(\nu) - i\, b(\nu) \right)^{\frac{1}{3}}} \left[x(\nu) \left(a(\nu) - i\, b(\nu) \right) \right. \\ &\quad \left. + \left\{ -x(\nu)^2 + \alpha_2(\nu) + 2 \left(a(\nu)^2 + b(\nu)^2 \right)^{\frac{1}{3}} \right\} \left(a(\nu)^2 + b(\nu)^2 \right)^{\frac{1}{3}} \right] . \end{aligned} \tag{H.24}$$

Finally, we determine $x(\nu)$. From the first equation in (H.21), we have $y_4(\nu) = x(\nu)\, y_3(\nu) - 3\, \alpha_2(\nu)\, |\Delta(\nu)|^2$. Using this and rewriting $y_5(\nu)$ as

$$\begin{aligned} y_5(\nu) &= \left(n(\nu)\, \Delta(\nu)^2 + n^*(\nu)\, \Delta^*(\nu)^2 \right) \left(\Delta(\nu)^3 + \Delta^*(\nu)^3 \right) \\ &\quad - n(\nu)\, \Delta(\nu)^2\, \Delta^*(\nu)^3 - n^*(\nu)\, \Delta^*(\nu)^2\, \Delta(\nu)^3 \\ &\quad + 5\, |\Delta(\nu)|^2 \left(\Delta(\nu)^3 + \Delta^*(\nu)^3 \right) + 10\, |\Delta(\nu)|^4 \left(n^*(\nu)\, \Delta(\nu) + n(\nu)\, \Delta^*(\nu) \right) \\ &= \left(y_2(\nu) + 3\, |\Delta(\nu)|^2 \right) \left(\Delta(\nu)^3 + \Delta^*(\nu)^3 \right) + 9\, |\Delta(\nu)|^4\, x(\nu) \end{aligned} \tag{H.25}$$

and substituting Eq. (H.21) and Eq. (H.22) and Eq. (H.11) and Eq. (H.12) we find the relation,

$$\begin{aligned} y_5(\nu) - x(\nu)\, y_4(\nu) &= -4\, x(\nu)^3\, \alpha_2(\nu) + 12\, x(\nu)^2\, \alpha_3(\nu) \\ &\quad +6\, x(\nu)\, \left(\alpha_2(\nu)^2 - \alpha_4(\nu) - 2\, \frac{\alpha_3(\nu)^2}{\alpha_2(\nu)} \right) \\ &\quad -8\, \alpha_2(\nu)\, \alpha_3(\nu) + 12\, \frac{\alpha_3(\nu)\, \alpha_4(\nu)}{\alpha_2(\nu)} \, . \end{aligned} \tag{H.26}$$

We analyse this expression for $y_5(\nu) - x(\nu)\, y_4(\nu)$ with the aid of Eq. (H.13–H.14) which yields

$$\begin{aligned} y_5(\nu) - x(\nu)\, y_4(\nu) &= -4\, x(\nu)^3\, \alpha_2(\nu) + 12\, x(\nu)^2\, \alpha_3(\nu) \\ &\quad +12\, x(\nu)\, \left(\alpha_2(\nu)^2 + 2\, \alpha_4(\nu) \right) \\ &\quad -20\, \alpha_2(\nu)\, \alpha_3(\nu) + 24\, \alpha_5(\nu) \, . \end{aligned} \tag{H.27}$$

That leads to an equation for $x(\nu)$ with the solution

$$x(\nu) = \frac{2\, \left(2\, \alpha_2(\nu)\, \alpha_5(\nu) - \alpha_2(\nu)^2\, \alpha_3(\nu) - \alpha_3(\nu)\, \alpha_4(\nu) \right)}{3\, \alpha_2(\nu)\, \alpha_4(\nu) - \alpha_2(\nu)^3 - 2\, \alpha_3(\nu)^2} \, . \tag{H.28}$$

We have stated above that these are non–linear equation systems which may have several solutions. Surprisingly, here, we finally have a *unique* solution. This is because the other solutions are related to this unique solution by the permutations of the three levels.

H.2.1 Physical conditions on the parameters

We have stated in the very beginning of the Appendix that there are two conditions which our primary parameters $n_j(\nu)$ and $E_j(\nu)$ have to fulfil. Here, after changing variables many times, we emphasise the following conditions required for our present parameters $n(\nu)$ and $\Delta(\nu)$.

1. $-\frac{1}{2} < \Re[n(\nu)] < 1$ and $\left| \Im[n(\nu)] \right| < \frac{-1}{\sqrt{3}} \left(\Re[n(\nu)] - 1 \right)$
2. $\Im[b(\nu)] = 0$.

The first condition means that all $n_j(\nu)$ satisfy the condition $0 < n_j(\nu) < 1$. The second condition guarantees that $\Delta(\nu)$ is complex and, that equivalently, all $\Delta_j(\nu)$ have different values. That means, all these three energy levels are different. We can represent the first condition by an equilateral triangle on the n plane. The area inside the triangle fulfils the first condition. The second condition can also be represented,

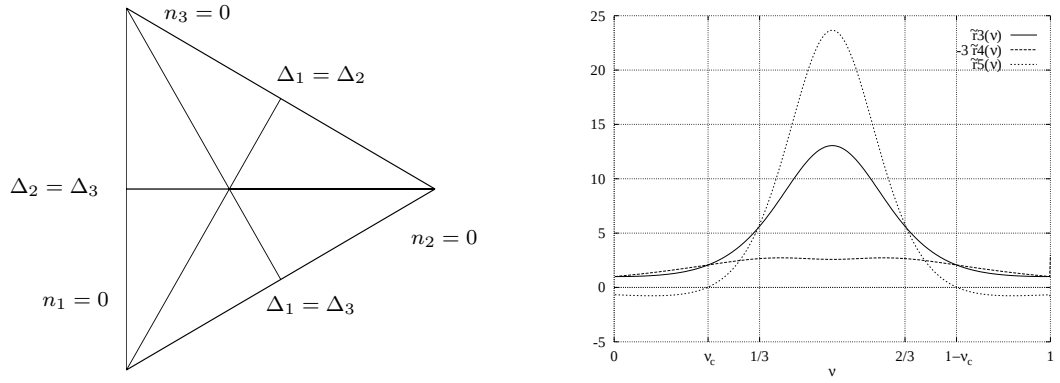

Figure H.1: The equilateral triangle and the three lines represent the physical conditions for the parameters $n(\nu)$ and $\Delta(\nu)$(Left). The dimensionless parameters $\tilde{r}_3(\nu), \tilde{r}_4(\nu)$ and $\tilde{r}_5(\nu)$ plotted for the W_1–interaction (Right).

related to the equilateral triangle mentioned above, by lines which divide the equilateral triangle into two right triangles. On each line, two of those three energy levels become equal. In Fig. H.1, we show how the two conditions are represented. Finally, the *allowed area* is inside the triangle with the exclusion of the lines.

Here, we check whether the solution of the previous section fulfils these conditions. In order to simplify this analysis, we introduce dimensionless parameters replacing the high–temperature expansion coefficients, $\alpha_n(\nu)$ as following :

$$\tilde{r}_3(\nu) = 1 - \frac{\alpha_2(\nu)^3}{\alpha_3(\nu)^2} \tag{H.29}$$

$$\tilde{r}_4(\nu) = -1 + \frac{\alpha_2(\nu)\ \alpha_4(\nu)}{\alpha_3(\nu)^2} \tag{H.30}$$

$$\tilde{r}_5(\nu) = -1 + \frac{\alpha_2(\nu)^2\ \alpha_5(\nu)}{\alpha_3(\nu)^3} \tag{H.31}$$

Then, we define dimensionless variables $\overline{x}(\nu)$, $\overline{a}(\nu)$ and $\overline{b}(\nu)$ by

$$x(\nu) = \frac{\alpha_3(\nu)}{\alpha_2(\nu)}\ (\overline{x}(\nu) + 1)\ , \tag{H.32}$$

$$a(\nu) + i\ b(\nu) = \frac{\alpha_3(\nu)}{\alpha_2(\nu)}^3\ (\overline{a}(\nu) + i\ \overline{b}(\nu)) \tag{H.33}$$

and get

$$\overline{x}(\nu) = \frac{4\ \tilde{r}_5(\nu) - 5\ \tilde{r}_4(\nu) + \tilde{r}_3(\nu)}{3\ \tilde{r}_4(\nu) + \tilde{r}_3(\nu)} \tag{H.34}$$

$$\overline{a}(\nu) = -\Big(\overline{x}(\nu)^3 + 3\,\overline{x}(\nu)\,\tilde{r}_4(\nu) + \tilde{r}_3(\nu) + 3\,\tilde{r}_4(\nu)\Big) \tag{H.35}$$

$$\overline{a}(\nu)^2 + \overline{b}(\nu)^2 = \Big(\overline{x}(\nu)^2 + 2\,\tilde{r}_4(\nu) + \tilde{r}_3(\nu)\Big)^3 . \tag{H.36}$$

The dimensionless parameters $\tilde{r}_3(\nu), \tilde{r}_4(\nu)$ and $\tilde{r}_5(\nu)$ are smooth and well defined in whole range of the filling factor, as shown in Fig. H.1. Thus, we express the solution for $n(\nu)$ by these dimensionless parameters,

$$\begin{aligned} n(\nu) = {} & \frac{i}{2\,\overline{b}(\nu)\,\Big(\overline{a}(\nu) - i\,\overline{b}(\nu)\Big)^{\frac{1}{3}}}\,\Big[(\overline{x}(\nu)+1)\,\Big(\overline{a}(\nu) - i\,\overline{b}(\nu)\Big) \\ & + \Big(\overline{x}(\nu)^2 - 2\,\overline{x}(\nu) + \tilde{r}_3(\nu) + 4\,\tilde{r}_4(\nu)\Big)\,\Big(\overline{a}(\nu)^2 + \overline{b}(\nu)^2\Big)^{\frac{1}{3}}\Big] . \end{aligned} \tag{H.37}$$

There is a divergence in the parameter $\overline{x}(\nu)$ when $\tilde{r}_3(\nu) + 3\,\tilde{r}_4(\nu) = 0$. We define ν_c by

$$\tilde{r}_3(\nu_c) + 3\,\tilde{r}_4(\nu_c) = 0 . \tag{H.38}$$

Finally, we find the ground state energy of the three–level model as the energy of the lowest energy level of the three energy levels. The result for the energies is

$$E_j(\nu) = \alpha_1(\nu) - x(\nu) + 2\,|\Delta(\nu)|\,\cos\left(\phi(\nu) + \frac{4\pi}{3}(k-1)\right) , \qquad j = 1,2,3 \tag{H.39}$$

where $\phi(\nu) = \frac{1}{3}\,\arctan[\,b(\nu)/a(\nu)\,]$.

Now we consider the case of the W_1–interaction. From Eq. (H.38) we find

$$\nu_c = \frac{1}{2} \mp \frac{1}{2}\,\sqrt{\frac{3957167}{12202751}} \tag{H.40}$$

We check the limit of $n(\nu)$ where $\overline{x}(\nu)$ goes to infinity using Eq. (H.35) and Eq. (H.36) in Eq. (H.37) and find that

$$n(\nu_c) = \lim_{\overline{x}(\nu)\to\infty} n(\nu) = -\frac{1}{2} - \frac{i\sqrt{3}}{2}\,\frac{1}{\sqrt{r_3^*}} \tag{H.41}$$

where $r_3^* = \lim\limits_{\nu\to\nu_c}\,\tilde{r}_3(\nu) \sim 2.069902123$. Here, we can see, that at these critical filling factors, our parameter, $n(\nu_c)$, has arrived at the border of the allowed area for the three–level model. From Eq. (H.41), $\Re[n(\nu_c)] = -1/2$ which leads to $n_1(\nu_c) = 0$, and that means one energy level, i. e., $E_1(\nu_c)$, is empty. This leads us to conclusion that at this filling factor, our three–level model collapses into a two–level model. We check the value of $n(\nu)$ beyond this critical point, where $\nu \leq \nu_c$ and $\nu \geq 1 - \nu_c$, and find that both conditions cannot be fullfiled in that area. The behaviour of parameter $n(\nu)$ in neighbourhood of ν_c is shown in Fig. H.2.

However, inside the region where $\nu_c < \nu < 1 - \nu_c$ both requirements are fulfilled.

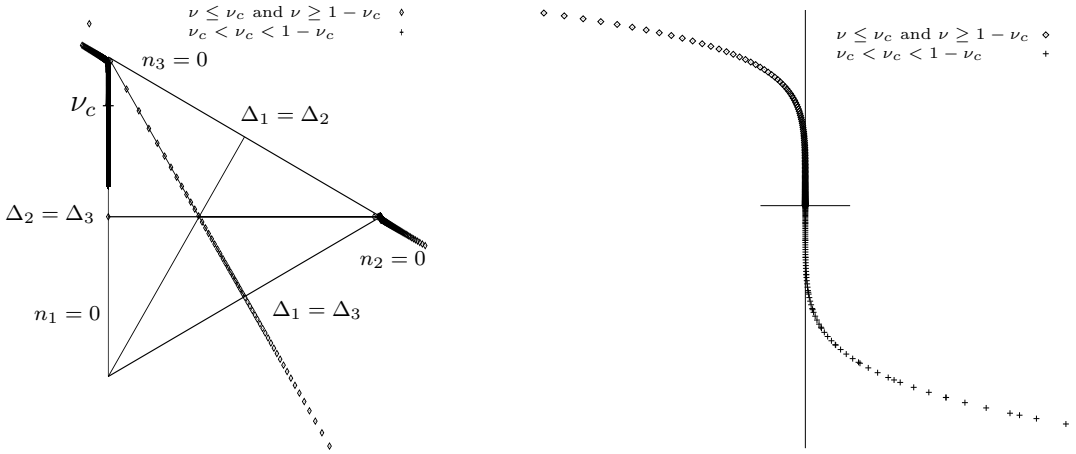

Figure H.2: The plots of the parameter $n(\nu)$ in the n–complex plane, in which the triangle and the lines represent the required conditions, (a) for whole range of filling factor (b) for filling factors in the neighbourhood of ν_c.

Part VII

References

Bibliography

[1] K. von Klitzing, G. Dorda, and M. Pepper, Phys. Rev. Lett. **45**, 494 (1980).

[2] T. Ando, Y. Matsumoto, and Y. Uemura, J. Phys. Soc. Japan **39**, 279 (1975).

[3] S. Kawaji, T. Igarashi, and J. Wakabayashi, Prog. Theor. Phys. Suppl. **57**, 176 (1975).

[4] R. B. Laughlin, Phys. Rev. B **23**, 5632 (1981).

[5] B. I. Halperin, Phys. Rev. B **25**, 2185 (1982).

[6] D. C. Tsui, H. L. Stormer, and A. C. Gossard, Phys. Rev. Lett. **48**, 1559 (1982).

[7] R. B. Laughlin, Phys. Rev. Lett. **50**, 1395 (1983).

[8] *The Quantum Hall Effect*, edited by R. E. Prange and S. M. Girvin (Springer–Verlag, New York, 1987).

[9] *Perspectives in Quantum Hall Effects : Novel Quantum Liquids in Low-Dimensional Semiconductor Structures*, edited by S. Das Sarma and A. Pinczuk (John Wiley & Sons, New York, 1996).

[10] O. Heinonen, *Composite Fermions in the Quantum Hall Effect* (World Scientific, Singapore, 1999).

[11] *Aspects topologiques de la physique en basse dimension. Topological aspects of low dimensional systems*, *Les Houches – Ecole d'Ete de Physique Theorique, Session LXIX*, edited by A. Comtet, T. J. amd S. Ouvry, and F. David (Springer–Verlag, Berlin/Heidelberg Germany, 1999).

[12] J. K. Jain, Phys. Rev. Lett. **63**, 199 (1989).

[13] J. K. Jain, Phys. Rev. B **40**, 8079 (1989).

[14] J. K. Jain, Phys. Rev. B **41**, 7653 (1990).

[15] A. Lopez and E. Fradkin, Phys. Rev. B **44**, 5246 (1991).

[16] B. I. Halperin, P. A. Lee, and N. Read, Phys. Rev. B **47**, 7312 (1993).

[17] R. R. Du *et al.*, Phys. Rev. Lett. **70**, 2944 (1993).

[18] J. K. Jain, in *Perspectives in Quantum Hall Effects : Novel Quantum Liquids in Low-Dimensional Semiconductor Structures*, edited by S. Das Sarma and A. Pinczuk (John Wiley & Sons, New York, 1996), Chap. 7.

[19] B. I. Halperin, in *Perspectives in Quantum Hall Effects : Novel Quantum Liquids in Low-Dimensional Semiconductor Structures*, edited by S. Das Sarma and A. Pinczuk (John Wiley & Sons, New York, 1996), Chap. 6.

[20] H. L. Stormer and D. C. Tsui, in *Perspectives in Quantum Hall Effects : Novel Quantum Liquids in Low-Dimensional Semiconductor Structures*, edited by S. Das Sarma and A. Pinczuk (John Wiley & Sons, New York, 1996), Chap. 10.

[21] T. Ando, J. Phys. Soc. Japan **37**, 622 (1974).

[22] R. E. Prange, Phys. Rev. B **23**, 4802 (1981).

[23] B. I. Halperin, Helvetica Physica Acta **56**, 75 (1983).

[24] R. B. Laughlin, Rev. Mod. Phys. **71**, 863 (1999).

[25] A. H. MacDonald, in *Introduction to the physics of the quantum Hall regime*, *Les Houches – Ecole d'Ete de Physique Theorique, Session LXI*, edited by E. Akkermans, G. M. amd J.-L. Pichard, and J. Zinn-Justin (Elsevier Science B. V., Netherlands, 1995), Chap. 12, pp. 663–720.

[26] Y. A. Bychkov, JETP Lett. **43**, 388 (1986).

[27] Y. A. Bychkov, Sov. Phys. – Solid State **31**, 1130 (1989).

[28] L. Zheng and A. H. MacDonald, Surf. Sci. **305**, 101 (1994).

[29] K. Tevosyan and A. H. MacDonald, Phys. Rev. B **56**, 7517 (1997).

[30] D. Yoshioka, B. I. Halperin, and P. A. Lee, Phys. Rev. Lett. **50**, 1219 (1983).

[31] D. Yoshioka and P. A. Lee, Phys. Rev. B **27**, 4986 (1983).

[32] F. D. M. Haldane and E. H. Rezayi, Phys. Rev. Lett. **54**, 237 (1985).

[33] F. D. M. Haldane, in *The Quantum Hall Effect*, edited by R. E. Prange and S. M. Girvin (Springer–Verlag, New York, 1987), Chap. 8.

[34] S. M. Girvin, A. H. MacDonald, and P. M. Platzman, Phys. Rev. Lett. **54**, 581 (1985).

[35] R. Morf and B. I. Halperin, Phys. Rev. B **33**, 2221 (1986).

[36] C. Gros and A. H. MacDonald, Phys. Rev. B **42**, 9514 (1990).

[37] T. Chakraborty and P. Pietiläinen, Phys. Rev. Lett. **76**, 4018 (1996).

[38] T. Chakraborty and P. Pietiläinen, Phys. Rev. B **55**, R1954 (1997).

[39] A. H. MacDonald, K. L. Liu, S. M. Girvin, and P. M. Platzman, Phys. Rev. B **33**, 4014 (1986).

[40] B. I. Halperin, Phys. Rev. Lett. **52**, 1583 (1984).

[41] R. B. Laughlin, Surf. Sci. **141**, 11 (1984).

[42] J. K. Jain, Phys. Rev. B **40**, 2723 (1989).

[43] J. K. Jain, Adv. Phys. **41**, 105 (1992).

[44] F. C. Zhang and T. Chakraborty, Phys. Rev. B **30**, 7320 (1984).

[45] X. C. Xie, Y. Guo, and F. C. Zhang, Phys. Rev. B **40**, 3487 (1989).

[46] R. J. Haug *et al.*, Phys. Rev. B **36**, 4528 (1987).

[47] J. P. Eisenstein, H. L. Stormer, L. N. Pfeiffer, and K. W. West, Phys. Rev. B **41**, 7910 (1990).

[48] S. Kronmüller *et al.*, Phys. Rev. Lett. **81**, 2526 (1998).

[49] S. Kronmüller *et al.*, Phys. Rev. Lett. **82**, 4070 (1999).

[50] A. S. Yeh *et al.*, Phys. Rev. Lett. **82**, 592 (1999).

[51] W. Pan *et al.*, cond-mat/9910182 (unpublished).

[52] W. Pan and H. L. Stormer, Phys. Rev. B **61**, R5101 (2000).

[53] R. Willet *et al.*, Phys. Rev. Lett. **59**, 1776 (1987).

[54] F. D. M. Haldane and E. H. Rezayi, Phys. Rev. Lett. **60**, 956 (1988).

[55] G. Moore and N. Read, Nucl. Phys. B **360**, 362 (1991).

[56] R. H. Morf, Phys. Rev. Lett. **80**, 1505 (1998).

[57] E. H. Rezayi and F. D. M. Haldane, Phys. Rev. Lett. **84**, 4685 (2000).

[58] J. P. Eisenstein *et al.*, Phys. Rev. Lett. **61**, 997 (1988).

[59] W. Pan *et al.*, cond-mat/0103144 (unpublished).

[60] M. P. Lilly *et al.*, Phys. Rev. Lett. **82**, 394 (1999).

[61] R. Moessner and J. T. Chalker, Phys. Rev. B **54**, 5006 (1996).

[62] A. H. MacDonald and M. P. A. Fisher, Phys. Rev. B **61**, 5724 (2000).

[63] S. M. Girvin, in *Aspects topologiques de la physique en basse dimension. Topological aspects of low dimensional systems*, *Les Houches – Ecole d'Ete de Physique Theorique, Session LXIX*, edited by A. Comtet, T. J. amd S. Ouvry, and F. David (Springer–Verlag, Berlin/Heidelberg Germany, 1999), Chap. 2, pp. 53–176, lectures delivered at Ecole d'Ete Les Houches, July 1998; also in cond-mat/9907002.

[64] M. Shayegan, in *Aspects topologiques de la physique en basse dimension. Topological aspects of low dimensional systems*, *Les Houches – Ecole d'Ete de Physique Theorique, Session LXIX*, edited by A. Comtet, T. J. amd S. Ouvry, and F. David (Springer–Verlag, Berlin/Heidelberg Germany, 1999), Chap. 1, pp. 1–50, lectures delivered at Ecole d'Ete Les Houches, July 1998.

[65] A. V. Andreev and Y. A. Bychkov, Phys. Rev. B **45**, 1443 (1992).

[66] V. L. Pokrovsky and A. L. Talapov, J. Phys.: Condens. Matter **18**, L691 (1985).

[67] V. L. Pokrovskii and A. L. Talapov, JETP Lett. **42**, 80 (1985).

[68] S. A. Trugman and S. Kivelson, Phys. Rev. B **31**, 5280 (1985).

[69] A. H. MacDonald, Phys. Rev. B **30**, 3550 (1984).

[70] C. Domb and M. S. Green, *Phase Transition and Critical Phenomena* (Academic Press, New York, 1974), Vol. 3.

[71] Y. A. Bychkov, S. V. Iordanskii, and G. M. Eliashberg, JETP Lett. **33**, 143 (1981).

[72] D. Vollhardt, Phys. Rev. Lett. **78**, 1307 (1997).

[73] J. P. Eisenstein, L. N. Pfeiffer, and K. W. West, Phys. Rev. B **50**, 1760 (1994).

Acknowledgements

I wish to thank Herr Priv.–Doz. Dr. Walter Apel for his guidance, furthermore, for his care and support during the whole period of my study in Germany. His push and encouragement profit me directly and greatly. I thank Prof. Dr. Mario Liu for his suggestion and advice concerning the way a young physicist may want to examine their works and also for his care as a referee of my thesis. I thank Prof. Dr. Rolf J. Haug for suggestion and encouragement he gave to me and my work. These are useful interactions. I am grateful for help, support, hospitality and encouragement from Herr Prof. Dr. Wolfgang Weller (Leipzig) since the very beginning. It was through him that I experienced German education tradition in person for the first time. That was before I actually came to Germany. I thank my colleagues at PTB and other places for useful discussion. I thank a friend of mine, Annette Bäker, for her help and support during the whole period of my study in Germany. I thank another friend of mine, Vanisa Surapipith, for her help and support all the while. Thanks the Apel family for their lively and cheerful support. Finally, I thank my family with whole–heartedly gratitude for their patient, understanding and support due to my study.

I thank my host the Physikalisch–Technische Bundesanstalt (PTB) for its hospitality and funding support. I thank the Deutsche Forschungsgemeinschaft (DFG) for funding support. I appreciate support from the Helmholtz Fonds e. V..

It was a great opportunity for me to come and study physics in Germany. It was a great experience and I have had a good time.

Curriculum vitae

Name	Sivinee Sawatdiaree
Date of birth	19.08.1972
Place of birth	Chiang Mai, Thailand

Primary education

05.1976 – 03.1984	Lampoon Kindergarten, Lampoon, Thailand
05.1984 – 03.1987	Suanboon Yopatham School, Lampoon, Thailand
05.1987 – 03.1989	The Prince Royal College , Chiang Mai, Thailand

Higher education

06.1989 – 04.1994	Department of Physics, Faculty of Science, Chiang Mai University, Thailand
04.1994	Bachelor of Science (Physics), Chiang Mai University
06.1994 – 04.1997	Department of Physics, Faculty of Science, Chulalongkorn University, Thailand
04.1997	Master of Science (Physics), Chulalongkorn University
06.1997	Bogoliubov Institute for Theoretical Science, Dubna, Russia Under the supervision of Prof. Dr. Vladimir Yarunin
07.1997 – 06.2000	Fachbereich Q. 1, Physikalisch–Technische Bundesanstalt, Braunschweig, Germany Sponsorship by Deutsche Forschungsgemeinschaft
07.2000 – 06.2001	Fachbereich Q. 1, Physikalisch–Technische Bundesanstalt, Braunschweig, Germany Sponsorship by Physikalisch–Technische Bundesanstalt

Publication

S. Sawatdiaree and W. Apel,
"On the high–temperature expansion
for a partially filled lowest Landau level",
Physica **E 6**, 75–78 (2000).